UNIVERSITY OF OKLAHOMA

GRADUATE COLLEGE

EFFECTS OF PROCESS PARAMETERS AND MOLD DESIGN ON RESIN TRANSFER MOLDED COMPOSITES

A DISSERTATION

SUBMITTED TO THE GRADUATE FACULTY

in partial fulfillment of the requirements for the

degree of

Doctor of Philosophy

By

KRISTIAN ALLEN OLIVERO
Norman, Oklahoma
2004

Downloaded from SHAREOK. Persistent Handle URL: https://hdl.handle.net/11244/709

UMI Number: 3122293

INFORMATION TO USERS

The quality of this reproduction is dependent upon the quality of the copy submitted. Broken or indistinct print, colored or poor quality illustrations and photographs, print bleed-through, substandard margins, and improper alignment can adversely affect reproduction.

In the unlikely event that the author did not send a complete manuscript and there are missing pages, these will be noted. Also, if unauthorized copyright material had to be removed, a note will indicate the deletion.

UMI®

UMI Microform 3122293

Copyright 2004 by ProQuest Information and Learning Company.

All rights reserved. This microform edition is protected against unauthorized copying under Title 17, United States Code.

ProQuest Information and Learning Company
300 North Zeeb Road
P.O. Box 1346
Ann Arbor, MI 48106-1346

©Copyright by KRISTIAN ALLEN OLIVERO 2004
All Rights Reserved

EFFECTS OF PROCESS PARAMETERS AND MOLD DESIGN ON RESIN TRANSFER MOLDED COMPOSITES

A Dissertation APPROVED FOR THE
SCHOOL OF AEROSPACE AND MECHANICAL ENGINEERING

BY

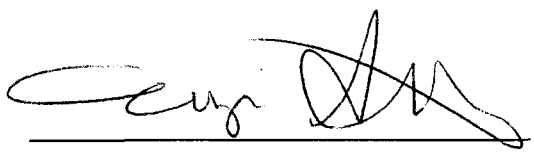

Dr. M. Cengiz Altan

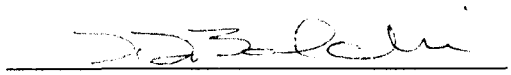

Dr. James D. Baldwin

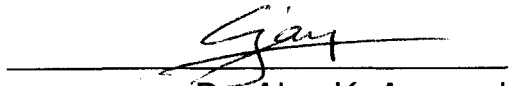

Dr. Ajay K. Agrawal



Dr. Ramkumar N Parthasarathy

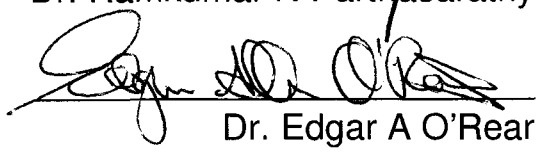

Dr. Edgar A O'Rear

Acknowledgments

This dissertation would not have been possible without the support of so many. Special thanks to the following:

I would like to thank my advisor, M. Cengiz Altan, for setting such a high academic standard by example. I would also like to thank the other members of my committee, Dr. Baldwin, Dr. Parthasarathy, Dr. O'Rear, and Dr. Agrawal for their contributions. Each of these professors has been a guide and model throughout all of my higher education.

Appreciation is also due to my peers who have supported these research efforts and who have become close friends, in particular, Levent Aktas, Youssef Hamidi, and Randal Fuller. Also, Harry Barraza for his contributions to this work through microscopic void analysis of molded test specimens.

This research would not have been possible without the support and expertise of Billy Mays, Greg Williams, and the rest of University of Oklahoma Aerospace and Mechanical Engineering machine shop. Their assistance has been invaluable.

I have missed my parents Robert and Terri, and each of my brothers, Michael, Bobby, Bryan, Brett, and Brad, but have not received any less from them. I can't forget Aunt Mary, and my ace in the hole, Tatarun; they have never forgotten me. Finally, my wife, Tra My, and my children, Samson, Rocco, and Kayla, who this is for.

This research work has been partially supported by the NASA Microgravity Materials Research Program under Grant NAG8-1271.

Nomenclature

D	inlet gate diameter
H	half gap width
K	permeability
K_{rr}	permeability in radial direction
L	gap width
p, P	pressure
Q	volume flow rate
r, R	radial location
R^*	radial location of the fluid front
t	time
w	width of flow perpendicular to flow direction
U, V	velocity components
x	coordinate in flow direction
X	linear location of the fluid front
ϕ	preform volume fraction
μ	viscosity

Table of Contents

Title Page i
Signature Page ii
Copyright Page iii
Acknowledgments iv
Nomenclature v
Table of Contents vi
List of Tables viii
List of Illustrations x
Abstract xviii
1 Introduction 1
1.1 Resin Transfer Molding 1
1.2 Importance of Process Parameters in Resin Transfer Molding 1
1.3 Permeability of the Fibrous Preform in Resin Transfer Molding 4
1.4 Importance of Void Content in Resin Transfer Molding 5
1.5 Mechanical Characterization of Resin Transfer Molded Parts 7
1.6 Pressure Reduction in Resin Transfer Molding 9
1.7 Scope of the Presented Research 12
2 Experimental Setup 14
2.1 Molding Apparatus Used to Fabricate RTM Parts 14
2.2 Tensile Testing of Molded Composites 17
2.3 Three-Point Bending Test of Molded Composites 19
2.4 Microscopic Analysis to Quantify Void Content 20
3 Effect of Injection Rate and Post-Fill Cure Pressure on Mechanical Properties and Void Content of Resin Transfer Molded Disks 32
3.1 Introduction 32
3.2 Effect of Injection Rate on Properties of Resin Transfer Molded Disks 33
3.3 Effect of Post-Fill Cure Pressure on Mechanical Properties and Void Content of Resin Transfer Molded Disks 35
3.4 Correlation Between Void Content and Mechanical Properties 37
3.5 Concluding remarks 40
4 Effect of Preform Thickness and Volume Fraction on Injection Pressure and Mechanical Properties of Resin Transfer Molded Composites 54
4.1 Introduction 54
4.2 Molding Apparatus Used to Fabricate RTM Parts 55
4.3 Pressure in a Disk Shaped Cavity Containing Porous Media 59
4.4 Permeability Measurement Using a Single Pressure Transducer 61
4.5 Results and Discussion 62
4.6 Concluding Remarks 69

5 Mold Modifications to Facilitate Reduced Molding Pressure 84
5.1 Introduction 84
5.2 Modified Channel Mold Cavity 85
5.3 Obtaining Permeability from Transient Inlet Pressure Data 89
5.4 Pressure Drop in a Channel 93
5.5 Theoretical Pressure Predictions for Mold with Single Channel 96
5.6 Theoretical Pressure Predictions for Mold with Two Channels 98
5.7 Fluid Front Profile Measurement for Channel Molds 101
5.8 Visual Characterization of Disks Fabricated Utilizing Channels 103
5.9 Identifying Intermediate Fluid Front Positions in Channel Molding 109
5.10 Pressure Reduction Results Observed in Channel Molds 116
5.11 Concluding Remarks 121
6 Concluding Remarks 175
7 References 179
8 Appendix A: Data Tables 188

List of Tables

Table 3.1 Molding parameters used to determine effect of volume flow rate on mechanical properties 41
Table 3.2 Molding parameters used to determine effect of packing pressure on mechanical properties and void content 46
Table 4.1 Experimental configurations used to examine effect of preform thickness and fiber volume fraction 71
Table 4.2 Measured permeability for each mat configuration and ratio between permeabilities of thick and thin mats 83
Table 5.1 Experimental configurations of fabricated disks used to observe effect of different channel configurations on molded parts 124
Table 5.2 Experimental configurations used to examine effect of channels on pressure reduction 126
Table 5.3 Maximum pressures (kPa) measured for 1-Channel molds with different channel lengths, expressed as percentage of disk radius, using different molding configurations. Average from three filling for each disk 161
Table 5.4 Maximum pressures (kPa) measured for 2-Channel molds with different channel lengths, expressed as percentage of disk radius, using different molding configurations. Average from three filling for each disk 162
Table 5.5 Measured permeability values obtained from curve fitting inlet pressure data 169
Table 6.1 Tensile strength data (in kPa) for position 1 and position 2 specimens used to quantify effects of injection rate on properties for each injection rate. Packing pressure=228 kPa 189
Table 6.2 Stiffness data (in kPa) for all position 1 and position 2 specimens used to quantify effects of injection rate on properties for each injection rate. Packing pressure=228 kPa 190
Table 6.3 Tensile strength data (in kPa) for position 1 and position 2 specimens used to quantify effects of packing pressure on properties for each packing pressure. Injection rate=0.067 cm^3/s 191
Table 6.4 Stiffness data (in kPa) for position 1 and position 2 specimens used to quantify effects of packing pressure on properties for each packing pressure. Injection rate=0.067 cm^3/s 192
Table 6.5 Void shape distribution data (in %) and total voids based on packing pressure. Injection rate=0.067 cm^3/s 193
Table 6.6 Void size distribution data (in %) and total voids based on packing pressure. Injection rate=0.067 cm^3/s 194

Table 6.7 Tensile strength of each specimen (in kPa) used to determine effect of mat thickness and volume fraction on properties 195
Table 6.8 Stiffness of each specimen (in kPa) used to determine effect of mat thickness and volume fraction on properties 196

List of Illustrations

Figure 2.1 Experimental setup used to fabricate resin transfer molded disks 23

Figure 2.2 Photograph of a molded disk cut into five tensile test specimens (left), chopped strand glass fiber mat (right), and Statomix inline mixer (top) 24

Figure 2.3 Top view of the disk-shaped mold cavity used to fabricate resin transfer molded disks (left) and exploded view of mold cavity components showing top plate, spacer plate, and bottom plate (right) 25

Figure 2.4 Photograph of the mold cavity components. Top mold wall with two flow channels (left), spacer plate (center), and bottom mold wall (right) 26

Figure 2.5 Representative injection force during mold filling showing four different packing pressures after filling is completed. Force is measured at constant flow rate during filling, followed by the application of a constant force applied for 300 seconds 27

Figure 2.6 Diagram of a molded disk depicting locations of the tensile test specimens 28

Figure 2.7 Tensile test specimen mounted in MTS machine showing extensometer location 29

Figure 2.8 Representative stress-strain curves of two position 1 specimens molded at two different packing pressures 30

Figure 2.9 Representative microscopic images obtained from specimen cross-sections at 100x magnifications. a: Example of fibers perpendicular to and parallel to cross section; b: Large, circular void at 0 kPa packing pressure; c: Smaller, circular void at 228 kPa; d: Irregular in-tow void at 683 kPa 31

Figure 3.1 Photograph of a transparent part that undergoing 683 kPa packing pressure (left), and a cloudy part with no applied packing pressure (right) 42

Figure 3.2 Ultimate tensile strength variation with injection flow rate for positions 1 and 2. Packing pressure=228 kPa 43

Figure 3.3 Ultimate tensile strength variation with injection flow rate averaged over positions 1 and 2. Packing pressure=228 kPa 44

Figure 3.4 Stiffness variation with injection rate averaged over positions 1 and 2. Packing pressure=228 kPa 45

Figure 3.5 Ultimate tensile strength variation with packing pressure averaged over positions 1 and 2. Injection rate=0.067 cm^3/s 47

Figure 3.6 Stiffness variation with packing pressure averaged over positions 1 and 2. Injection rate=0.067 cm^3/s 48

Figure 3.7 Void area fraction variation based on packing pressure. Injection rate=0.067cm^3/s 49

Figure 3.8 Void shape distribution based on packing pressure. Injection rate=0.067 cm^3/s 50
Figure 3.9 Void size distribution based on packing pressure. Injection rate=0.067 cm^3/s 51
Figure 3.10 Strength variation with void fraction averaged over positions 1 and 2. Injection rate=0.067 cm^3/s 52
Figure 3.11 Stiffness variation with void fraction averaged over positions 1 and 2. Injection rate=0.067 cm^3/s 53
Figure 4.1 Setup used to fabricate RTM parts and measure pressure to determine permeability 72
Figure 4.2 Photograph of the setup used to fabricate RTM parts and measure pressure to determine permeability 73
Figure 4.3 Representative stress strain curves from tensile tested specimens. TN4: 4 layers of thin mats (i.e., v_f =9.8%); TN8: 8 layers of thin mats (i.e., v_f =21.2%); TN12: 12 layers of thin mats (i.e., v_f =33.1%) 74
Figure 4.4 Example pressure curves from filling disks containing each of the six preform configurations 75
Figure 4.5 Cross section of disk shaped cavity labeled for pressure calculations. R_f is the transient radial location of the fluid front during filling 76
Figure 4.6 Ultimate tensile strength of specimens for each preform configuration 77
Figure 4.7 Elastic modulus of specimens for each preform configuration 78
Figure 4.8 Short beam shear strength of specimens from each preform configuration 79
Figure 4.9 Example pressure curves from disks containing thick mats and theoretical curve fit used to determine permeability. TK2: 2 layers of thick mats (i.e., v_f =9.8%); TK4: 4 layers of thick mats (i.e., v_f =21.2%); TK6: 6 layers of thick mats (i.e., v_f =33.1%) 80
Figure 4.10 Example pressure curves from disks containing thin mats and theoretical curve fit used to determine permeability. TN4: 4 layers of thin mats (i.e., v_f =9.8%); TN8: 8 layers of thin mats (i.e., v_f =21.2%); TN12: 12 layers of thin mats (i.e., v_f =33.1%) 81
Figure 4.11 Permeability results obtained for each preform configuration. Theoretical permeability for empty mold is obtained from Equation 4.14 82
Figure 5.1 a:(left) Original top mold wall with no flow channels; b:(middle) Top mold wall with a single flow channel; c:(right) Top mold wall with two perpendicular flow channels 123
Figure 5.2 Pressure curves obtained from center-gated disk containing 21.2% fiberglass preform at R =12.7 mm 127

Figure 5.3 Pressure difference observed between inlet and R =12.7 mm from center-gated disk containing 21.2% fiberglass preform 128
Figure 5.4 First second of inlet pressure measurement for 0-Channel and 1-Channel molds containing 4 layers (≅20%) of thick fiberglass preform impregnated with 118 cp corn syrup. Channel length set to disk radius. Each curve represents average of three pressure profiles 129
Figure 5.5 Diagram of geometry used to calculate theoretical inlet pressure for 1-Channel mold. Only one half of flow drawn due to symmetry 130
Figure 5.6 Diagram of geometry used to calculate theoretical inlet pressure for 2-Channel mold 131
Figure 5.7 Theoretical inlet pressures for 0, 1, and 2-Channel molds..... 132
Figure 5.8 Photograph of all molded disks used to determine effect of flow channels on filling 133
Figure 5.9 Photograph of disk 0K4R molded with 4 layers of preform and no flow channels. a: top; b: bottom 134
Figure 5.10 Photograph of disk 0K6R molded with 6 layers of preform and no flow channels. a: top; b: bottom 134
Figure 5.11 Photograph of disk 1K2R molded with 2 layers of preform and 1 flow channel. a: top; b: bottom 135
Figure 5.12 Photograph of disk 1K4R molded with 4 layers of preform and 1 flow channel. a: top; b: bottom 135
Figure 5.13 Photograph of disk 1K6R molded with 6 layers of preform and 1 flow channel. a: top; b: bottom 136
Figure 5.14 Photograph of disk 1K8R molded with 8 layers of preform and 1 flow channel. a: top; b: bottom 136
Figure 5.15 Photograph of disk 2K2R molded with 2 layers of preform and 2 flow channels. a: top; b: bottom 137
Figure 5.16 Photograph of disk 2K4R molded with 4 layers of preform and 2 flow channels. a: top; b: bottom 137
Figure 5.17 Photograph of disk 2K6R molded with 6 layers of preform and 2 flow channels. a: top; b: bottom 138
Figure 5.18 Photograph of disk 2K8R molded with 8 layers of preform and 2 flow channels. a: top; b: bottom 138
Figure 5.19 Photograph of disk 1K4R-1/3B molded with 4 layers of preform and 1 flow channel which has had the final 1/3 of its length blocked. a: top; b: bottom 139
Figure 5.20 Photograph of disk 1K6R-1/3B molded with 6 layers of preform and 1 flow channel which has had the final 1/3 of its length blocked. a: top; b: bottom 139
Figure 5.21 Photograph of disk 2K4R-1/3B molded with 4 layers of preform and 2 flow channels which have had the final 1/3 of their length blocked. a: top; b: bottom 140

Figure 5.22 Photograph of disk 2K6R-1/3B molded with 6 layers of preform and 2 flow channels which have had the final 1/3 of their length blocked. a: top; b: bottom 140
Figure 5.23 Photograph of disk 1K4R-1/2B molded with 4 layers of preform and 1 flow channel which has had the final 1/2 of its length blocked. a: top; b: bottom 141
Figure 5.24 Photograph of disk 1K6R-1/2B molded with 6 layers of preform and 1 flow channel which has had the final 1/2 of its length blocked. a: top; b: bottom 141
Figure 5.25 Photograph of disk 2K4R-1/2B molded with 4 layers of preform and 2 flow channels which have had the final 1/2 of their length blocked. a: top; b: bottom 142
Figure 5.26 Photograph of disk 2K6R-1/2B molded with 6 layers of preform and 2 flow channels which have had the final 1/2 of their length blocked. a: top; b: bottom 142
Figure 5.27 Photograph of disk 1K4R-2/3B molded with 4 layers of preform and 1 flow channel which has had the final 2/3 of its length blocked. a: top; b: bottom 143
Figure 5.28 Photograph of disk 1K6R-2/3B molded with 6 layers of preform and 1 flow channel which has had the final 2/3 of its length blocked. a: top; b: bottom 143
Figure 5.29 Photograph of disk 2K4R-2/3B molded with 4 layers of preform and 2 flow channels which have had the final 2/3 of their length blocked. a: top; b: bottom 144
Figure 5.30 Photograph of disk 2K6R-2/3B molded with 6 layers of preform and 2 flow channels which have had the final 2/3 of their length blocked. a: top; b: bottom 144
Figure 5.31 Photograph of disk 1K4R-SS2 molded with 4 layers of preform and 1 flow channel. Partially filled for 2 seconds. a: top; b: bottom 145
Figure 5.32 Photograph of disk 1K6R-SS2 molded with 6 layers of preform and 1 flow channel. Partially filled for 2 seconds. a: top; b: bottom 145
Figure 5.33 Photograph of disk 1K2R-SS4 molded with 2 layers of preform and 1 flow channel. Partially filled for 4 seconds. a: top; b: bottom 146
Figure 5.34 Photograph of disk 1K4R-SS4 molded with 4 layers of preform and 1 flow channel. Partially filled for 4 seconds. a: top; b: bottom 146
Figure 5.35 Photograph of disk 1K6R-SS4 molded with 6 layers of preform and 1 flow channel. Partially filled for 4 seconds. a: top; b: bottom 147
Figure 5.36 Photograph of disk 1K8R-SS4 molded with 8 layers of preform and 1 flow channel. Partially filled for 4 seconds. a: top; b: bottom 147

Figure 5.37 Photograph of disk 2K4R-SS2 molded with 4 layers of preform and 2 flow channels. Partially filled for 2 seconds. a: top; b: bottom 148
Figure 5.38 Photograph of disk 2K6R-SS2 molded with 6 layers of preform and 2 flow channels. Partially filled for 2 seconds. a: top; b: bottom 148
Figure 5.39 Photograph of disk 2K2R-SS4 molded with 2 layers of preform and 2 flow channels. Partially filled for 4 seconds. a: top; b: bottom 149
Figure 5.40 Photograph of disk 2K4R-SS4 molded with 4 layers of preform and 2 flow channels. Partially filled for 4 seconds. a: top; b: bottom 149
Figure 5.41 Photograph of disk 2K6R-SS4 molded with 6 layers of preform and 2 flow channels. Partially filled for 4 seconds. a: top; b: bottom 150
Figure 5.42 Photograph of disk 2K8R-SS4 molded with 8 layers of preform and 2 flow channels. Partially filled for 4 seconds. a: top; b: bottom 150
Figure 5.43 Photograph of disk 1K4R-1/2B-SS4 molded with 4 layers of preform and 1 flow channel which has had the final 1/2 of its length blocked. Partially filled for 4 seconds. a: top; b: bottom 151
Figure 5.44 Photograph of disk 1K6R-1/2B-SS4 molded with 6 layers of preform and 1 flow channel which has had the final 1/2 of its length blocked. Partially filled for 4 seconds. a: top; b: bottom 151
Figure 5.45 Photograph of disk 2K4R-1/2B-SS4 molded with 4 layers of preform and 2 flow channels which have had the final 1/2 of their length blocked. Partially filled for 4 seconds. a: top; b: bottom 152
Figure 5.46 Photograph of disk 2K6R-1/2B-SS4 molded with 6 layers of preform and 2 flow channels which have had the final 1/2 of their length blocked. Partially filled for 4 seconds. a: top; b: bottom 152
Figure 5.47 Photograph of disk 1K4R-HG molded with 4 layers of preform and 1 flow channel. Mold cavity surrounding preform filled with a ring of hot glue prior to filling.. a: top; b: bottom 153
Figure 5.48 Photograph of disk 1K6R-HG molded with 6 layers of preform and 1 flow channel. Mold cavity surrounding preform filled with a ring of hot glue prior to filling.. a: top; b: bottom 153
Figure 5.49 Photograph of disk 2K4R-HG molded with 4 layers of preform and 2 flow channels. Mold cavity surrounding preform filled with a ring of hot glue prior to filling.. a: top; b: bottom 154

Figure 5.50 Photograph of disk 2K6R-HG molded with 6 layers of preform and 2 flow channels. Mold cavity surrounding preform filled with a ring of hot glue prior to filling.. a: top; b: bottom 154
Figure 5.51 Inlet pressure measurement for 0, 1, and 2-Channel molds containing 4 layers (≅20%) of thick fiberglass preform impregnated with 118 cp corn syrup. Channel length set to disk radius. Bold curves are theoretically generated. Each experimental curve represents average of three pressure profiles 155
Figure 5.52 Inlet pressure measurement for 0, 1, and 2-Channel molds containing 4 layers (≅20%) of thick fiberglass preform impregnated with 118 cp corn syrup. Channel length set to 67% of disk radius. Each curve represents average of three pressure profiles 156
Figure 5.53 Inlet pressure measurement for 0, 1, and 2-Channel molds containing 4 layers (≅20%) of thick fiberglass preform impregnated with 118 cp corn syrup. Channel length set to 50% of disk radius. Each curve represents average of three pressure profiles 157
Figure 5.54 Inlet pressure measurement for 0, 1, and 2-Channel molds containing 4 layers (≅20%) of thick fiberglass preform impregnated with 118 cp corn syrup. Channel length set to 33% of disk radius. Each curve represents average of three pressure profiles 158
Figure 5.55 Inlet pressure measurement for 1-Channel molds containing 4 layers (≅20%) of thick fiberglass preform impregnated with 118 cp corn syrup for channel lengths blocked to 33, 50, 67, and 100% of the disk radius. Limiting case is 0% channel length, represented by 0-Channel mold. Each curve represents average of three pressure profiles 159
Figure 5.56 Inlet pressure measurement for 2-Channel molds containing 4 layers (≅20%) of thick fiberglass preform impregnated with 118 cp corn syrup for channel lengths blocked to 33, 50, 67, and 100% of the disk radius. Limiting case is 0% channel length, represented by 0-Channel mold. Each curve represents average of three pressure profiles 160
Figure 5.57 Inlet pressure measurement for 0, 1, and 2-Channel molds containing 8 layers (≅20%) of thin fiberglass preform impregnated with 138 cp corn syrup. Channel length set to disk radius. Bold curves are theoretically generated. Each experimental curve represents average of three pressure profiles 163
Figure 5.58 Inlet pressure measurement for 0, 1, and 2-Channel molds containing 8 layers (≅20%) of thin fiberglass preform impregnated with 138 cp corn syrup. Channel length set to

67% of disk radius. Each curve represents average of three pressure profiles 164
Figure 5.59 Inlet pressure measurement for 0, 1, and 2-Channel molds containing 8 layers (≅20%) of thin fiberglass preform impregnated with 138 cp corn syrup. Channel length set to 50% of disk radius. Each curve represents average of three pressure profiles 165
Figure 5.60 Inlet pressure measurement for 0, 1, and 2-Channel molds containing 8 layers (≅20%) of thin fiberglass preform impregnated with 138 cp corn syrup. Channel length set to 33% of disk radius. Each curve represents average of three pressure profiles 166
Figure 5.61 Inlet pressure measurement for 1-Channel molds containing 8 layers (≅20%) of thin fiberglass preform impregnated with 138 cp corn syrup for channel lengths blocked to 33, 50, 67, and 100% of the disk radius. Limiting case is 0% channel length, represented by 0-Channel mold. Each curve represents average of three pressure profiles 167
Figure 5.62 Inlet pressure measurement for 2-Channel molds containing 8 layers (≅20%) of thin fiberglass preform impregnated with 138 cp corn syrup for channel lengths blocked to 33, 50, 67, and 100% of the disk radius. Limiting case is 0% channel length, represented by 0-Channel mold. Each curve represents average of three pressure profiles 168
Figure 5.63 Inlet pressure measurement for 0, 1, and 2-Channel molds containing 12 layers (≅30%) of thin fiberglass preform impregnated with 63.2 cp corn syrup. Channel length set to 67% of disk radius. Bold curves are theoretically generated for 100% channel length. Each experimental curve represents average of three pressure profiles 170
Figure 5.64 Inlet pressure measurement for 0, 1, and 2-Channel molds containing 12 layers (≅30%) of thin fiberglass preform impregnated with 63.2 cp corn syrup. Channel length set to 50% of disk radius. Each curve represents average of three pressure profiles 171
Figure 5.65 Inlet pressure measurement for 0, 1, and 2-Channel molds containing 12 layers (≅30%) of thin fiberglass preform impregnated with 63.2 cp corn syrup. Channel length set to 33% of disk radius. Each curve represents average of three pressure profiles 172
Figure 5.66 Inlet pressure measurement for 1-Channel molds containing 12 layers (≅30%) of thin fiberglass preform impregnated with 63.2 cp corn syrup for channel lengths blocked to 33, 50, and 67% of the disk radius. Limiting case is 0% channel length, represented by 0-Channel mold. Each curve represents average of three pressure profiles 173

Figure 5.67 Inlet pressure measurement for 2-Channel molds containing 12 layers (≅30%) of thin fiberglass preform impregnated with 63.2 cp corn syrup for channel lengths blocked to 33, 50, and 67% of the disk radius. Limiting case is 0% channel length, represented by 0-Channel mold. Each curve represents average of three pressure profiles 174

Abstract

The effects of flow rate and post-fill cure pressure, i.e., packing pressure, on the mechanical properties of resin transfer molded disks are experimentally investigated. Disks are molded at different flow rates and packing pressures in order to observe the effects of these parameters on the mechanical properties and void content of the final parts. Increased injection rate is found to reduce both the strength and stiffness of the molded parts due to the formation of more voids behind the faster moving fluid front. At higher packing pressures, fewer voids and improved strength and stiffness are observed. Mechanical properties are correlated with the total void fraction for disks molded at different packing pressures. A decrease in both tensile strength and elastic modulus is observed with increasing void fraction. Doubling the void volume fraction from 0.35% to 0.72% results in about 15% decrease in strength and stiffness.

An experimental study is performed to characterize the effect of the thickness of random preforms on injection pressure and mechanical properties of RTM parts. Center-gated, disk-shaped parts are molded using two different chopped strand, glass fiber preforms. Both preforms have random microstructure but different planar densities (i.e., different uncompressed layer thicknesses). Tensile strength, short-beam shear strength, and elastic modulus are measured for parts molded with each preform type at three different volume fractions of 9.8, 21.2, and 33.1%. Although mechanical properties are found to increase linearly with volume fraction, significant difference is not observed between disks containing thick and thin mats at equivalent fiber volume fractions.

However, at the same fiber content, parts molded with thin mats require significantly lower injection pressures compared to parts containing thick mats.

The final phase of the presented research goes beyond traditional RTM. An enhancement to the molding process is presented which is expected to yield substantial reduction in molding pressure. Small flow channels are machined in mold walls, resulting in low resistance flow paths for resin flow during impregnation. Experiments are performed to evaluate the effects of channels on molding process. Disk-shaped parts are fabricated via RTM utilizing molds modified with either 1 or 2 flow channels on the top mold wall. Channel length is varied to 33%, 50%, 67%, and 100% of the mold cavity to further characterize the process. Molded parts are visually observed for void content and dry spots to verify that pressure reduction does not occur at the expense of overall part quality. Transient pressure measurements are compared for each configuration.

Channels are observed to significantly alter the flow pattern, by allowing the fluid front to reach the mold edge early in the filling process for longer channel lengths. Ray tracing effect is observed in these cases, as the fluid is observed to quickly move along the mold edge, eventually trapping air and resulting in dry areas and areas of high macrovoid concentration. However, at shorter channel lengths, defect-free parts are realized. A channel length of 67% is found to yield good parts for 2-Channel molds, and a channel length of 50% results in good parts for 1-Channel molds. Best case of 77% pressure reduction for a 2-Channel mold and 57% for 1-Channel mold are observed, thus channels are shown to be effect enhancement to RTM process for reduction of pressure.

1 Introduction

1.1 Resin Transfer Molding

Resin transfer molding (RTM) is frequently used to fabricate medium to large, geometrically complex, high performance composite parts in a cost-effective manner. In this process, a fibrous reinforcing preform is placed in the mold cavity and subsequently impregnated by a relatively low viscosity thermosetting resin. The polymeric resin cures in the cavity, typically within several hours, after which the solid part is demolded. Depending on the shape complexity, size, and performance requirements, a wide variety of resins and preform types can be used. Compared to other molding operations that use higher viscosity thermoplastics, the complete RTM process can be accomplished with much simpler, lighter, and less expensive tooling and molding equipment. Resin transfer molding has become increasingly popular because it offers improved properties at a lower cost. Overall cost reduction is primarily due to increased production rates as a result of automation, low capital cost, and low scrap rate.

1.2 Importance of Process Parameters in Resin Transfer Molding

Several process parameters are important to the properties and quality of RTM parts. Process parameters influence phenomena during molding such as wetting, air entrapment, and thermal gradients. Poor wetting and air entrapment during molding lead to voids that degrade mechanical properties and surface finish in the final part, while thermal gradients can cause the part to deform or

buckle as it cures. Parameters such as injection rate, gate and vent locations, packing pressure, and preform microstructure are commonly known to contribute to void formation. Quantitative details about how individual process parameters lead to void formation, and the resulting change in mechanical performance are vital to the understanding and design of effective resin transfer molding processes.

The mechanical performance of resin transfer molded parts is shown to depend on the fiber volume fraction [1,2], microstructure of the preform [3-5], void content [6], and impregnation parameters [7]. In most cases, mechanical properties of composite parts can be improved by increasing fiber volume fraction. Higher fiber volume fractions, however, require increased injection pressure, which may significantly affect the properties of the final part. Patel et al. [8] molded composite parts containing E-glass fibers at constant injection pressure. They observed that doubling the injection pressure results in an 11% decrease in tensile strength of parts. Similarly, significant variation of the mechanical performance of RTM composites has been observed by Lee and Wei [9] for composites molded at different injection pressures. Lee and Wei [9] reported as much as a 38% decrease in the flexural strength at same fiber volume fraction due to a 25% increase in the injection pressure. Both references suggested that increased injection pressure causes higher flow velocities during molding, leading to more air entrapment at the fluid front and thus increased void formation.

Injection pressure is also influenced by cavity thickness, preform microstructure, and lay up sequence. Brickerton et al. [10,11] reported that even a small variation in mold cavity thickness has a drastic impact on the injection pressure. A decrease in local mold thickness leads to higher local fiber volume fraction, lower preform permeability, and thus, increased molding pressure. Mogavero and Advani [12] investigated the effects of varying the multilayer preform architecture on resin flow. Their results showed that varying the lay up order for a fixed number of layers did not result in significant differences in the process. Pearce et al. [13] showed that, using the same fiber type, surface treatment, and fiber volume fraction, permeabilities differed based on fiber weave. A 5 harness satin weave was found to have the lowest permeability and yielded parts with the highest interlaminar shear strength (ILSS) compared to 5 harness satin Injectex and 2x2 twill weave. The 2x2 twill weave had the highest permeability and lowest ILSS. Adams and Rebenfeld [14] showed that the flow characteristics are very sensitive to preform microstructure. The effect of having multilayer fabric assemblies on the permeability was investigated by using two isotropic fabrics. It was found that the presence of a single high permeability layer among other layers considerably increased the permeability. In addition, the lay up sequence of multilayer fabrics was observed to be important for the average permeability.

1.3 Permeability of the Fibrous Preform in Resin Transfer Molding

In most theoretical models developed for RTM, the required injection pressure is governed by the preform permeability. The commonly used Darcy's law [15] characterizes the permeability as the ratio between the superficial velocity and the pressure drop in the porous media. Several models have been proposed to estimate the value of the permeability for various porous media. Capillary models such as those proposed by Carman [16] and Gutowsky et al. [17] use the fiber radius and porosity to predict the permeability, but several discrepancies with experimental data have been reported [17-21]. Theoretical models have also been developed for different idealized media structures [18-21]. Most models may not provide accurate prediction of permeabilities since fibrous mats used in RTM are often more complex than the idealized unit cell patterns used in theoretical derivations. Thus due to the lack of adequate predictive models, permeability of RTM performs is usually determined experimentally.

A number of permeability measurement methods have been developed; however, there is no standardized measurement technique for RTM applications. Trevino et al. [22] and Young et al. [23] determined unidirectional permeability using two pressure transducers at the inlet and the exit in conjunction with an equation based on Darcy's law applied to their flow geometry. Calhoun et al. [24] presented a technique based on placing several pressure transducers at various locations inside the mold. Adams and Rebenfeld [25-27] developed a technique that quantified the planar permeability using the position and shape of

the advancing resin front as a function of time. A transparent mold was used to enable the monitoring of the advancing front. Other techniques based also on the observation of the moving resin front are common in the literature [10,11,17,25-31]. However, transparent mold walls may not have enough strength to avoid deflection, which has been shown to perturb the measured permeability values [10,11,22,23]. In addition, the use of a camera or multiple transducers placed on the mold walls may not be practical for many RTM applications.

1.4 Importance of Void Content in Resin Transfer Molding

One of the main effects of varying the process parameters in RTM is changing void occurrence and characteristics in the molded parts. Microvoids are common defects formed in the liquid molding of composite materials due to the flow dynamics and the interactions between the resin and the fiber surfaces inside the mold cavity, and are the major contributor to mechanical degradation of RTM parts. Voids occur at different length scales, such as the fiber, tow, and part scales, with different factors contributing to the formation of voids at each scale. A composite part having a high void content usually exhibits low structural integrity, in terms of tensile strength and interlaminar shear strength (ILSS) [6,32,33]; as well as an increased propensity to absorb moisture from the environment [34]. Crack propagation and failure mechanisms have also been shown to correlate, not only with void content, but also with the void size and shape distribution along the composite [35,36].

Variation in mechanical properties between two parts molded with identical processing parameters, or between specimens obtained from different locations in the same part, may be attributed to porosity concentration in specific regions within the composite. One-dimensional numerical models have been used to predict the formation of voids resulting from flow disruption due to local permeability variations [37,38]. Many researchers have studied various fill parameters, the level of voids formed, and methods to minimize void content. The effects of mat architecture and liquid properties [39], vibrating mold walls, and mold surface treatments [40] have been presented. Ikegawa et al. proposed a technique to modify the RTM process, in which mold walls are compressed during filling, resulting in fewer voids [41].

Various studies have shown that pressure applied at different locations and times during filling significantly affects void formation. For example, vacuum assistance has been investigated as a method to decrease overall void content in molded parts. Chang and Hourng developed a model predicting that vacuum assistance would cause voids formed in the transverse impregnation of unidirectional fibers to shrink and disappear [42]; while Lundström and Gebart actually observed a decrease in measured void content in composites molded with vacuum assistance, with very few voids observed at the highest vacuum levels [43]. Similarly, the effects of injection pressure and injection rate or local velocity have been observed by both Patel and Lee [52], and Lee and Wei [44]. Patel and Lee [52] used flow visualization to investigate flow patterns for several fiber mat architectures at different injection rates, while Lee and Wei [44]

investigated the effect of these variables on void formation in a radially expanding flow. However the importance of post-fill cure pressure has not been studied in detail, even though cure pressure is known to have a significant effect on void content [43]. In the present study, packing pressure is found to have a more significant effect on the mechanical properties compared with the injection rate for the parts molded.

Glass preforms typically used in RTM contain fibers of 10 to 20-μm in diameter, so voids with dimensions approximately 10 to 100 microns are expected to form. Assuming a true randomness in the composite structure when selecting a particular cross-section, the void area fraction in the cross-section is equivalent to the void volume fraction inside the part [45]. With this concept borrowed from stereology, Ghiorse [46] demonstrated that, dependent on the resolution of the system, image analysis is among the most accurate methods for assessing the true void content. Usually, the choice of the image resolution is a trade off between the demand for high resolution to detect voids of all sizes and the demand for coverage of a large area to minimize the number of micrographs necessary to cover the entire cross section [43].

1.5 Mechanical Characterization of Resin Transfer Molded Parts

A number of mechanical testing methods are utilized in literature to measure the performance of RTM parts fabricated using varied process parameters. Callus et al. examined molded parts containing several fiber weave architectures, each consisting of 60% glass fibers, that had been impregnated by

Derakane 411-c50 vinyl ester resin [47]. Parts were tensile tested in both the warp and weft directions. Three distinct regions were observed in the stress-strain curves-an elastic regime, a hardening phase, and a softening phase. Mechanical testing was complimented by optical microscopy, in which they observed resin between tows failing at low strains, although this did not reduce the elastic modulus. De Oliveira Simões and Marques obtained the stiffness properties of glass and hybrid carbon-glass fiber reinforced epoxy resin [48]. Stiffness properties were determined from the axial and circumferential strains recorded during internal water pressure tests of tubular specimens. Hillermeier and Seferis investigated a method of improving the toughness of RTM parts by manufacturing interlayered RTM composite structures [49]. Several tests were performed on the molded parts to detect improved toughness by dynamic mechanical analysis (DMA), double cantilever beam (DCB) method for mode I interlaminar fracture toughness, and an end notch flexture (ENF) test to measure mode II interlaminar fracture toughness. Margueres et al. compared ultrasonic testing to several stiffness and damage measurement techniques, including tension, torsion, impact, fatigue, post-impact fatigue [50]. For undamaged samples all of the methods were shown to be adequate. Their results also showed the capability of non-destructive methods in qualitatively and quantitatively describing the behavior of a damaged material. Most of the studies on mechanical characterization of RTM parts focus on the effect of the reinforcement type and properties such as the weave pattern. Studies

attempting to correlate mechanical properties with the process parameters such as injection rate and packing pressure are limited.

1.6 Pressure Reduction in Resin Transfer Molding

Lowering injection pressure could considerably reduce the cost of the resin transfer molding process, by allowing the use of less expensive molds and injection equipment. However, lower injection pressures often result in slower fills and longer cycle times. Higher void content and bigger voids are also observed when injection pressure is considerably reduced [51,52]. At significantly slower injection rates, void entrapment in the interstices of the preform tows is observed to increase exponentially with decreasing fluid front velocity. On the other hand, at high injection speeds cited earlier [8,9,52], inter-tow void entrapment within fiber bundles increases at a slower rate with increasing fluid front velocity. Thus, there are tradeoffs associated with the selection of optimum process parameters for a composite part. Although a priori selection of optimum process parameters is desirable, in practice they are most often determined empirically after several production trials.

A number of modifications have been made to the overall resin transfer molding process aimed at reducing molding pressure and cost of the process. The simplest of these modifications leverage the process parameters fundamental to RTM. For example, Han et al. worked on theoretically optimized vent and gate locations aimed at minimizing fill times and avoiding dry spots [53]. Adams and Rebenfeld [14] showed that molding pressure could be reduced

using a single layer of high permeability preform, which lowered the overall average permeability. Johnson and Pitchumani investigate local induction heating of the mold cavity during filling to reduce the viscosity of the filling fluid, allowing a degree of control over the process by allowing the heated areas to flow more easily [54].

Several processes have been developed which go beyond simple manipulation of process parameters and modify the fundamental mechanics of RTM. For example, vacuum assisted resin transfer molding (VARTM), sometimes referred to as vacuum assisted resin injection (VARI), is an enhancement to RTM that utilizes a vacuum applied during molding. In this process, a vacuum is applied, typically at the exit vents, to draw resin through the preform and help hold the mold closed during processing [54]. Presence of vacuum in the cavity not only reduces required molding pressure, but has the added advantage of reducing void formation during filling [42,43]. VARTM has a relatively low volume of parts produced each year.

Reaction injection molding (RIM), and the similar structural reaction injection molding (SRIM), represent another process in which the fundamental mechanics of RTM are varied to improve molding characteristics. RIM and SRIM differ from each other only in that structural reaction molding is performed at a larger scale. Reaction injection molding involves the high-speed mixing of two or more reactive chemicals, typically a resin and curing agent, prior to injecting them into the mold. The mixture flows into the mold at a relatively low temperature, pressure and viscosity. Curing occurs in the mold, at a relatively

low temperature and pressure. The mixture of reactive chemicals in RIM is usually less viscous than the thermosetting resins utilized in traditional RTM, thus injection pressure is reduced and cost savings are realized.

In thermal expansion resin transfer molding (TERTM), elements of compression molding are added to the RTM process. In TERTM, a rigid thermoelastic foam core is initially formed via direct molding or compression molding. This core is wrapped with a dry fabric reinforcement and placed into the RTM mold cavity. After the mold is filled with the matrix resin, the cavity is heated, causing the foam core to expand, creating a compression molding type effect. RTCM, resin transfer compression molding, bring RTM even closer to compression molding utilizing one or more mold walls which can compress the part. Several families of RTCM processes are identified and investigated in literature, depending on if the injected fluid is at constant flow or pressure, if the mold cavity compresses during or after filling, and if a vent is opened during compression to allow resin to exit the cavity [55,56].

An interesting process was developed in the late 80's by Seemann's Composites, which is a hybrid of RTM, VARTM, and the vacuum bagging used in curing of pre-impregnated composites [53]. The Seemann Composites resin infusion molding process (SCRIMP^{TM}) utilizes a one-sided mold cavity. The preform is laid on a single mold wall, and covered with a vacuum bag that is sealed at the mold edges. Vacuum assisted injection is usually achieved through the use of a high-permeability surface layer that quickly impregnates, followed by through-the-thickness flow. This process allows for low pressure

injection, high voume fraction, low void content, low scrap rates, and the ability to manufacture very large components, such as boat hulls and structural components.

1.7 Scope of the Presented Research

In the context of the literature covering resin transfer molding, the present work attempts to further characterize and improve the process. A laboratory-based molding setup is constructed to allow controlled fabrication of resin transfer molded parts. The setup allows for a number of variations in the molding process to be controlled and studied, such as injection rate, part thickness, and fiber volume fraction. Specific details covering the molding setup are presented in Chapter 2. Molded parts are utilized to perform an experimental study of RTM. Molding setup also allows for flow simulation experiments in order to collect data during filling of RTM parts. In Chapter 3, a study is presented covering the effect of flow rate and an applied post cure packing pressure on the molded parts. Applied post cure packing pressure is anticipated to be a method that can be used to improve properties of the final part by reducing voids. Mechanical properties, determined by tensile testing specimens cut from the molded parts, and void content are characterized for each flow rate and packing pressure.

Chapter 4 covers effects of preform thickness on mechanical properties and fill pressure in RTM. A short beam shear test is added to the mechanical tests for parts examined in this chapter in order to capture variations in shear

properties that might be introduced when the number of mat interfaces is varied. A method of measuring permeability using a single pressure transducer upstream of the mold cavity is presented to measure the differences in permeability that govern changes in injection pressure. Results show that similar mechanical properties can be obtained at same volume fraction by varying preform thickness, while reducing molding pressure.

Finally, an extension to the resin transfer molding process is presented in Chapter 5. Small flow channels devoid of fibrous preform are shown to significantly reduce molding pressure. These flow channels are recommended as advancement to the process, due to the reduction in molding pressure, with a caveat: part quality is a concern. Flow channels significantly alter the progression of resin through the mold, leading to weld lines and dry spots in many cases. A number of parts are molded using different channel configurations. Comparisons made in observed part quality and pressure reduction show that with care, appropriate configuration can be selected to obtain quality parts and still achieve lower pressures.

2 Experimental Setup

2.1 Molding Apparatus Used to Fabricate RTM Parts

An experimental molding setup is constructed to fabricate resin transfer molded disks. This setup is used exactly as described here for the study presented in Chapter 3. Studies presented in Chapters 4 and 5 utilize modifications to the basic molding setup which are described in those chapters. The basic setup, depicted in Figure 2.1, is composed of a molding press that injects a polymeric resin at either a specified flow rate or pressure, and a modular disk-shaped mold cavity. The molding press contains two hollow cylinders, which are for resin and curing agent respectively. Plungers attached to the top plate of the press displace the resin and curing agent in the cylinders by equal distances when the top plate is moved. The flow from the two cylinders merges, then passes through a Statomix brand motionless inline mixer (Technical Resin Packaging, Inc.) which facilitates thorough mixing of the two components. The Statomax mixer is depicted in Figure 2.2 (top). The outer body of the mixer is a 155 mm long, polypropylene tube (ID= 5 mm, OD= 8). Inside the tube, mixing is performed by 32 alternating helical segments, visible in Figure 2.2. The mixture is then injected into the center of the disk-shaped cavity. The entire press is mounted in a materials testing system (MTS) machine, which provides the force necessary to inject the mixed resin. The MTS machine is computer-controlled, and is run with either constant linear velocity, resulting in constant volume flow rate, or at constant force for a fixed inlet pressure.

The mold cavity, depicted in Figure 2.3, is constructed by placing an aluminum spacer plate having a thickness of 3.18 mm (0.125 in.) between two 6.35 mm (0.25 in.) thick aluminum mold walls. Alternatively, 25.4 mm (1.0 in.) thick plexiglass mold walls are used for flow visualization experiments. Photographs of three aluminum mold cavity components are contained in Figure 2.4. A 15.24 cm (6.0 in.) diameter circle is cut from the center of the spacer plate to form the disk-shaped cavity, visible in Figure 2.4 (center). After filling, holding a packing pressure on the mold has been demonstrated to produce higher quality parts [43,57]. This phenomenon is the focus of one part of the study presented in Chapter 3. In order to maintain pressure in the cavity, a 4 mm wide o-ring groove is machined into each mold wall to form a pressure-tight seal. An inlet gate, positioned at the center of the disk-shaped cavity, is drilled and tapped for a polypropylene hose fitting (ID=6.2mm) on the top mold wall. Four vents are also drilled in the top mold wall and tapped for hose fittings (ID=1.6 mm). Vents are positioned evenly around the cavity at a radius of 8.89 cm (3.5 in). The top mold wall is shown on the left in Figure 2.4. In the photograph, the o-ring is in place, and tapped holes for inlet and exit gates are visible. The two perpendicular grooves passing through the inlet in this image are flow channels which are described in Chapter 5. O-ring is also shown on the bottom mold wall in Figure 2.4 (right).

Two different chopped-strand glass fiber mats having different planar densities i.e., 0.228 kg/m^2 (0.75 oz/ft^2, Fiberglast part #248), and 0.459 kg/m^2 (1.5 oz/ft^2, Fiberglast part #250) are used in this study. Preforms are cut into

15.24 cm (6.0 in.) diameter circles and layered in the mold cavity to achieve desired fiber volume fraction prior to filling. One of the dense mats cut into a 15.24 cm circle is visible on the right in Figure 2.2. Mats have a randomly distributed, in-plane fiber orientation.

An epoxy resin, EPON 815C, manufactured by Shell Chemicals, is selected for the molding experiments. Attractive properties of this resin include its low viscosity, which facilitates moderate injection pressures, and its low toxicity. The desired gel time of about 20 minutes is achieved by selecting EPICURE 3282 (Shell Chemicals) as the curing agent. Flow rate for each cylinder is proportional to flow area, thus the internal diameters of the two stainless steel cylinders are machined to 55.47 mm (2.18 in.) and 25.53 mm (1.00 in.) in order to achieve the appropriate mix ratio, 4.7 to 1 by volume, of resin to curing agent. The cylinders contain enough resin and curing agent to mold six of the disks during a single stroke. Thus, six disks are molded in each session utilizing multiple mold assemblies.

The parts are molded at constant flow rates, with typical fill times ranging between 20 and 900 seconds. Constant flow rate is achieved by setting the MTS to the appropriate constant displacement rate. After filling, the mold is left attached to the press, the vents closed, and the selected packing pressure is applied for 300 seconds. The inlet hose is then clamped to maintain the pressure, and the part cures in the mold for 24 hours before demolding. The part is then cured for a minimum of 24 hours more before the specimens are machined and polished, and for at least one week before testing, to ensure

complete post curing. The entire process is performed at room temperature. A representative figure depicting the increase in molding force for a 300 second mold filling is given in Figure 2.5. A representative inlet pressure is obtained by dividing the molding force, measured by the MTS during filling, by the cross sectional area of the two plungers (29.3 cm^2). After an initial rise, the injection force increases gradually for the first 300 seconds during the mold filling at constant flow rate. Between 300 and 350 seconds, the force increases more substantially, as the mold is nearly full, and resin is forced, still at constant injection rate, between the spacer plate and mold wall into all exit vents. After the mold is completely filled, one of four packing pressures (shown in Figure 2.5) is selected. The MTS is switched to a constant force control mode, and the force corresponding to the desired pressure is applied for 300 seconds. Figure 2.5 shows all four packing pressures for comparative purposes, however only one of these pressures is selected and applied for each mold filling operation.

2.2 Tensile Testing of Molded Composites

Each molded disk is cut into five 11.43x1.27x0.318 cm (4.50x0.50x0.125 in.) rectangular tensile test specimens in accordance with ASTM D3039/D3039M standards [58]. Figure 2.6 depicts the relative spatial positions of the five specimens within the molded disk. A photograph of a disk that has been cut into the five specimens can be seen in Figure 2.2(left). Angular position of the specimen array within each disk is arbitrary due to the random planar fiber orientation. Each disk yields one specimen in the center of the disk, with the

inlet passing through the center of the specimen at position 3. Two specimens at position 2 are located symmetrically on either side of the center specimen, and two specimens at position 1 are near the edge of the disk as shown in Figure 2.6. An aluminum cutting template is used to hold the disk in place on a vertical milling machine so specimens can be cut to the best tolerances possible. Each cut specimen is slightly polished with sandpaper to remove edge defects that might result in premature mechanical failure. A micrometer is used to measure the thickness and width at five locations on each specimen. Variations in the injection pressure and difference in the o-ring compression during molding result in a thickness variation up to 0.1 cm (0.039 in.) among specimens. Average measured thickness of all specimens used for the study presented in Chapter 3 is 0.34 cm (0.134 in.), with a standard deviation of 0.013 cm (0.005 in.). Average measured thickness for specimens used for the study presented in Chapter 4 is 0.434 cm (0.171 in.), with a standard deviation of 0.046 cm (0.018 in.).

Specimens at position 1 and 2 are tested under tension using the MTS machine at room temperature. A specimen mounted in the MTS machine is displayed in Figure 2.7. Position 3 contains a large surface defect at the inlet where the cured resin column contained in the inlet has been broken off during demolding, thus these specimens typically fail early and are not used. The testing force is increased linearly from 0 to 8.90 kN (0-2000 lbs) over 120 seconds; depending on fiber content, specimens typically fail at lower forces between 2.7 and 8.0 kN (600-1800 lbs). Strain is measured directly using an

extensometer, visible in Figure 2.7, attached over a 2.54 cm (1.00 in.) span at the center of the specimen during testing. The stress is calculated by dividing the force by the average cross sectional area, and stress-strain curves are generated for each specimen. Two representative stress-strain curves for position 1 specimens molded using different packing pressures studied in Chapter 3 are depicted in Figure 2.8. Stress-strain curves have no distinct yield point, and exhibit nearly linear behavior until failure. From the tensile data, maximum stress is obtained for each specimen, and the elastic modulus is calculated over the linear region between 1000 and 3000 microstrain, as specified by ASTM D3039/D3039M [58].

2.3 Three-Point Bending Test of Molded Composites

Additional mechanical characterization of the parts is obtained by performing a three-point bending test in order to determine the short-beam shear strength. Short-beam shear strength can be a good indicator of matrix-fiber adhesion and interlaminar shear strength. Testing is performed in accordance with the ASTM D2344/D2344M standard for short-beam strength of high-modulus fiber-reinforced composite materials [59]. One specimen from position 1 in each disk is utilized for three-point bending test. Three-point bending specimens are cut into three 38.1 mm (1.5 in.) segments. The center segment, which is symmetric about a diameter of the disk, is used for testing. An adjustable three-point bend fixture, (MTS Series #642) is mounted on the MTS machine. The specimen is placed on two 3.175 mm (0.125 in.) diameter bottom

rollers, adjusted to a center-to-center span of 25.4 mm (1 in.). A third roller, 6.35 mm (0.25 in.) in diameter, exerts force on the specimen center from above, moving down at a constant linear displacement of 1.27 mm/min. (0.05 in./min.). After failure, specimens are examined visually to ensure the failure mechanism is by shear, indicated for these particular specimens by a cloudy white failure band visible through the thickness.

2.4 Microscopic Analysis to Quantify Void Content

Microscopic analysis performed on specimens cut from position 3 in each kind of molded part is used to assess the void volume fraction, as well as other important parameters such as void size, shape, and roundness. Voids with different characteristics are likely to originate from different sources during filling, and will contribute to mechanical properties and failure mechanisms differently. For example void size directly affects void mobility and thus, void distribution. Void shape affects mechanical properties, with irregular voids being more likely to induce early crack formation. Cross sections of each specimen are embedded using a commercial resin (Embed 812-DER 736), and then machined to have a flat base surface for further polishing. A series of silicon carbide pastes of different grit sizes ranging from 240 to 1200 insured a smooth finish. Finish with aluminum powder was not necessary to obtain good surfaces for the composite used in this study, however specimens are cleaned to remove paste residue. Once polished, the cross sections are analyzed and pictures of individual voids taken at 100x with an optical microscope (Nikon OPTIPHOT-2)

and attached CCD camera (Hammatsu C2400). Individually captured pictures are processed with the aid of an image analysis software (Optimas v4.1), which has features such as area morphometry that enable not only void area measurement, but also the classification of the voids according to their size and shape (i.e., circularity, j= perimeter^2/area). Assuming a linear equivalence, the volumetric void content was simply taken as the percentage ratio of the total cross sectional void area divided by the cross sectional area of the entire sample.

Voids are classified into three categories based on their circularity values: circular, ellipsoidal/irregular, and very irregular. A circularity of 12.58 is used for circular voids, while values greater than 20 were assigned to highly irregular voids. Intermediate values represent ellipsoidal to irregular geometries. The longest axis is used as the sole indicator to account for void size. Representative images obtained from the microscopic analysis are depicted in Figure 2.9. Figure 2.9a depicts the matrix containing fibers perpendicular to the cross section, seen as small circular dots in the figure. Elliptical white objects observed in the figure are fibers oriented nearly parallel to the cross section. Fibers with similar orientations are observed in close proximity to one another in the image. These are fiber tows containing groups of similarly-aligned fibers bundled together within the random mats.

A large circular void, with a diameter of approximately 100 μm, about 10 times the fiber diameter, and a smaller irregular void are visible in Figure 2.9b. These voids are representative of those found at 0 packing pressure. At slightly

higher packing pressure, 228 kPa, fewer large circular voids are found. Most voids are smaller and slightly irregular, such as the one depicted in Figure 2.9c. At higher packing pressures, voids are irregular and trapped in fiber tows (Figure 2.9d).

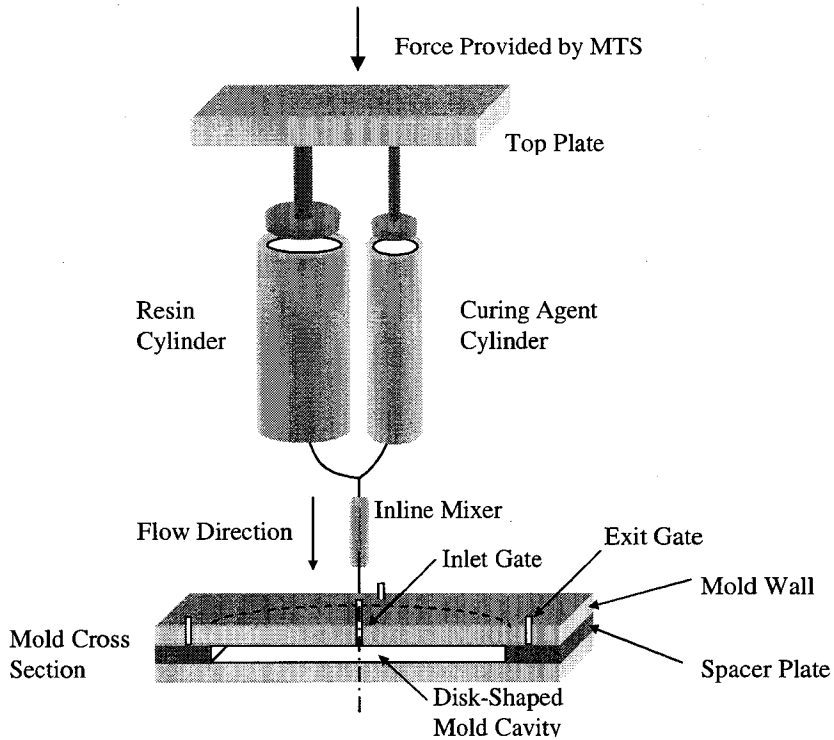

Figure 2.1 Experimental setup used to fabricate resin transfer molded disks

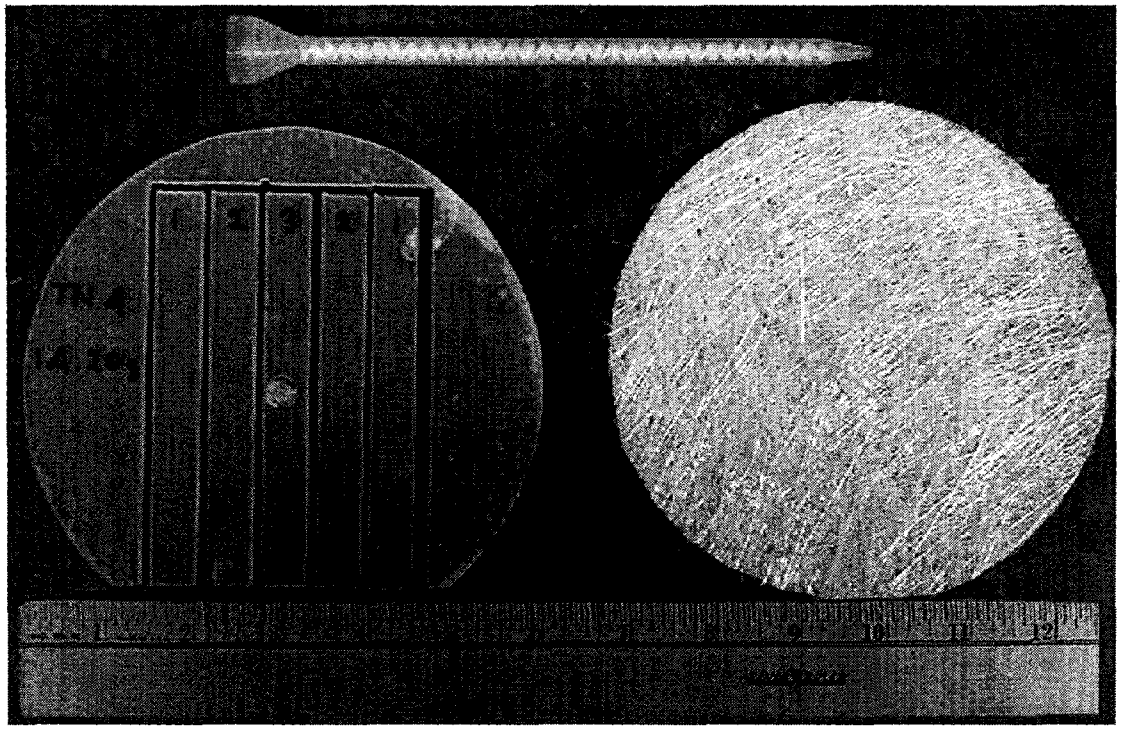

Figure 2.2 Photograph of a molded disk cut into five tensile test specimens (left), chopped strand glass fiber mat (right), and Statomix inline mixer (top)

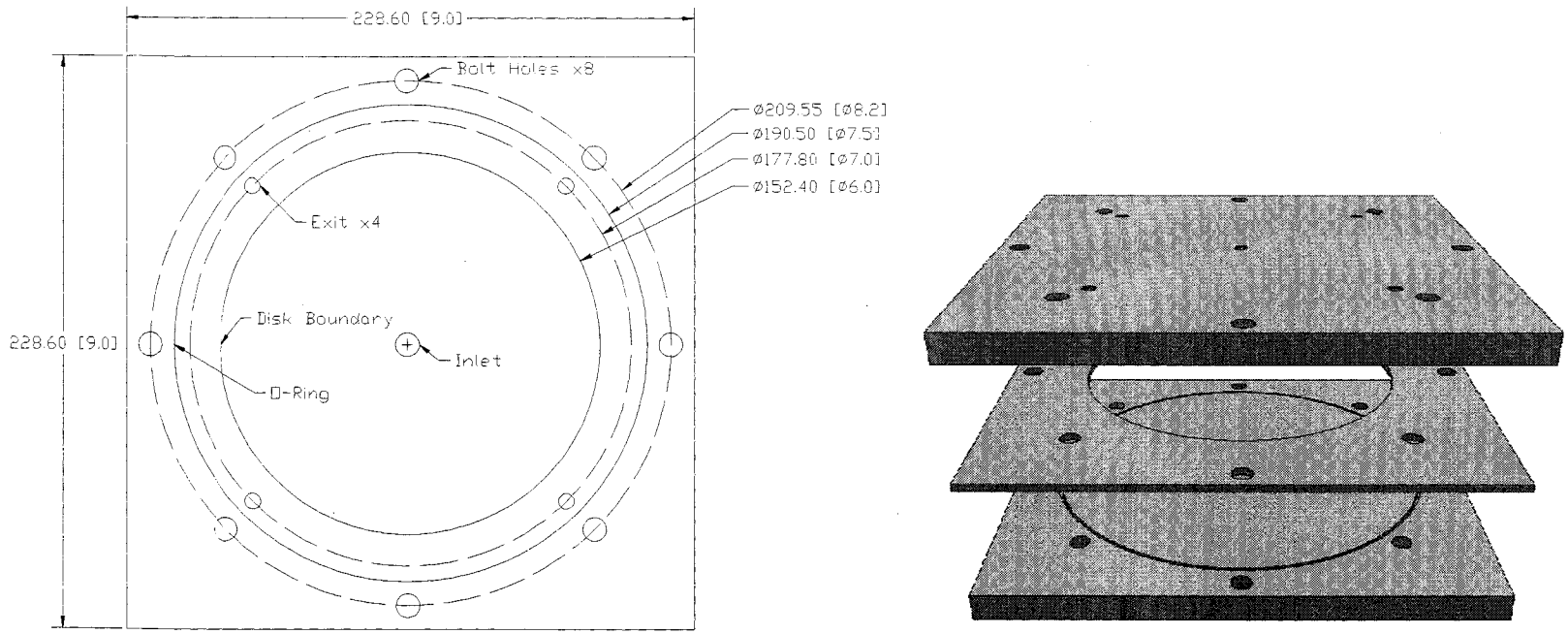

Figure 2.3 Top view of the disk-shaped mold cavity used to fabricate resin transfer molded disks (left) and exploded view of mold cavity components showing top plate, spacer plate, and bottom plate (right)

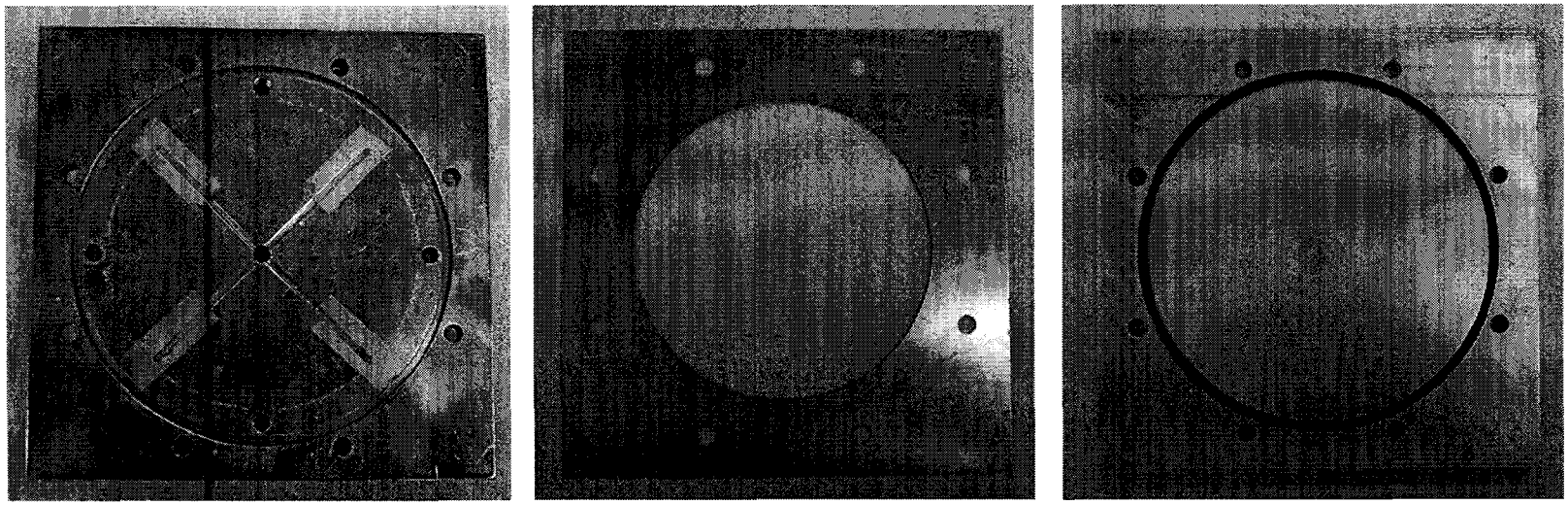

Figure 2.4 Photograph of the mold cavity components. Top mold wall with two flow channels (left), spacer plate (center), and bottom mold wall (right)

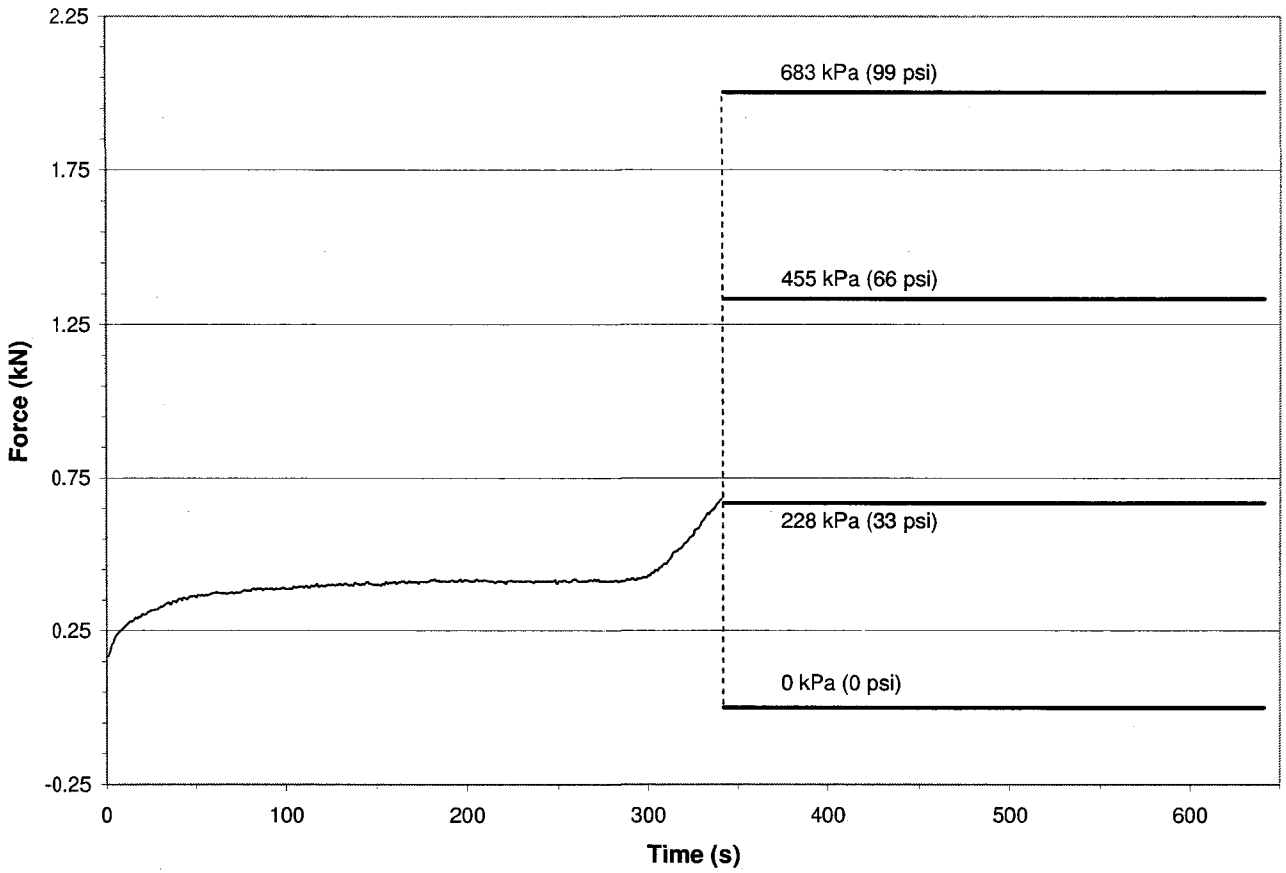

Figure 2.5 Representative injection force during mold filling showing four different packing pressures after filling is completed. Force is measured at constant flow rate during filling, followed by the application of a constant force applied for 300 seconds

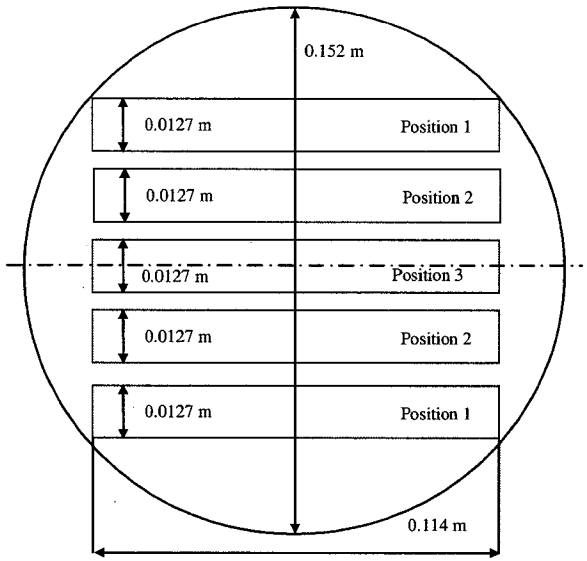

Figure 2.6 Diagram of a molded disk depicting locations of the tensile test specimens

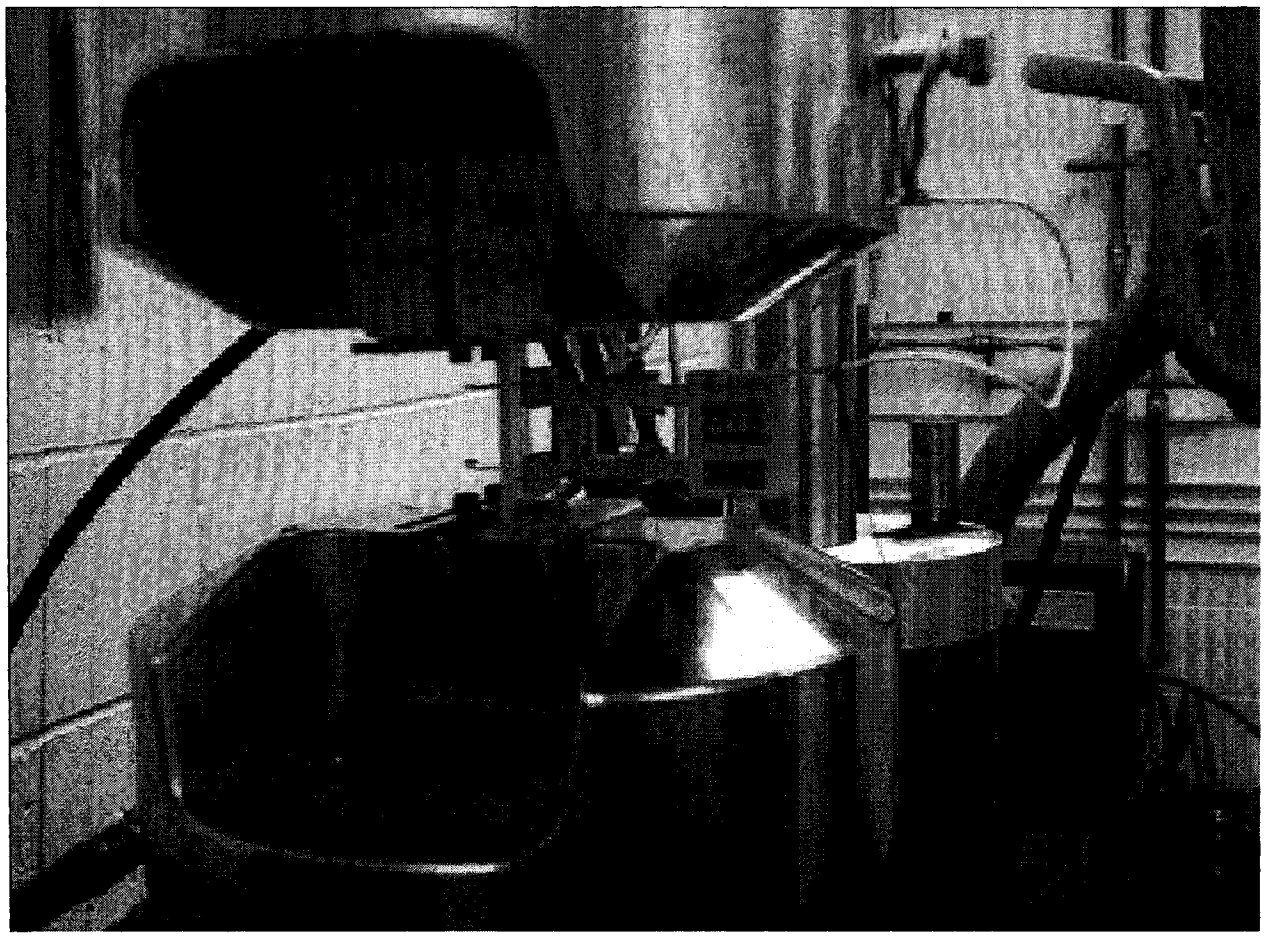

Figure 2.7 Tensile test specimen mounted in MTS machine showing extensometer location

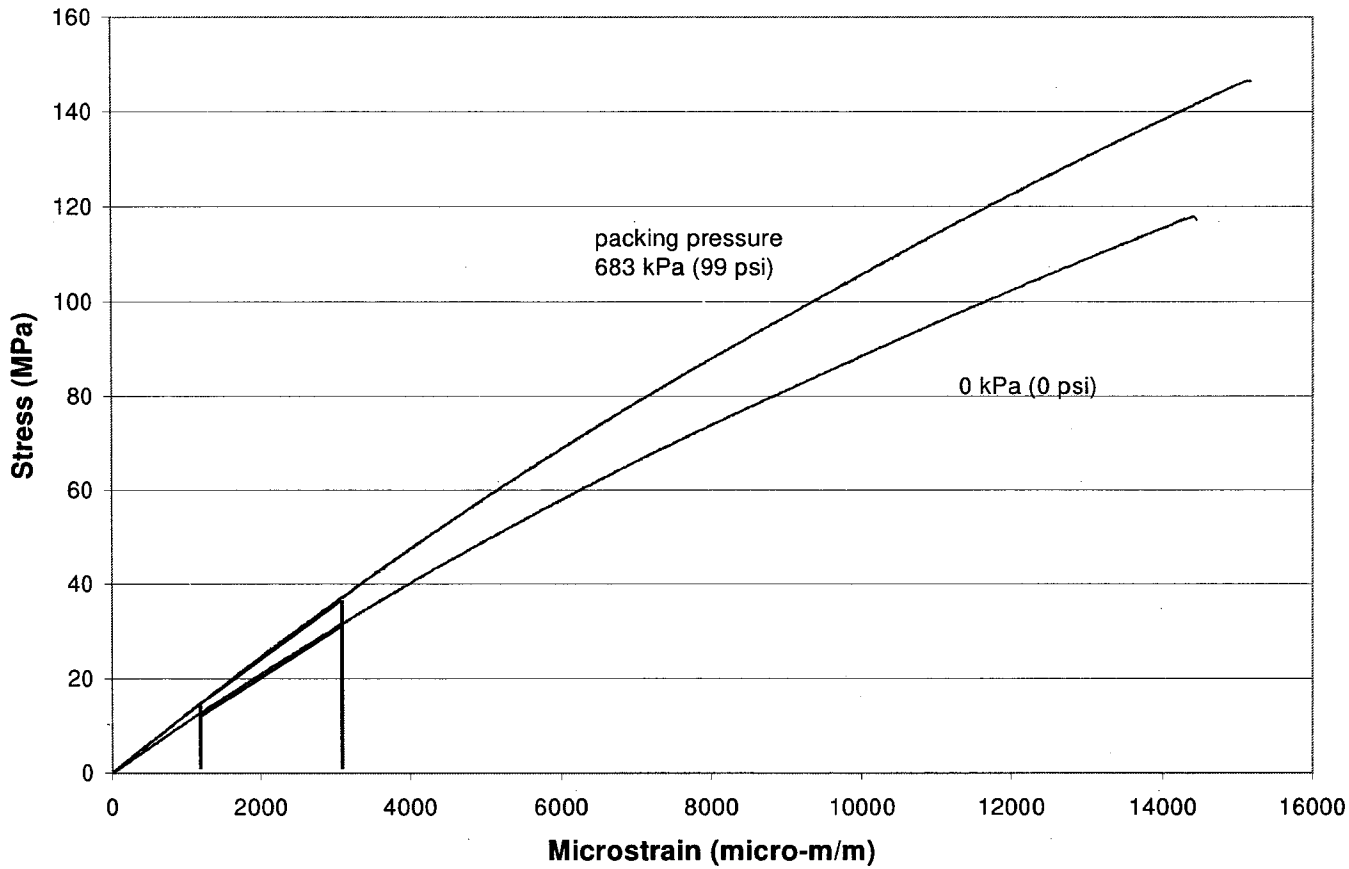

Figure 2.8 Representative stress-strain curves of two position 1 specimens molded at two different packing pressures

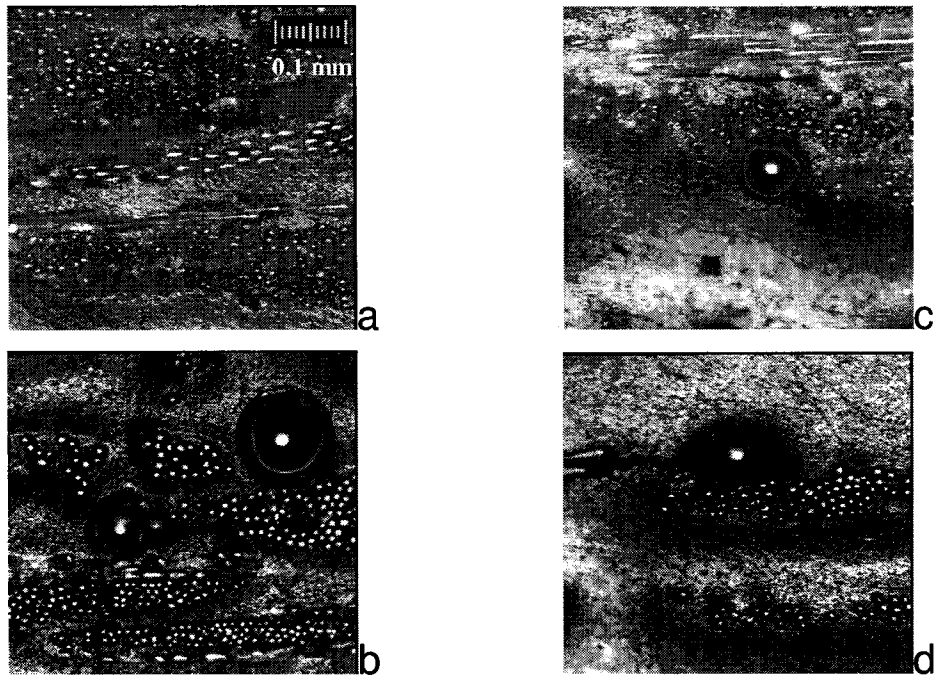

Figure 2.9 Representative microscopic images obtained from specimen cross-sections at 100x magnifications. a: Example of fibers perpendicular to and parallel to cross section; b: Large, circular void at 0 kPa packing pressure; c: Smaller, circular void at 228 kPa; d: Irregular in-tow void at 683 kPa

3 Effect of Injection Rate and Post-Fill Cure Pressure on Mechanical Properties and Void Content of Resin Transfer Molded Disks

3.1 Introduction

Two of the most readily controlled process variables in resin transfer molding are injection pressure (or comparably, injection flow rate), and post fill cure pressure. Injection rate has been shown to affect void content with increases in void content at very low injection pressures [51,52] and at very high injection rates [8,9,52]. It is known that curing pressure affects void content [43], and preliminary results show that an applied post-fill cure pressure reduces void content. A corresponding increase in mechanical properties is expected. Figure 3.1 shows two parts which have just been filled. For the part on the left in this figure, a packing pressure of 683 kPa (99 psi) is being applied; the part on the right has a packing pressure of 0 kPa. The part with the higher packing pressure is noticeably clearer due to lower void content. Voids refract light passing through the part causing this cloudy appearance, thus part transparency represents a good qualitative assessment of void content.

In the current study, center-gated disk-shaped parts are fabricated at four different injection rates and four different packing pressures in order to determine the effects of these process parameters on the void content and mechanical properties in RTM. Mechanical testing data and characterization of voids with an optical microscope are used to determine the interrelation between void content

and mechanical properties. This dependence could be utilized to develop predictive models for molding processes or used in controlling the molding to fabricate parts with better properties.

3.2 Effect of Injection Rate on Properties of Resin Transfer Molded Disks

Initially, the disks are molded at different flow rates in order to ascertain the effect of this parameter on mechanical properties. Four different constant injection rates of 0.067, 0.2, 0.6, and 1.0 cm^3/s, representing more than an order of magnitude change in this parameter, are used. These injection rates result in fill times of 300, 100, 33 and 20 seconds respectively. The 20 and 33 second fill times are consistent with fill times observed in industrial molding of small to medium sized RTM parts. The slower fill times are expected to yield better overall part quality as fewer voids will be entrapped by a slower moving fluid front.

Chopped-strand glass mats (1.5 oz/ft^2, Fiberglast part #250) cut into 15.24 cm (6.0 in.) diameter circles are layered in the mold cavity prior to filling to reinforce the resin transfer molded parts. The mats have a randomly distributed, in-plane fiber orientation. For this study, 4 mat layers are stacked in the cavity, representing a 21% fiber volume fraction.

All disks in this series are molded with a packing pressure of 228 kPa (33 psi). All pressures given in this study are gage pressures. Molding parameters for this series are tabulated in Table 3.1. At least five disks are molded at each

flow rate, and the measured ultimate tensile strength and elastic modulus at each velocity are averaged from all specimens to reduce statistical error. Positions 1 and 2 have two symmetric specimens from each disk, resulting in a total of 10 specimens to average for each data point. However, data from specimens which broke at a location within one thickness of the MTS grips is discarded, resulting in fewer specimens for some data points.

The tensile strength variation with volume flow rate for positions 1 and 2 is depicted in Figure 3.2. Error bars are calculated using a 95% confidence interval, and a maximum uncertainty of about 9% is observed. Tensile strength results from positions 1 and 2 are similar, and exhibit a decrease in strength with increased flow rate. The decrease in strength is about 14% from 123 MPa (17.8 ksi) to 108 MPa (15.7 ksi) for position 1, over the range of flow rates studied. A straight line is fit to the data on a semi-log plot, with all experimental points fitting the curve within the associated uncertainties. Data for this curve suggests strength may be approaching an asymptotic minimum, however linear curve fit is still used as it is found to represent mechanical properties over a wide range of flow rates. The decrease in strength at higher flow rates is most likely due to increased void formation resulting from more air being trapped by the faster moving fluid front.

Due to very similar results observed between positions 1 and 2, data from these two positions are combined to reduce uncertainty and generate the single curve depicted in Figure 3.3. It has been shown that the local fluid velocity at the fluid front as it passes a particular location is one of the primary factors

influencing lag-lead or fingering [60], and thus void formation and properties in the cured part. The change in local velocity between positions 1 and 2 is small compared with change in velocity between disks molded at different injection rates, thus results from these two positions are expected to be similiar. Combining data from the two positions results in a reduction in the maximum observed uncertainty for a 95% confidence to approximately 5%.

Stiffness data from these specimens is shown in Figure 3.4. Similar to the strength behavior, the data is plotted on a semi-log graph based on injection rate. Again, error bars are drawn with a 95% confidence interval, and data from positions 1 and 2 are averaged due to their similar behavior, thus reducing uncertainty. The average statistical error is about 8%, which is slightly greater compared with the strength results. The stiffness is also found to decrease with increased velocity, with a slightly smaller reduction with increased flow rate compared with the decrease in strength data. Stiffness drops about 12% from 9.7 GPa (1.4 ksi) to 8.7 GPa (1.3 ksi) over the range of injection rates used.

3.3 Effect of Post-Fill Cure Pressure on Mechanical Properties and Void Content of Resin Transfer Molded Disks

Twelve additional disks are molded at an injection rate of 0.067 cm^3/s with varied packing pressures of 0, 455, and 683 kPa (0, 66, and 99 psi) to determine the effect of packing pressure on properties of the final part. The data presented in the previous section, obtained from disks molded at a flow rate of 0.067 cm^3/s and a packing pressure of 228 kPa (33 psi), provides an additional packing

pressure for comparison. Table 3.2 contains the molding parameters for these 4 sets of disks. Position 1 and 2 specimens from these disks are tested under tension to determine the mechanical properties, while position 3 specimens are analyzed optically for void characterization.

Packing pressure is found to have a greater effect on the mechanical properties compared with injection rate. The ultimate tensile strength based on packing pressure for the average of positions 1 and 2 is depicted in Figure 3.5. Error bars in Figure 3.5 are calculated with a 95% confidence interval. Tensile strength increase by a total of 15% from 125 MPa (18.1 ksi) at 0 kPa packing pressure, to 144 MPa (20.9 ksi) at 683 kPa packing pressure. The increase in strength between 0 and 228 kPa pressure is observed to be much smaller than the increase in strength observed over the other pressure ranges. This indicates that a minimum packing pressure may be required to observe improvements in mechanical properties. There is a significant improvement in strength is between 455 and 683 kPa, the highest pressure used; thus higher strengths may be obtained at higher packing pressures. It is believed that packing pressure improves strength mainly by reducing the size and quantity of voids. Increased pressure may also improve wetting of fibers by forcing resin into fiber bundles that are not fully wetted during filling. An upper limit on useful packing pressures is anticipated, due to limits on void reduction and complete wetting.

Figure 3.6 depicts elastic modulus based on packing pressure for the average of position 1 and 2 data. Similar to the results for disks molded at different injection rates, the average observed error for stiffness is lower

compared with strength results. An average statistical error of about 4% is obtained, with little variation in error at different packing pressures. Stiffness increases less than strength at increased pressure, with an increase of 13% to 12.2 GPa (174 ksi) at the maximum packing pressure. There is a small increase in stiffness from 0 and 228 kPa pressure, further indicating that a minimum packing pressure is required for the benefits to be observed. There is also a small increase of 2.5% in stiffness over the final interval from 455 to 683 kPa, indicating a possible upper limit on improved stiffness is being approached at this level of packing.

3.4 Correlation Between Void Content and Mechanical Properties

Microscopic analysis is performed on specimen cross sections from each of the four packing pressures. Void content is found to decrease with increased pressure, with fairly low void fractions of 0.72%, 0.52%, 0.32%, and 0.34% measured for packing pressures of 0, 228, 455, and 683 kPa, respectively. Figure 3.7 depicts an exponentially decaying function of void fraction based on the four post-fill cure pressures used in the current study. The three-parameter exponential curve is fit to the data by minimizing the sum of the squared differences between the measured and analytical values using the solver feature in Microsoft Excel. It is clear from this graph that the application of higher resin pressures after the molds have been filled significantly reduces the porosity inside the composite parts. This particular reduction in porosity can be correlated to an increase in the post-fill cure pressure by considering the

establishment of a high local pressure that shrinks individual bubbles and possibly cause smaller voids to dissolve into the resin. Although the radial distribution of voids inside the parts was not measured in this study, a careful examination of the size and shape distribution of the voids encountered in each one of the specimens would give some indications of the actual mobility of the voids. As can be seen in Figure 3.8, the combined relative percentage of both circular and ellipsoidal bubbles decreases as the post-fill pressure increases. Both circular and ellipsoidal voids are usually located in the inter-tow spaces. Thus a smaller relative presence of these type of voids at high post-fill pressures is indicative of more voids in the interstitial areas. It is observed that the contribution of very irregular voids is increased at higher packing pressures, although the total void fraction and number of voids has decreased. It seems that the irregular voids, which are typically found inside fiber bundles, are less susceptible to removal by increased pressure compared with the more circular voids found in the interstitial areas.

A second characterization of void content with increased post-fill cure pressure is presented in Figure 3.9. Void shape distribution is given for each of the packing pressures. Circular and ellipsoidal voids have sizes that are mostly in the range 50-150 μm. Based on the total number of voids in this particular range, it is clear that as long as the local pressure is increased, the contribution of the small-to-medium circular voids decreases thus increasing the relative percentage of large irregular voids. During image analysis the large irregular voids are observed primarily in the intra-tow spacing. Varna et al. [35] recently

suggested that laminates with highest average content of voids also had the highest content of spherical voids, which concentrated in regions away from the inlet gate. Our results, presented in Figure 3.8 and Figure 3.9, agree with those presented by Varna et al. These data suggest that increasing the post-fill cure pressure is a potentially viable method for removing or compressing entrapped air, thus decreasing void content of a molded part.

As a consequence of decreased void content at higher packing pressures, it is expected that the mechanical properties would be improved. The strength and stiffness are directly correlated with the measured total void content to investigate this effect. In Figure 3.10, the strength is observed to decrease exponentially by nearly 15% from 143 to 125 MPa with increased void content. The four parameters from the exponential curve fits in both Figure 3.10 and Figure 3.11 are found by minimizing the sum of the squared differences between the measured and analytical values using the solver feature in Microsoft Excel. The maximum strength observed at the minimum void content, 0.35%, represents the highest packing pressure. The stiffness based on void content, depicted in Figure 3.11, demonstrates a similar behavior. An exponential decrease in modulus from about 12.2 to 10.7 GPa is observed as the void content doubles from about 0.35% to 0.73%. These results clearly show that the decreased void content obtained at higher post-fill cure pressures directly translates into improved mechanical properties of the final part.

3.5 Concluding remarks

Increased injection rate is found to have a detrimental effect on the mechanical properties of resin transfer molded composite disks. Both the stiffness and tensile strength are measured to decrease by 12% and 14%, respectively, with 15-fold increase in injection rate. At higher injection rates, the fluid front moves faster and traps more air leading to increased void formation. Increased packing pressure is presented as a method for decreasing void content in RTM process. Increased packing pressure is observed to improve mechanical properties, with 15% increase in strength and 13% increase in elastic modulus over the pressure ranges studied. This is due to lower void content which decreased from 0.72% to 0.35% by increasing pressure from 0 kPa to 683 kPa. It is observed that there are fewer, more irregularly shaped voids at higher packing pressures. Average void size is also observed to increase at higher packing pressures. Close examination of the data and micrographs reveals that this is due to a reduction in total number of small voids, while the quantity of larger irregular voids remains unchanged. Strength and stiffness are correlated directly with void fraction. An exponential decrease in both strength and stiffness is observed as the void fraction increased from 0.35 to 0.72%.

Table 3.1 Molding parameters used to determine effect of volume flow rate on mechanical properties

Flow Rate (cm^3/s)	Fill Time (s)	Packing Pressure (kPa)
0.067	300	228
0.2	100	228
0.6	33	228
1.0	20	228



Figure 3.1 Photograph of a transparent part that undergoing 683 kPa packing pressure (left), and a cloudy part with no applied packing pressure (right)

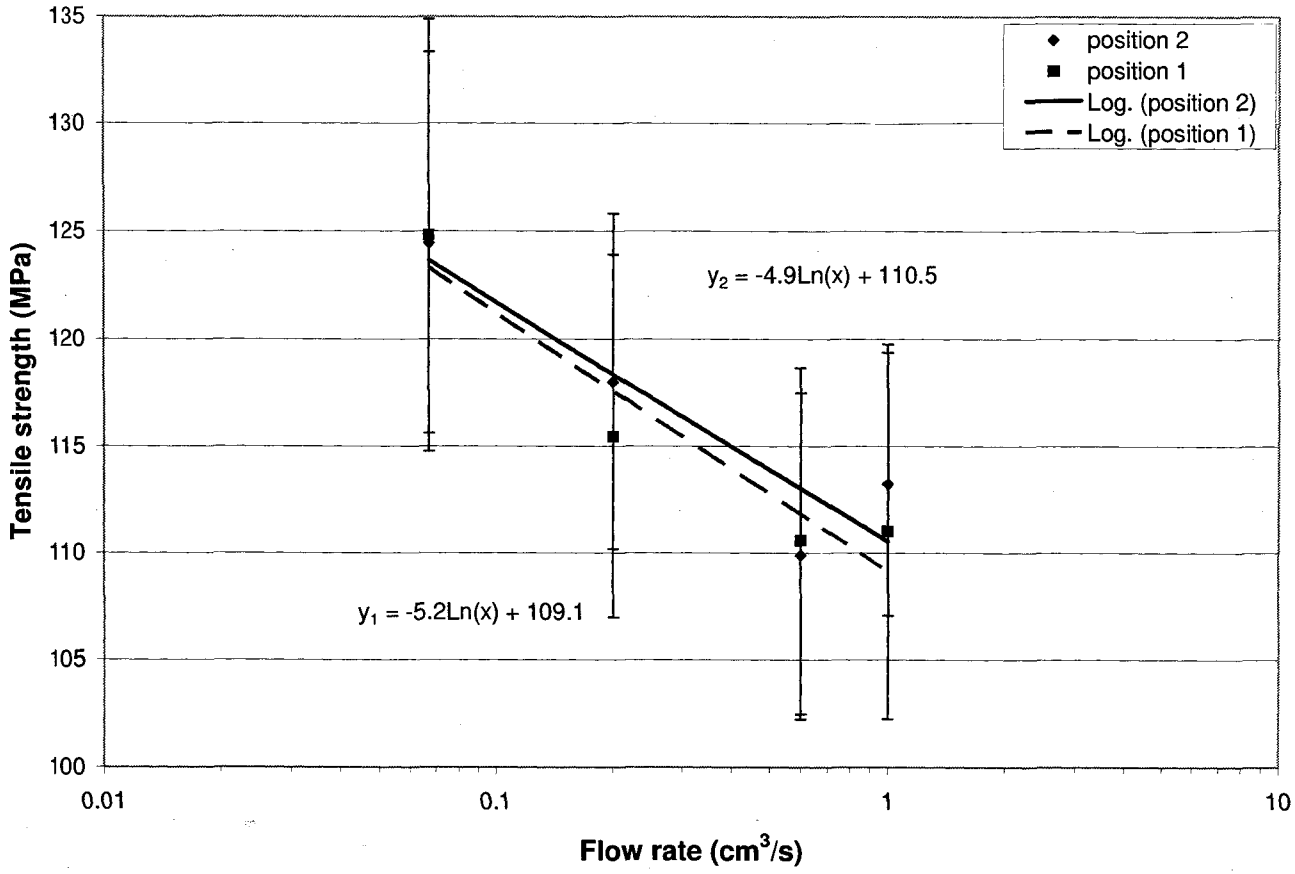

Figure 3.2 Ultimate tensile strength variation with injection flow rate for positions 1 and 2. Packing pressure=228 kPa

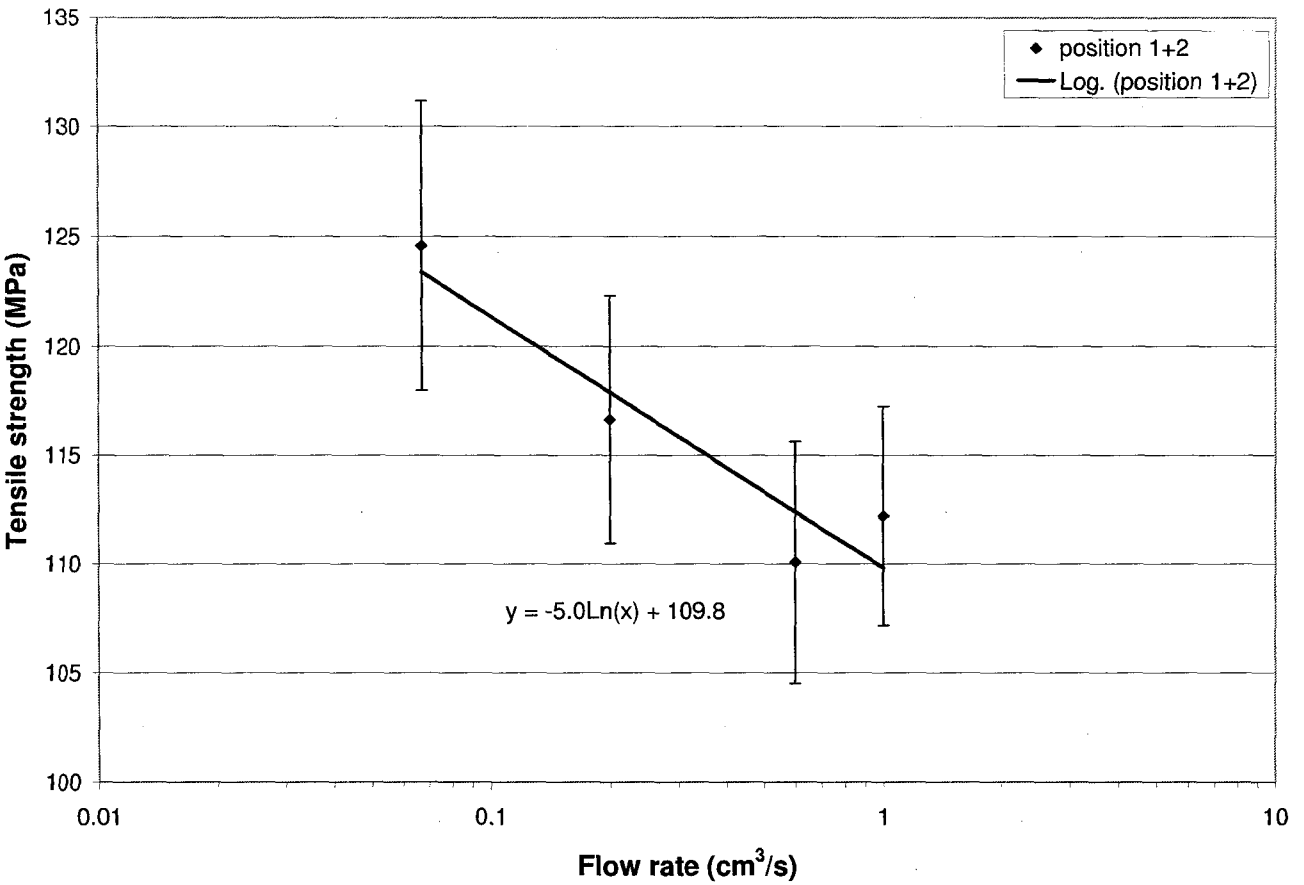

Figure 3.3 Ultimate tensile strength variation with injection flow rate averaged over positions 1 and 2. Packing pressure=228 kPa

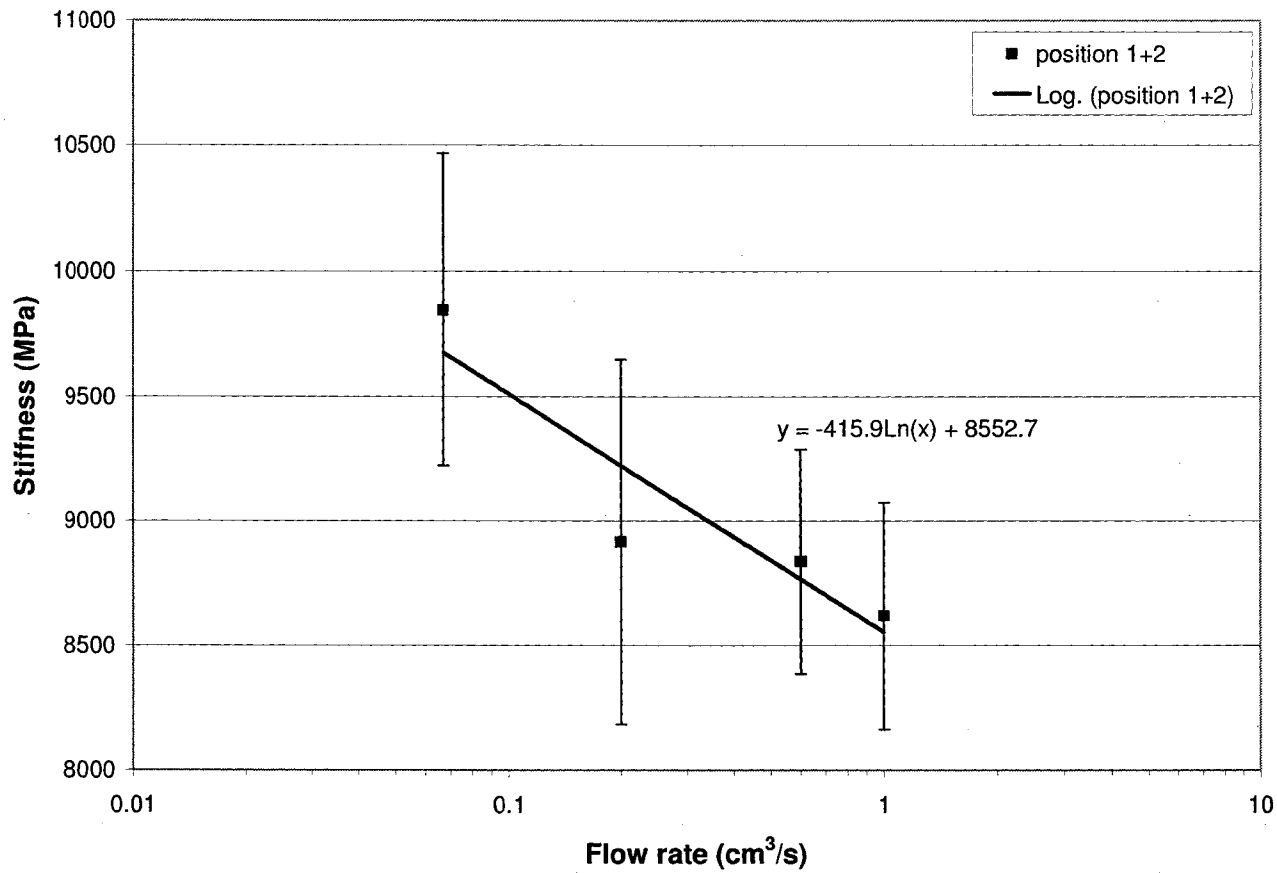

Figure 3.4 Stiffness variation with injection rate averaged over positions 1 and 2. Packing pressure=228 kPa

Table 3.2 Molding parameters used to determine effect of packing pressure on mechanical properties and void content

Flow Rate (cm^3/s)	Fill Time (s)	Packing Pressure (kPa)
0.067	300	0
0.067	300	228
0.067	300	455
0.067	300	683

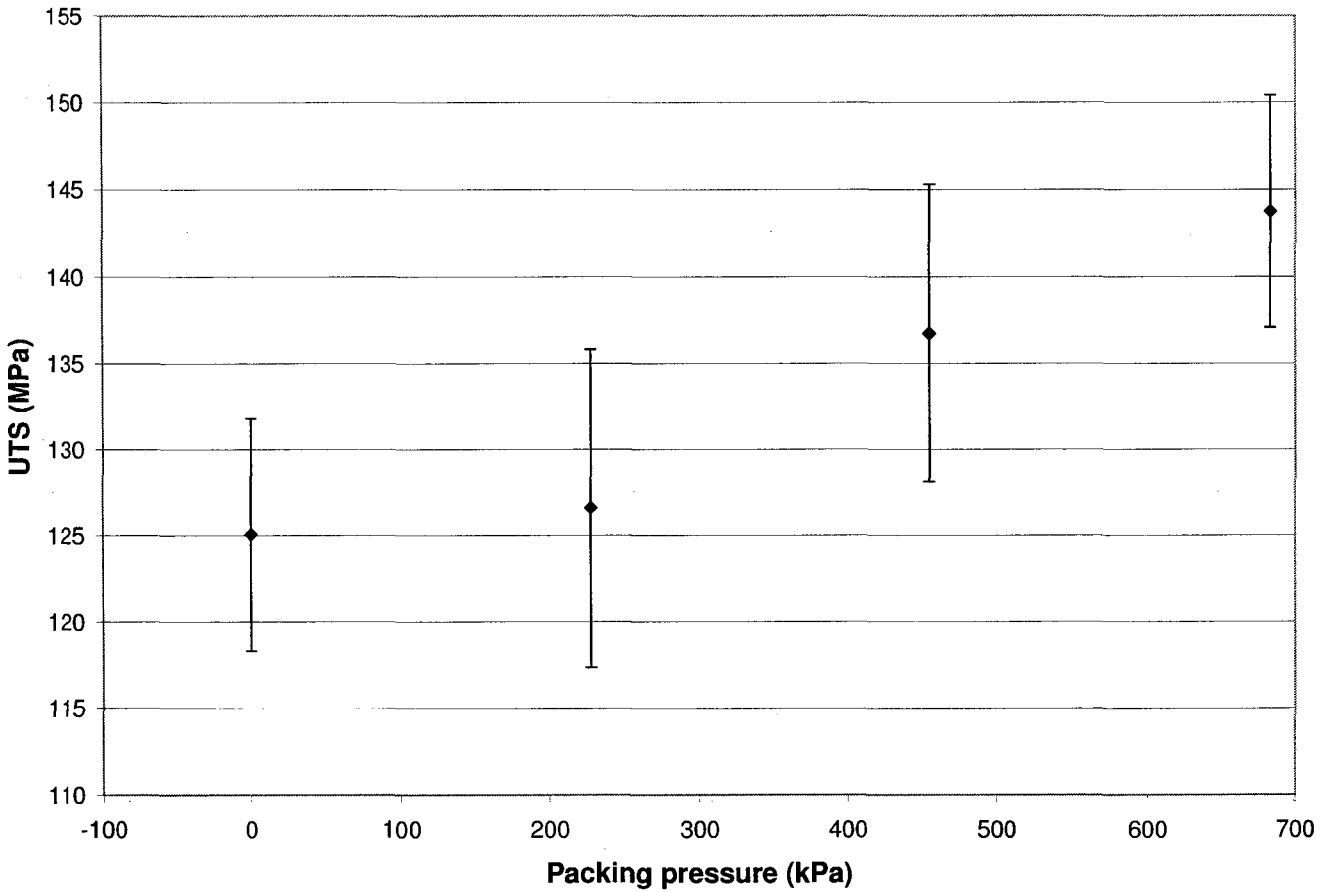

Figure 3.5 Ultimate tensile strength variation with packing pressure averaged over positions 1 and 2. Injection rate=0.067 cm^3/s

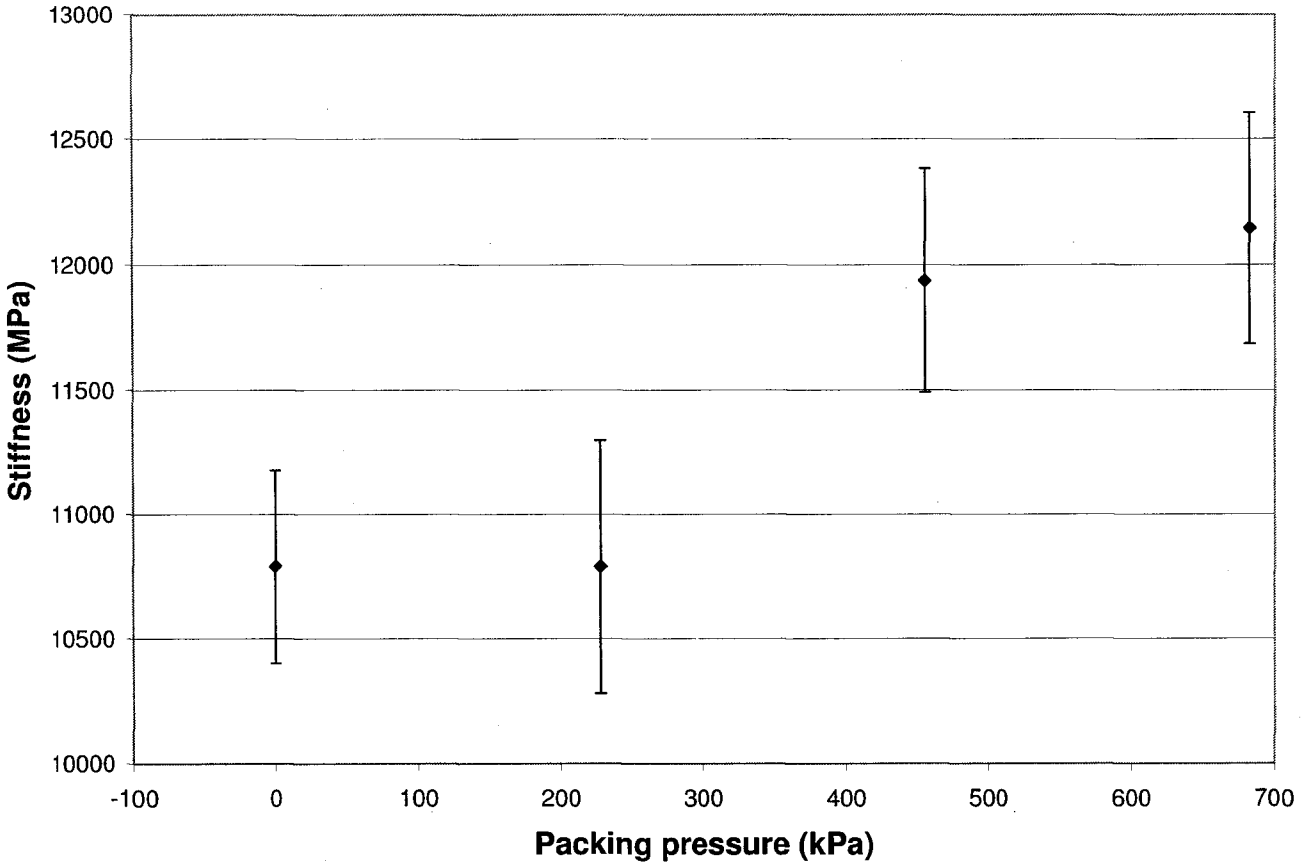

Figure 3.6 Stiffness variation with packing pressure averaged over positions 1 and 2. Injection rate=0.067 cm^3/s

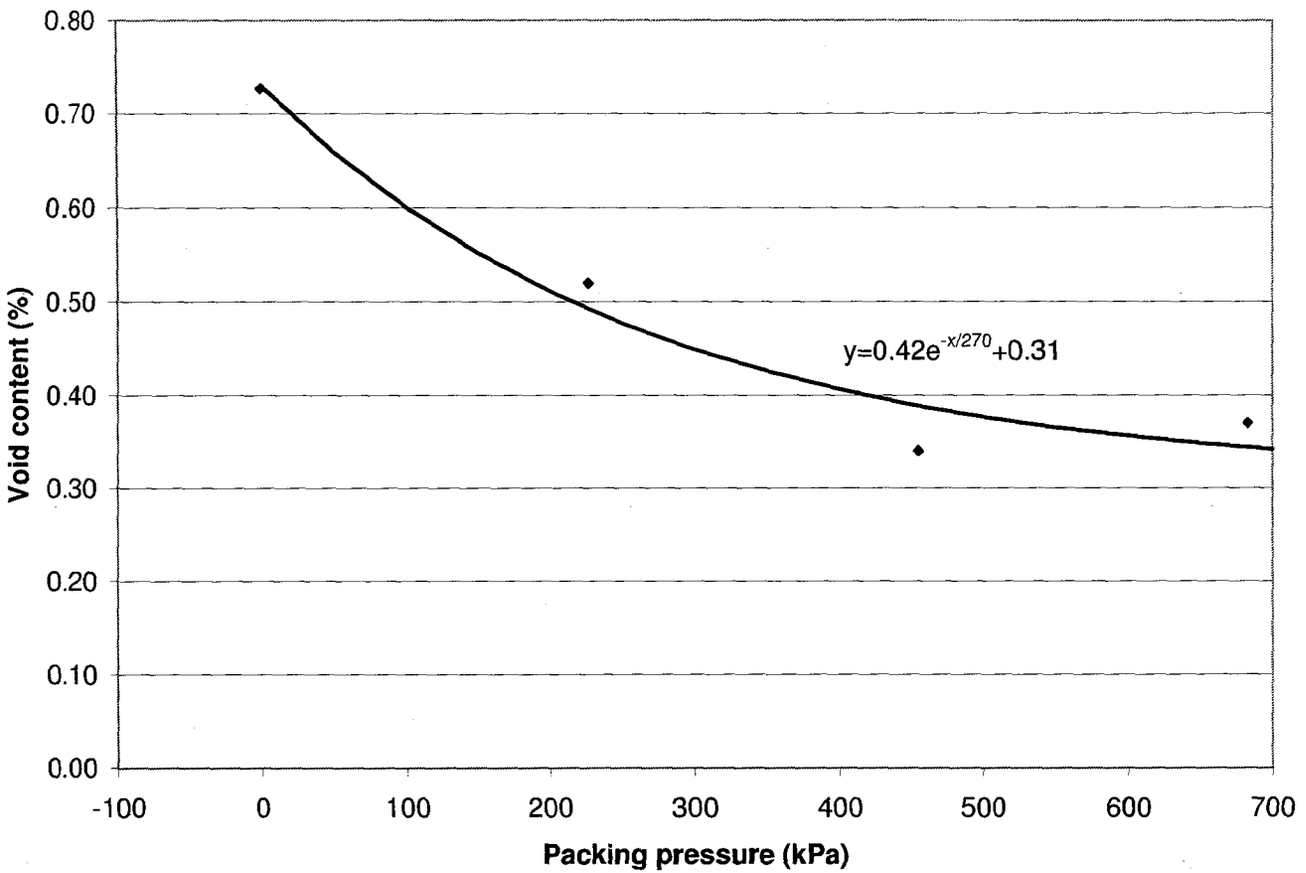

Figure 3.7 Void area fraction variation based on packing pressure. Injection rate=0.067cm^3/s

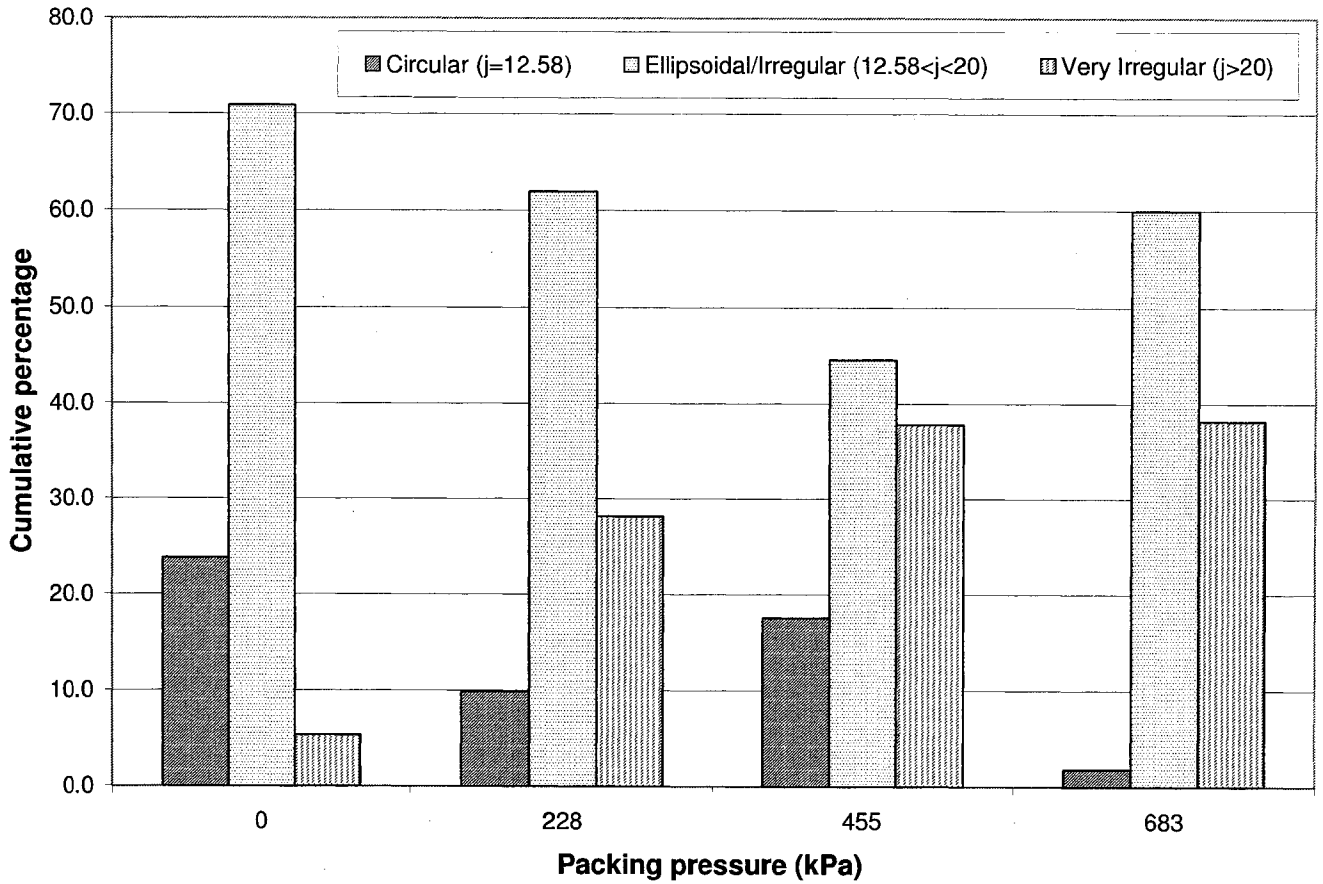

Figure 3.8 Void shape distribution based on packing pressure. Injection rate=0.067 cm^3/s

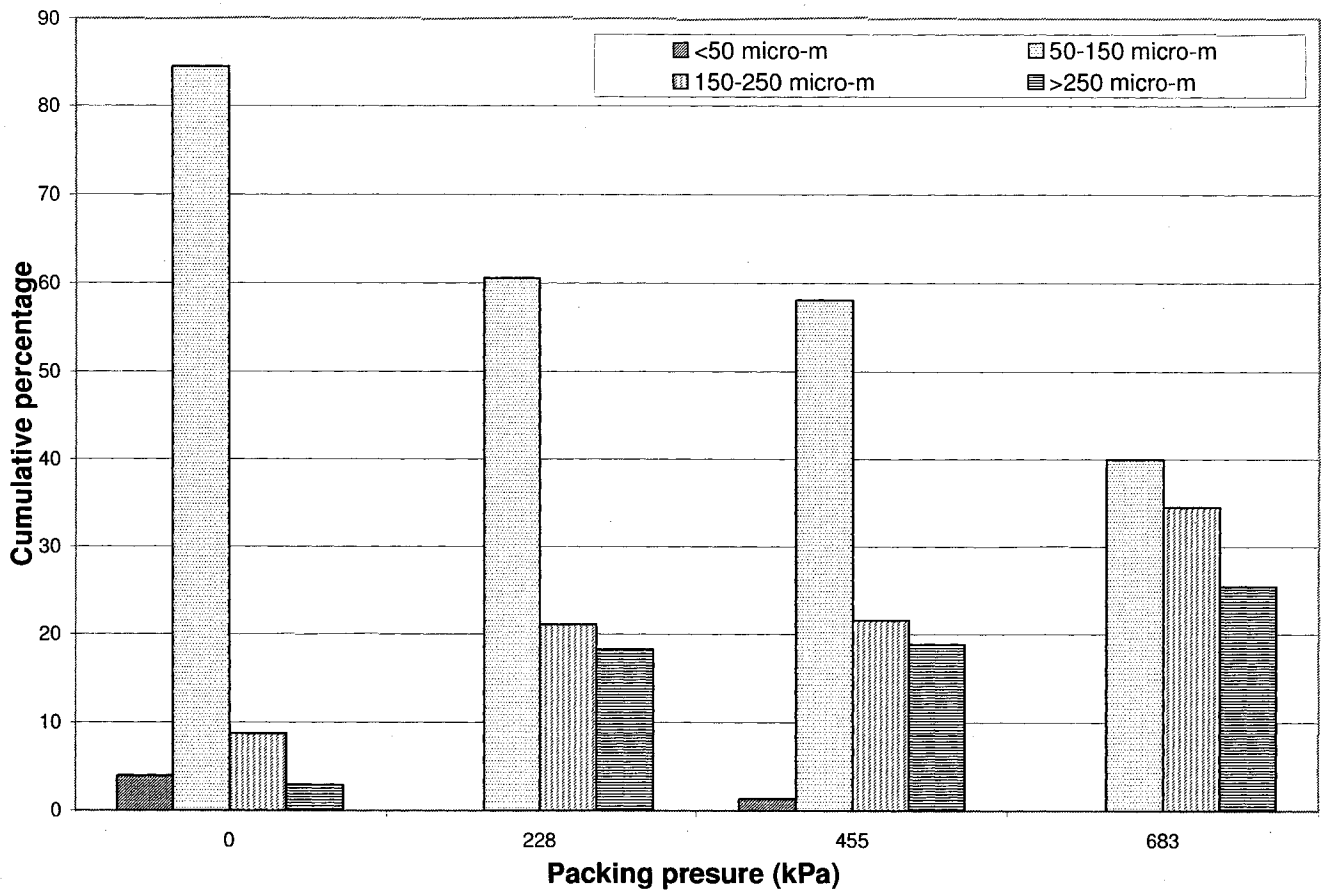

Figure 3.9 Void size distribution based on packing pressure. Injection rate=0.067 cm^3/s

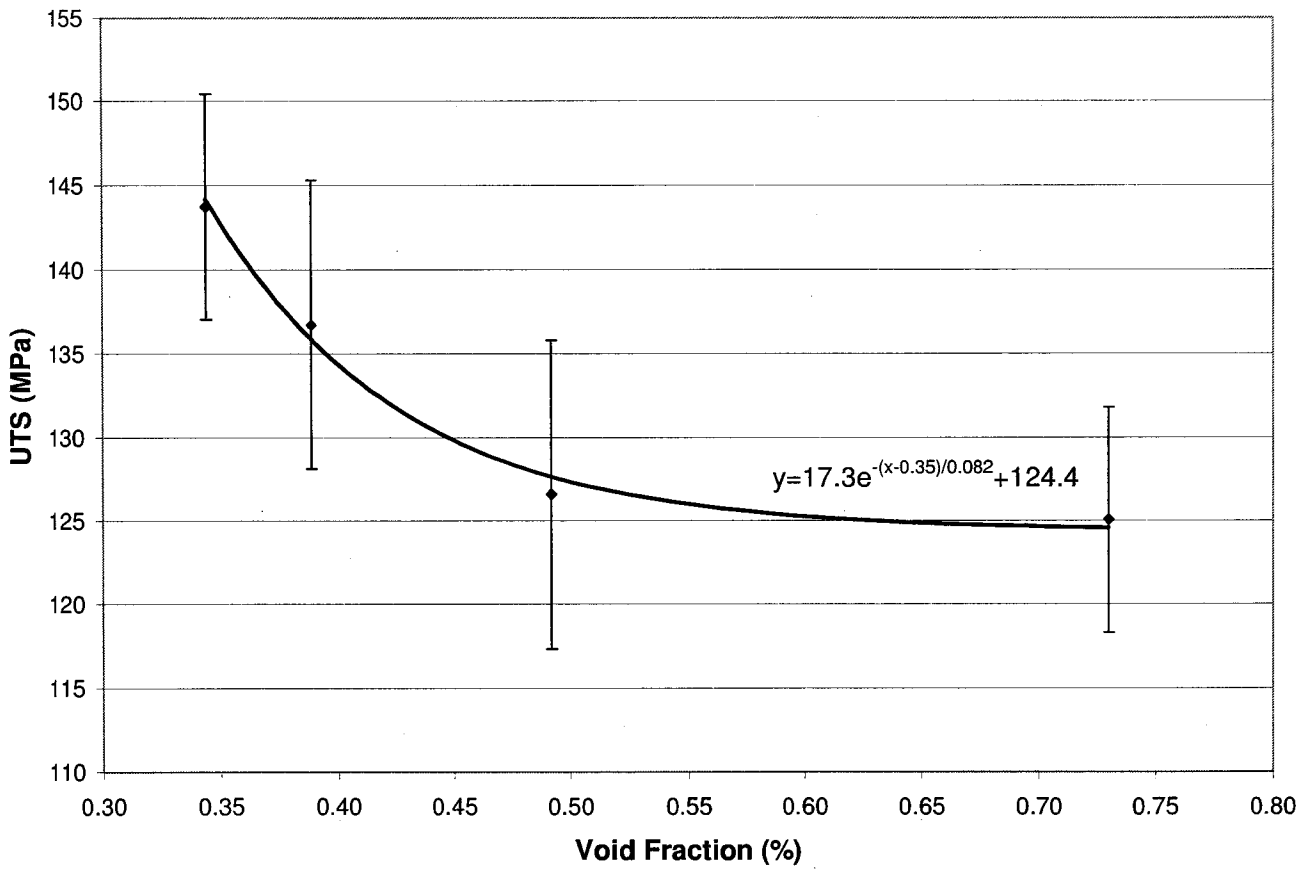

Figure 3.10 Strength variation with void fraction averaged over positions 1 and 2. Injection rate=0.067 cm^3/s

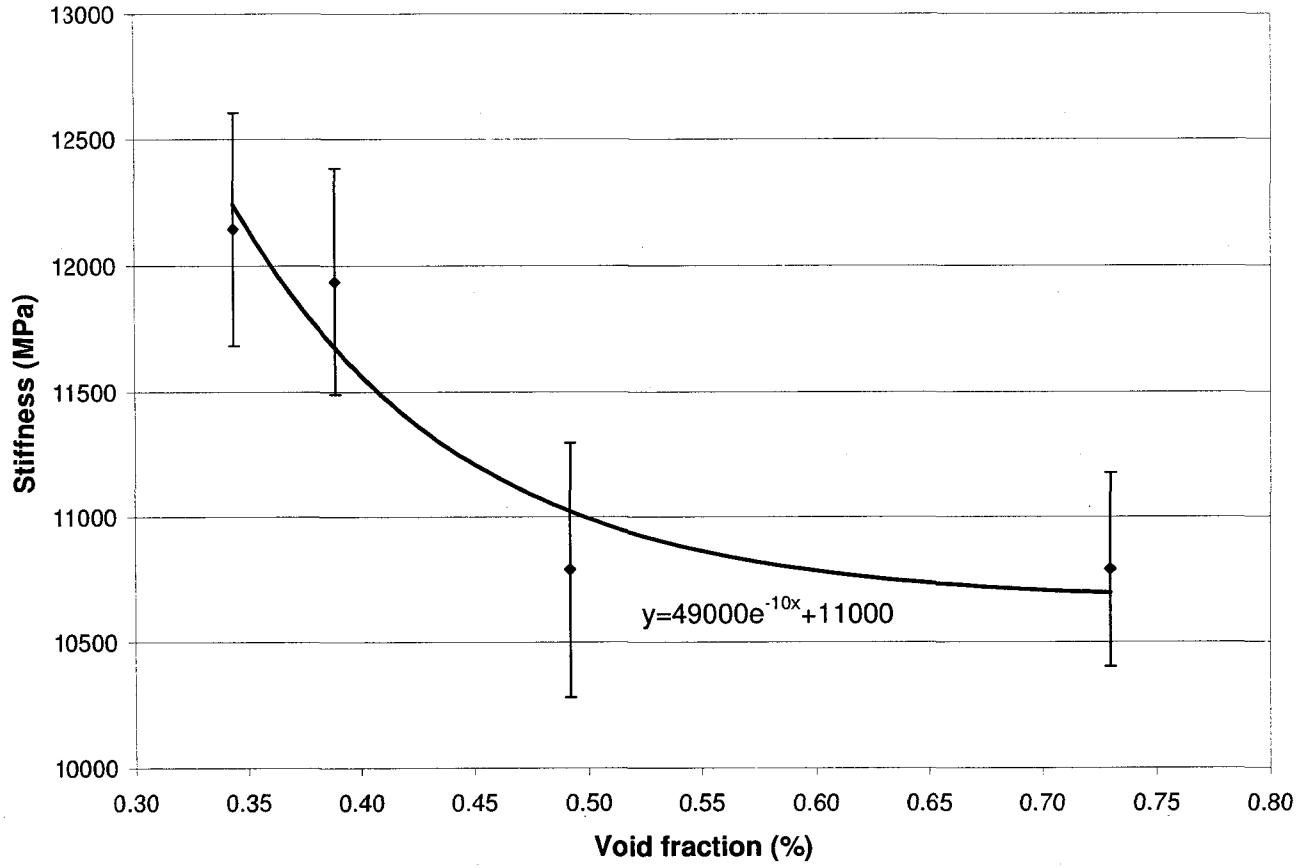

Figure 3.11 Stiffness variation with void fraction averaged over positions 1 and 2. Injection rate=0.067 cm^3/s

4 Effect of Preform Thickness and Volume Fraction on Injection Pressure and Mechanical Properties of Resin Transfer Molded Composites

4.1 Introduction

In the RTM industry, random glass fiber preforms are commonly used because of their availability, lower cost, and planar isotropy. In this study, preform architecture was varied using two different glass fiber mats. Both mat types have identical random microstructure, but have different planar densities and thus different thicknesses. Six series of disks were molded using the same process parameters and fiber volume fraction (i.e., 9.8, 21.2, and 33.1%) for both preform types. Table 4.1 contains fiber quantities, preform type, and configuration ID, for each designation. For each of the six cases, test samples were cut from disk-shaped parts, then tensile strength, short-beam shear strength, and elastic modulus were measured. Transient pressure data was recorded at a radial location 12.7 mm from the disk center during molding. A new technique is presented in this work, in which radial planar permeability is measured by fitting an analytical pressure expression derived from Darcy's law to the measured transient pressure data. Permeabilities of different configuration are compared in order to quantify effect of preform density on injection pressure.

When thin mats are used, microstructure is similar, although additional layer interfaces are introduced. Effects of these additional interfaces on fill characteristics and mechanical properties are unknown. One may expect the

short-beam shear strength and tensile properties to be similar at same fiber volume fraction. However, flow characteristics, in particular injection pressure, which is observed to be lower for thin mats, seem to be influenced by number of layers. Changes in flow could result in differences in void formation and thus, variations in mechanical properties. However, it may be advantageous to use thin mats due to lower pressure requirements, if similar mechanical properties can be obtained at the same fiber content.

4.2 Molding Apparatus Used to Fabricate RTM Parts

An experimental molding setup is constructed to fabricate resin transfer molded disks. The experimental molding setup described in Chapter 2 is updated to mold disks at conditions more like those expected in industrial RTM. The modified setup, presented in Figure 4.1, is composed of a molding press assembly that injects a two-part thermosetting resin at constant flow rate, and a modular disk-shaped mold cavity. The setup is still well represented by Figure 2.1, with small changes such as the addition of a pressure transducer on the bottom wall of the mold cavity. There is also an added pressure transducer in the line just before the fluid enters the mold cavity which can be used for obtaining injection pressure. Injection pressure is measured as near to the mold inlet as possible, and only represents pressure requirements for the mold cavity. Additional molding pressure is required due to losses in the fluid lines and mixer, which are not addressed in the present study.

A photograph of the modified experimental setup with each component labeled is depicted in Figure 4.2. The inlet pressure transducer is not shown in this photo. The molding press contains two hollow cylinders, which hold resin and curing agent respectively. Plungers attached to the top plate of the press displace the resin and curing agent in the cylinders by equal distances when the top plate is pushed down. Flow from the two cylinders merges, and again passes through a Statomax inline mixer before being injected into the center of the disk-shaped cavity. The modified setup is mounted on a hydraulic press (ARCAN, 80,000 lb. capacity) shown in Figure 4.2, which provides the force necessary to inject the mixed resin. The press moves at a constant linear velocity of $2x10^{-3}$ m/s through most of its 152.4 mm (6 in.) stroke, thus resulting in constant injection rate.

The mold cavity is constructed by placing a 3.18 mm (0.125 in.) thick aluminum spacer plate between two 6.35 mm (0.25 in.) thick aluminum mold walls. Mold wall thickness is doubled in order to reduce bulging at higher pressures that occur at increased volume fraction and flow rate. A 15.24 cm (6.0 in.) diameter circle is cut from the center of the spacer plate to form the disk-shaped cavity. By replacing the space plate, parts having different thickness can be molded, however in the current study only 3.18 mm (0.125 in.) thick disks are molded. O-ring, inlet, and exit vent configuration is unchanged compared to the original setup. Vents on the top mold wall with hoses that have white hose clamps attached to seal the exits are visible in Figure 4.2. After the mold is completely full, the press is run for a few additional seconds until resin comes

out of all four vent hoses. Then the four vent hoses and the inlet hose are sequentially clamped to maintain the final fill pressure.

For this study, three fiber volume fractions are investigated (i.e., 9.8, 21.2, and 33.1 %). These fiber contents are achieved by layering 2, 4, or 6 layers, respectively, of the thick mats (Fiberglast part #250), or 4, 8, or 12 layers, respectively, of the thin mats (Fiberglast part #248) inside the mold cavity. Details of each of the six resulting fiber configurations are listed in Table 4.1. Configurations are designated TK2, TK4, and TK6 for thick mats and TN4, TN8, and TN12 for thin mats. EPON 815C resin mixed with and Epicure 3282 curing agent are used as the filling fluid for molded parts.

The parts are molded at constant flow rate of 5.83×10^{-6} m^3/s, with fill times ranging between 6 and 9 seconds, depending on fiber volume fraction. Fill times are consistent with those expected in industrial molding of similar-sized parts. After the vents and inlet hose are clamped to maintain the pressure, the part is left to cure in the mold for 48 hours before demolding. The part is then post cured at room temperature and pressure for a minimum of two additional weeks before the specimens are machined, polished, and tested to ensure the completion of cross-linking and development of mechanical properties. Three representative stress-strain curves for specimens from position 1 molded at the three fiber contents used in this study are shown in Figure 4.3. These curves show the typical shape of the tensile curves, and give a sample of the differences in slope and ultimate tensile strength observed in the tensile data.

During filling, transient pressure data is collected at a radial location of 12.7 mm (0.5 in.) away from the inlet. Pressure is measured using a pressure transducer (Omega Model PX180-100GV, 100 psi max, 0.3% accuracy) flush mounted on the bottom mold wall, as depicted in Figure 4.1. The pressure transducer is attached to a custom built signal amplification circuit based on an i640 in-amp, which conditions the signal for data acquisition system by amplifying voltage, isolating the signal, and lower transducer output impedance. The voltage amplification is adjustable by changing resistors in the circuit with typical amplifications being on the order of 100. Pressure data is sampled at 10 Hz using a laptop computer controlled Omega Daqbook data acquisition system. The circuit, Daqbook, and computer are all visible in Figure 4.2. For pressure measurement, mold filling experiments are performed using corn syrup as the filling fluid to avoid damaging the pressure transducer. The corn syrup is diluted with water to adjust its viscosity, allowing fill pressures for all the six mat configurations to be obtained within the pressure transducer's most accurate range.

Representative pressure measurements at 12.7 mm away from the inlet during filling experiments for each fiber content are shown in Figure 4.4 (i.e., configurations TK2, TK4, and TK6 for thick mats and TN4, TN8, and TN12 for thin mats). Filling begins at t =0 s, and continues for several seconds after the mold cavity is completely full as the exit hoses are left unclamped to allow continued discharge of the fiiling fluid. Pressure is first recorded when flow contacts the transducer, however the time each pressure curve starts in Figure

4.4 has been shifted to allow all curves to be clearly observed without any overlapping.

4.3 Pressure in a Disk Shaped Cavity Containing Porous Media

Darcy's law [15] is used to model flow through a porous media by relating velocity to pressure gradient with a permeability tensor,

$$\mathbf{u} = -\frac{1}{\mu}\mathbf{K}\nabla p\,. \tag{4.1}$$

In Equation 4.1 **u** is the average Darcy velocity, μ is the dynamic viscosity, ∇p is the pressure gradient, and **K** is the second-order permeability tensor. For the molding of center-gated disk-shaped parts, purely radial flow in the cavity is expected. (There is no flow component or non-zero derivatives in the tangential direction, thus the flow is axisymmetric). Figure 4.5 depicts the cross section of a center-gated disk labeled with the coordinate system used. Important dimensions in Figure 4.5 are the half gap width, H, and the transient radial location of the fluid front, $R_f(t)$. In radial coordinates and with axisymmetric radial flow assumption, Darcy's law simplifies to the following,

$$u_r = -\frac{1}{\mu}\frac{\partial p}{\partial r}K_{rr}\,, \tag{4.2}$$

where u_r is the radial velocity component, and K_{rr} is the radial permeability. In addition, conservation of mass simplifies to,

$$\frac{\partial}{\partial r}(ru_r) = 0\,. \tag{4.3}$$

Equation 4.3 can be integrated straightforwardly to yield,

$$ru_r = c(t), \tag{4.4}$$

where $c(t)$ is a constant dependent only on time. Equation 4.4 is then substituted into Equation 4.2, to obtain,

$$\frac{dr}{r} = -\frac{K_{rr}}{\mu}\frac{dp}{c(t)}. \tag{4.5}$$

Equation 4.5 is integrated from the radius at the location of the pressure transducer, $r = R$, to the radial location of the fluid front, $r = R_f(t)$, and from the pressure at the transducer, $p = P(t)$, to the pressure at the free surface, P_f, to obtain,

$$-\frac{K_{rr}}{c(t)\mu}(P_f - P(t)) = \ln\left(\frac{R_f(t)}{R}\right). \tag{4.6}$$

The velocity in Equation 4.4 can be expressed in terms of the volume flow rate, Q, and geometry using the volume flowing through area of the ring in the disk at the radius of the transducer, R, as,

$$u_r = \frac{c(t)}{R} = \frac{Q}{A} = \frac{Q}{(1-v_f)4\pi RH}, \tag{4.7}$$

where v_f is the preform volume fraction. The velocity u_r remains constant at a given radial location if the fluid is injected at constant volume flow rate; thus, c is a constant that does not depend on time. At the free surface, the fluid front is in contact with atmosphere if the vents are kept open during filling, thus, $P_f = 0$, and Equations 4.6 and 4.7 can be combined to yield,

$$P(t) = \frac{Q\mu}{(1-v_f)4\pi HK_{rr}}\ln\frac{R_f(t)}{R}. \tag{4.8}$$

Equation 4.8 gives the transient pressure in a disk at the radius R based on the flow rate, viscosity, gap width, radial permeability, and the radial position of the fluid air interface, $R_f(t)$.

4.4 Permeability Measurement Using a Single Pressure Transducer

The majority of methods for permeability measurement published in literature require the use of two pressure transducers placed at different locations in the mold cavity [29,61,62]. These transducers are used to measure a pressure difference between two locations, from which the permeability is calculated from Darcy's equation. Equation 4.8, however, is in a form that allows the permeability to be calculated using the known pressure at the fluid front and data from only one pressure transducer [63]. The viscosity, gap width, flow rate, and volume fraction are measured prior to filling. The location of the fluid front with time, $R_f(t)$, is obtained based on the volume flow rate and geometry. The volume of the disk that has been filled at a time, t, is given by the following two expressions.

$$V = Qt\,; \tag{4.9}$$

$$V = 2(1-v_f)\pi H R_f^2(t)\,. \tag{4.10}$$

These are combined to obtain $R_f(t)$ in terms of experimental parameters and time,

$$R_f(t) = \sqrt{\frac{Qt}{2(1-v_f)\pi H}}\,. \tag{4.11}$$

Equation 4.11 is substituted into Equation 4.8, to obtain the final form used to obtain permeability from a single set of pressure data,

$$P(t) = \frac{Q\mu}{(1-v_f)4\pi HK_{rr}} \ln \frac{\sqrt{\frac{Qt}{2(1-v_f)\pi H}}}{R} \tag{4.12}$$

The permeability, K_{rr}, can now be obtained by using a least squares curve fit varying K_{rr} to match Equation 4.12 to transient pressure data.

4.5 Results and Discussion

At least five disks are molded using each of the six preform configurations designated in Table 1 in order to obtain mechanical properties based on preform configuration. All specimens from position 2 and half of the specimens from position 1 are tested under tension as described by ASTM D3039/D3039M. In a previous study of composite disks molded similarly, tensile results were found to be statistically indistinguishable for positions 1 and 2 [64], thus data from these specimens are combined yielding at least 15 specimens for each data point to reduce statistical variation. The use of a large number of specimens is preferred because random preforms have been shown to have large local variations in planar density [28], which leads to higher statistical variation in tensile results. Fifteen preforms from each mat type are cut to size, and weighed in order to characterize planar density variation for the mats used in this study. Thick mats have a measured planar density of 0.446 kg/m^2, which is slightly lower than the 0.459 kg/m^2 reported by the manufacturer, and a standard deviation of 0.0485 kg/m^2. Planar densities are observed in the range of 0.374 to 0.526 kg/m^2

representing a 40% variation. Planar density for thin mats is also observed to be lower than the reported value of 0.228 kg/m^2, with an average measured value of 0.200 kg/m^2 and a standard deviation of 0.31 kg/m^2. Thin mats exhibit greater variation of 64%, with individual values ranging between 0.163 and 0.266 kg/m^2.

Measured values for ultimate tensile strength for each configuration are presented in Figure 4.6. Strength values are plotted with error bars calculated using a 95% confidence interval. Tensile strength is observed to be equivalent within the range of statistical error for thick and thin mats at each of the three equivalent fiber volume fractions, with thick mats exhibiting slightly higher strengths at the lower two fiber volume fractions, and thin mats having slightly higher strength at highest fiber content. Both thick and thin mat strengths are observed to increase linearly with increasing fiber content, with 130% increase in strength for thick mats when fiber content is increased from 9.8% and 33.1%. Thin mats exhibit a 169% increase in strength over the same range of fiber content. For these six cases the uncertainty using the 95% confidence interval ranges between 7.5% to 18.2% with an average value of 13.4%. Overall, tensile strengths found in Figure 4.6 are observed to be lower than results presented in Chapter 3. This is due in part to the higher injection rate and lower post-fill cure pressures used during molding of the disks utilizing the molding setup mounted on the hydraulic press.

Figure 4.7 contains data for elastic modulus for the six preform configurations, with error bars drawn again using a 95% confidence interval. Stiffness results are observed to follow trends similar to those exhibited by

strength. The stiffness is found to be similar for thick and thin mats at the same fiber content, and increases linearly with fiber content. Stiffness data, however, exhibits less improvement with increased fiber volume fraction, with only 100% increase in modulus between 9.8 and 33.1% fiber volume fraction. Stiffness data is found to have lower statistical variation, with a range between 6.0% to 14.7% and an average of 9.5%. Stiffness results exhibit even lower variation between thick and thin mats compared with strength results. The linear increase of tensile modulus of resin transfer molded composites up to 50% fiber volume fraction is also reported by Oksman [2].

Three point bending test is also performed on molded parts to examine more subtle variations in mechanical properties introduced by additional layer interfaces for thin mats. It may be possible that these additional interfaces could weaken interlaminar shear strength of the composite material. Half of the specimens from position 1 are cut into three 38.1 mm (1.5 in.) segments, and the center segment is used for three point bending test. A total of 5 tests are performed for each configuration. The measured short-beam shear strength values obtained from this test are presented in Figure 4.8. The short-beam shear strength is observed to be similar for thick and thin mats, with larger variation (7%) between mat types at 33.1% volume fraction. Although increase in shear strength is linear with volume fraction, thin mats exhibit the largest deviation in linearity of all mechanical data presented. This slight deviation from linearity may be attributed to higher statistical variations, particularly at lower

fiber content. At lower fiber content, variations in mats are less likely to even out due to lower number of layers, thus leading to higher uncertainties.

Ultimate tensile strength, elastic modulus, and short-beam shear strength results show that the planar preform density does not affect mechanical properties within the volume fractions studied. However the potential for flow differences between thick and thin configurations still exists, particularly at low volume fractions where fluid paths between layers may be significantly altered by changing the number of layers used. Experiments are performed, as explained in the previous section on pressure measurement, measuring transient pressure on the bottom mold wall at R =12.7 mm (0.5 in.). To quantify effect of mat type on pressure, permeability is obtained from pressure data using Equation 4.12. Permeability is calculated by using a least squares curve fit varying the value of K_{rr} to match Equation 4.12 to transient pressure data during filling.

Maximum pressure observed increases with fiber content with maximum pressures of approximately 40, 110, and 160 kPa (5.8, 16.0, and 23.2 psi) observed for TK2, TK4, and TK6, respectively. For the lowest volume fraction, pressure is seen to follow a logarithmic increase for the duration, however higher volume fractions, pressure is seen to deviate from a logarithmic fit for an initial short duration. This deviation is due to expansion of hoses when filling starts due to the higher pressure at these runs, and is reduced by reinforcing the tubing connecting the molding press assembly to mixer and the mold. At higher volume fractions the mold fills more quickly, thus the pressure is observed to level off

after about 6 seconds for the TK6 case. Data after the mold has filled is not used in least squares calculation to determine permeability.

Permeability fits to the representative pressure curves from the filling of three disks containing preform configurations TK2, TK4, and TK6 (i.e., 2, 4, and 6 layers of thick mats), respectively are depicted in Figure 4.9. Solid lines in Figure 4.9 represent measured valued, while dashed lines show curve fits used to obtain permeability. A brief startup period is observed in which curve fits do not match measured pressure values due to hose bulging and possibly inlet effects, especially at higher volume fraction. It has been shown that mat deformation at the inlet gate may have considerable effect on fill pressure [65,66], which may also contribute to the observed startup effects. Deviation in pressure at startup from theoretical values is minimized both by reinforcing tubing leading to mold inlet, and reducing tubing length. Results show that pressure data follows the anticipated trend, and thus curve fits are quite good after startup period. The theoretical pressure curve deviates from measured values after about 7 seconds for configuration TK6 due to mold being full earlier at higher fiber volume fraction. The best curve fit is obtained for configuration TK2, due to the lowest pressure for this configuration. The highest fill pressure of about 160 kPa (23.2 psi) is observed for configuration TK6. Permeabilities obtained from configurations TK2, TK4, and TK6 for these representative runs are 170, 5.2, and 1.75 Darcy, respectively.

Representative pressure measurement for thin mat configurations TN4, TN6, and TN12, and their respective curve fits, are shown in Figure 4.10. The

observed molding pressures for thin mat configurations are lower compared to thick mat configurations at same fiber volume fraction. The theoretical pressure curves generated from the permeability fits match measured values after startup period, with TN12 pressure fit ending earlier than the others since the cavity fills more quickly higher fiber content. The measured permeabilities for TN4, TN6, and TN12 configurations are 575, 7.8, and 2.8 Darcy, respectively, which are higher than thick mat configurations, indicating lower molding pressure requirements.

The permeability values for the six preform configurations are presented in Figure 4.11, with error bars drawn using 95% confidence interval. Permeability values for the six configurations are also given in Table 4.2. The permeability ratio in Table 4.2 is defined as the ratio of thin mat permeability to thick mat permeability at same fiber volume fraction, and represents the multiple pressure is increased by when using thick mats instead of thin. Permeability values are observed to be higher for thin mats at all fiber volume fractions. The permeability decreases by two orders of magnitude as volume fraction increases from 9.8% to 33.1%, with the largest decrease in permeability observed between 9.8% and 21.2% fiber content. At 9.8% fiber volume fraction, the permeability ratio is the highest at 3.3, indicating thick mats have over three times the molding pressure requirement of thin mats. At 21.2% and 33.1%, permeability ratios of 1.5 and 1.6, respectively are obtained. These are lower than those observed at 9.8% fiber content, but still represent considerable increases in molding pressure for thick mats.

The measured permeability values are similar in magnitude to those reported for random mats in the literature [67-70]. For example, Wirth and Gauvin, using pressure transducers mounted in a channel-shaped mold, measure permeabilities of 99 and 49 $x10^{-10}$ m^2 for volume fractions of 11 and 18%, respectively [67]. At 17% fiber volume fraction, Luce et al. measure a permeability value of 30 $x10^{-10}$ m^2 using radial flow experiments [68]. Trevino et al. report permeabilities for random mats between 1.5 and 3.5 $x10^{-10}$ m^2 for fiber contents between 25 to 45% [22]. Values presented in the current study are also consistent with results from Kim et al. [69], and Berker and Sun [70].

An effective permeability, calculated from pressure data obtained by injecting corn syrup into a mold cavity containing zero preform, along with a theoretically predicted value, is depicted in Figure 4.11. Effective permeability is obtained by comparing theoretical pressure in an empty disk with pressure obtained by Equation 4.8 for a porous media. The pressure at the transducer for the configuration depicted in Figure 4.5 is obtained using Navier-Stokes Equations. Neglecting inertia terms, pressure at $r=R$ is found to be,

$$P(t)=\frac{3Q\mu}{(1-v_f)4\pi H^3}\ln\frac{R_f(t)}{R}. \tag{4.13}$$

Equating Equations 4.8 and 4.13, an effective permeability can be defined for the case of an empty mold as,

$$K_{eff}=\frac{H^2}{3}. \tag{4.14}$$

The theoretical value of effective permeability in Figure 4.11 is calculated to be 8400 Darcy, and is consistent with the measured value. Empty mold

permeability represents the limiting case of zero fiber volume fraction, and obtained values follow the trend observed in other measured permeability values.

4.6 Concluding Remarks

Results are presented demonstrating effect of fiber volume fraction and planar preform density (i.e., mat thickness) on mechanical properties and injection pressure of resin transfer molded disks. At same fiber content, planar preform density has negligible effect on mechanical properties, demonstrated by comparable values for elastic modulus, tensile strength, and short-beam shear strength. Mechanical properties are observed to increase linearly between 9.8% and 33.1% fiber volume fraction, with average increase of about 150% for ultimate tensile strength, and 100% for elastic modulus and short-beam shear strength. Despite having negligible effect on mechanical properties, mat thickness is shown to have significant effect on injection pressure. Effect of mat thickness on injection pressure is quantified using differences in permeability values. A new technique to measure permeability using the transient pressure data from a single pressure transducer is presented. The measurement technique is simpler and more advantageous than the techniques currently used in the literature, that require the use of multiple transducers or tracking of fluid front motion in addition to pressure measurement. Permeabilities measured for thin mats are observed to be 47% to 226% higher than those measured for thick mats, thus resulting in significant reduction of injection pressure by 50% to 260%

for fiber volume fractions ranging from 33.1% to 9.8%, respectively. Ability to reduce injection pressure or cycle time at same fiber content without degradation in mechanical properties could lead to less expensive molding processes.

Table 4.1 Experimental configurations used to examine effect of preform thickness and fiber volume fraction

Designation	Description	Volume fraction in mold (v_f)
TN4	4 thin layers of chopped-strand glass fiber mat. Planar density- Listed: 0.228 kg/m^2 (0.75 oz/ft^2) Measured: 0.200 kg/m^2	9.8%
TN8	8 thin layers of chopped-strand glass fiber mat. Planar density- Listed: 0.228 kg/m^2 (0.75 oz/ft^2) Measured: 0.200 kg/m^2	21.2%
TN12	12 thin layers of chopped-strand glass fiber mat. Planar density- Listed: 0.228 kg/m^2 (0.75 oz/ft^2) Measured: 0.200 kg/m^2	33.1%
TK2	2 thick layers of chopped-strand glass fiber mat. Planar density- Listed: 0.459 kg/m^2 (1.5 oz/ft^2) Measured: 0.446 kg/m^2	9.8%
TK4	4 thick layers of chopped-strand glass fiber mat. Planar density- Listed: 0.459 kg/m^2 (1.5 oz/ft^2) Measured: 0.446 kg/m^2	21.2%
TK6	6 thick layers of chopped-strand glass fiber mat. Planar density- Listed: 0.459 kg/m^2 (1.5 oz/ft^2) Measured: 0.446 kg/m^2	33.1%

TN-thin mats, TK-thick mats, #-number of layers

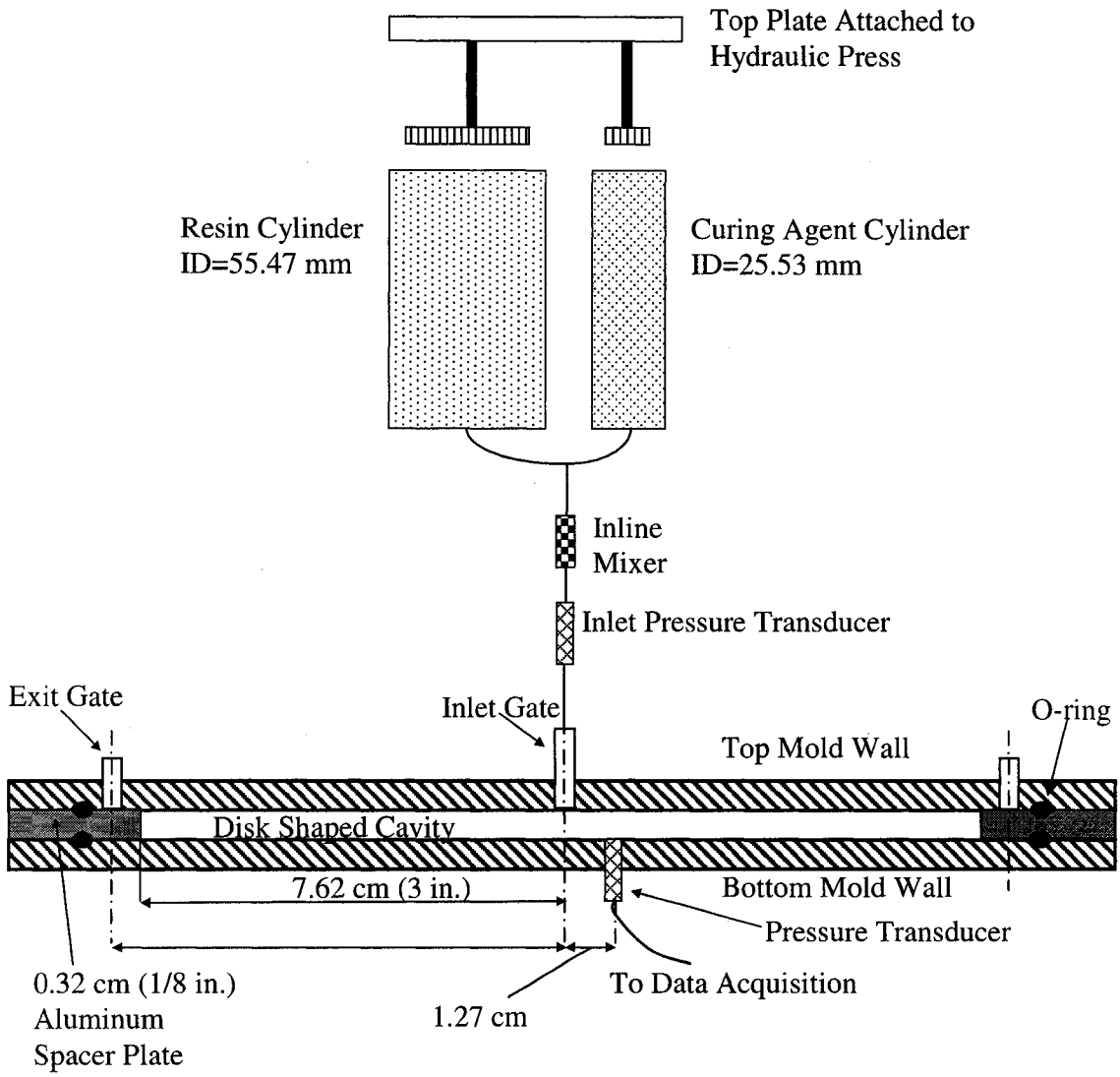

Figure 4.1 Setup used to fabricate RTM parts and measure pressure to determine permeability

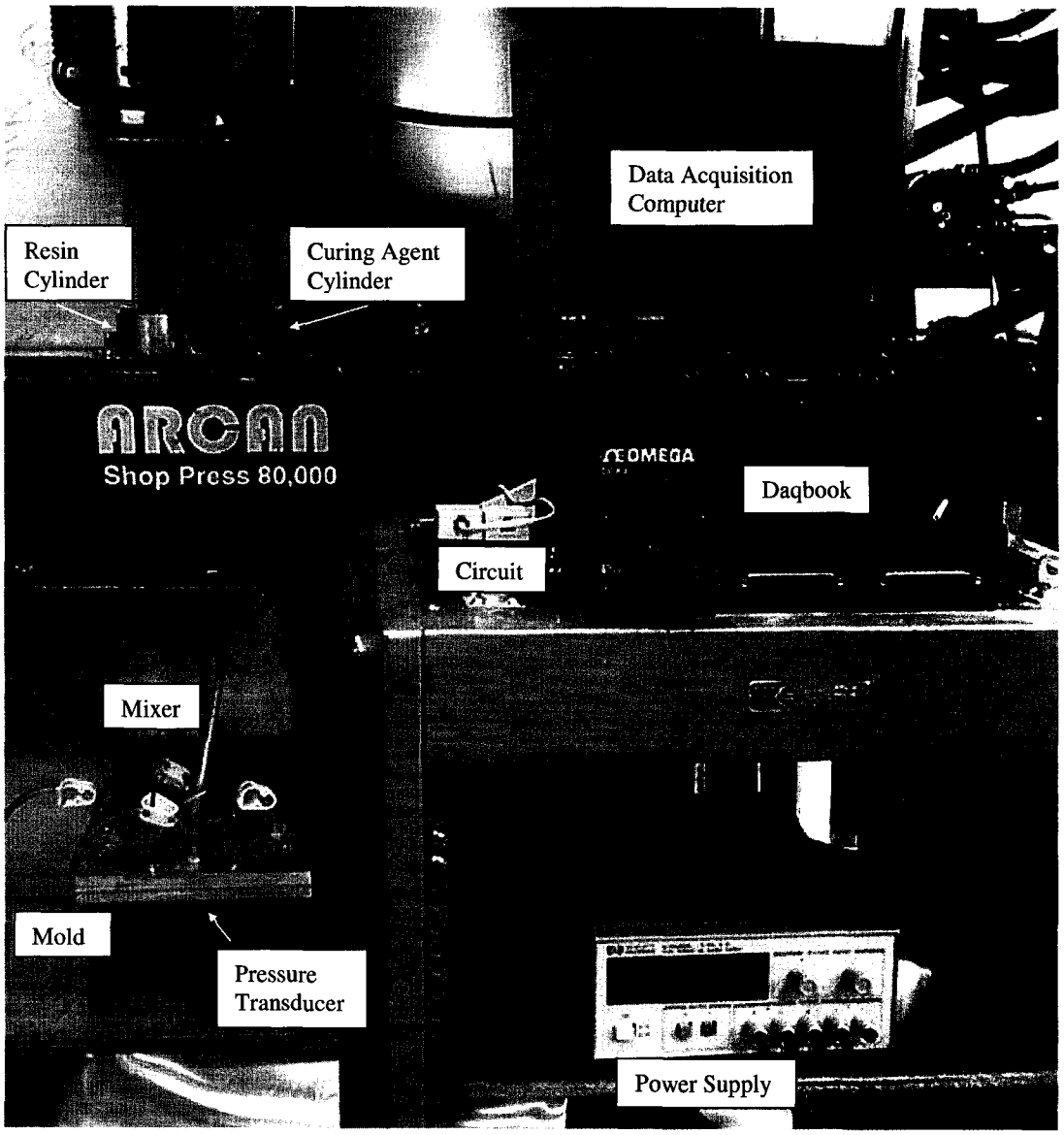

Figure 4.2 Photograph of the setup used to fabricate RTM parts and measure pressure to determine permeability

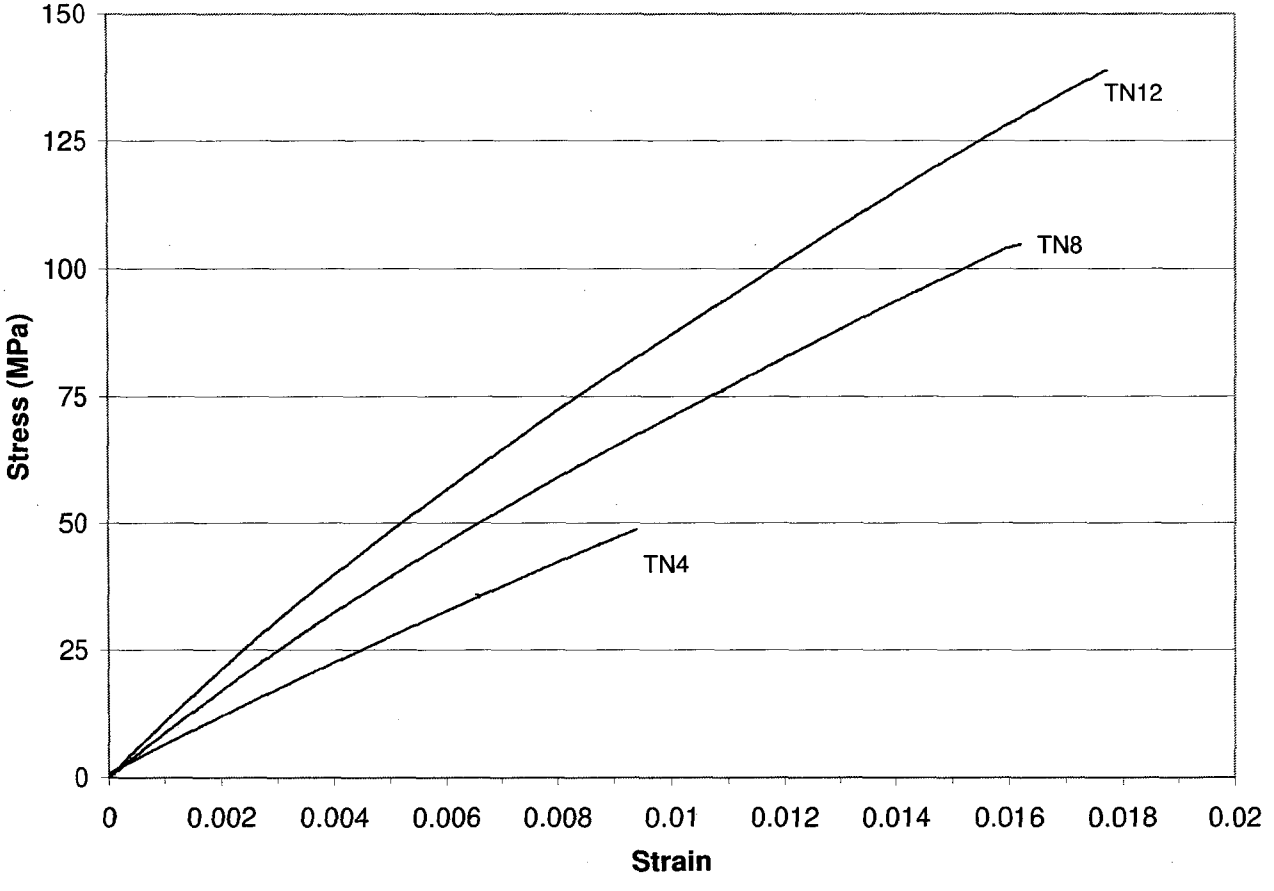

Figure 4.3 Representative stress strain curves from tensile tested specimens. TN4: 4 layers of thin mats (i.e., v_f =9.8%); TN8: 8 layers of thin mats (i.e., v_f =21.2%); TN12: 12 layers of thin mats (i.e., v_f =33.1%)

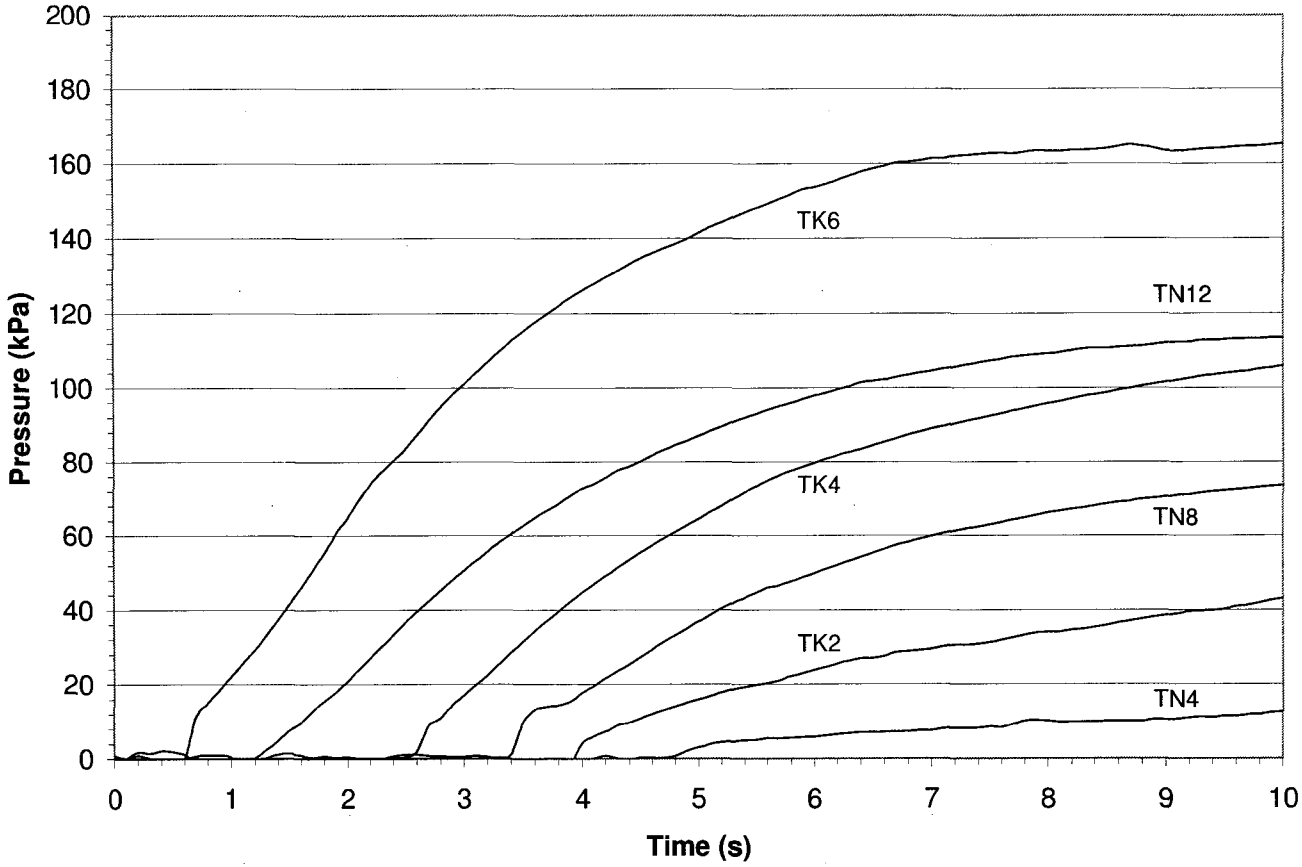

Figure 4.4 Example pressure curves from filling disks containing each of the six preform configurations

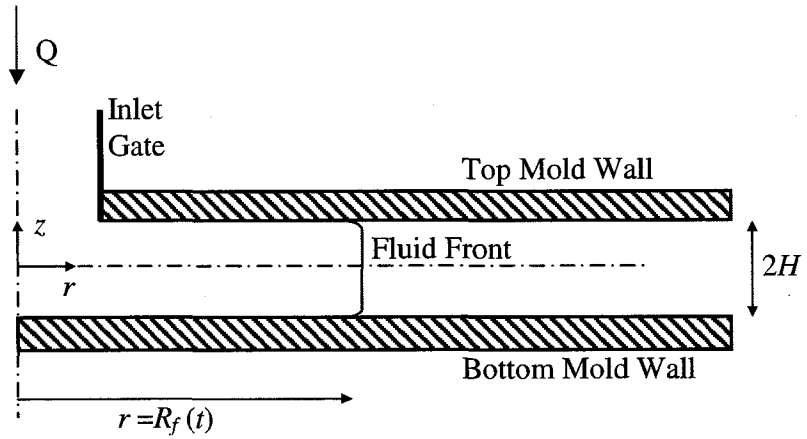

Figure 4.5 Cross section of disk shaped cavity labeled for pressure calculations. R_f is the transient radial location of the fluid front during filling

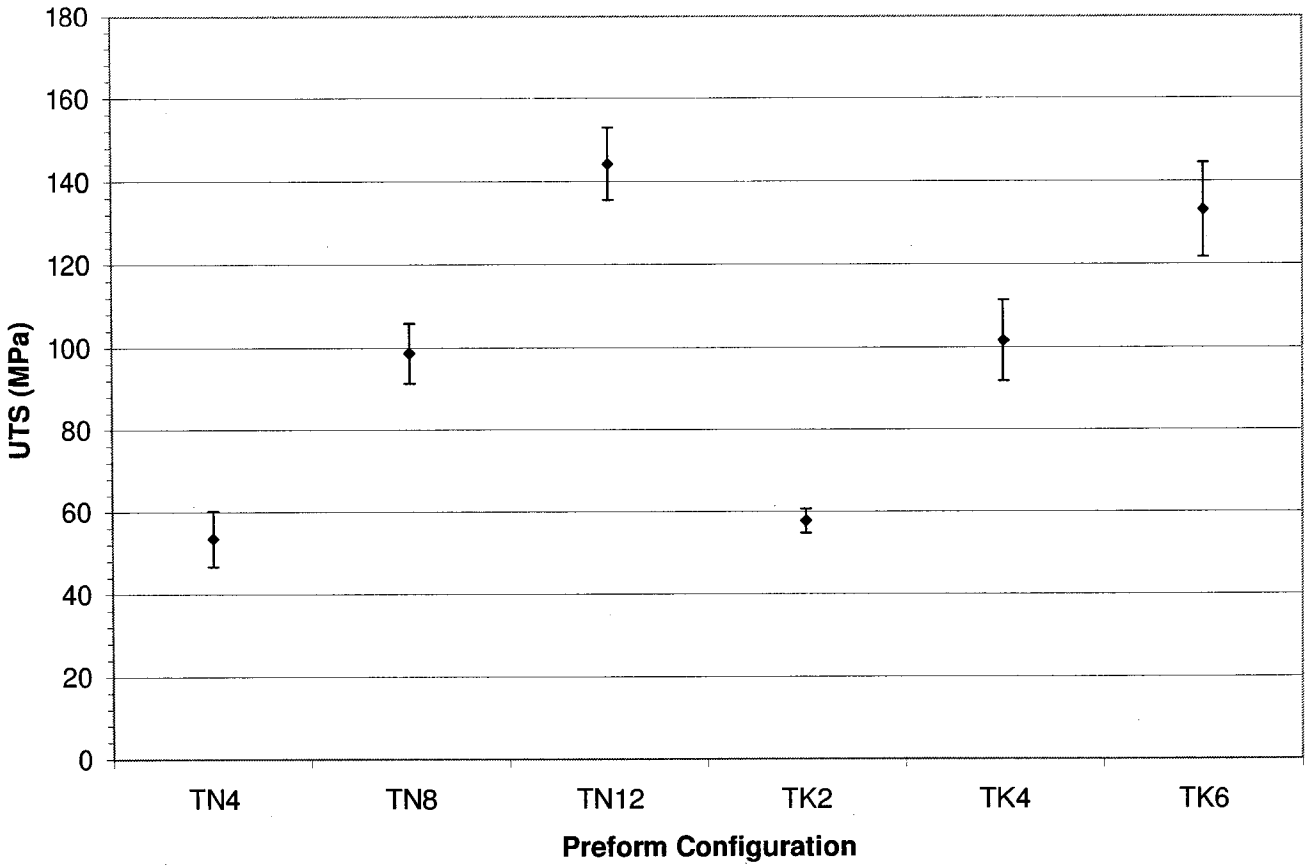

Figure 4.6 Ultimate tensile strength of specimens for each preform configuration

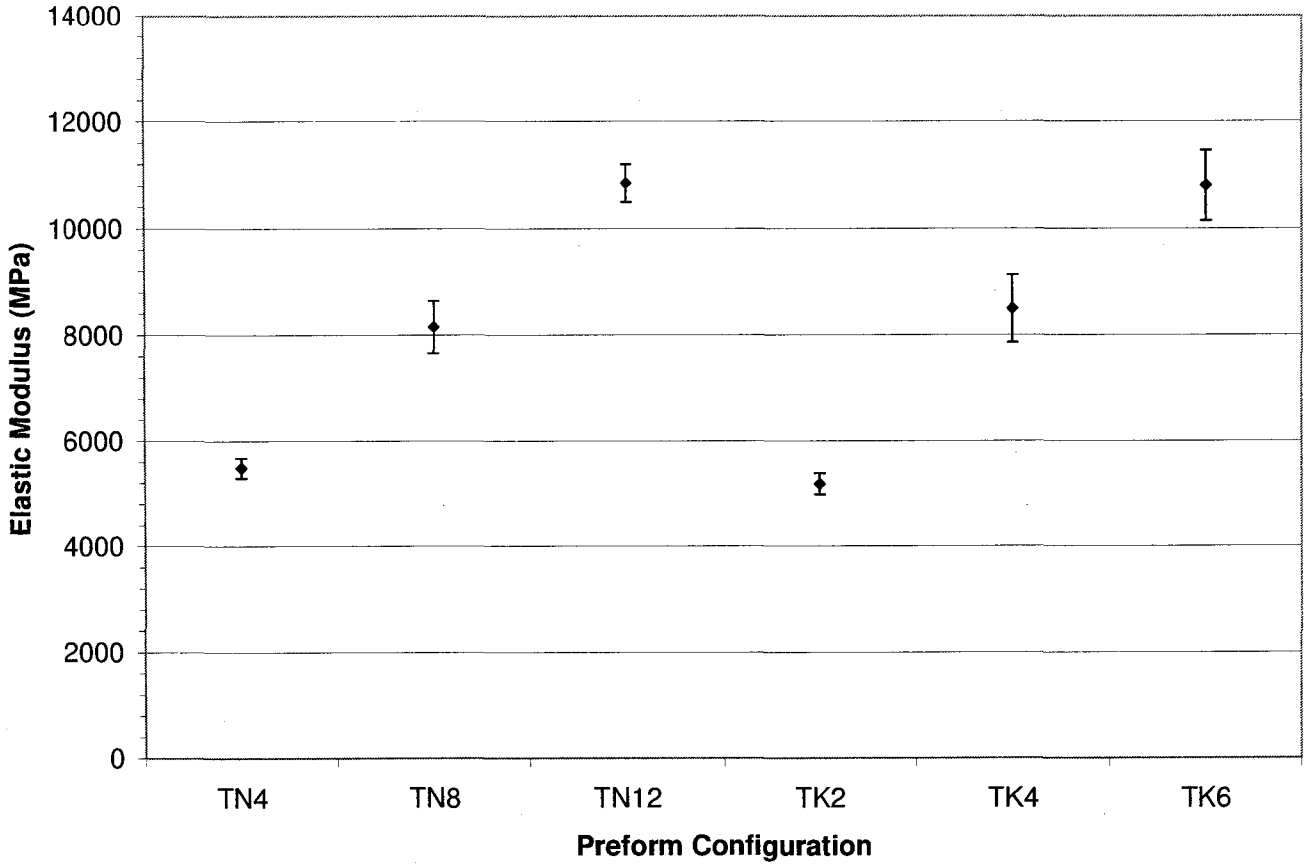

Figure 4.7 Elastic modulus of specimens for each preform configuration

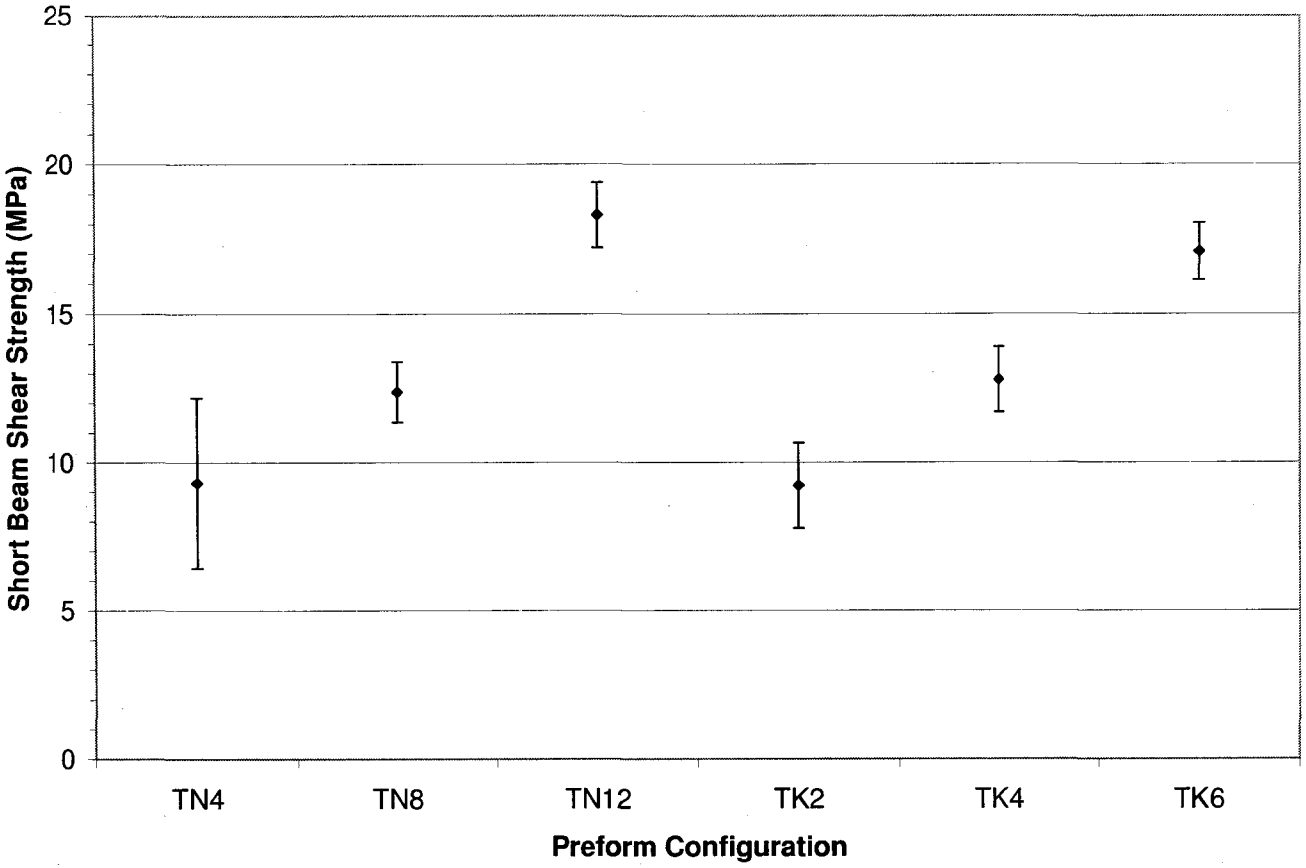

Figure 4.8 Short beam shear strength of specimens from each preform configuration

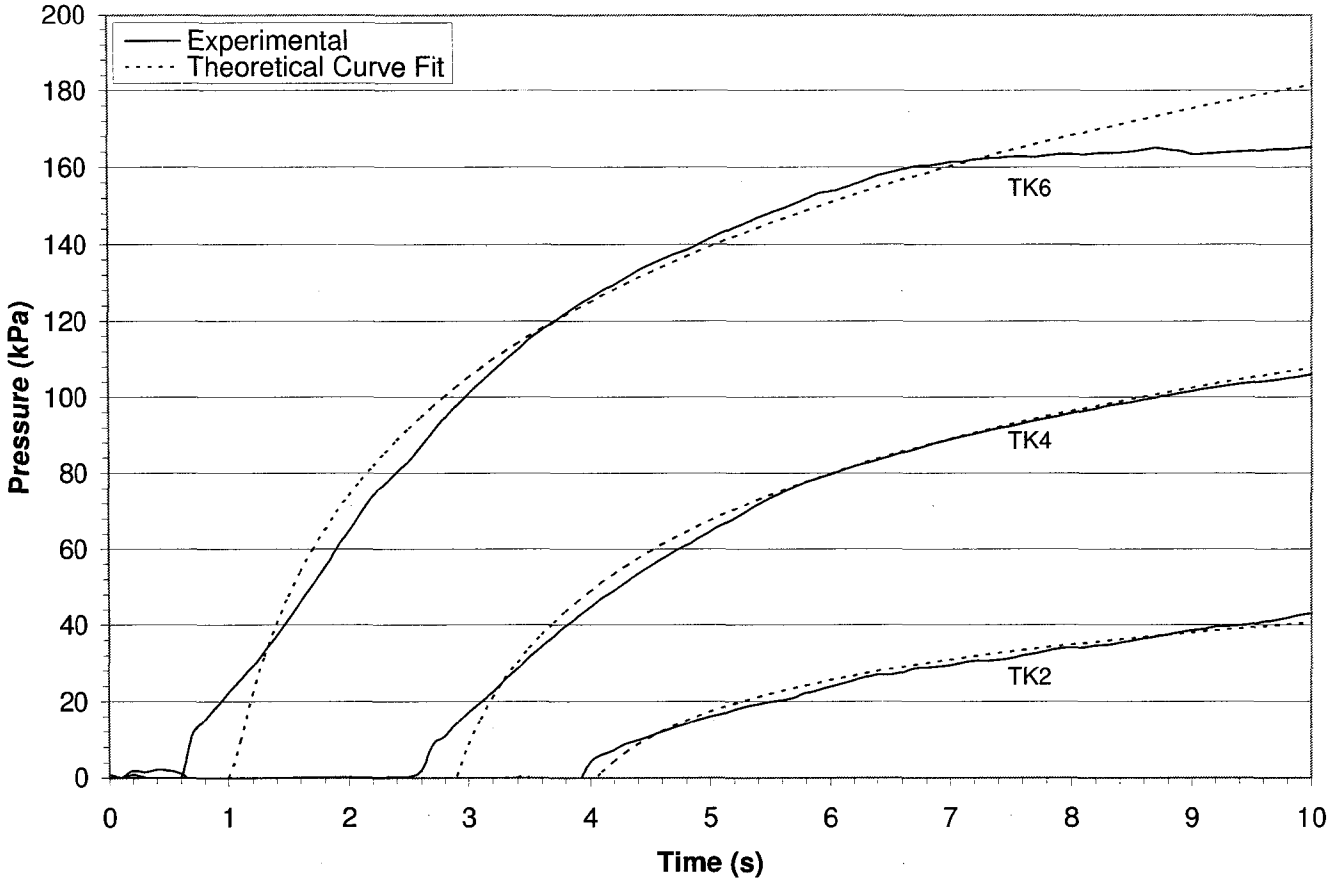

Figure 4.9 Example pressure curves from disks containing thick mats and theoretical curve fit used to determine permeability. TK2: 2 layers of thick mats (i.e., v_f =9.8%); TK4: 4 layers of thick mats (i.e., v_f =21.2%); TK6: 6 layers of thick mats (i.e., v_f =33.1%)

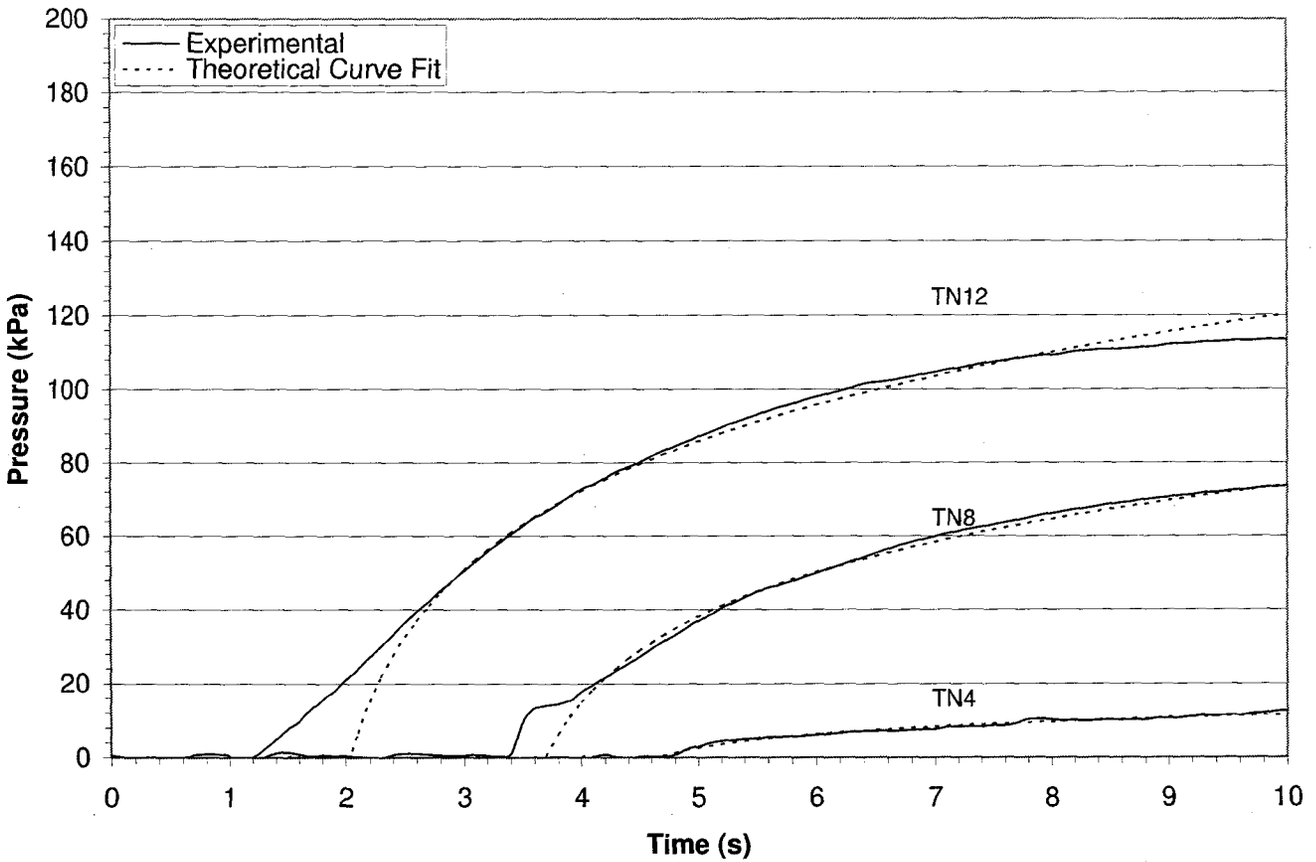

Figure 4.10 Example pressure curves from disks containing thin mats and theoretical curve fit used to determine permeability. TN4: 4 layers of thin mats (i.e., v_f =9.8%); TN8: 8 layers of thin mats (i.e., v_f =21.2%); TN12: 12 layers of thin mats (i.e., v_f =33.1%)

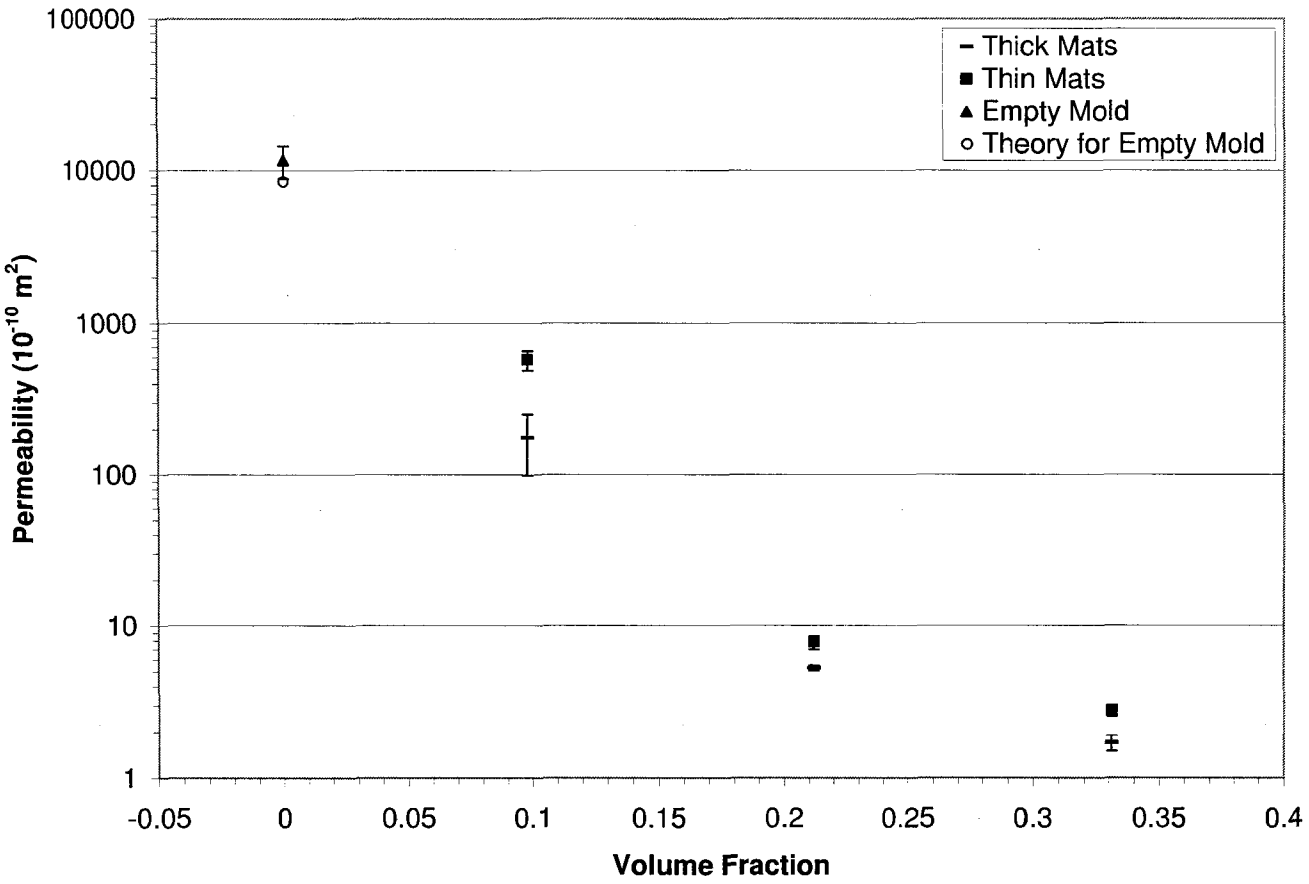

Figure 4.11 Permeability results obtained for each preform configuration. Theoretical permeability for empty mold is obtained from Equation 4.14

Table 4.2 Measured permeability for each mat configuration and ratio between permeabilities of thick and thin mats

v_f	**Thick mats TK2, TK4, TK6 permeability (10^{-10} m^2)**	**Thin mats TN4, TN8, TN12 permeability (10^{-10} m^2)**	**Permeability ratio (TN/TK)**
9.8%	176	575	3.6
21.2%	5.3	7.8	1.5
33.1%	1.7	2.8	1.6

5 Mold Modifications to Facilitate Reduced Molding Pressure

5.1 Introduction

The benefits of pressure reduction in RTM were described in Chapter 1. Significant cost saving potential exists through less expensive tooling or faster cycle times using equivalent tooling. In Chapter 3, the effect of reducing injection rate directly, and thus, injection pressure, is quantified. It is shown that parts with improved mechanical properties can be obtained with lower injection pressure, however the increased cost associated with longer cycle times will make this an undesirable tradeoff in many cases. Additionally, there is a limit to how much injection rate can be reduced before increased void formation is observed [51,52], primarily due to lag lead and fingering effects [60]. In Chapter 4, lower pressures are obtained by modifying preform thickness without adverse affects on mechanical properties or production capabilities. These studies can be grouped with many found in literature aimed at optimizing process parameters in RTM.

The study presented in this chapter attempts to go beyond the optimization of process parameters and implements a fundamental improvement to resin transfer molding, as has been done in processes such as vacuum assisted resin transfer molding, and compression resin transfer molding. Small flow channels in the mold cavity are proposed as a method to significantly decrease injection pressure requirements by providing low resistance flow paths. These paths are expected to yield an effect similar to that observed by Adams

and Rebenfeld [14] in which bulk permeability increased significantly when including a single high permeability layer.

Experiments are performed using mold cavities modified to include one or two flow channels. Flow experiments are utilized to quantify pressure reduction observed due to addition of flow channels, and disks are molded using molds with one or two flow channels, and compared to disks molded without flow channels. It is known that in a center-gated disk highest pressure drop occurs near the inlet, thus experiments are performed to ascertain necessary channel length required to achieve improved results.

5.2 Modified Channel Mold Cavity

Modified mold cavities are constructed to characterize the effects of flow channels on molding of resin transfer molded parts. Initially, channel mold assemblies are fabricated according to the basic mold cavity specifications described in Chapter 2.1, and depicted in Figure 2.3. Mold wall thickness is increased to 12.7 mm (0.5 in.) to help ensure mold walls don't bulge under fill pressure due to decreased wall thickness in the channel regions. Molds having three channel configurations are fabricated, having zero, one, and two channels on the top mold wall respectively.

The 0-Channel mold is identical to the mold used in previous studies, thus, no modifications are necessary on the top mold wall (Figure 5.1a). Molds with one and two channels require extra steps to produce. For the 1-Channel mold, a single 3.175 mm (0.125 in.) wide by 3.175 mm (0.125 in.) deep groove is

machined along a diameter of the disk as depicted in Figure 5.1b. The single channel results in two additional radial flow paths for flow leaving the inlet. The resulting flow has 2 axes of symmetry. The channel intersects the outer edge of the disk at two points that lie between exit gates so that flow will not fill the channel then immediately exit the disk. The 2-Channel mold top is fabricated by machining a single groove identical to that used for the 1-Channel mold, followed by another 3.175 mm (0.125 in.) wide by 3.175 mm (0.125 mm) deep groove machined along the diameter perpendicular to the first groove, as depicted in Figure 5.1c. As in the single channel mold, all channel endpoints lie between exit gates to prevent premature flow exit. The 2-Channel mold introduces four additional flow paths leaving the inlet gate, thus, resulting in a flow with four axes of symmetry. A photograph of a top mold wall with two machined flow channels is given in Figure 2.4 (left).

Minimizing the amount of excess material that needs to be trimmed off the cured parts is an important consideration for the potential use of channels to minimize molding pressure. Maximum pressure gradient in the disk is observed at the inlet, with smaller increases in pressure as fluid front moves away from the inlet. It is expected that reducing the channel length will not significantly reduce the benefits to molding pressure, while reducing waste and facilitating easier demolding. Additional channel configurations are obtained by shortening the channel length. Channels are shortened by filling the channel completely with hot glue, then removing the necessary hot glue to obtain the desired channel length, with the channel always starting at the inlet. Hot glue is covered with

scotch tape to give a smooth mold surface. Channel lengths of 0, 33, 50, 67, and 100% of the disk radius are used in this study, with 0% representing the special, limiting case of a 0-Channel mold, and 100% representing a completely unblocked channel. The channels in Figure 2.4 (left) are blocked to 50% of the disk diameter using hot glue.

An additional polishing step is performed on the surface of the mold walls used for channel flow characterization experiments. A very smooth surface is obtained using a buffing wheel and buffing compound. This higher quality surface makes the flow less susceptible to anomalies due to surface defects. The smooth surface also facilitates easy cleanup for corn syrup used in flow simulation experiments, and makes demolding of cured parts much easier.

For this study, four fiber volume fractions are investigated (approximately 10, 20, 30, and 40%). Fiber contents are achieved by layering 2, 4, 6, or 8 layers, respectively, of chopped strand glass fiber mats (Fiberglast part #250) inside the mold cavity. EPON 815C resin mixed with and Epicure 3282 curing agent are used as the filling fluid for molded parts. The parts are molded at a constant flow rate of 5.83×10^{-6} m^3/s, with fill times ranging between 5 and 9 seconds, depending on fiber volume fraction. For molded parts, vents and inlet hose are clamped after filling to maintain the pressure, and the part is left to cure in the mold for 48 hours before demolding. For some configurations short shots are molded, in which filling is performed for only 2 or 4 seconds and the part is cured, in order to visualize intermediate flow front positions. Molding is performed at a number of configurations, with changes to number of channels,

channel length, fiber volume fraction, and at intermediate fills. Table 5.1 contains configuration data for all molded disks used in this study, described in further detail later in this chapter.

Corn syrup, diluted with water to obtain desired viscosity, is used as the filling fluid for pressure experiments. Pressure measurements are made using three preform combinations, given in Table 5.2. Viscosity is selected for each preform combination to yield pressures that match the pressure transducer range. Combinations are designated TK4CH for 118 cp fluid and 4 thick mats (20% Fiberglast part #250), TN8CH for 138 cp fluid and 8 thin mats (≅20% Fiberglast part #248), and TN12CH for 63.2 cp fluid and 12 thin mats (≅30% Fiberglast part #248). For each viscosity/preform combination, pressure measurements are collected from three fill experiments for each of all possible combinations of 0, 1, and 2-Channels versus 0, 33, 50, 67, and 100% channel length. As an exception, experiments are not performed for TN12CH at 100% channel length, as this configuration results in the fluid exiting from the exit gates before any useful data pressure can be collected. Fill experiments show some configurations have significant dry areas at the end of the fill, thus some pressure configurations will not represent complete fill times. Viscosity and temperature of corn syrup is measured before and after fill experiment to verify properties have remained constant over the process of filling.

5.3 Obtaining Permeability from Transient Inlet Pressure Data

For radially symmetric flow in a 0-Channel mold, the pressure profile at a fixed radius gives a meaningful value for comparison with the theoretical Equation 4.12. The flow and pressure fields are expected to be complex and three-dimensional due to lack of radial symmetry and non-uniform features through the thickness for 1-Channel and 2-Channel molds. Additionally, 0-Channel, 1-Channel, and 2-Channel molds may have significantly different spatial pressure distribution. Thus, pressure measurement made at a single location on an internal mold wall is less meaningful for comparison and theoretical validation.

Transient inlet pressure is selected as the measured value to quantify effect of channel configuration on molding pressure. Inlet pressure shows the total reduction in pressure achieved by introducing channels. In addition, inlet pressure yields the maximum molding pressure, a meaningful characterization of the molding operation as a whole.

In Equation 4.12, pressure in a disk at a given radial location becomes undefined as R approaches 0, and thus cannot be used to generate inlet pressure curves, however with some manipulation a more useful form of the equation can be obtained. Equation 4.8 can be expressed for the transient pressures $P_1(t)$ and $P_2(t)$ at radii R_1 and R_2.

$$P_1(t) = \frac{Q\mu}{(1-v_f)4\pi HK_{rr}} \ln \frac{R_f(t)}{R_1}, \text{ and} \tag{5.1}$$

$$P_2(t) = \frac{Q\mu}{(1-v_f)4\pi HK_{rr}} \ln \frac{R_f(t)}{R_2}. \tag{5.2}$$

Then, Equations 5.2 and 5.2 are subtracted to find the pressure drop between the two points as,

$$P_2(t) - P_1(t) = \frac{Q\mu}{(1-v_f)4\pi HK_{rr}} \ln \frac{R_2}{R_1}. \tag{5.3}$$

The fluid front must have passed both locations of interest for the expressed pressure drop to be meaningful. When the two radial locations of interest R_1 and R_2 are fixed, the pressure difference between two radial locations is observed to be constant; independent of time, and a function of only constant experimental parameters. This constant pressure difference also implies that all pressure curves are identical in shape, and can be superimposed by shifting along the pressure axis.

It is expected that the inlet pressure curves can be similarly superimposed on curves from locations within the mold, since at constant flow rate pressure drop between the inlet and a given radial location will remain constant barring any upstream or downstream influences on the flow over time. This behavior is confirmed experimentally. The pressure at the inlet and at R=12.7 mm (0.5 in.) along with the corresponding theoretical pressure curve are depicted in Figure 5.2. The difference between the inlet pressure and the R=12.7 mm pressure is shown in Figure 5.3. The pressure difference does in fact remain constant after an initial startup period. Startup period is believed to result due to inlet effects. In particular, data tends to indicate that inlet effects are present due to hose bulging during the sharp increase in pressure at startup. This causes an initial reduction in flow rate into the cavity as system volume upstream of the inlet increases. Reduced inlet effects are observed when reinforced tubing is used.

Some inlet effects may also be due to reduction in the permeability as the incoming flow compresses the fiber preforms, or due to increased surface interface effects which are more prevalent at startup. For the ideal case, pressure difference would be constant from the time wall transducer initially registers a pressure reading, so some error is expected due to inlet effects.

Using Equation 5.3 and the knowledge that pressure drop between the inlet and a given radius is a constant, C_r, the pressure at the inlet, $P_i(t)$, can be expressed in terms of the pressure, $P_r(t)$, at the arbitrary radial location, $R=r$, and constant molding parameters as,

$$P_i(t) = \frac{Q\mu}{(1-v_f)4\pi HK_{rr}} \ln \frac{R_f(t)}{r} + C_r . \tag{5.4}$$

This equation states that the pressure at the inlet is equal to the sum of the pressure drop between a given location and the fluid front and the pressure drop between the inlet and that location. For curve fitting, it is more convenient to substitute Equation 4.11 into Equation 5.4 to obtain pressure in terms of t and t_r, the time that the fluid front crosses $R=r$, to obtain

$$P_i(t) = \frac{Q\mu}{(1-v_f)8\pi HK_{rr}} \ln \frac{t}{t_r} + C_r . \tag{5.5}$$

In this study, Equation 5.5 is used to curve fit to inlet pressure data. The time, t_r, is arbitrary, and sets the time at which curve fitting starts. It also affects the value of C_r obtained, which for a good curve fit is very near the pressure at time t_r. The time, t_r, is selected to avoid the region of inlet effects. Similarly, the end time, t_e, is selected to avoid artifacts at the end of filling, if they are present. All other parameters are measured fill parameters, except K_{rr}. Similar

manipulation is performed in ref [63] for molding of a disk in the absence of preform, in which an equivalent radius is presented that allows the theoretically undefined inlet pressure to be expressed using flow equation for inside the disk.

In order to fit Equation 5.5 to pressure data, a least squares error fit is used. The difference between the pressure data and the value from Equation 5.5 is squared for each data point between t_r and t_e, then all squares are summed to obtain the total error value. Each error point multiplied by an appropriately sized scalar, in order to obtain a total error value that is within several orders of magnitude of 1. This scaling method is used, rather than dividing by the number of data points, to ensure stability when using numerical methods in Microsoft Excel, which yields poor results for extreme values, and does not affect the parameters which result in the overall minimum error. The "Solver" feature in Microsoft Excel XP is used to solve for the K_{rr} and C_r to obtain the minimum total error.

Using this method, permeability can be measured using a single inlet transducer. Although this method is more complex, it has several substantial advantages over the permeability measurement method described in Chapter 4. Most importantly, inlet pressure represents the limiting, maximum pressure, which is an important molding parameter. Additionally, a transducer mounted in the actual mold cavity is intrusive, and may not be well suited to many molding operations. The inlet pressure transducer used for this study is located on the hose just upstream of the inlet gate, as shown in Figure 4.1. This location only captures pressure generated in the cavity, and does not include losses in the line

or mixer. The anticipated pressure drop is expected to be constant in the line and mixer at constant flow rate, thus it is expected the proposed method could be used upstream to measure permeability based on total required pressure.

5.4 Pressure Drop in a Channel

Pressure drop in a single channel is calculated as a starting point towards predicting the effectiveness of channels at reducing mold pressure. It is obvious that there will be less resistance to fluid flow and thus, lower pressure drop in the channel compared to flow through bulk preform. However the magnitude of the difference is relevant. If the resistance to flow is not significantly lower in the channel only marginal overall pressure reduction may be observed. On the other end of the spectrum, determining necessary channel dimensions to make sure specified channel size is not larger than required to help reduce scrap and post molding cleanup is important.

The channel is modeled as a rectangular duct. For duct flow head loss, h_L, is calculated using,

$$\frac{h_L}{l} = \frac{f}{D_h}\frac{V_S^2}{2g}, \tag{5.6}$$

where l is the duct length, f is the friction factor, V_s is the superficial velocity, g is the acceleration due to gravity, and D_h is the hydraulic diameter. The hydraulic diameter, D_h, is calculated from the rectangle cross section side lengths a and b as,

$$D_h = \frac{2ab}{a+b}. \tag{5.7}$$

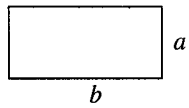

And the Reynolds number is defined as

$$\mathrm{Re}_h = \frac{\rho V_S D_h}{\mu}, \tag{5.8}$$

and the constant, *C*, is defined as,

$$C = f\,\mathrm{Re}_h. \tag{5.9}$$

Head loss is converted to pressure drop using,

$$\Delta p = h_L \rho g. \tag{5.10}$$

Substituting Equations 5.8-10 into Equation 5.6 yields,

$$\frac{\Delta p}{l} = \frac{C\mu}{D_h^2}\frac{V_S}{2}, \tag{5.11}$$

in which the constant, *C*, is dependent on *a*/*b*, and is tabulated in fluid mechanics textbooks to be C =56.9 [71].

The pressure drop for both 1 and 2 unblocked channels is desired. The unblocked channel length is l =76.2 mm (3 in), and the channel depth and width are a=b=3.175 mm (0.125 in). The hydraulic diameter is calculated using Equation 5.7 to be D_h =0.003175 m. The fluid viscosity is assumed to be 100 cp, which is representative of the flow simulation experiments. Assuming that the entire flow rate, Q =5.83x10^{-6} m^3/s, enters and remains in the channels, the superficial velocity for N channels (n=2N) is found using conservation of mass to be,

$$V_S = \frac{Q}{nA} = \frac{Q}{nab}. \tag{5.12}$$

The resulting pressure drop in a 1-Channel mold is Δp = 6219 Pa (0.90 psi), and for a 2-Channel mold is Δp = 3109 Pa (0.45 psi). The actual pressure drop in the channel is expected to be lower, since some fluid will bleed off into the preform. The predicted channel pressure drop is significantly less than the 100-200 kPa (15-30 psi) typically measured in filling experiments, thus, the fluid is expected to prefer the channels.

An effective permeability for the channel is calculated as another comparative indicator resistance of the channel compared with that of the preform. From Darcy's law,

$$V = \frac{K}{\mu}\frac{dp}{dx}. \tag{5.13}$$

Thus, by equating Equations 5.11 and 5.13,

$$K_{eff} = \frac{2D_h^2}{C}. \tag{5.14}$$

The effective permeability for the channels is calculated to be K_{eff} = 3.54 x10^{-7}m^2, which is three orders of magnitude higher than the typical permeabilities for mats used in this study at about 20% fiber content. Thus, effective permeability is a second indicator that fluid paths will prefer channels to preform. This preference is visible in Figure 5.4 in which the first two seconds of inlet pressure measured for both 0-Channel and 1-Channel molds are graphed. The 0-Channel pressure is seen to increase immediately, while the 1-Channel mold has exhibits linear pressure increase for a short duration as the channel on the top mold wall fills,

after which pressure begins to increase more substantially. A linear pressure increase is expected behavior at the inlet for pure duct flow. This behavior is observed at the beginning of many channel mold pressure profiles, and is not seen in 0-Channel moldings.

5.5 Theoretical Pressure Predictions for Mold with Single Channel

A simplified theory to predict the inlet pressure profile for a single channel mold is developed. Several assumptions reduce the complexity of the calculations. First, it is assumed that pressure drop in the channel is small in comparison to pressure changes throughout the rest of the mold cavity, and resistance to flow in the channel is assumed to be negligible, such that fluid can easily feed any point along the channel. These assumptions allow the entire channel to be treated as an inlet at uniform pressure. Effects in the thickness direction are ignored, and the flow is treated as if it enters the cavity with a uniform in-plane velocity. The channel is assumed to start completely full of fluid. The volume and width of the channel are ignored, thus flow originates along a line segment that is represented by a diameter on the disk; not from the line segment along the channel edge a half channel width away from the diameter segment. Figure 5.5 depicts the geometry used for the calculation. In Figure 5.5, x represents the distance from the centerline, and $w(x)$ is the width of the cavity parallel to the channel at a distance x from the channel. The fluid velocity is assumed to be uniform at a given x. This implies that edge effects are neglected; a common assumption used for flows through porous media.

The given assumptions lead to simple "channel" flow through porous media with varying channel width (i.e., $w(x)$), where "channel" refers to the mold cross section perpendicular to the flow direction, not the pressure reducing flow channels. The solution to this flow is a straightforward application of Darcy's law in one dimension,

$$V(x) = \frac{K}{\mu}\frac{dp}{dx}. \tag{5.15}$$

To obtain the velocity as a function of x, we need an expression for the width, $w(x)$, as a function of x, given as,

$$\left(\frac{w(x)}{2}\right)^2 + x^2 = R^2, \tag{5.16}$$

which can be rearranged to yield

$$w(x) = 2\sqrt{R^2 - x^2}. \tag{5.17}$$

Due to symmetry, half of the flow enters each half of the disk, and the velocity is given using the half the flow rate divided by cross-sectional area as,

$$V(x) = \frac{0.5Q}{A} = \frac{0.5Q}{2Hw(x)} = \frac{Q}{8H\sqrt{R^2 - x^2}}. \tag{5.18}$$

Equation 5.15 is rearranged, and integrated from the inlet to the fluid front location, X, as

$$\int_0^X V(x)dx = \frac{K}{\mu}\int_{inlet}^{front} dp. \tag{5.19}$$

The pressure is 0 at the fluid front, thus the integral becomes,

$$p_{inlet} = \frac{Q\mu}{8KH}\sin^{-1}\left(\frac{X}{R}\right). \tag{5.20}$$

Finally, the maximum pressure occurs when the mold is full at $X=R$, and is,

$$p_{\max} = \frac{Q\mu\pi}{16KH}. \tag{5.21}$$

The fluid front location, X, can be calculated at any time from the flow rate and geometry, thus Equation 5.20 is sufficient to generate pressure profiles for a 1-Channel mold.

5.6 Theoretical Pressure Predictions for Mold with Two Channels

The assumptions and initial setup used for pressure calculation in the 1-Channel mold serve as the starting point for pressure calculations in a 2-Channel mold. Both channels are assumed to act as the inlet, and one-dimensional flow is assumed. The solution differs in the geometry used to calculate the flow cross section. The flow geometry used for calculations is shown in Figure 5.6. Due to symmetry, only one eight of the disk needs to be used in calculations. Fluid is drawn in an eighth of the disk in the top right of Figure 5.6, clockwise of line OR shown in Figure 5.6. The flow in this octant is assumed to remain parallel to the horizontal channel, and due to flow symmetry, the fluid in a given octant does not cross the symmetry line. The one dimensional flow assumption requires the OR line to be treated as a solid edge with negligible effect on flow, resulting in a perpendicular flow front junction as flow moves along the OR line. However, it is more reasonable that the flow will curve at this line, thus, the assumption may not hold as well as those for the 1-Channel case.

To get the velocity as a function of x, an expression for the width as a function of x, $w(x)$, is used,

$$w(x) = R\cos\left(\sin^{-1}\left(\frac{x}{R}\right)\right) - x. \tag{5.22}$$

Due to symmetry, 1/8 of the flow enters each 1/8 of the disk, and the velocity is given using the half the flow rate divided by the area of a cross-section as,

$$V(x) = \frac{1}{8}\frac{Q}{A} = \frac{1}{8}\frac{Q}{2Hw(x)} = \frac{Q}{16H\left(R\cos\left(\sin^{-1}\left(\frac{x}{R}\right)\right) - x\right)}. \tag{5.23}$$

Integration in one-dimension from the inlet to the fluid front location, X, yields

$$\int_0^X V(x)dx = \frac{K}{\mu}\int_{inlet}^{front} dp. \tag{5.24}$$

The pressure is 0 at the fluid front, thus the inlet pressure is

$$p_{inlet} = \frac{Q\mu}{16HK}\int_0^X \frac{1}{R\cos\left(\sin^{-1}\left(\frac{x}{R}\right)\right) - x}. \tag{5.25}$$

This equation is integrated numerically using the trapezoid rule and a 0.1 second time step to generate pressure curves. For this integration value of X at each step is calculated from time and mold geometry. Pressure in Equation 5.25 becomes unbounded at the fill time of the disk, due to cross sectional flow area converging to zero which results in infinite flow velocity. Under no circumstances would one expect maximum fill pressure to increase above the baseline pressure upon addition of lower resistance fluid paths, thus Equation 5.25 is not a good representation of pressure at the end of the flow.

Figure 5.7 depicts theoretically generated transient pressure curves based on parameter values typically used for molding experiments performed in this study for 0-Channel, 1-Channel, and 2-Channel molds, using Equations 5.5, 5.20, and 5.25, respectively. Mold dimensions are used for geometric parameters, and measured volume flow rate of 5.83×10^{-6} m^3/s is used. Representative values are selected for fluid and mat properties, with a fluid viscosity of 100 cp and mat permeability of 5.2×10^{-10} m^2 selected. Additionally, an offset pressure which results in the resulting maximum pressure being consistent with experimentally measured values is assumed for the 0-Channel mold theory.

Addition of channels is observed to significantly alter the flow behavior. For the 0-Channel mold, the pressure increases dramatically at the beginning of the flow, and increases more gradually towards the end of filling. For 1-Channel and 2-Channel molds, the theoretical equations predict pressure gradual pressure increase at the beginning of the flow and much more quickly at the end of filling. At half of the fill time, the addition of a single channel is predicted to reduce fill pressure to about one fourth of its original value, and the pressure in the 2-Channel mold is about a third of that in the 1-Channel mold. The final pressure in the 1-Channel mold has increased to about 85% of the 0-Channel pressure value. The 2-Channel pressure is undefined at the end of filling, but it is observed to be less than 50% of the 0-Channel pressure just before filling is complete.

The channels result in such a fundamental change in pressure requirements due to the way they affect flow area. In a 0-Channel mold, the fluid around the inlet has a small flow area, resulting in high local velocities and an immediate increase in pressure. Initial flow with one or more channels is spread out along the length of the channel This leads to an additional expected benefit, with reduced void formation anticipated due to the slower moving fluid front. It is possible that the increase in pressure for the 1-Channel and 2-Channel molds at the end of filling is purely an artifact resulting from the assumed cross sectional flow area reducing to zero, and that end pressures will remain at lower values due to deviations from assumptions at end of filling.

5.7 Fluid Front Profile Measurement for Channel Molds

The first step towards experimentally characterizing the effect of channels on molding operations is to mold, cure, and examine disks covering the spectrum of available channel configurations, and at several preform volume fractions. A total of 42 disks are fabricated for this purpose, using zero-channel, 1-Channel, and 2-Channel top mold walls. All channel lengths, i.e., 0, 33, 50, 66, and 100% of disk radius, are considered. Molds are filled with 2, 4, 6, and 8 layers of the thick chopped-strand glass fiber mat, planar density measured to be 0.446 kg/m^2, representing fiber volume fractions of approximately 10, 20, 30, and 40%, respectively. Filling for some disks is stopped at two or four seconds, resulting in a short shot showing intermediate fluid front profile shapes. Table 5.1 contains configurations details for each of the 42 disks. Table 5.1 also includes a special

column, which is used to designate mold edges have been treated with hot glue in order to reduce so-called ray tracing effects. A photograph of all disks molded is shown in Figure 5.8.

Each disk is observed and photographed top and bottom. Major features of interest are for macrovoids, fluid front shape, clarity, and color. Special care is taken in the preparation of figures generated from disks. Images must be processed in order to have sufficient contrast to view important macro scale features when printed. However, clarity and color are important indicators of microvoid content, so figures must be prepared as uniformly as possibly to allow visual comparison. A uniformly lit white background is used behind the disks. A Sony Cybershot 2.1 megapixel digital camera is set on a tripod as closely to the disk as possible to maximize resolution of final images. Each disk is placed in the same location, and camera, background, and lighting are left in place for each photographs, so raw images are as uniform as possible.

Disk images are prepared using Adobe Photoshop image processing software. Each image is processed using the same sequence in Photoshop. Initially, the image size is cropped to 320x320 pixels. The "auto contrast" filter and "auto levels" filter are used on the image in succession to set appropriate contrast and brightness levels. The disk and white background are the only entities in the pictures, so these filters adjust the images in a consistent fashion. Finally, pure white is filled over the background and any shadows around the disk for a more attractive print.

5.8 Visual Characterization of Disks Fabricated Utilizing Channels

Figures 5.9-5.50 represent photographs of all molded disks in the channel study. In each figure, a photograph of the top of the disk labeled "a" is presented on the left, and a photograph of the bottom of the disk labeled "b" is on the right. Parts are molded with inlet gate on the top mold wall, and the location of inlet gate is visible at the center of each of the "a" figures. For more transparent disks, the inlet location is visible through the disk in the bottom picture as well. A thin black ring is visible around a substantial percentage of the perimeter of each disk is the shadow of the disk which is lit from above.

Figure 5.9 and Figure 5.10 are photographs representing the baseline case of disks molded without flow channels. Figure 5.9 is from disk 0K4R containing 20% fiber volume fraction, and Figure 5.10 is from disk 0K4R containing 30% fiber volume fraction. Each disk is observed to have filled completely, and appears similar from both the top and bottom. The disk molded at 30% fiber volume fraction is less transparent, which can be determined by noting that Figure 5.10 is darker than Figure 5.9. In general, higher quality parts are observed to be more transparent due to lower void content. Lower volume fraction parts are also more transparent, as there is a mismatch in the index of refraction between the cured resin and the glass fibers. At lower volume fractions, there are fewer fiber-matrix interfaces, and more light passes through the part.

Several features can be seen in the photographs, which are not artifacts of the molding process. Small dark line segments are visible in both figures.

Fiber mats are marked with a black felt tip pen so they can be cut to shape, and during handling some of the black glass fibers get spread. This also results in a black or green ring just inside the outer edge of some disks. Slight green discoloration is visible in the upper right quadrant in Figure 5.10a. Discoloration is due to an identifying label that has permanently discolored the surface of the disk. The slightly darker region in the top left of Figure 5.9a is due to slightly non-uniform lighting. Image processing is designed to highlight molding features, and also enhances this non-uniformity in the lighting which was undetectable to the eye during photographing. Since no dark region is visible in the photograph from the bottom of the disk, it can be ascertained that the dark region does not represent a less transparent region.

Figures 5.11-5.14 are photographs of disks molded in 1-Channel molds at fiber volume fractions of 10, 20, 30, and 40%, respectively. In each image, the resin remaining in the single flow channel after molding is visible in the picture from the top of the part. Damage to this resin can occur during demolding, such as the section visible on the right of Figure 5.14a. The disk depicted in Figure 5.11, molded at 10% fiber volume fraction, is observed to be very transparent. This results from the low volume fraction. Large macrovoids are visible around the perimeter of the disk. Flow channel makes no observable difference in the low volume fraction case, as the two layers of preform do not completely fill the mold cavity, resulting in very high permeability throughout the cavity. At the three higher volume fractions, however, effect of channel on flow is dramatically visible.

In Figure 5.12, a transparent band approximately 1 in. wide is visible straddling the channel. This region is the result of flow nearly uniformly moving out from the channels. Outside this band, there are two semicircular opaque high void content regions observed. These regions occur as a result of an unwanted side effect induced by the channel. Fluid reaches the edge of the disk quickly through the channel, and finds a continued low resistance flow path between the preform and mold edge. The flow quickly circles the perimeter of the disk, then flows inward trapping the semicircular region of air. Fluid traveling ahead at preform boundaries is an effect called ray tracing, which is typically avoided in RTM. At 20% volume fraction, permeability is lower, and a completely dry spot is not observed in Figure 5.12, however dry spots are observed at 30% and 40% volume fractions in Figures 5.13 and 5.14, respectively. It is thought that this is due to more similar flow resistances between channels, edge gap, and preform, Resin is also expected to more easily flowing into the dry regions after molding, but before resin has cured. The dry region observed at 40% volume fraction is observed to be smaller, and closer to the edge of the disk. At this higher volume fraction, more mat layers result in more layers touching the mold edge at any given location, resulting in less ray tracing. The linear fluid front in this case lasts longer before fluid completely rings the mold and creating the dry spot. All disks depicted in Figures 5.11-5.14 appear similar from both the top and bottom, two-dimensional flow may be a good approximation.

Figures 5.15-5.18 are photographs of disks molded using 2-Channel molds at fiber volume fractions of 10, 20, 30, and 40%, respectively. In each

image, the resin remaining in the each flow channel after molding is visible in the picture taken of the top of the part. Parts molded utilizing 2-Channel mold are observed to be very similar in nature to those molded with 1-Channel molds. The part molded with 10% fiber volume fraction, depicted in Figure 5.15, is observed to have high transparency and no macrovoids or dry spots. At a slightly higher volume fraction of 20%, four regions of high void content with many large macrovoids are observed in each quadrant in Figure 5.16. At the higher two volume fractions of 30 and 40%, 4 quarter-circle shaped dry spots clearly resulting from air trapped by ray tracing effect are observed. A plus shaped area of resin around the two flow channels shows that initial flow is predicted-first filling the flow channel, then flowing out with a very linear flow front from the channels. In Figure 5.18, the dry section is observed to have a wider band of resin on the perimeter of the disk, indicating that significant flow occurred from the edge towards the center, and thus, high volume fraction is not a guarantee of reduced ray tracing effect. Dry areas in the 2-Channel mold are nearer to mold wall than those observed in 1-Channel mold indicating more of the disk has been filled when ray tracing effects become prominent.

To counteract ray tracing effects, channel length is shortened to cover 2/3 the disk diameter, with channel centered at the inlet. Equation 5.5 can be used to show the pressure gradient near the edge of the disk is much lower than at the inlet, thus it is expected that the pressure relieving benefit of the channel will not be significantly reduced at this shortened channel length. Figures 5.19 and 5.20 depict photographs of disks which were molded with a single flow channel,

reduced to 67% of its original length containing 20% and 30% fiber volume fraction, respectively. At 20% volume fraction, a very small area of high void content is observed near the edge at the two locations furthest from the channel; otherwise visually the part quality appears quite good. At 30% volume fraction, a small internal dry area is visible in the same location. This dry area has been covered with resin on the top and mold walls, so it is completely encased in resin. The fact that these problem areas are near the mold wall indicates that the mold was nearly full before ray tracing effects took over and trapped air in the part. The patch of visible fibers visible at the top of Figure 5.20a is the result of damage during demolding, not the fill dynamics. Reducing channel length to 67% is observed to significantly decrease ray tracing and improve part quality, however deficiencies are still present.

Disks are molded utilizing 2 flow channels reduced to 67% percent of the disk diameter. Figure 5.21 depicts disk molded with 20% fiber volume fraction, and Figure 5.22 depicts disk molded with 30% fiber volume fraction. Good part quality with no visible dry patches or void concentration zones is achieved in both cases. Parts are observed to be transparent, with channel resin being clearly visible through the part in the photographs taken from the bottom of the mold cavity. The two flow paths added by the second channel near the regions of air entrapment have eliminated problems observed in molded disks with 1-Channel mold. The four areas where voids might be expected between channels near the edge of the mold wall exhibit good part quality. The exit gate is just past the mold edge in these locations, and probably contributes to expulsion of voids at

these locations. Additionally, at full channel length dry zones are observed to be nearer the channel edge for 2-Channel molds compared with 1-Channel molds, and the dry zones were already quite near the edge for 1-Channel reduced to 2/3 of the initial length.

Channel length is further reduced to 50% of the disk diameter in an effort to completely eliminate ray tracing effects. Figure 5.23 and Figure 5.24 are photographs of disks utilizing 1-Channel molds containing 20% and 30% fiber volume fraction, respectively, and Figure 5.25 and Figure 5.26 are photographs of disks utilizing 2-Channel molds containing 20% and 30% fiber volume fraction, respectively. Part quality for all disks molded at 50% channel length is observed to be good. Figure 5.26 is much less transparent than the others, however no specific problem areas are observed, or expected considering the 2-Channel mold had good part quality at longer channel length. The odd opaque disk is observed during fabrication, and is typically due to additional microvoids formed when exit clamps leak, allowing cure pressure to decrease. In Chapter 3, benefit of post fill cure pressure is discussed on molded parts. Four additional disks are molded utilizing 1-Channel and 2-Channel molds which have had the channel length further reduced to 1/3 the disk diameter and both 20% and 30% volume fraction. No further variation in part quality compared with 50% length channels is expected or observed. These fill parameters, however, are expected to yield useful pressure measurement results. Photographs of these disks are included for completeness in Figures 5.27-5.30.

5.9 Identifying Intermediate Fluid Front Positions in Channel Molding

Transient fluid front shape during molding can be determined experimentally by direct observation of the fluid front through transparent mold walls, or by mounting sensors in the mold cavity which detect fluid contact [63]. In the present study, the fluid front shape is found by molding parts which are only partially filled. A series of parts are molded to gain a clearer understanding of flow pattern in disks molded using channels. During the filling stage, resin is only injected into the cavity for a fraction of the fill time, then the part is cured and demolded as usual. These "short shots" are performed using 2 and 4 second fill times for selected channel configurations. Prior to curing, capillary effects drive some fluid motion at the fluid-air interface. The resulting interfaces observed in the cured part are believed to be rough compared to the fluid front at the moment injection stops, however interfaces still give a clear picture of the fill status.

Figures 5.31-5.36 contain photographs of disks molded utilizing a single flow channel which have been only partially filled. Figures 5.31 and 5.32 depict disks containing 20% and 30% glass preform, respectively, that were filled for 2 seconds. Figures 5.33-5.36 depict disks containing 10%, 20%, 30%, and 40%, respectively, filled for 4 seconds before curing. In Figure 5.31, the fluid is observed to have completely filled the channel, and fluid front has traveled a fairly uniform distance from the channel at all radial locations, which is similar to the expected behavior. The distance between the channel and the fluid front is

observed to be slightly greater at a location between the mold wall and the symmetry line in the flow direction. This increase could be some combination of contracting flow area driving the fluid forward and ray tracing effects at the edge. It is likely that the effect is due to contraction rather than ray tracing, since the fluid front has advanced farthest at a location away from the mold boundary . In Figure 5.31b, the top of the fluid front has advanced considerably farther than the bottom, indicating at startup through-the-thickness effects are important. At higher volume fraction, fill pattern after 2 seconds is observed to be different. In Figure 5.32, several differences are observed in the disk molded at 30% fiber volume fraction. Fluid front is more uniform top to bottom, indicating that comparatively, fluid moves through the thickness more easily at the higher volume fraction, and thus, in-plane permeability has decreased more than through-the-thickness permeability. As a result, 2D flow models may be more applicable at higher volume fractions. Ray tracing effect is obvious in Figure 5.32, with fluid progressing much further along the edge of the disk.

Disks depicted in Figures 5.33-5.36 have been filled for 2 seconds longer, and additional volume fractions of 10% and 40% are included. At 10% volume fraction, presented in Figure 5.33, it is clear why dry spots are not observed in the completely filled disk molded at this configuration, depicted in Figure 5.11. Channel has influenced the front shape, resulting in an oblong front as opposed to a circular front expected without flow channel. However, channel does not completely dictate flow shape as it did at higher volume fractions. The observed flow front shape in Figure 5.33 will not result in any weld lines or trapped air

when it contacts the mold edge. Flow has barely contacted the center of the bottom mold wall in Figure 5.33b, even though the fluid front is well advanced at the top mold wall in Figure 5.33a, making it apparent that flow is mainly occurring between the preform and top mold walls. This will result in trapped air when the fluid begins to penetrate down through the thickness, and explains the large macrovoids observed in the final part depicted in Figure 5.11. The through-the-thickness flow is similar to flow pattern in SCRIMP™ process. In SCRIMP™, however, macrovoids are avoided by evacuating air prior to filling with vacuum assistance.

Disks depicted in Figures 5.34 and 5.35 contain same volume fractions as those Figures 5.31 and 5.32, respectively, and can be directly compared. In Figure 5.34, it appears that flow area contraction effects continue to dominate ray tracing effects at 20% fiber volume fraction. Flow has advanced further ahead near the flow edges, but the thin band of resin along the edge visible in Figure 5.35, which is an obvious ray tracing effect, is not apparent in Figure 5.34. It is possible that the higher permeability of 20% preform has allowed resin to more quickly flow from the edge inward at the lower volume fraction. In Figure 5.36, the disk molded at 40% fiber volume fraction is observed to have significant ray tracing effect on one side. Asymmetric ray tracing effect observed in Figure 5.36 is most likely result of preform not placed directly in the center of the cavity. Fluid front distance from channel and mold edge are similar and thus, mold edge appears to be behaving as an extended channel. This distance from channel is much shorter and more uniform along channel length and at top and

bottom mold walls than at lower volume fraction. The extreme mismatch in channel and preform permeability result in conditions which more closely match the assumptions the theoretical approximation was based on.

Two second short shots of disks molded with 2-Channels containing 20 and 30% fiber volume fraction are depicted in Figures 5.37 and 5.38, respectively. Results are similar to those observed for 1-Channel molds, with flow area reduction effects visible in mold containing 20% fiber volume fraction, and ray tracing effects observed more prominently at the higher volume fraction. Through-the-thickness flow effects are visible in both figures, with top of the fluid front being more advanced. The 2-Channel mold is thought to exhibit transverse effects at two seconds while the 1-Channel mold did not at this point due to doubled total channel length. Fluid spends more time filling channels, and has double flow area afterwards, resulting in the extension of startup effect duration.

Photographs of four second short shots for 2-Channel molds are depicted in Figures 5.39-5.42. Volume fractions of 10%, 20%, 30%, and 40% are represented in these figures. At 10% volume fraction, 2-Channel mold is observed to be quite different in Figure 5.39 compared to 1-Channel mold at this volume fraction. The 1-Channel mold exhibited flow between the top mold wall and the preform, with channels influencing, but not dominating front shape. In figure 5.39, flow front appears along the bottom mold wall, with fluid contacting top mold wall at random locations. Flow front shape is oblong and does not coincide with features that might be anticipated to result from the flow channels. It is believed that the flow probably followed a similar pattern as the 1-Channel

mold, and filled above the preform first, probably to an even larger extent as the flow front is observed to be more advanced. Subsequently, the fluid impregnated down through the preform under gravity effects and deposited on the bottom mold wall. It is unclear why gravity did not affect the 1-Channel molding. Perhaps different molding temperatures resulted in varied resin viscosity or quicker cure times for one of the parts.

Figure 5.40 is quite similar to Figure 5.37. These disks are molded at 20% fiber volume fraction at 4 and 2 seconds, respectively. Bottom flow front has advanced to nearer to top after 4 seconds, however no additional flow features are observed. At 30% volume fraction, Figure 5.41 captures the flow at an interesting point. Flow front near the channels remains in a similar location as it has been after 2 seconds. Additional fluid injected has contributed to ray tracing effect. Ray tracing progressed at slightly different rates from the end of each channel, resulting in one quadrants which has trapped the which will ultimately lead to one of four dry spots, and the other three quadrants nearing that point. The size of the dry spot in Figure 5.41 is considerably larger than in the completed part (depicted in Figure 5.17). Air in the dry spot is apparently compressed as molding progresses. In Figure 5.42, the disk molded at 40% fiber content does not exhibit a stage of flow as advanced as that observed at 30% fiber content after 4 seconds. It is possible that human error contributed to a shorter flow time for this disk. More likely, higher injection pressures at this high volume content has caused some of the fluid to contribute towards hose expansion. This is similar to problem encountered in pressure measurement

experiments previously. Top flow front is ahead of bottom in this figure, indicating that with additional channel contributes to increased inlet effects even at high volume fraction. Comparing Figures 5.39-5.42, it is apparent that higher volume fraction contributes to a more linear flow front moving away from each channel, and that ray tracing effects are more prevalent and higher volume fractions.

The observed part quality for molded disks with channel length restricted to 50% of disk diameter was found to be superior to those molded at longer channel lengths. Four second short shots are performed for 1-Channel and 2-Channel disks using this reduced channel width. Photographs of these disks are contained in Figures 5.43-5.46. Figure 5.43 depicts a disk molded with 4 layers of preform and a single flow channel with channel length set to of 50% of the disk diameter. The observed fluid front is much rougher than other disks molded at 20% fiber content-possibly due to aforementioned temperature effects after filling. Fluid front shape is much rounder compared with unblocked channel. Effect of rounder fluid front is less deviation in time fluid front first contacts mold edge, reducing likelihood of ray tracing effect and trapped air. At a higher volume fraction of 30%, depicted in Figure 5.44, the fluid front is very similar, however slightly less round. At higher volume fraction, radial flow from the inlet is delayed due to higher permeability. For 2-Channel molds, depicted in Figure 5.45 for 20% fiber content, and 5.46 for 30% fiber content, fluid front shape is even closer to round. Only slight extension of front is observed in the channel directions.

These four figures show significant difference in transient flow front compared with longer channels, and show why such improved part quality is observed for shorter channels. Flow for these cases deviates considerably from the assume flow used in theoretical approximations for the channel molds pressure, so deviation is expected at shorter channel length. Ray tracing effects are apparent within the first several seconds of molding at full channel length, however, so these curves are likely to deviate from predictions as well.

A small side study is performed, aimed at eliminating ray tracing for full length channels by removing flow path at disk edge. Prior to filling, hot glue is used to fill any potential flow gap at the disk edge. Parts are molded using 1 and 2-Channels, at 20% and 30% fiber content. Figures 5.47-5.50 depict disks molded using hot glue. At 20% fiber content, void regions are observed to be significantly reduced for the 1-Channel mold, and completely eliminated for the 2-Channel mold, as seen in Figure 5.49. At 30% fiber content, dry regions size is reducer for the 1-Channel mold in Figure 5.48, and are improved from a dry region to a high void region for the 2-Channel mold in Figure 5.49. The bottom of the 1-Channel disk depicted in Figure 5.48b sustained considerable damage during demolding, which can be distinguished from the dry region on close inspection. Although marked improvement is found for all cases, overall part quality is not improved enough to justify the overall configuration as viable. It may be possible to perform even better gap reduction, however the extra setup time most likely warrants addressing ray tracing issue by other means.

5.10 Pressure Reduction Results Observed in Channel Molds

It has been demonstrated in previous sections that parts can be molded that contain no visually detectably defects utilizing some channel configurations. With proper selection of number of channels and channel length, no macrovoids are observed. However, pressure measurements are necessary to quantify achieved pressure reduction and justify the process. Experiments are performed to compare pressure reduction observed in 1-Channel and 2-Channel molds compared with 0-Channel mold. Since reduced channel length is required to achieve good part quality, experiments are also performed to compare pressure reduction observed at channel lengths of 0%, 33%, 50%, 67%, and 100% of the disk diameter. Experiments are repeated at two additional preform configurations designated in Table 5.2, each with a fill viscosity set to allow good range of pressure measurements, as channel molded disks show variation in fill properties based on preform configuration used. Figures 5.51-5.67 depict transient pressure data from these experiments. Each experiment is repeated 3 times and each pressure curve in these charts represents an average of three experiments. Average curve is calculated by setting all curves to same start time, then taking a point by point pressure average.

Figures 5.51-5.56 depict results from pressure experiments performed with preform configuration TK4CH which involves 4 thick layers of chopped-strand glass fiber mat and corn syrup diluted to 118cp. Pressure results in Figure 5.51 represent the baseline pressure from a 0-Channel mold, along with pressure from 1 and 2-Channel molds with full channel length. Addition of a

single channel is observed to reduce significantly, with maximum observed pressure reduced by 68% from 158 to 49.8 kPa. A second flow channel further reduces the pressure by another 48% to a maximum observed inlet pressure of 26.1 kPa. Total pressure reduction from 0-Channel to 2-Channel case is 83%. This is a considerable reduction in pressure, and demonstrates channels are an effective pressure combatant. Maximum pressure values for all experiments in this series are tabulated in Tables 5.3 and 5.4.

Pressure curve in Figure 5.51 is fit to 0-Channel mold data as previously described to obtain permeability using Equation 5.5. Permeability is used to predict theoretical approximations of pressure in 1 and 2-Channel molds using Equations 5.20 and 5.25, respectively. Theoretical pressure predictions are observed to be considerably lower than measured pressure curve for approximately 2/3 of the fill. At the end of filling, theoretical pressure predicts higher rate of pressure increase, which is not observed in the experimental filling. Predicted pressure is too high at the end of filling, which is anticipated as the assumptions for linear flow front break down at end of fill. Differences also arise from the observed deviation of flow front shape from assumed profile. However, 1 and 2-Channel pressure curves are observed to increase nearly linearly for the duration, lending some credibility to the approximation. The linear increase of pressure as flow channels fill described previously is visible at the beginning of most fills with flow channel.

Figures 5.52-5.54 depict pressure results for TK4CH, at reduced channel lengths of 67%, 50%, and 33%, respectively. At each of these channel lengths,

pressure reduction between first and second channel is lower in magnitude, resulting in a decrease in the percent improvement achieved by adding a second channel. Of primary interest are results at 50% channel length, depicted in Figure 5.53, as this is the maximum channel length at which quality parts could be molded consistently for any number of channels and at any volume fraction. Pressure reduction from 0-Channel mold to 1-Channel blocked to 50% of its original length is 59%; pressure reduction for 2-Channels is by 64%. At this channel length, the addition of a second channel may not be worth the gain in reduced pressure.

Pressure results for TK4CH are presented grouped by number of channels in Figure 5.55 for 1-Channel and 5.56 for 2-Channels. These figures are useful to observe the effect of channel length on pressure reduction. The minimum reduction in pressure is observed at 33% channel length, with 50% reduction achieved by 1 channel, and 58% reduction for 2-Channels. Even at these short channel lengths, significant reduction in pressure is observed. For 1-Channel mold, little gain is observed when increasing channel length from 67% to 100%, however improvements are observed with each channel length increase for 2-Channel molds.

Fill experiments are repeated for configuration TN8CH, which has almost same fiber volume fraction, but uses 8 layers of thin preform to achieve it. TN8CH uses corn syrup diluted to 138 cp as the filling fluid. Results for these fills are presented in Figures 5.57-5.62. The fluid viscosity is increased for these experiments to compensate for increased permeability and flow channels in

order to achieve same magnitude of pressure as was observed for 0-Channel mold in Figure 5.57. Other pressures scale similarly in this set of results compared with TK4CH, with similar decreases in maximum pressures of 70% for 1 unblocked channel, and 82% for 2 unblocked channels observed in Figure 5.57. Theoretical pressure curves in Figure 5.57 are slightly closer to measured values than those in Figure 5.51. This is unexpected, as pressures are all similar in magnitude and relationship. The discrepancy occurs due to inlet permeability curve fit. Inlet permeabilities for this study are tabulated in Table 5.5. Table 5.5 also contains permeability results from similar volume fractions of the two preform types determined in Chapter 4. Permeability measured at the inlet is similar in magnitude and follows similar trends, but does not differ as much between preform configurations. Significant inlet effects need to be reduced before accurate permeabilities can be measured. Additionally, more measurements need to be taken to reduce statistical deviation, as results do not fall outside the range of individual measurements made in Chapter 4.

Figures 5.58-5.60 depict pressure results for reduced channel lengths reduced to 67%, 50%, and 33% of disk diameter, respectively. Percent reductions in pressure are nearly identical for each of these sets of curves. For channel length of 50%, identified as maximum channel length that quality disks can be fabricated using 1-Channel mold, 40% decrease in pressure is observed for single channel case. For channel length of 67%, the length which yielded defect free parts utilizing 2-Channel mold, pressure reduction of 71% is observed. At same channel length reduction in pressure due to second channel

is limited, however ability to increase channel length gives 2-Channel molds a significant advantage in this case.

In Figures 5.61 and 5.62, pressure results are again segregated into figures for 1 and 2-Channels. In Figure 5.61, differences are observed for 1-Channel mold compared with results for 4 thick mats. Almost identical pressure curves are observed for 33% and 50% channel lengths in Figure 5.61, while in Figure 5.55 reduction in pressure was observed over this range of channel lengths. However, thick mats were observed to have nearly identical pressure curves for 67% and 100% channel lengths, while difference is observed in thin mat pressure curves for these channel lengths. Some small variation in flow patterns exists between these two configurations that changes the maximum channel lengths after which no pressure change is observed.

Results for TN12CH are presented in Figures 5.63-5.67. TN12CH represents a higher volume fraction of ≅30%, composed of 12 thin mats, which is injected with a lower viscosity corn syrup blend (μ = 62.4 cp). Pressure results were unobtainable for 100% channel length, as ray tracing effects caused filling to end too soon after flow is initiated. The first set of curves, presented in Figure 5.63, are for channel length of 67% of disk diameter. Theoretical pressure curves are given on this chart, but are not directly comparable to any experimental data. At the higher volume fraction of TN12CH, addition of second flow channel is observed to have more significant effect on pressure reduction compared with lower volume fractions. For curves in Figure 5.63, maximum pressure is reduced by 57% for 1-Channel and and 77% for 2 flow channels.

Reduction percentage is similar to that observed lower volume fractions for 2-Channels mold, however the single channel is less effective at this channel length. From 5.64, pressure reduction for 1-Channel mold compared to 0-Channel is calculated to be 59% for 50% channel length, which is better than the reduction observed at lower volume fraction. Reduction in pressure for 2-Channel mold at 67% volume fraction is already given as 77%. Figures 5.66 and 5.67 group pressure results into those for 1 and 2-Channel molds, respectively. An important result, visible in these figures, is the similarity for both 1 or 2-Channel pressure measurements between channel lengths of 50% and 67%. This corresponds with very little difference in observed properties for parts molded with these channel lengths. This indicates that channel length must be carefully selected, as regions resulting in excess scrap and cleanup with no benefit to injection pressure exist.

5.11 Concluding Remarks

Addition of channels to RTM is shown to considerably reduce required injection pressure. Optical characterization of molded parts indicate that potential exists for macrovoids and degradation of part quality due to the addition of flow channels in the mold. This is mainly due to ray tracing effects, however combined study shows that channels can be configured such that good part quality is observed in conjunction with substantial reduction in pressure. Channel molding has several drawbacks, such as additional scrap and the necessity to remove the resin tabs from the final parts, but it is thought that

overall cost savings will result from the substantial reduction in pressure. In some cases, it is anticipated that the flow channels can be designed directly into the part, eliminating the need for their removal.

Greatest decrease in maximum observed fill pressure resulting from the addition of one flow channel is by 57%. This value is given for a channel length of 50% the disk diameter, which is the maximum channel length at which high quality parts are consistently observed. For channel lengths greater than 50%, further reduction in pressure is observed. However, large dry areas are observed in the molded parts for these channel lengths, thus part quality is unacceptable and no overall improvement is claimed. The addition of a second channels yields greater reduction in maximum observed fill pressure of 77%. The second flow channel is beneficial at reducing pressure because it adds a second low resistance flow path that brings fluid directly to the center of the large dry area observed in 1-Channel molded parts. This allows further pressure reduction as channel length at which no dry areas are observed is 67%, which is greater than the 1-Channel case. Overall, Addition of flow channels is shown to significantly reduce fill pressure as long as parameters such as channel length and channel location are correctly selected.

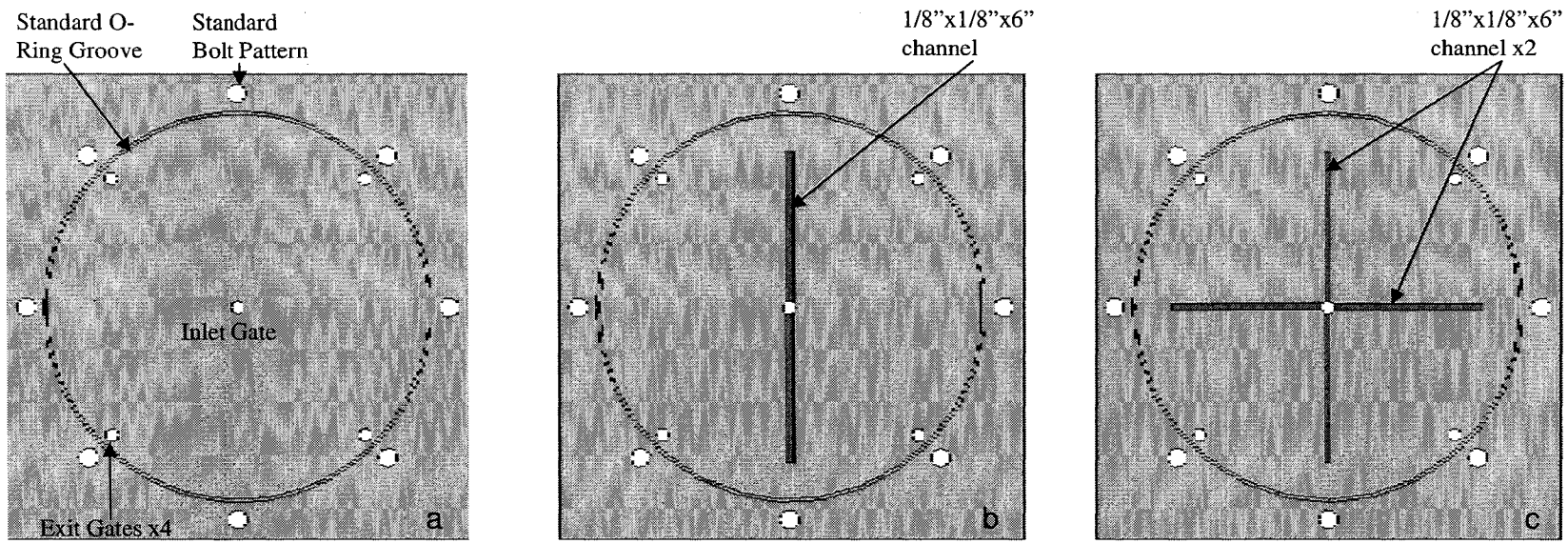

Figure 5.1 a:(left) Original top mold wall with no flow channels; b:(middle) Top mold wall with a single flow channel; c:(right) Top mold wall with two perpendicular flow channels

Table 5.1 Experimental configurations of fabricated disks used to observe effect of different channel configurations on molded parts

Designation	Channels	Channel Length	Fill Time	Mat Layers (≅ vf)	Special
0K4R	0	NA	Complete	4 (20%)	none
0K6R	0	NA	Complete	6 (30%)	none
1K2R	1	100%	Complete	2 (10%)	none
1K4R	1	100%	Complete	4 (20%)	none
1K6R	1	100%	Complete	6 (30%)	none
1K8R	1	100%	Complete	8 (40%)	none
2K2R	2	100%	Complete	2 (10%)	none
2K4R	2	100%	Complete	4 (20%)	none
2K6R	2	100%	Complete	6 (30%)	none
2K8R	2	100%	Complete	8 (40%)	none
1K4R-1/3B	1	67%	Complete	4 (20%)	none
1K6R-1/3B	1	67%	Complete	6 (30%)	none
2K4R-1/3B	2	67%	Complete	4 (20%)	none
2K6R-1/3B	2	67%	Complete	6 (30%)	none
1K4R-1/2B	1	50%	Complete	4 (20%)	none
1K6R-1/2B	1	50%	Complete	6 (30%)	none
2K4R-1/2B	2	50%	Complete	4 (20%)	none
2K6R-1/2B	2	50%	Complete	6 (30%)	none
1K4R-2/3B	1	33%	Complete	4 (20%)	none
1K6R-2/3B	1	33%	Complete	6 (30%)	none

Table 5.1 (cont.)

Designation	Channels	Channel Length	Fill Time	Mat Layers (≅ vf)	Special
2K4R-2/3B	2	33%	Complete	4 (20%)	none
2K6R-2/3B	2	33%	Complete	6 (30%)	none
1K4R-SS2	1	100%	2 s	4 (20%)	Short shot
1K6R-SS2	1	100%	2 s	6 (30%)	Short shot
1K2R-SS4	1	100%	4 s	2 (10%)	Short shot
1K4R-SS4	1	100%	4 s	4 (20%)	Short shot
1K6R-SS4	1	100%	4 s	6 (30%)	Short shot
1K8R-SS4	1	100%	4 s	8 (40%)	Short shot
2K4R-SS2	2	100%	2 s	4 (20%)	Short shot
2K6R-SS2	2	100%	2 s	6 (30%)	Short shot
2K2R-SS4	2	100%	4 s	2 (10%)	Short shot
2K4R-SS4	2	100%	4 s	4 (20%)	Short shot
2K6R-SS4	2	100%	4 s	6 (30%)	Short shot
2K8R-SS4	2	100%	4 s	8 (40%)	Short shot
1K4R-1/2B-SS4	1	50%	4 s	4 (20%)	Short shot
1K6R-1/2B-SS4	1	50%	4 s	6 (30%)	Short shot
2K4R-1/2B-SS4	2	50%	4 s	4 (20%)	Short shot
2K6R-1/2B-SS4	2	50%	4 s	6 (30%)	Short shot
1K4R-HG	1	100%	Complete	4 (20%)	Hot glue*
1K6R-HG	1	100%	Complete	6 (30%)	Hot glue*
2K4R-HG	2	100%	Complete	4 (20%)	Hot glue*
2K6R-HG	2	100%	Complete	6 (30%)	Hot glue*

*Edge of mold cavity filled with hot glue to reduce ray-tracing pathways.

Table 5.2 Experimental configurations used to examine effect of channels on pressure reduction

Designation	Description	Corn Syrup Viscosity (cp)	Volume fraction in mold (v_f)
TK4CH	4 thick layers of chopped-strand glass fiber mat. Planar density- Listed: 0.459 kg/m^2 (1.5 oz/ft^2) Measured: 0.4356+/-0.0060 kg/m^2 (95% confidence)	118	≅20%
TN8CH	8 thin layers of chopped-strand glass fiber mat. Planar density- Listed: 0.228 kg/m^2 (0.75 oz/ft^2) Measured: 0.2148+/-0.0022 kg/m^2 (95% confidence)	138	≅20%
TN12CH	12 thin layers of chopped-strand glass fiber mat. Planar density- Listed: 0.228 kg/m^2 (0.75 oz/ft^2) Measured: 0.2148+/-0.0022 kg/m^2 (95% confidence)	63.2	≅30%

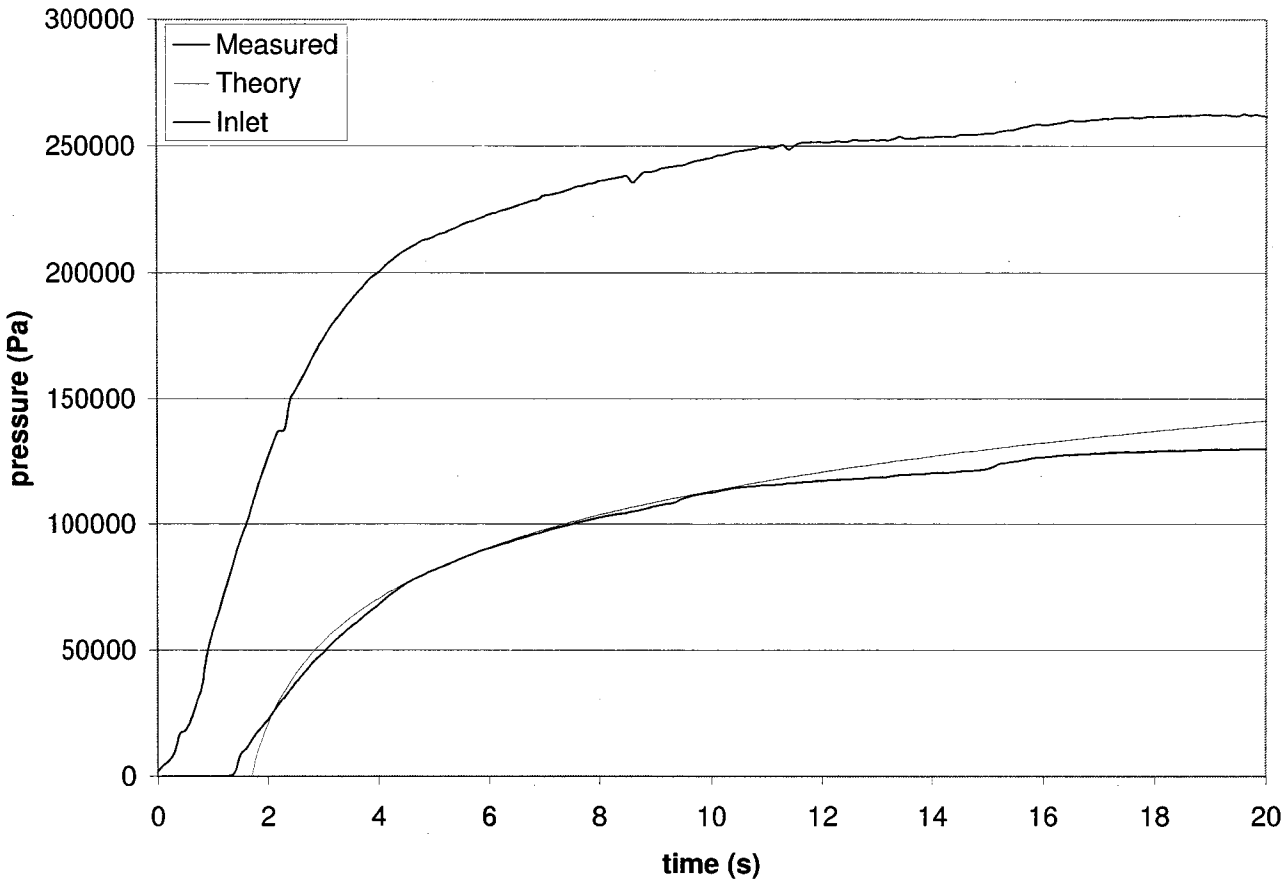

Figure 5.2 Pressure curves obtained from center-gated disk containing 21.2% fiberglass preform at R =12.7 mm

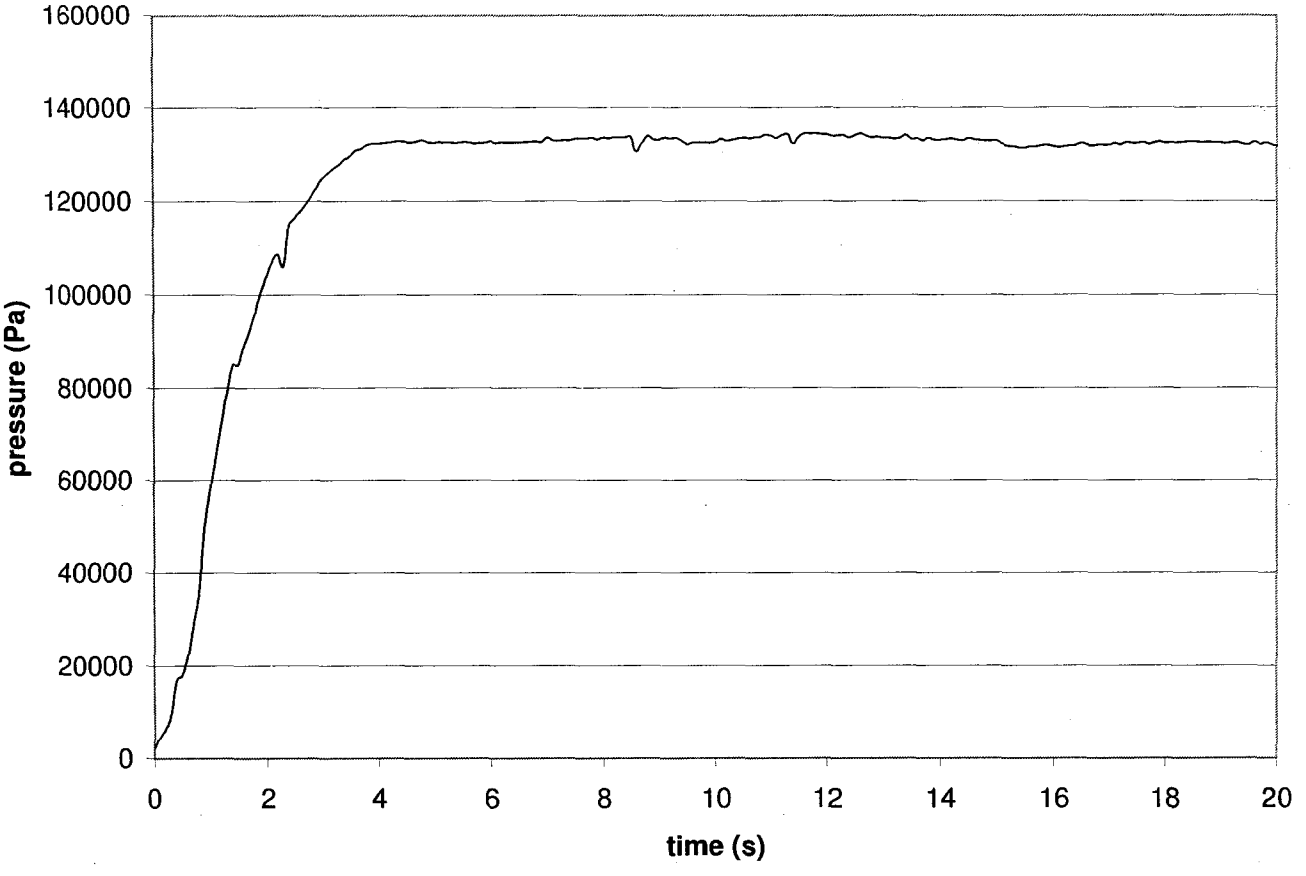

Figure 5.3 Pressure difference observed between inlet and R =12.7 mm from center-gated disk containing 21.2% fiberglass preform

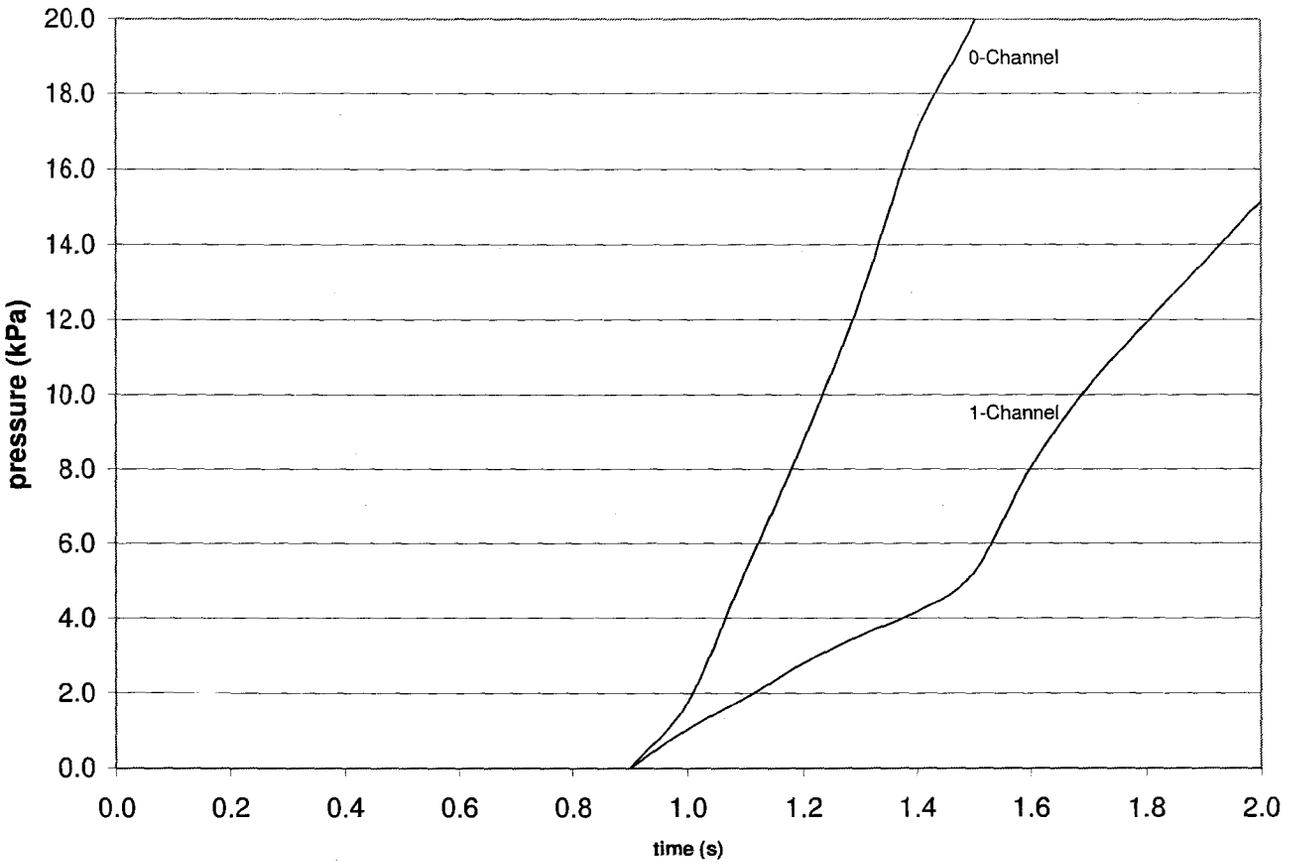

Figure 5.4 First second of inlet pressure measurement for 0-Channel and 1-Channel molds containing 4 layers (≅20%) of thick fiberglass preform impregnated with 118 cp corn syrup. Channel length set to disk radius. Each curve represents average of three pressure profiles

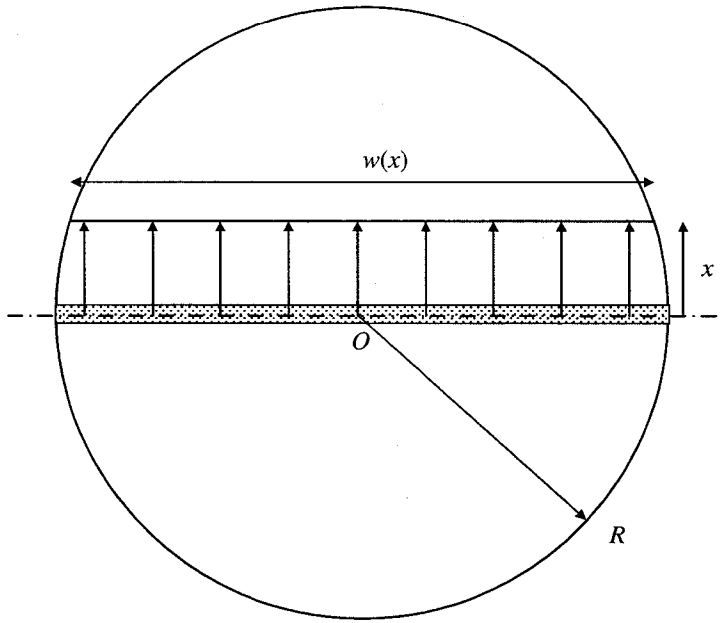

Figure 5.5 Diagram of geometry used to calculate theoretical inlet pressure for 1-Channel mold. Only one half of flow drawn due to symmetry

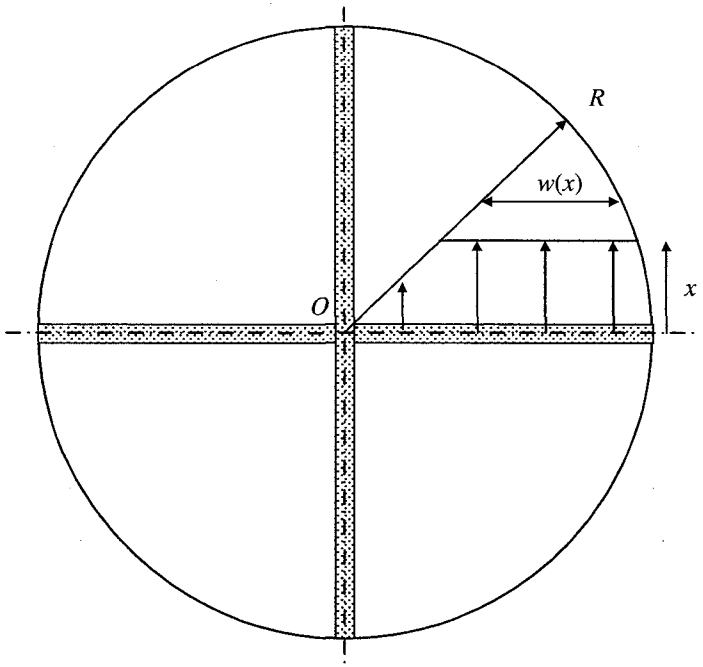

Figure 5.6 Diagram of geometry used to calculate theoretical inlet pressure for 2-Channel mold

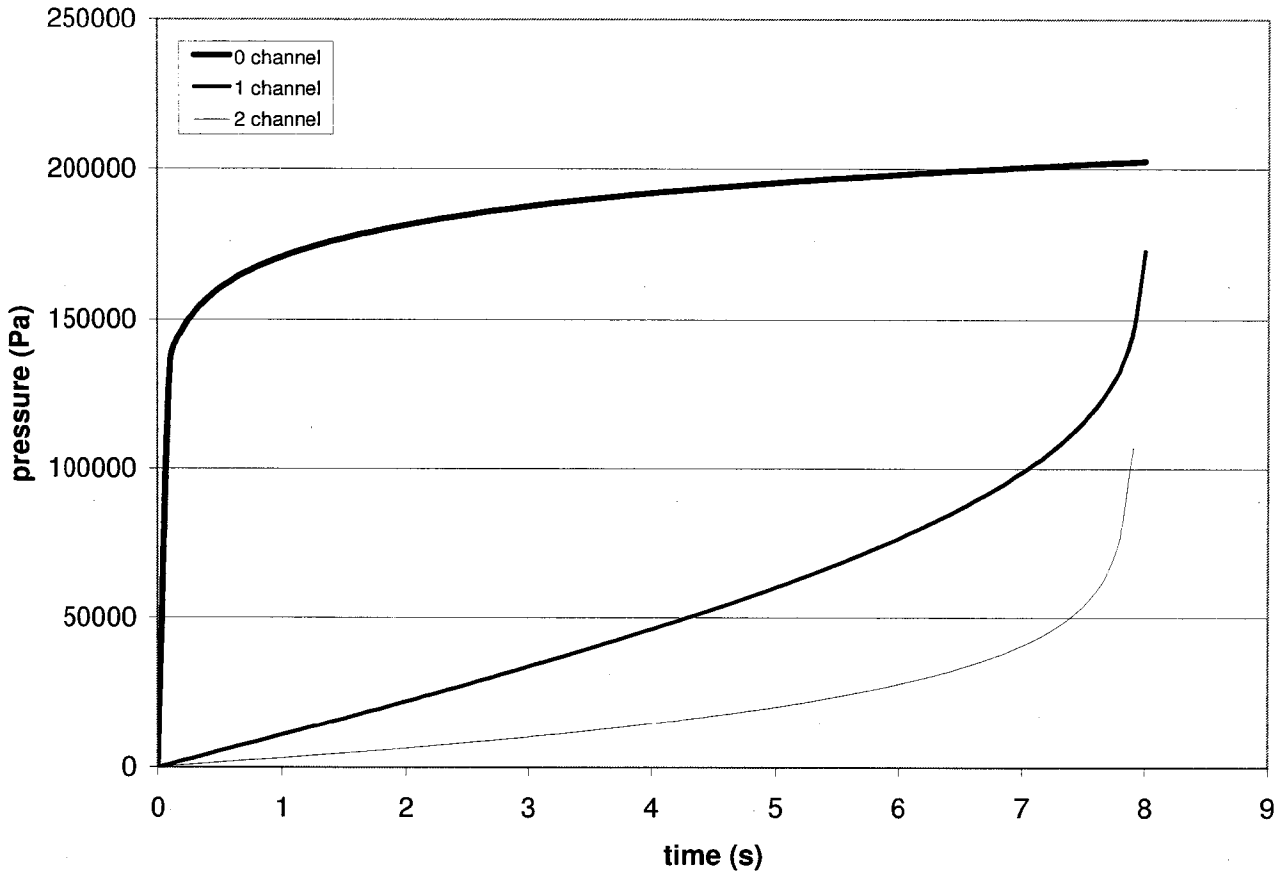

Figure 5.7 Theoretical inlet pressures for 0, 1, and 2-Channel molds

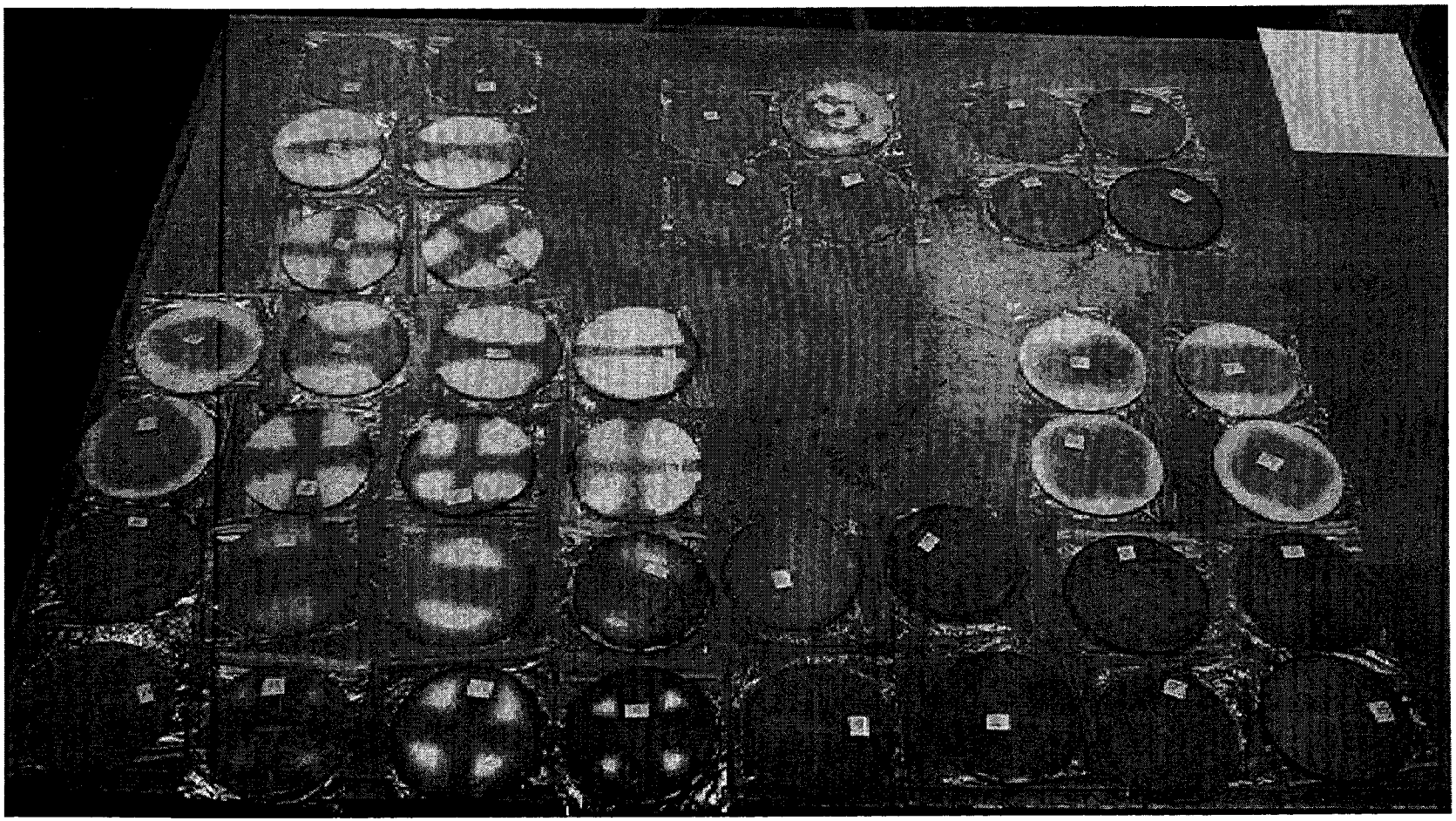

Figure 5.8 Photograph of all molded disks used to determine effect of flow channels on filling

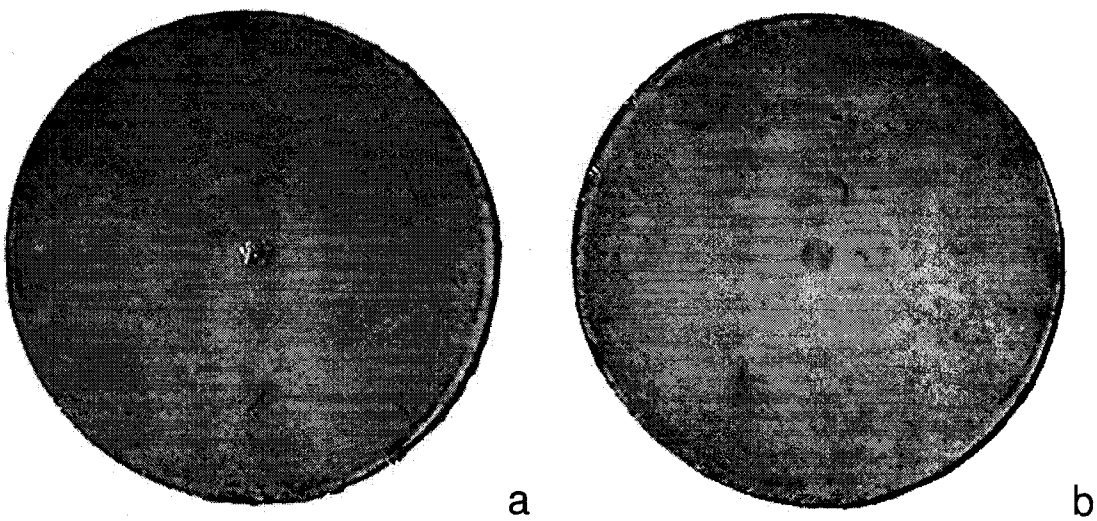

Figure 5.9 Photograph of disk 0K4R molded with 4 layers of preform and no flow channels. a: top; b: bottom

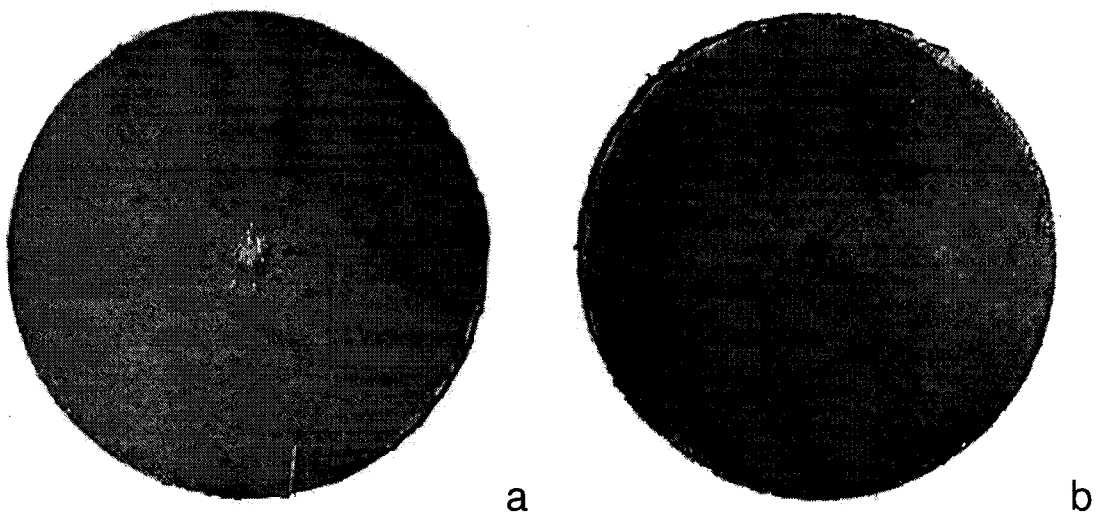

Figure 5.10 Photograph of disk 0K6R molded with 6 layers of preform and no flow channels. a: top; b: bottom

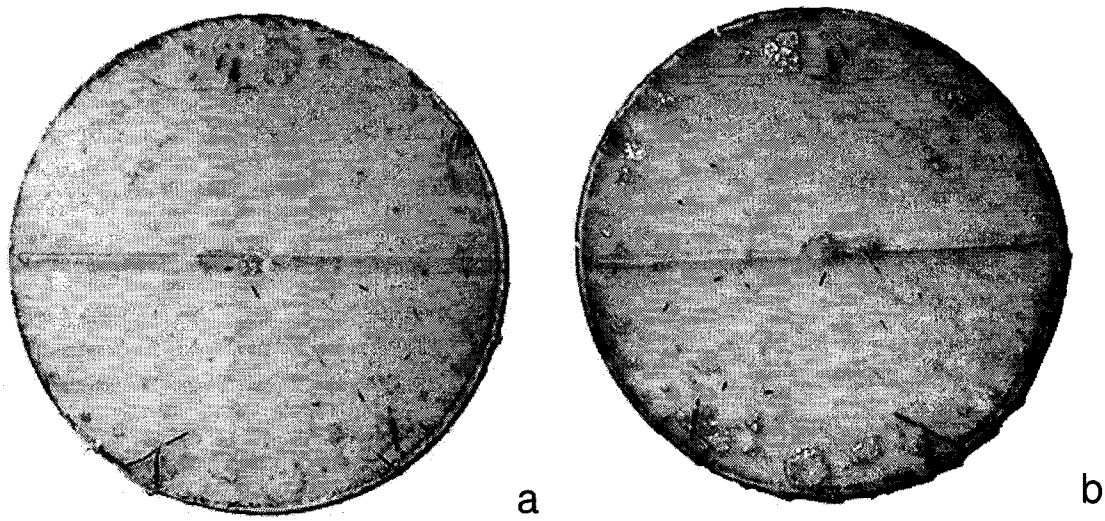

Figure 5.11 Photograph of disk 1K2R molded with 2 layers of preform and 1 flow channel. a: top; b: bottom

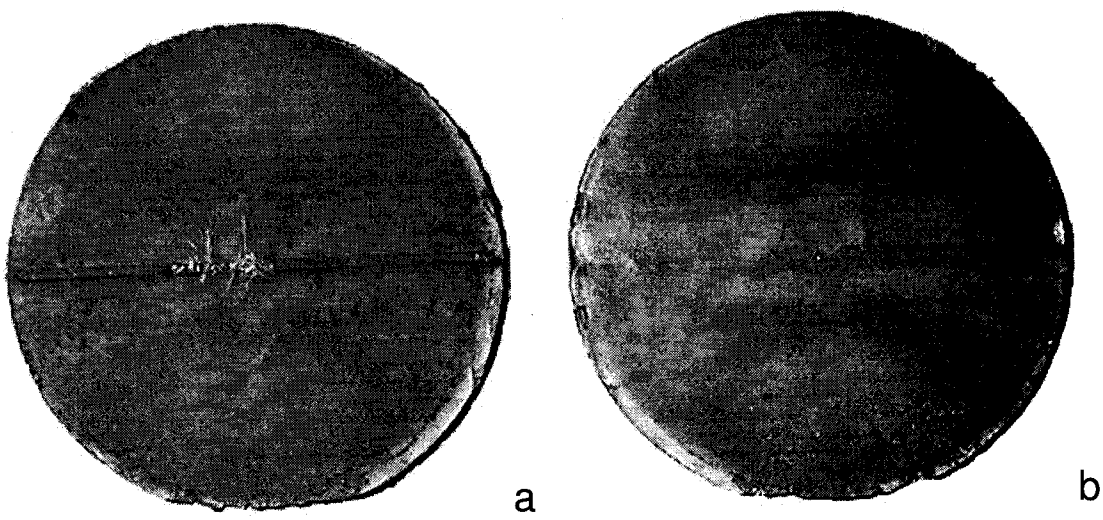

Figure 5.12 Photograph of disk 1K4R molded with 4 layers of preform and 1 flow channel. a: top; b: bottom

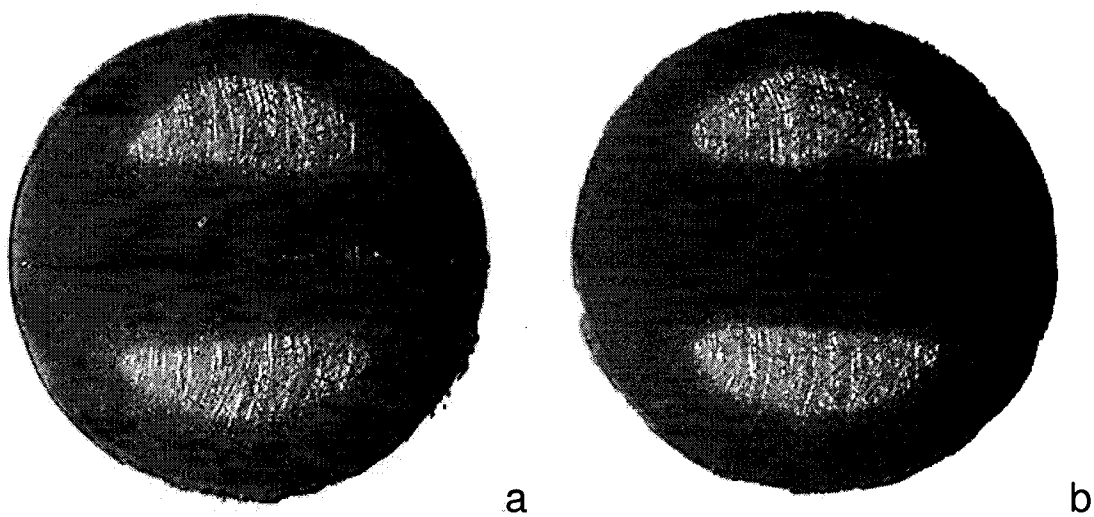

Figure 5.13 Photograph of disk 1K6R molded with 6 layers of preform and 1 flow channel. a: top; b: bottom

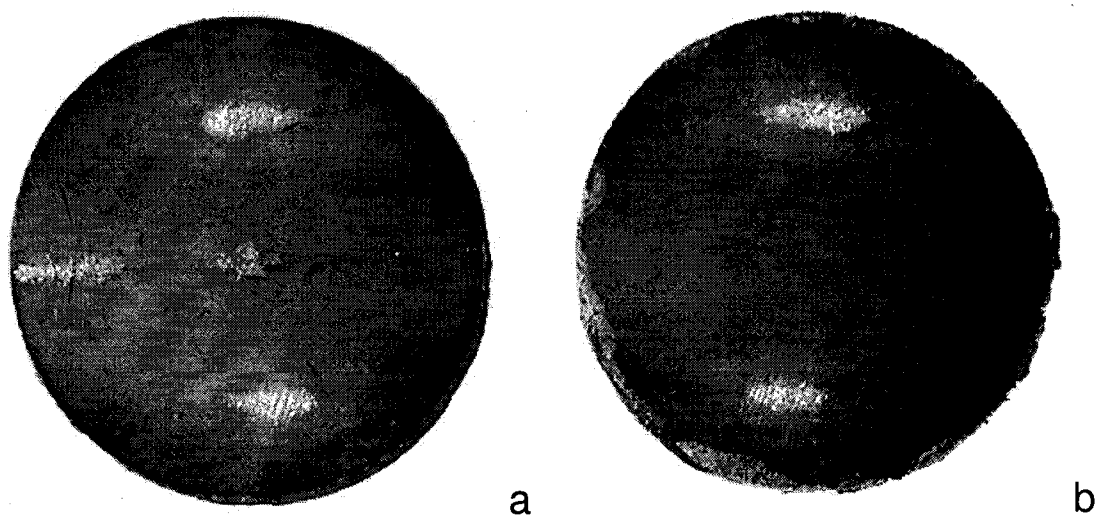

Figure 5.14 Photograph of disk 1K8R molded with 8 layers of preform and 1 flow channel. a: top; b: bottom

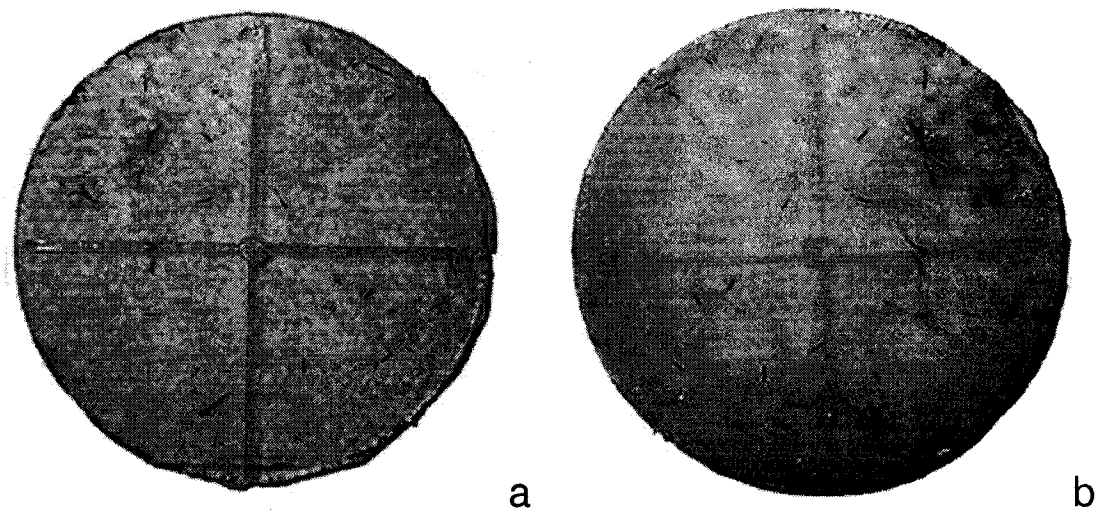

Figure 5.15 Photograph of disk 2K2R molded with 2 layers of preform and 2 flow channels. a: top; b: bottom

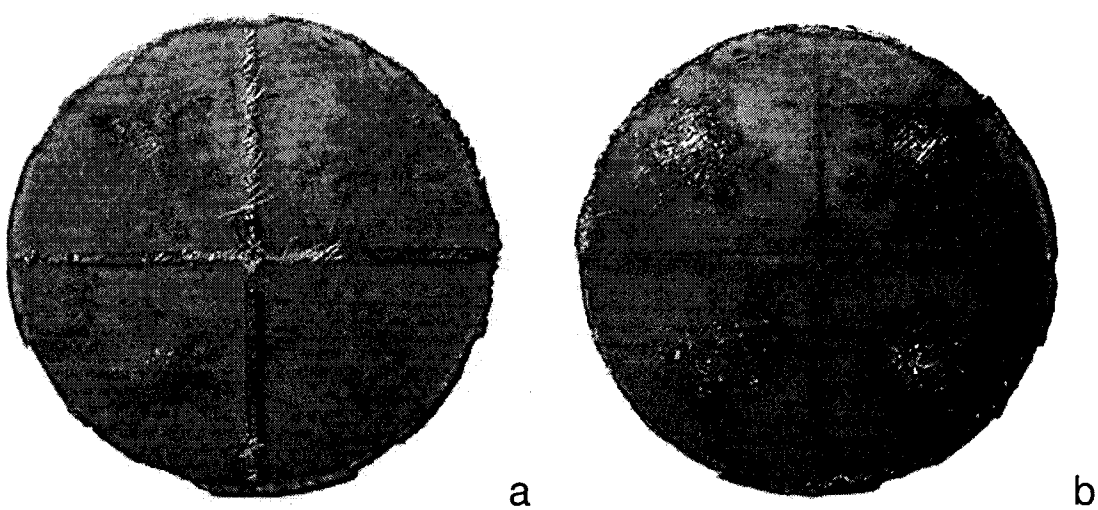

Figure 5.16 Photograph of disk 2K4R molded with 4 layers of preform and 2 flow channels. a: top; b: bottom

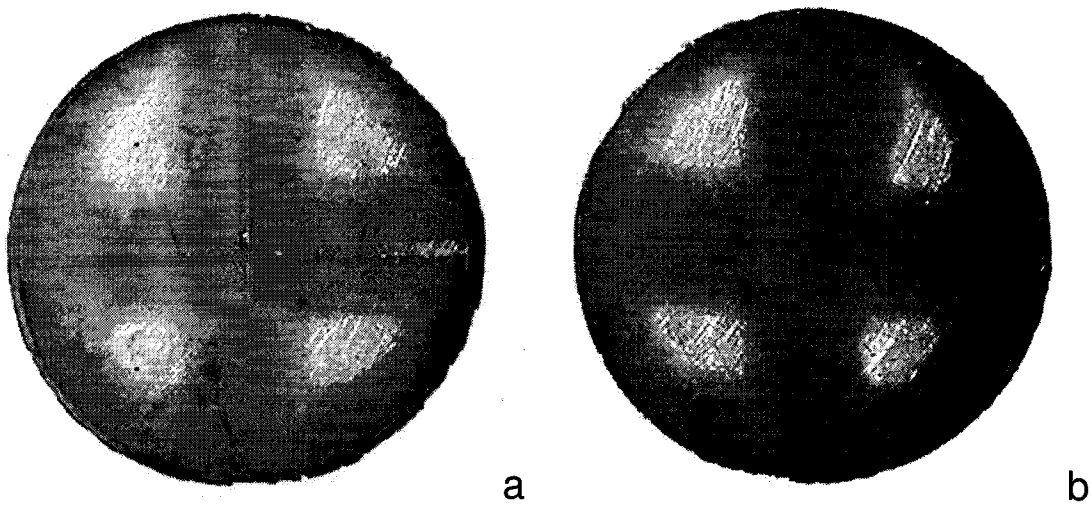

Figure 5.17 Photograph of disk 2K6R molded with 6 layers of preform and 2 flow channels. a: top; b: bottom

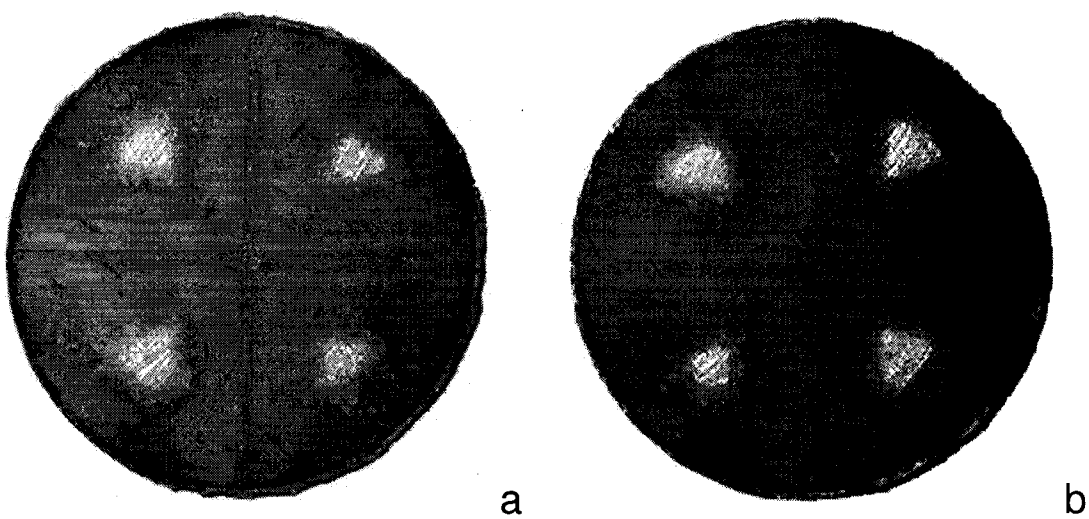

Figure 5.18 Photograph of disk 2K8R molded with 8 layers of preform and 2 flow channels. a: top; b: bottom

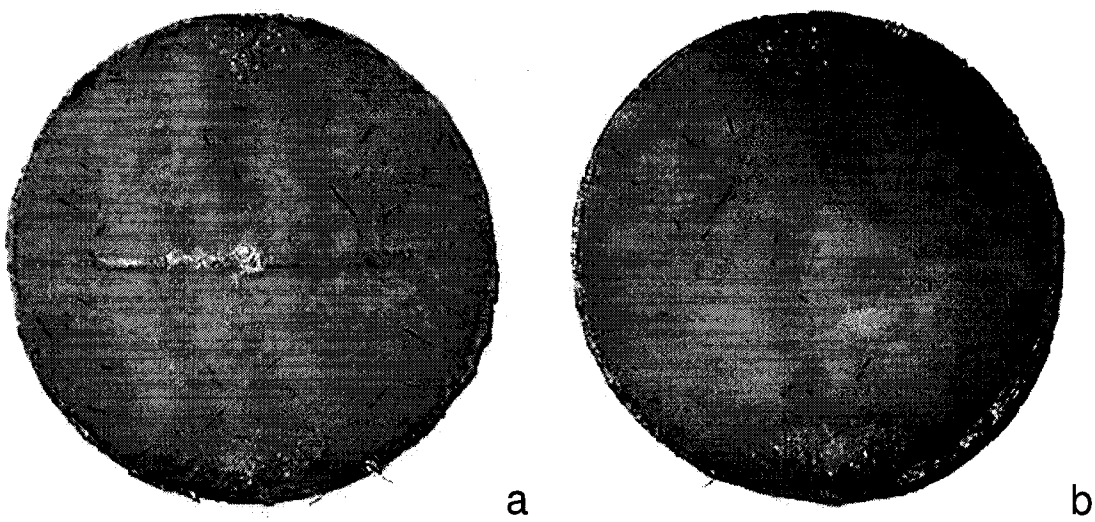

Figure 5.19 Photograph of disk 1K4R-1/3B molded with 4 layers of preform and 1 flow channel which has had the final 1/3 of its length blocked. a: top; b: bottom

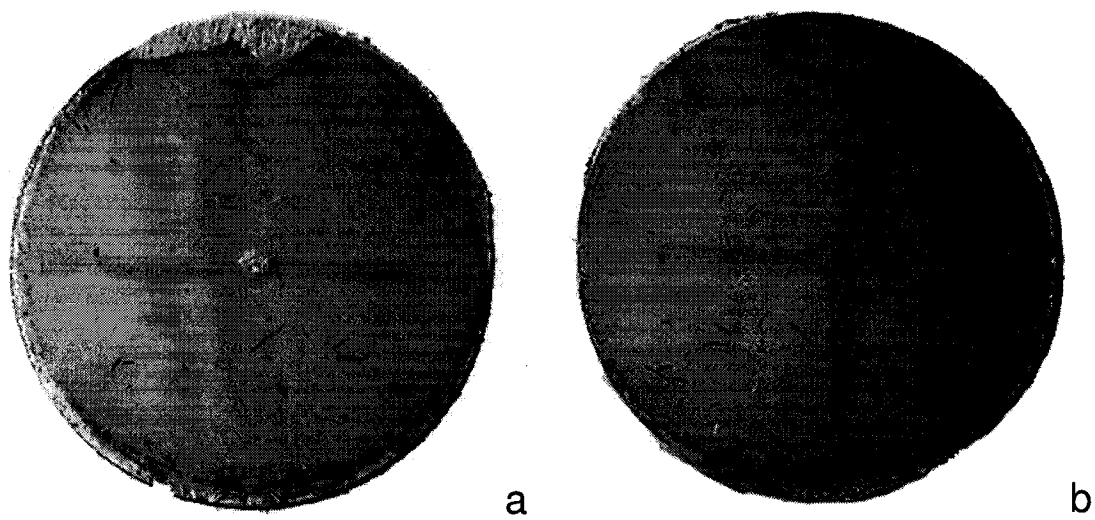

Figure 5.20 Photograph of disk 1K6R-1/3B molded with 6 layers of preform and 1 flow channel which has had the final 1/3 of its length blocked. a: top; b: bottom

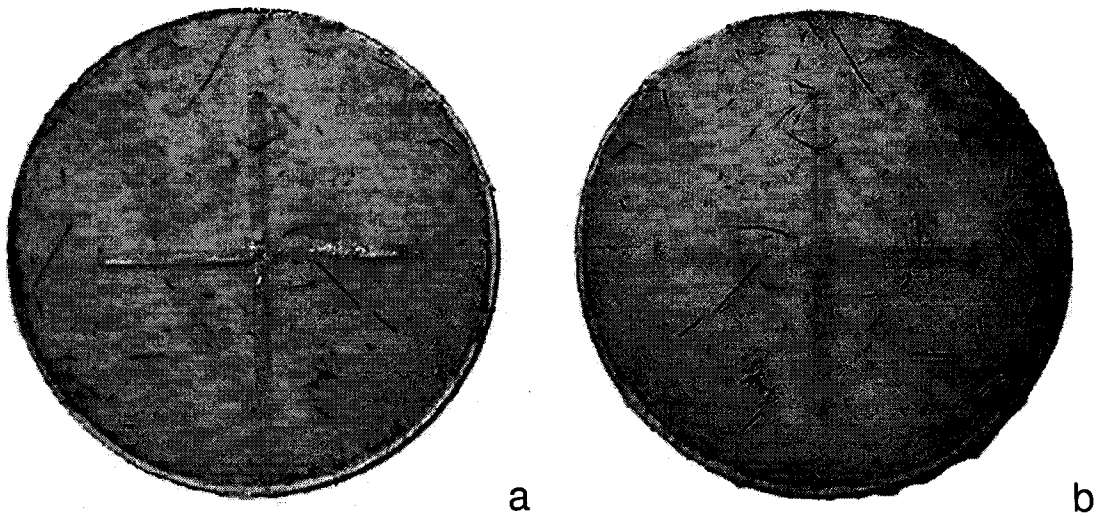

Figure 5.21 Photograph of disk 2K4R-1/3B molded with 4 layers of preform and 2 flow channels which have had the final 1/3 of their length blocked. a: top; b: bottom

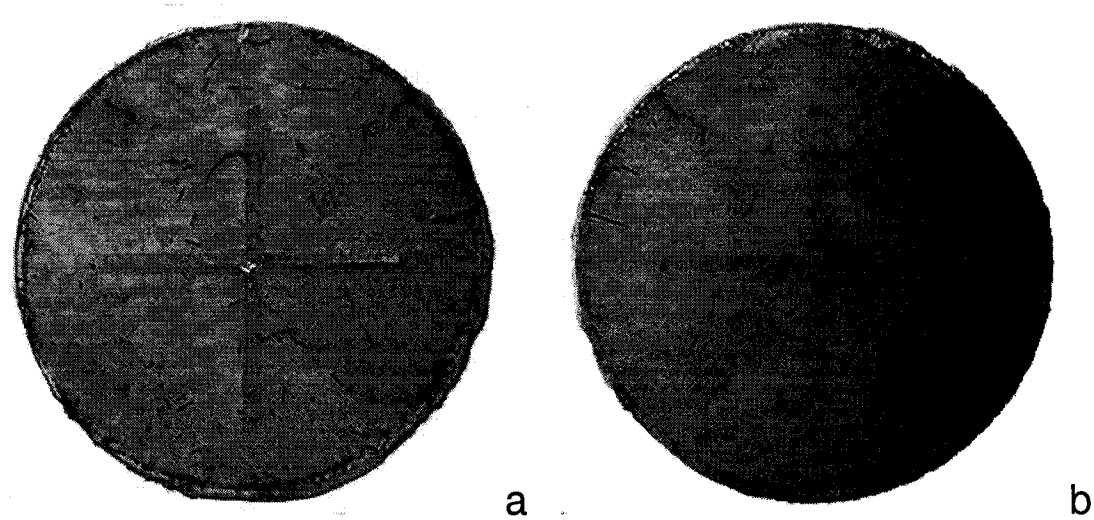

Figure 5.22 Photograph of disk 2K6R-1/3B molded with 6 layers of preform and 2 flow channels which have had the final 1/3 of their length blocked. a: top; b: bottom

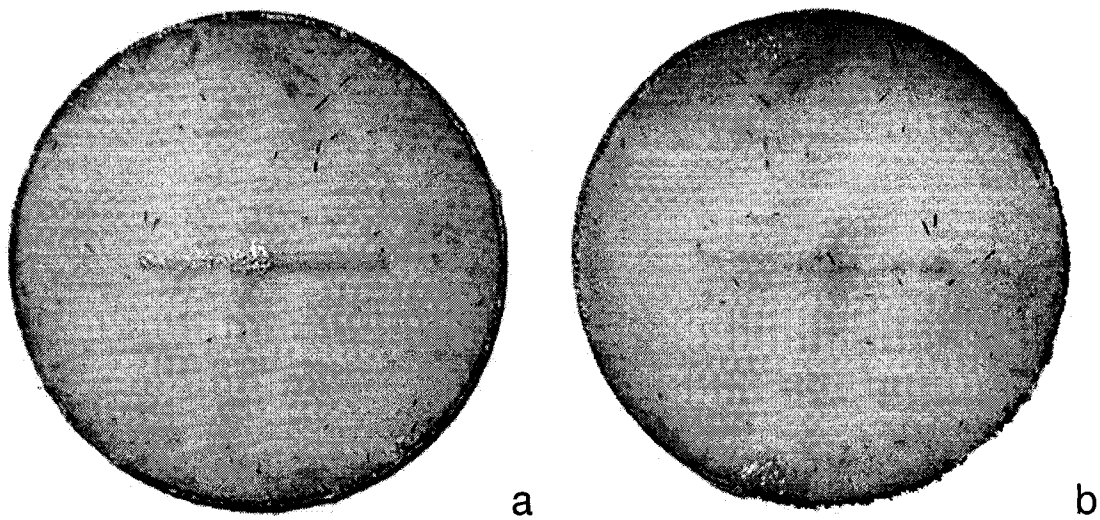

Figure 5.23 Photograph of disk 1K4R-1/2B molded with 4 layers of preform and 1 flow channel which has had the final 1/2 of its length blocked. a: top; b: bottom

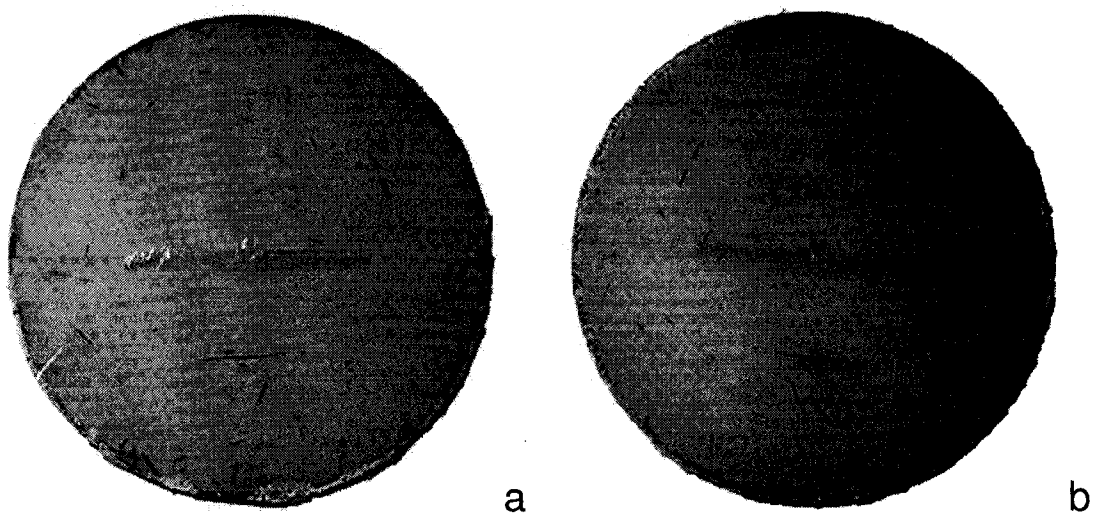

Figure 5.24 Photograph of disk 1K6R-1/2B molded with 6 layers of preform and 1 flow channel which has had the final 1/2 of its length blocked. a: top; b: bottom

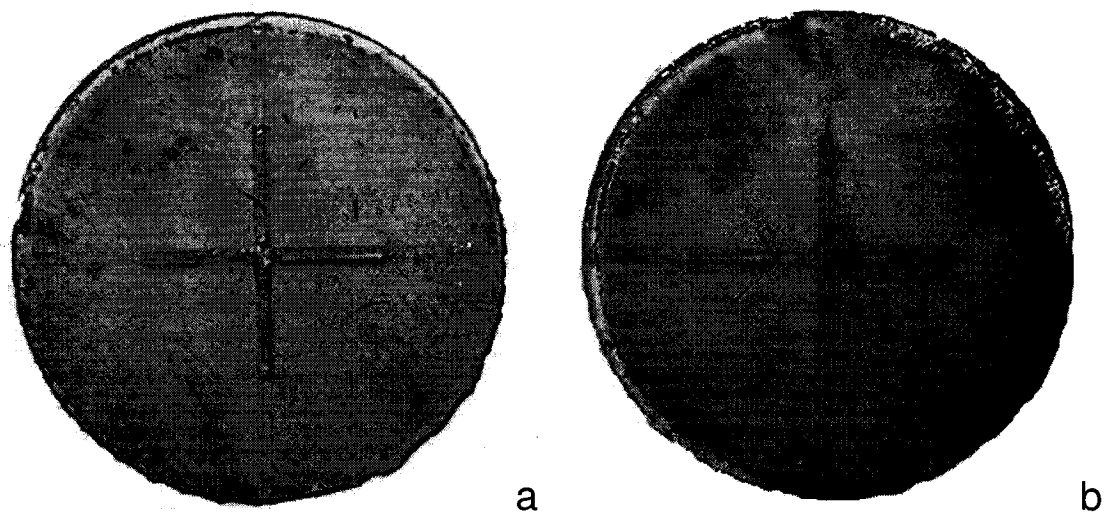

Figure 5.25 Photograph of disk 2K4R-1/2B molded with 4 layers of preform and 2 flow channels which have had the final 1/2 of their length blocked. a: top; b: bottom

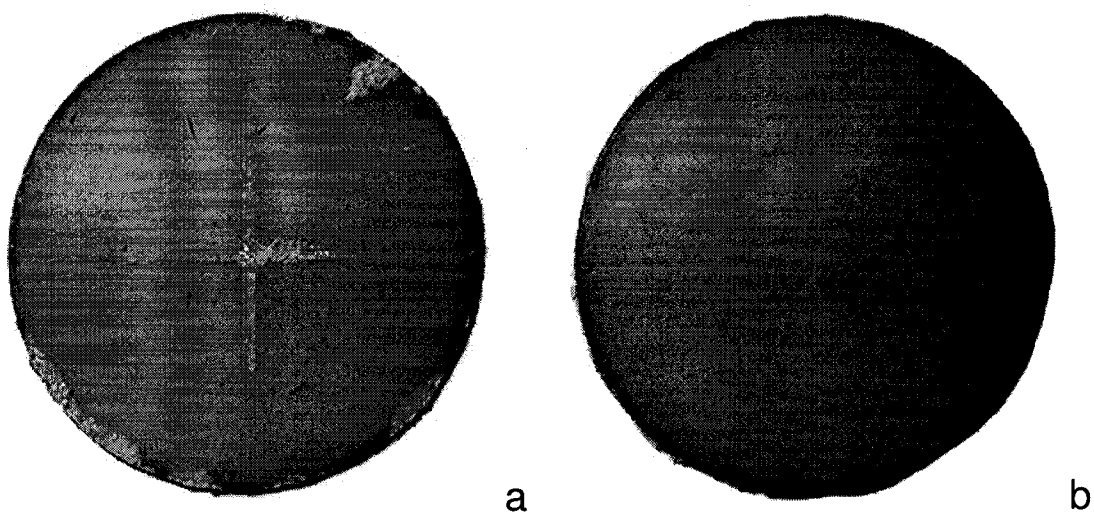

Figure 5.26 Photograph of disk 2K6R-1/2B molded with 6 layers of preform and 2 flow channels which have had the final 1/2 of their length blocked. a: top; b: bottom

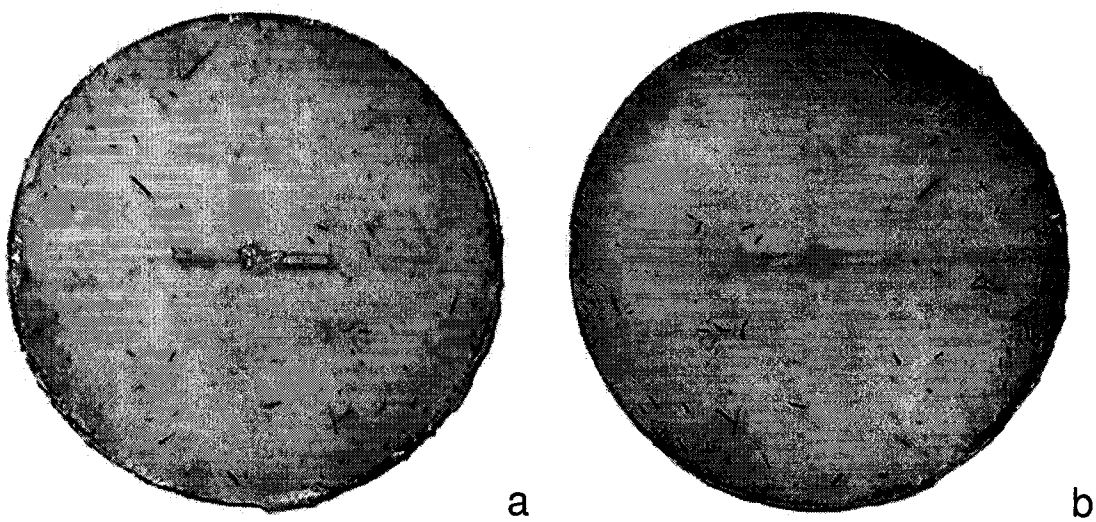

Figure 5.27 Photograph of disk 1K4R-2/3B molded with 4 layers of preform and 1 flow channel which has had the final 2/3 of its length blocked. a: top; b: bottom

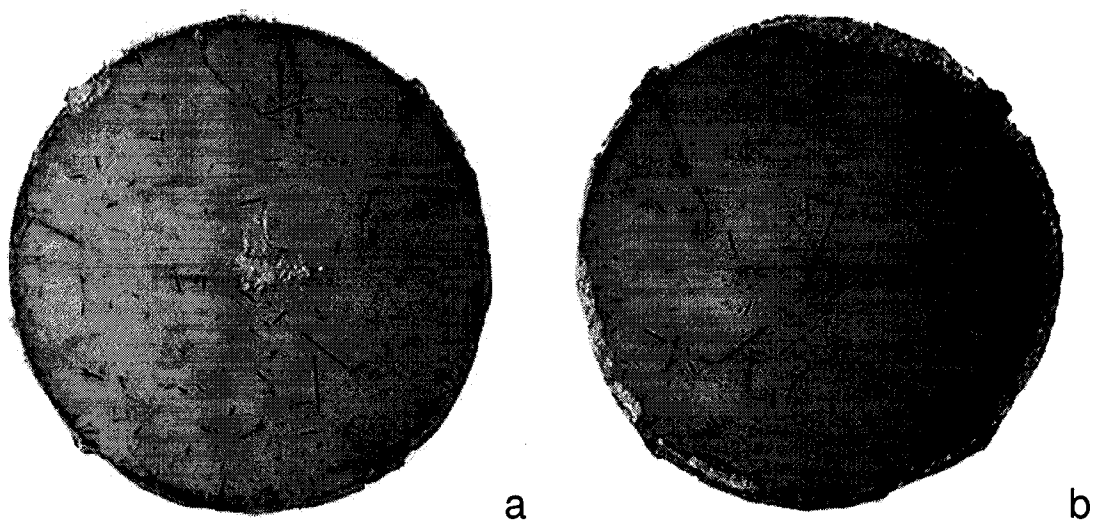

Figure 5.28 Photograph of disk 1K6R-2/3B molded with 6 layers of preform and 1 flow channel which has had the final 2/3 of its length blocked. a: top; b: bottom

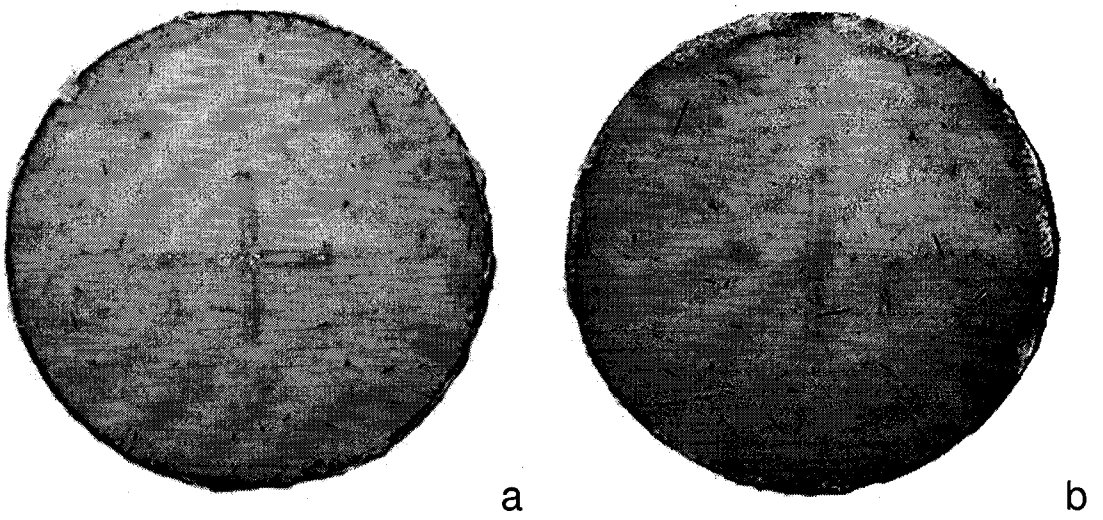

Figure 5.29 Photograph of disk 2K4R-2/3B molded with 4 layers of preform and 2 flow channels which have had the final 2/3 of their length blocked. a: top; b: bottom

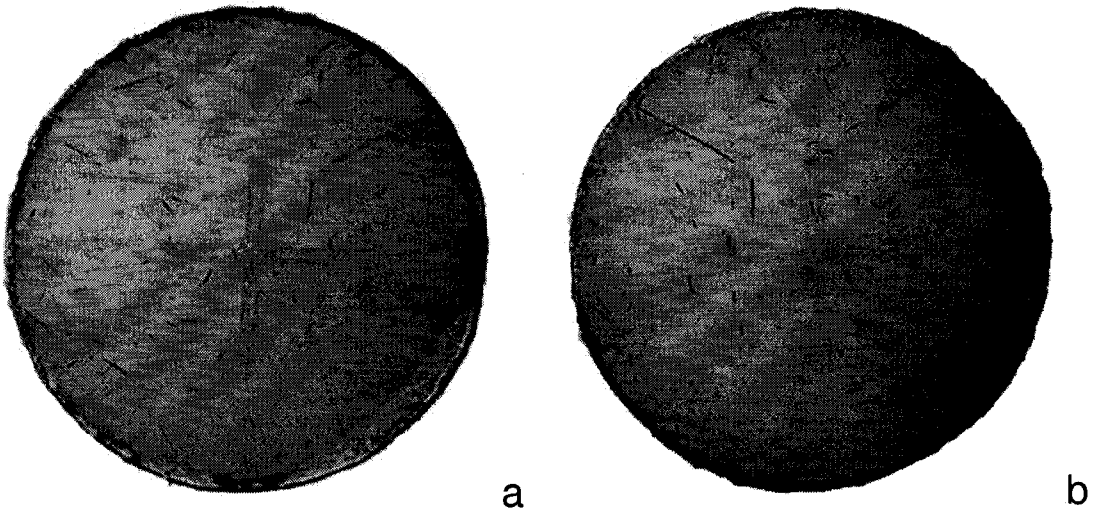

Figure 5.30 Photograph of disk 2K6R-2/3B molded with 6 layers of preform and 2 flow channels which have had the final 2/3 of their length blocked. a: top; b: bottom

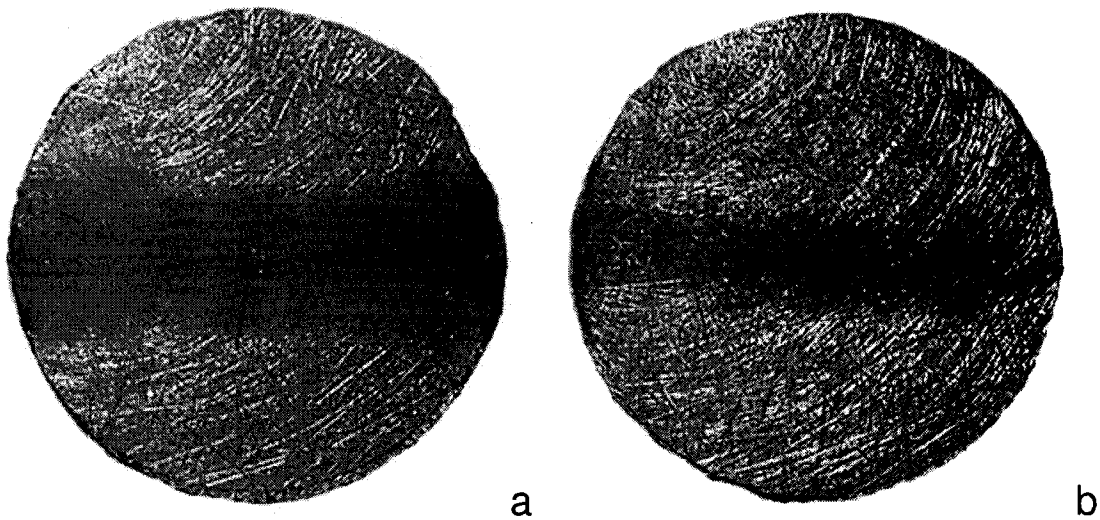

Figure 5.31 Photograph of disk 1K4R-SS2 molded with 4 layers of preform and 1 flow channel. Partially filled for 2 seconds. a: top; b: bottom

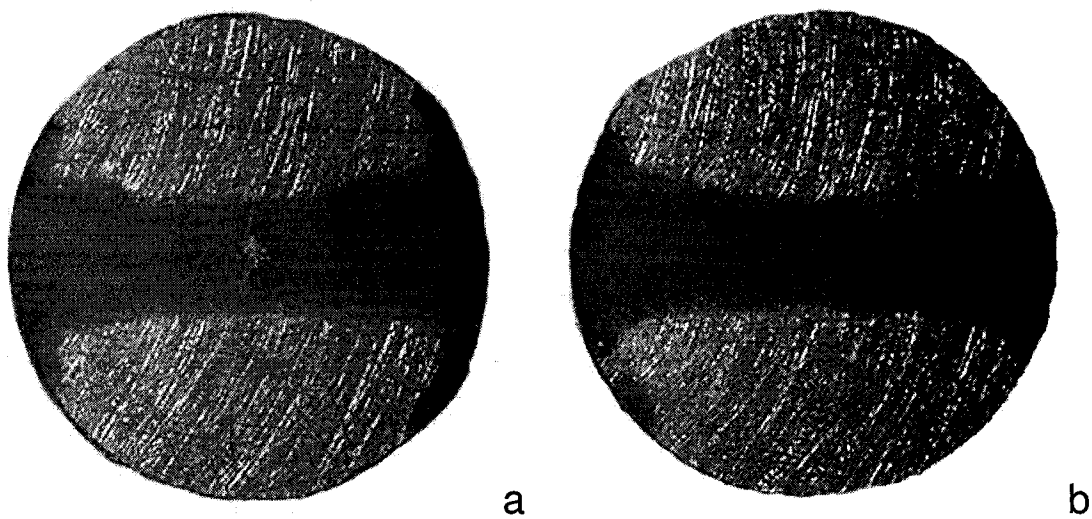

Figure 5.32 Photograph of disk 1K6R-SS2 molded with 6 layers of preform and 1 flow channel. Partially filled for 2 seconds. a: top; b: bottom

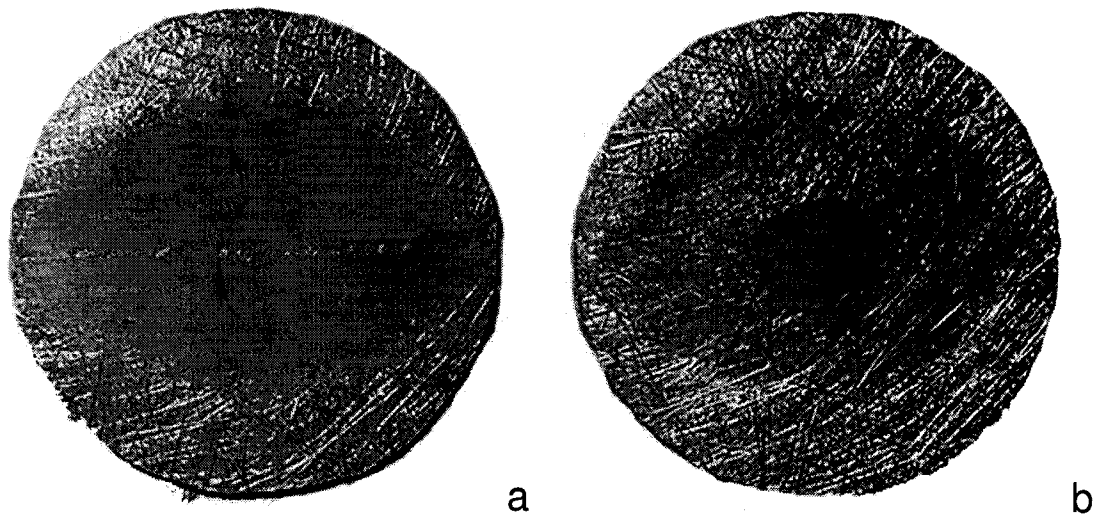

Figure 5.33 Photograph of disk 1K2R-SS4 molded with 2 layers of preform and 1 flow channel. Partially filled for 4 seconds. a: top; b: bottom

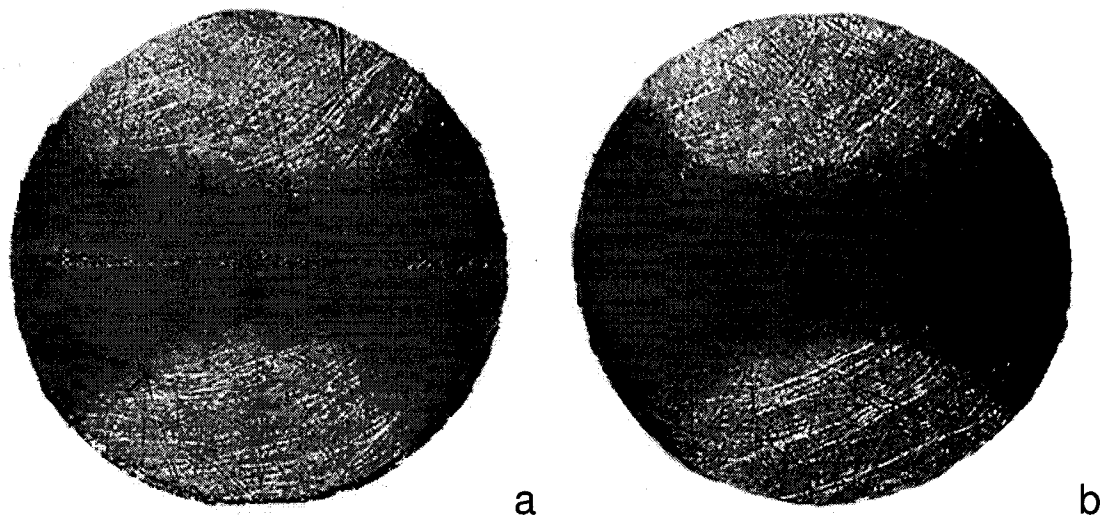

Figure 5.34 Photograph of disk 1K4R-SS4 molded with 4 layers of preform and 1 flow channel. Partially filled for 4 seconds. a: top; b: bottom

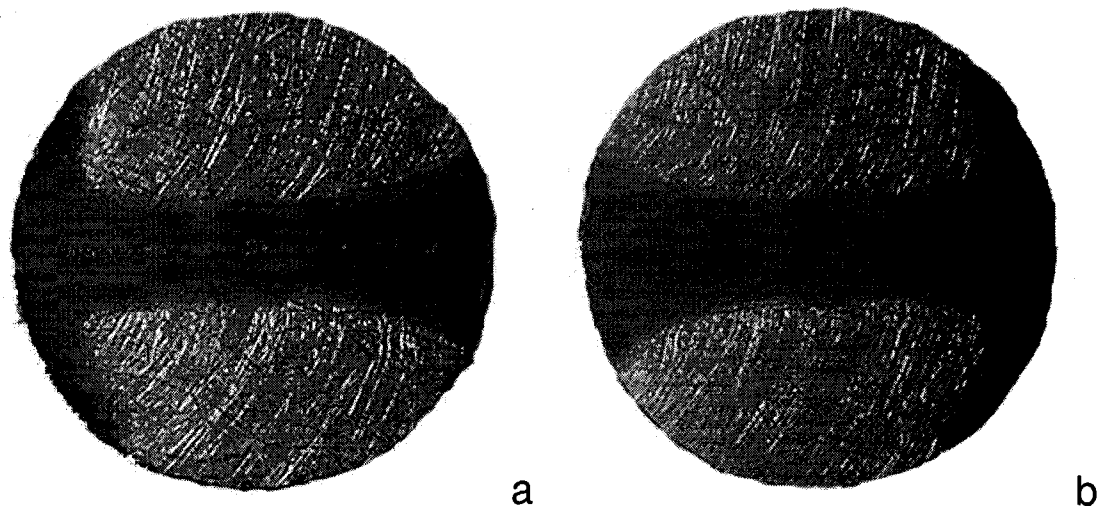

Figure 5.35 Photograph of disk 1K6R-SS4 molded with 6 layers of preform and 1 flow channel. Partially filled for 4 seconds. a: top; b: bottom

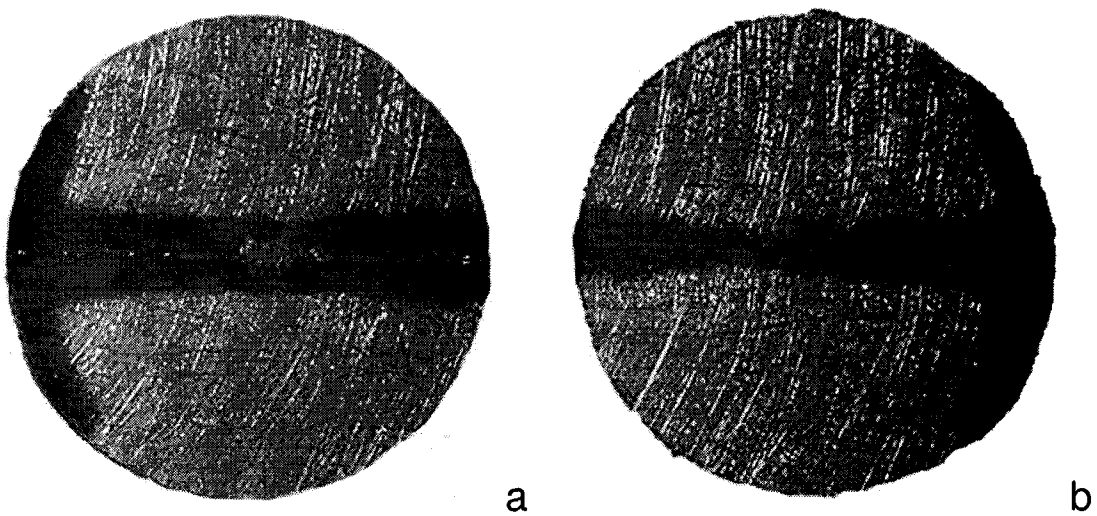

Figure 5.36 Photograph of disk 1K8R-SS4 molded with 8 layers of preform and 1 flow channel. Partially filled for 4 seconds. a: top; b: bottom

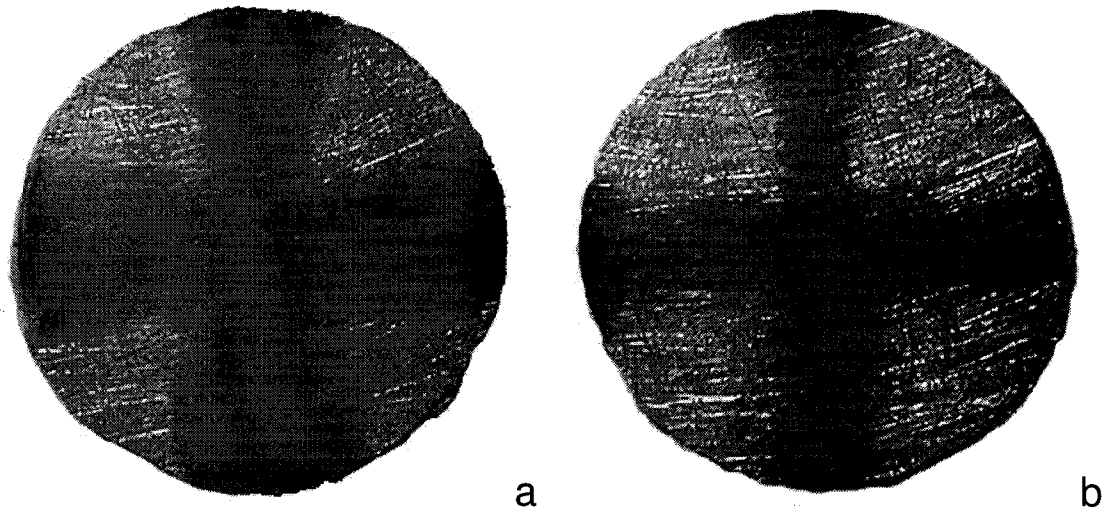

Figure 5.37 Photograph of disk 2K4R-SS2 molded with 4 layers of preform and 2 flow channels. Partially filled for 2 seconds. a: top; b: bottom

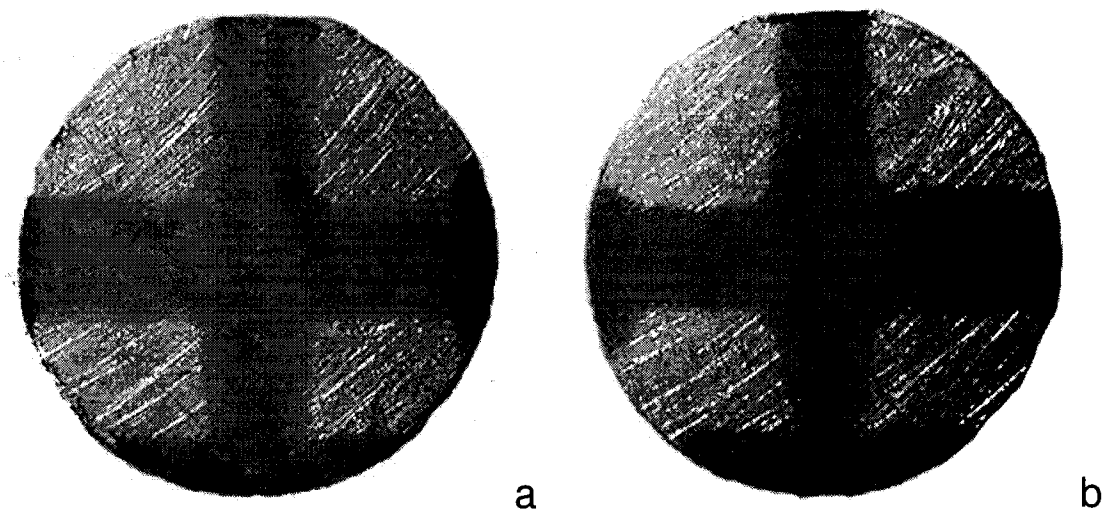

Figure 5.38 Photograph of disk 2K6R-SS2 molded with 6 layers of preform and 2 flow channels. Partially filled for 2 seconds. a: top; b: bottom

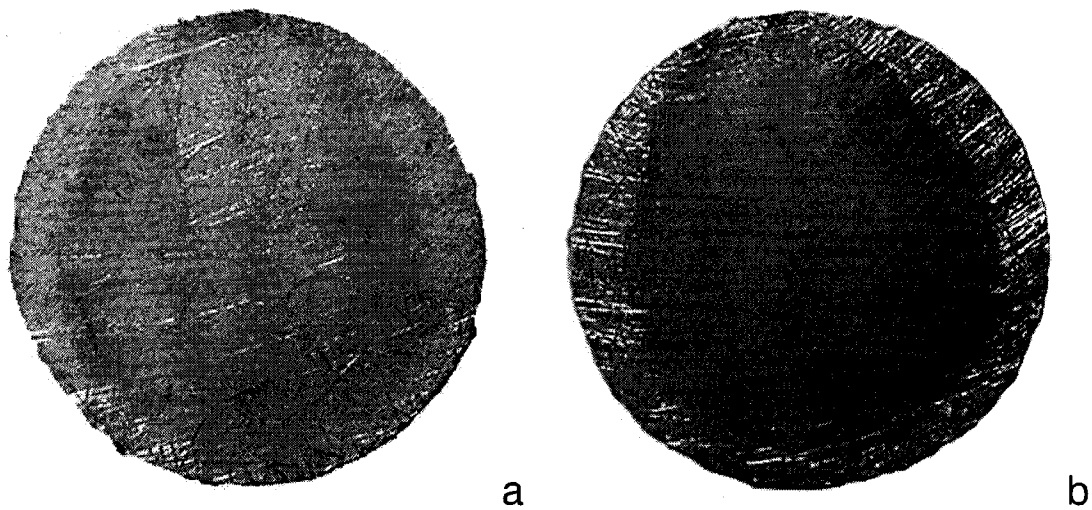

Figure 5.39 Photograph of disk 2K2R-SS4 molded with 2 layers of preform and 2 flow channels. Partially filled for 4 seconds. a: top; b: bottom

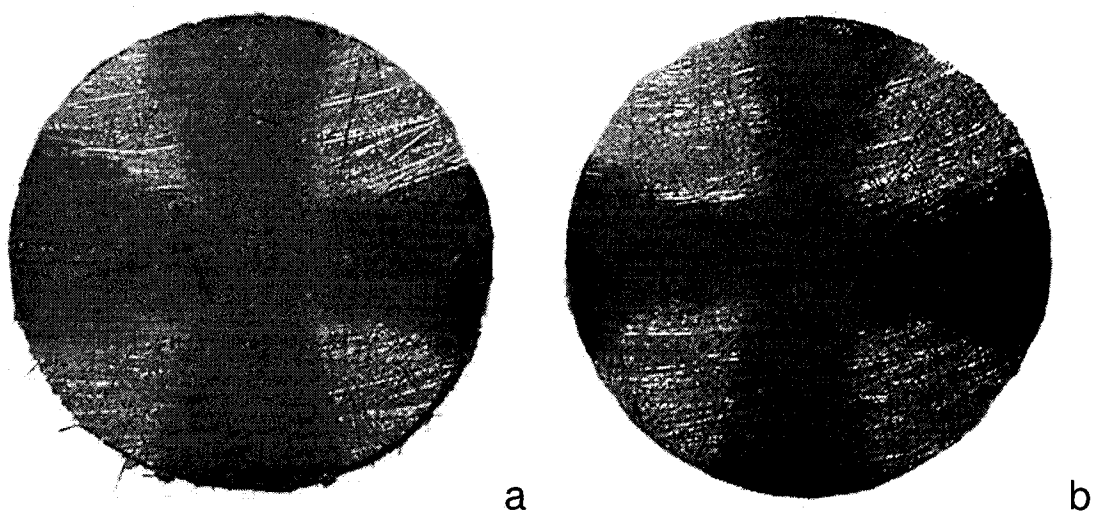

Figure 5.40 Photograph of disk 2K4R-SS4 molded with 4 layers of preform and 2 flow channels. Partially filled for 4 seconds. a: top; b: bottom

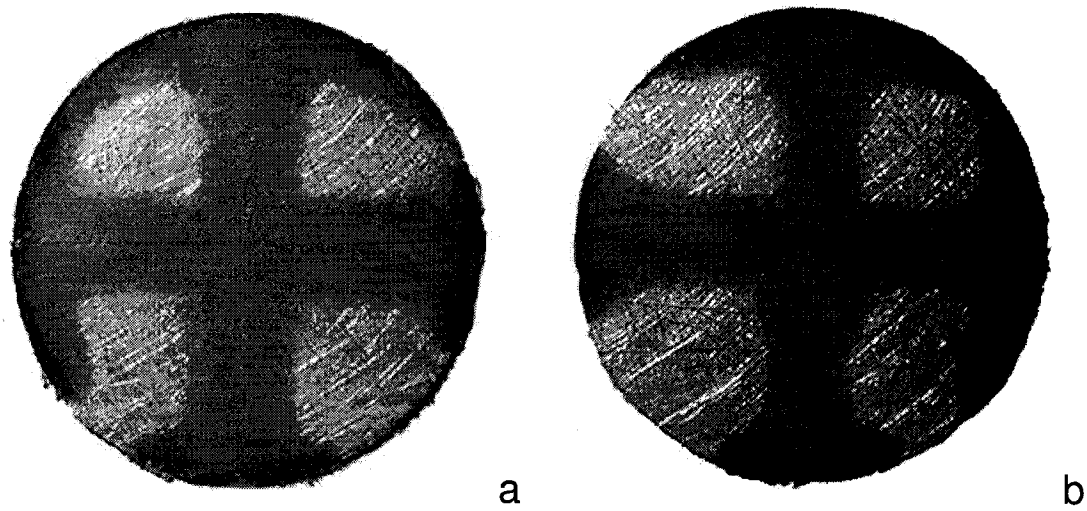

Figure 5.41 Photograph of disk 2K6R-SS4 molded with 6 layers of preform and 2 flow channels. Partially filled for 4 seconds. a: top; b: bottom

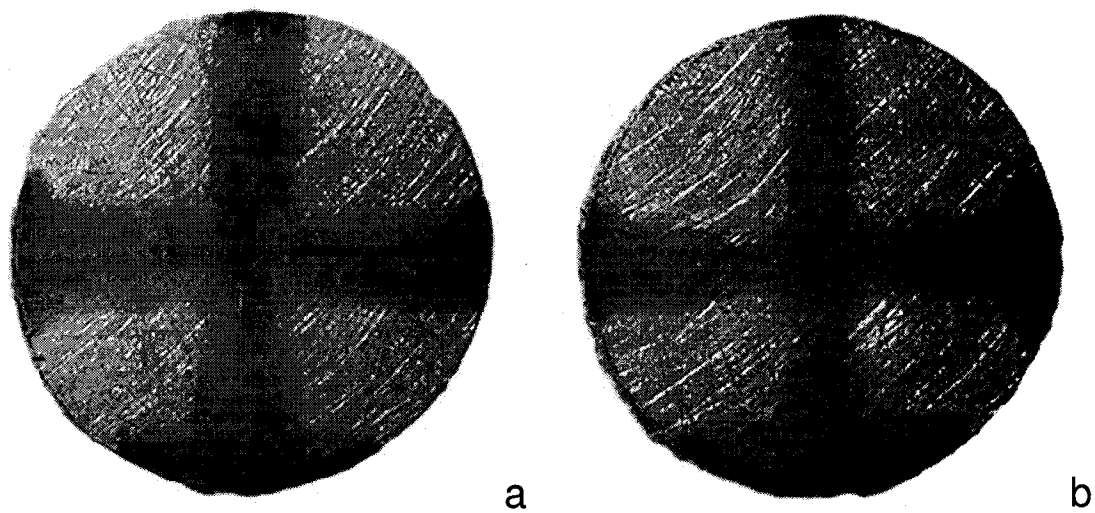

Figure 5.42 Photograph of disk 2K8R-SS4 molded with 8 layers of preform and 2 flow channels. Partially filled for 4 seconds. a: top; b: bottom

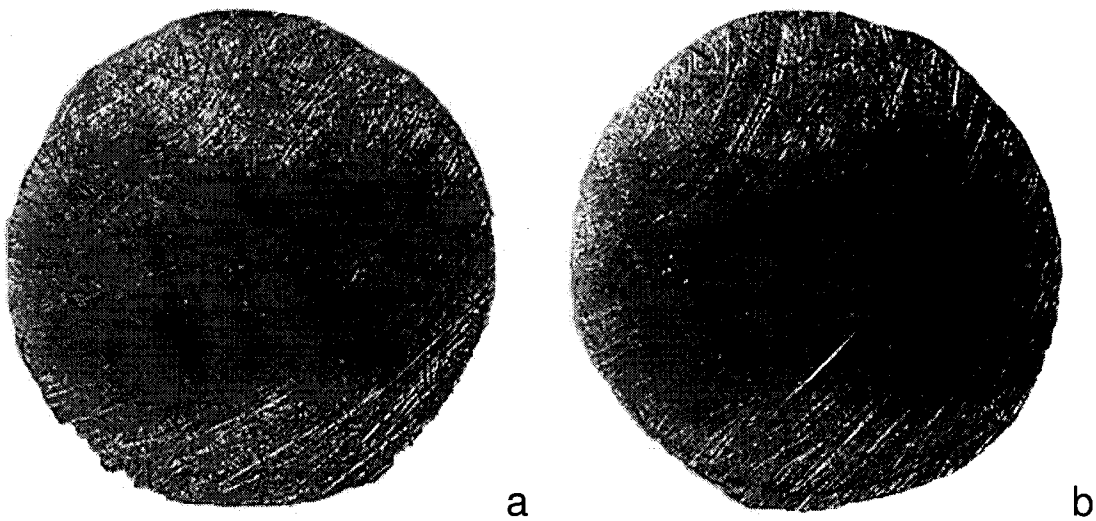

Figure 5.43 Photograph of disk 1K4R-1/2B-SS4 molded with 4 layers of preform and 1 flow channel which has had the final 1/2 of its length blocked. Partially filled for 4 seconds. a: top; b: bottom

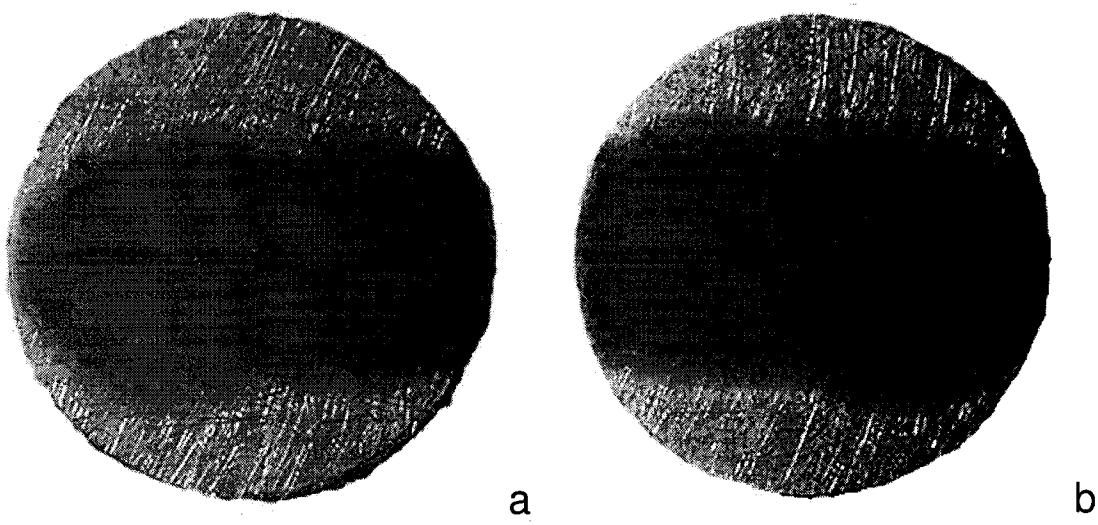

Figure 5.44 Photograph of disk 1K6R-1/2B-SS4 molded with 6 layers of preform and 1 flow channel which has had the final 1/2 of its length blocked. Partially filled for 4 seconds. a: top; b: bottom

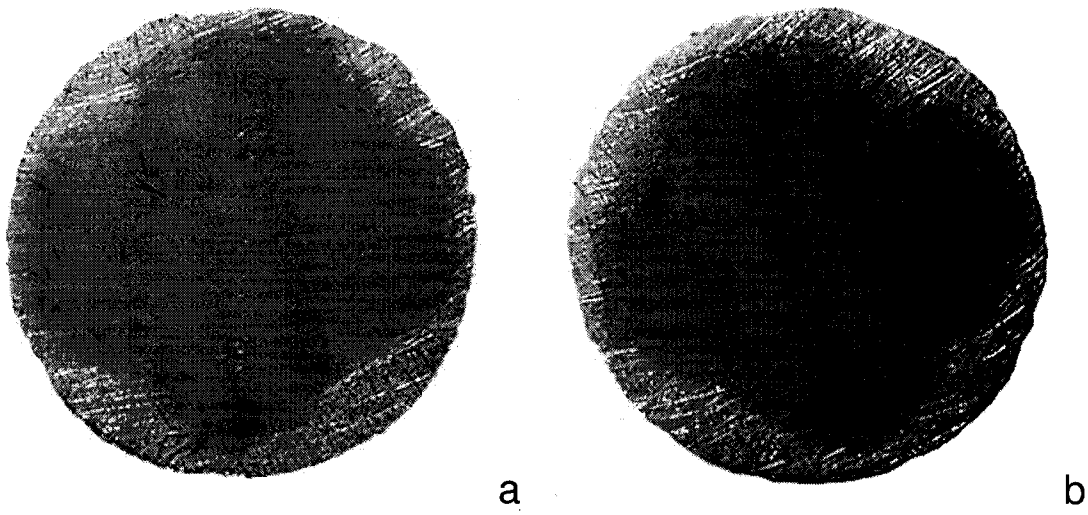

Figure 5.45 Photograph of disk 2K4R-1/2B-SS4 molded with 4 layers of preform and 2 flow channels which have had the final 1/2 of their length blocked. Partially filled for 4 seconds. a: top; b: bottom

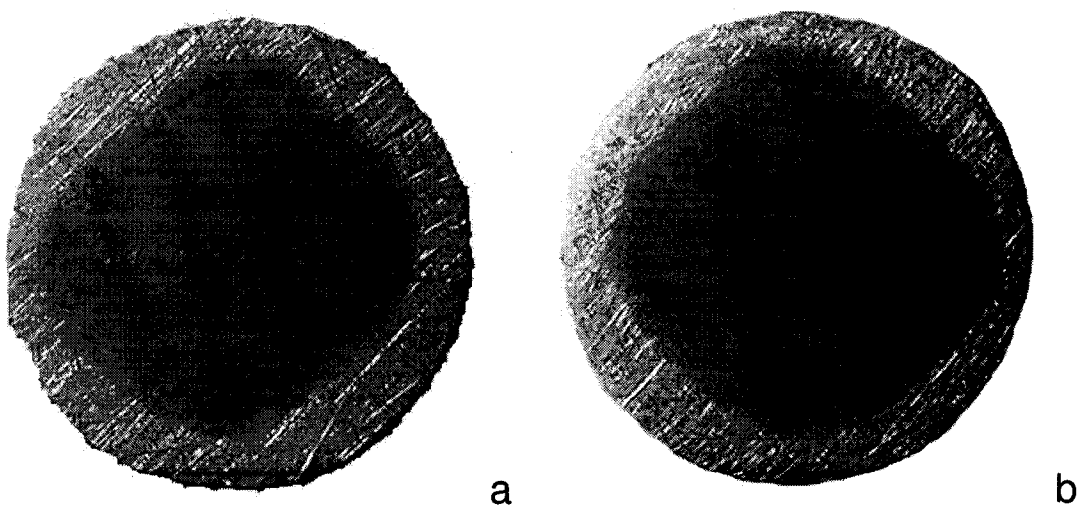

Figure 5.46 Photograph of disk 2K6R-1/2B-SS4 molded with 6 layers of preform and 2 flow channels which have had the final 1/2 of their length blocked. Partially filled for 4 seconds. a: top; b: bottom

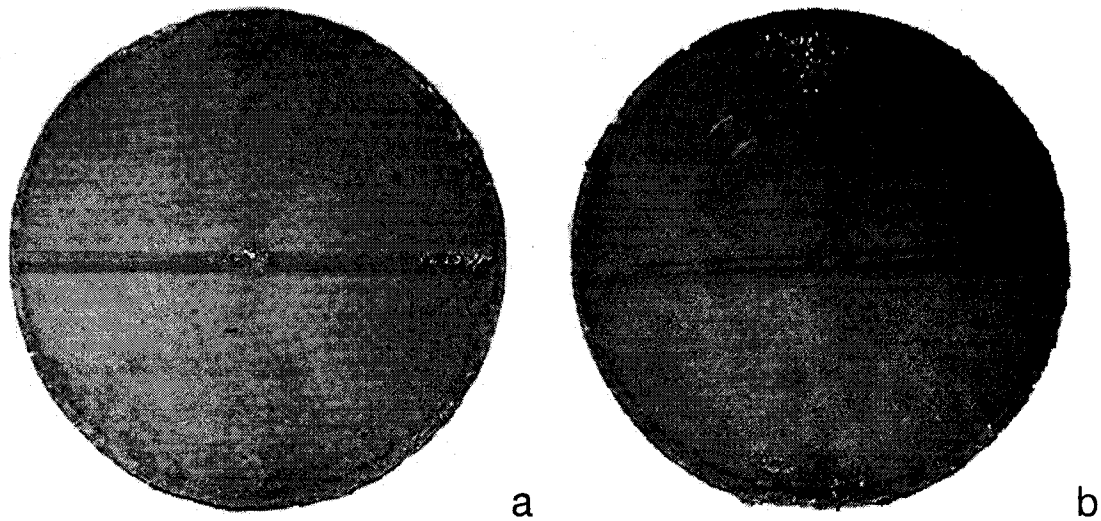

Figure 5.47 Photograph of disk 1K4R-HG molded with 4 layers of preform and 1 flow channel. Mold cavity surrounding preform filled with a ring of hot glue prior to filling.. a: top; b: bottom

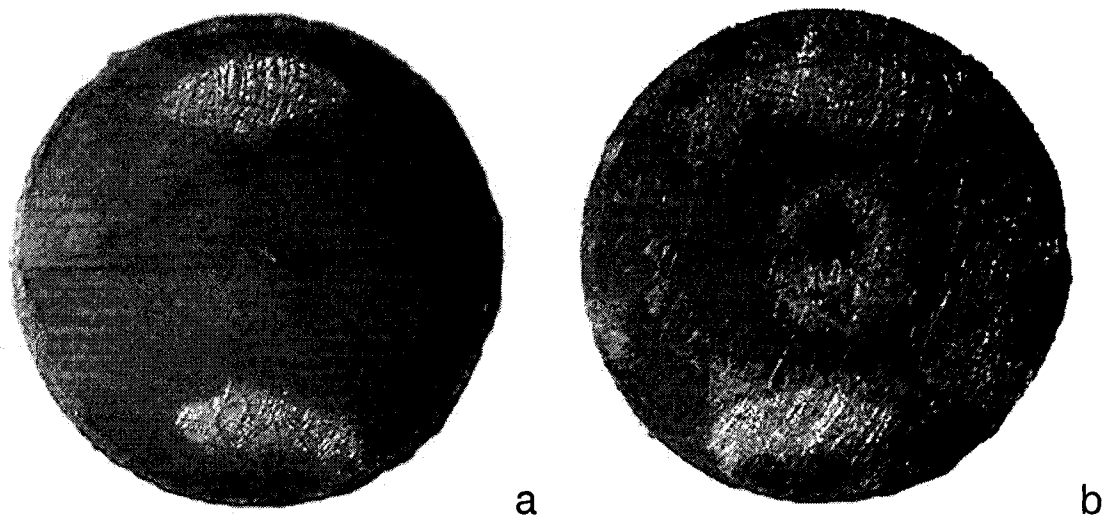

Figure 5.48 Photograph of disk 1K6R-HG molded with 6 layers of preform and 1 flow channel. Mold cavity surrounding preform filled with a ring of hot glue prior to filling.. a: top; b: bottom

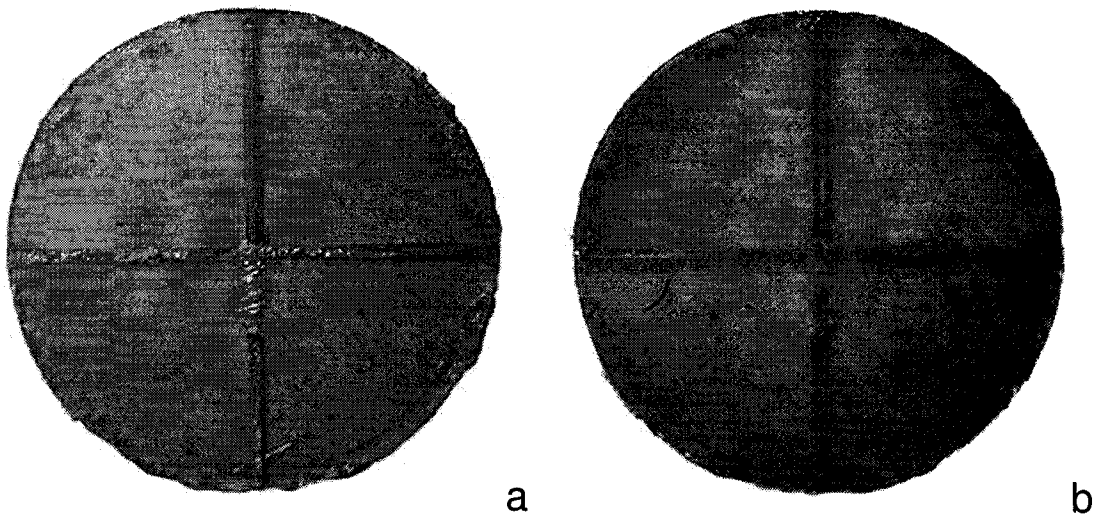

Figure 5.49 Photograph of disk 2K4R-HG molded with 4 layers of preform and 2 flow channels. Mold cavity surrounding preform filled with a ring of hot glue prior to filling.. a: top; b: bottom

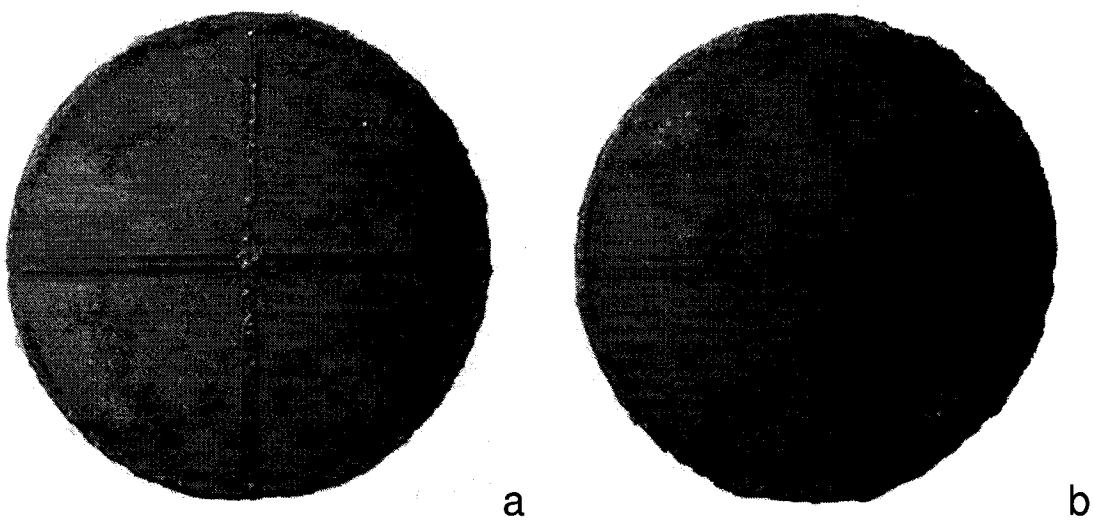

Figure 5.50 Photograph of disk 2K6R-HG molded with 6 layers of preform and 2 flow channels. Mold cavity surrounding preform filled with a ring of hot glue prior to filling.. a: top; b: bottom

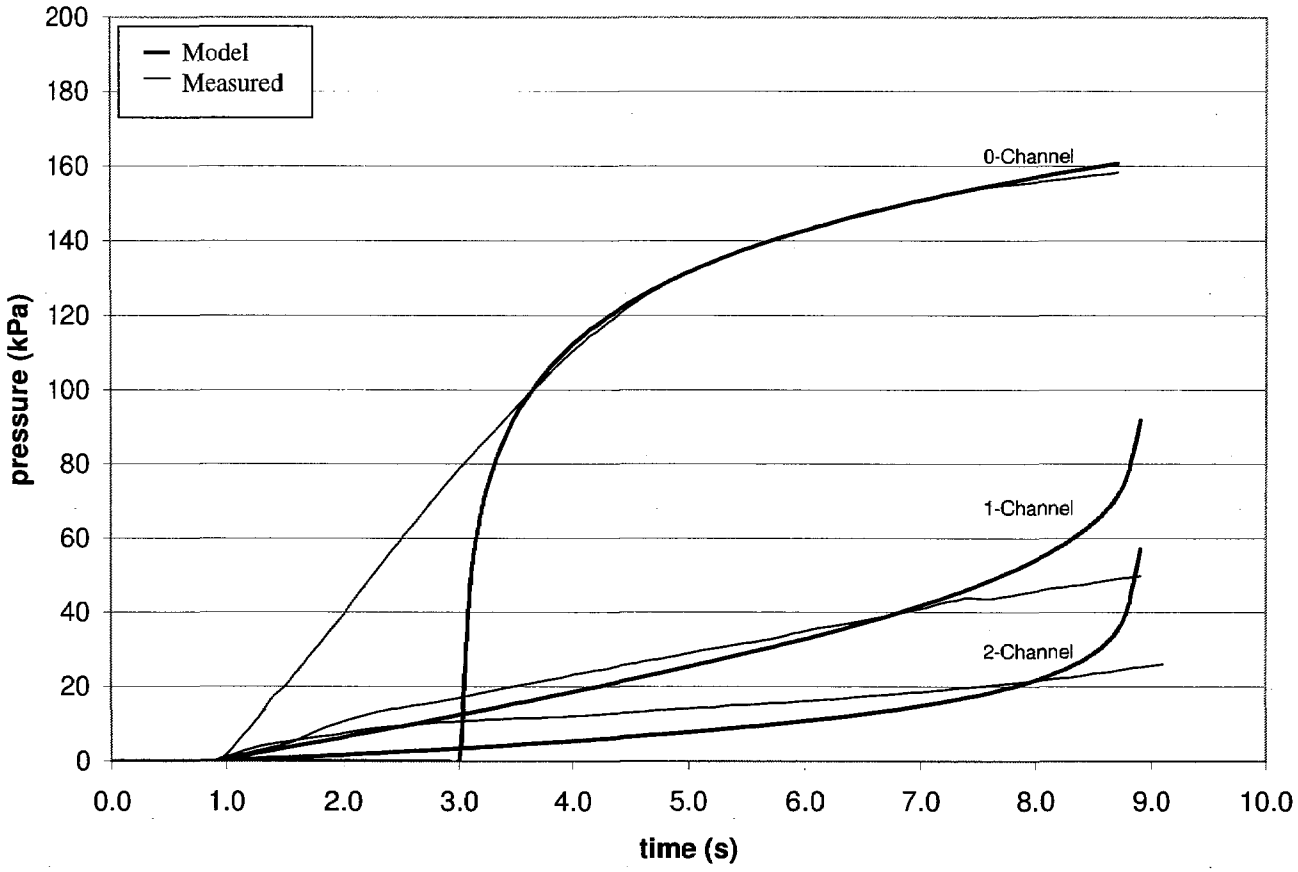

Figure 5.51 Inlet pressure measurement for 0, 1, and 2-Channel molds containing 4 layers (≅20%) of thick fiberglass preform impregnated with 118 cp corn syrup. Channel length set to disk radius. Bold curves are theoretically generated. Each experimental curve represents average of three pressure profiles

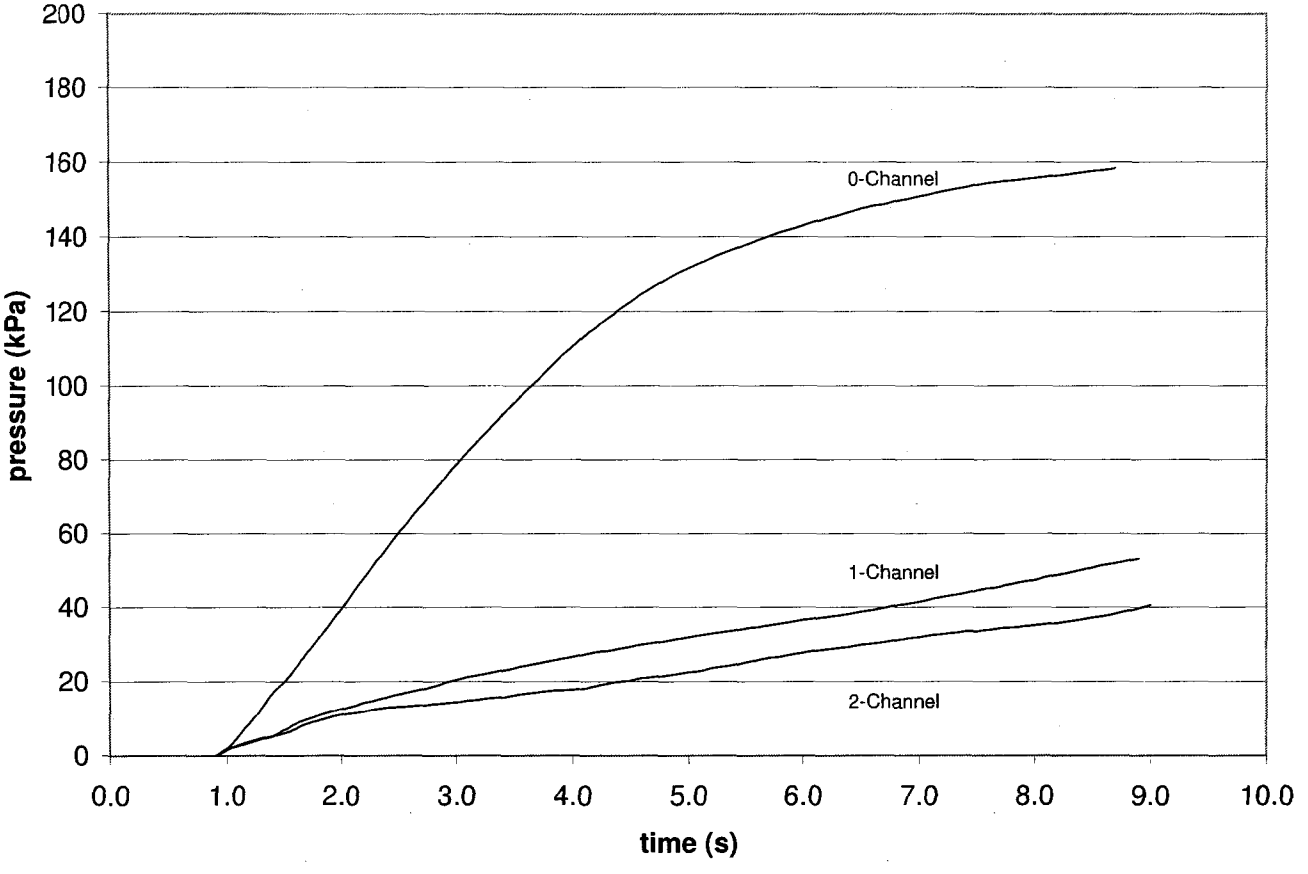

Figure 5.52 Inlet pressure measurement for 0, 1, and 2-Channel molds containing 4 layers (≅20%) of thick fiberglass preform impregnated with 118 cp corn syrup. Channel length set to 67% of disk radius. Each curve represents average of three pressure profiles

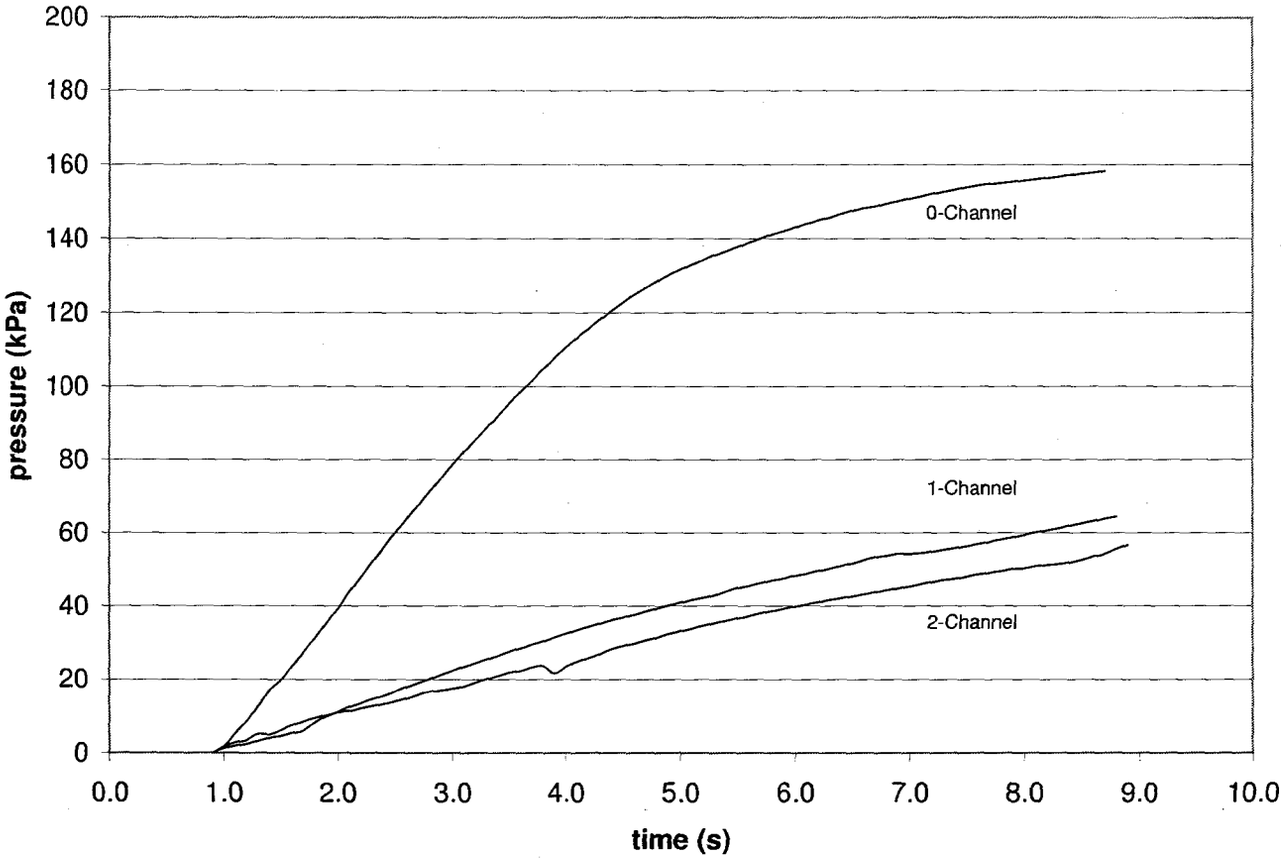

Figure 5.53 Inlet pressure measurement for 0, 1, and 2-Channel molds containing 4 layers (≅20%) of thick fiberglass preform impregnated with 118 cp corn syrup. Channel length set to 50% of disk radius. Each curve represents average of three pressure profiles

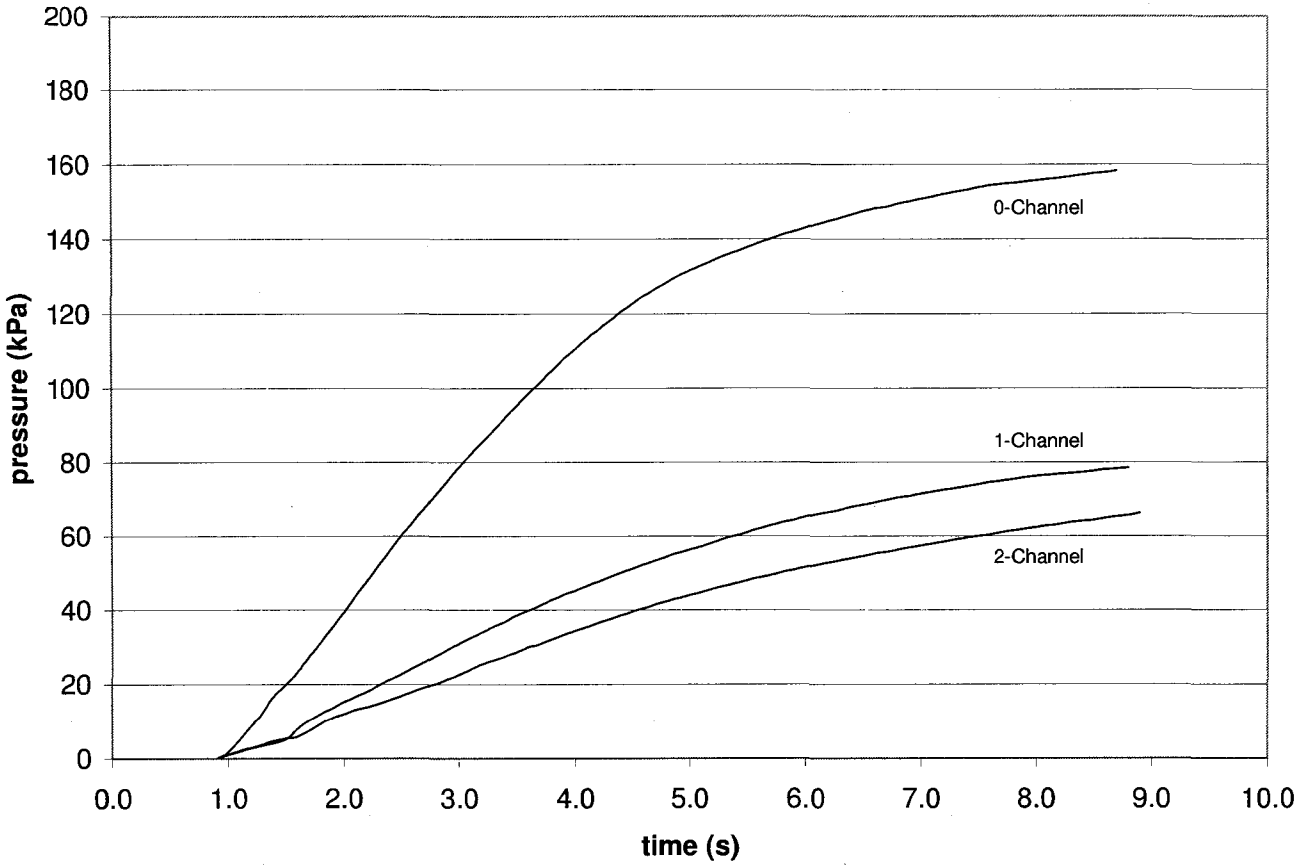

Figure 5.54 Inlet pressure measurement for 0, 1, and 2-Channel molds containing 4 layers (≅20%) of thick fiberglass preform impregnated with 118 cp corn syrup. Channel length set to 33% of disk radius. Each curve represents average of three pressure profiles

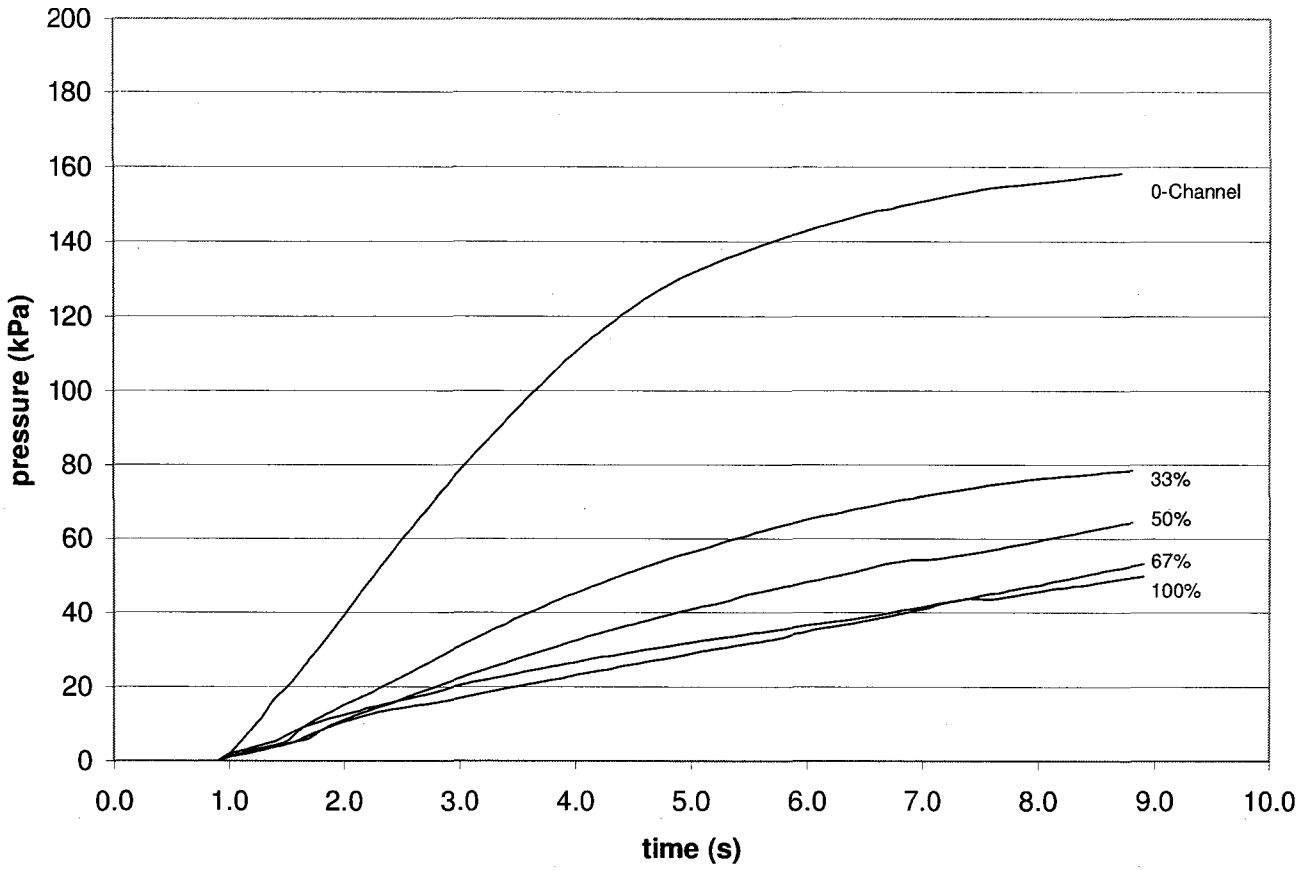

Figure 5.55 Inlet pressure measurement for 1-Channel molds containing 4 layers (≅20%) of thick fiberglass preform impregnated with 118 cp corn syrup for channel lengths blocked to 33, 50, 67, and 100% of the disk radius. Limiting case is 0% channel length, represented by 0-Channel mold. Each curve represents average of three pressure profiles

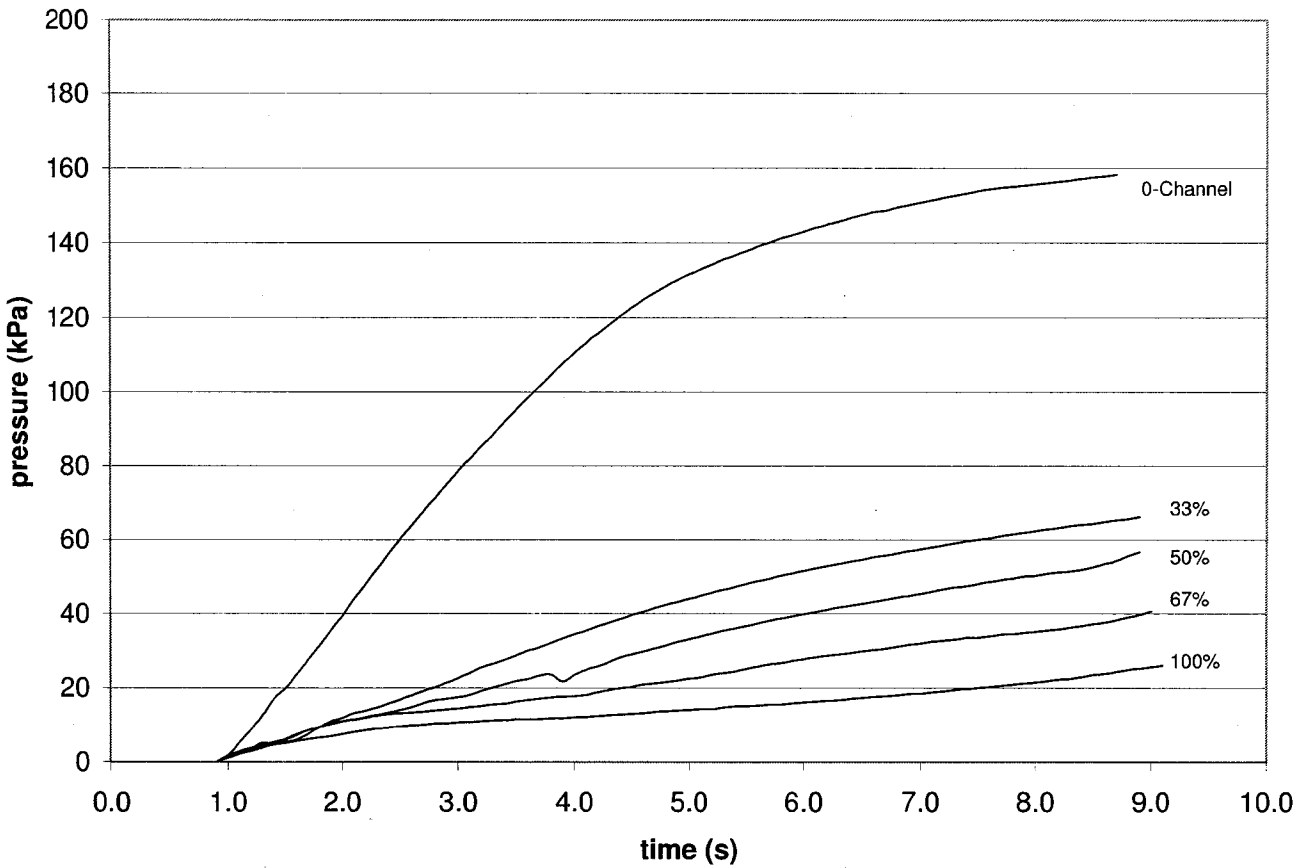

Figure 5.56 Inlet pressure measurement for 2-Channel molds containing 4 layers (≅20%) of thick fiberglass preform impregnated with 118 cp corn syrup for channel lengths blocked to 33, 50, 67, and 100% of the disk radius. Limiting case is 0% channel length, represented by 0-Channel mold. Each curve represents average of three pressure profiles

Table 5.3 Maximum pressures (kPa) measured for 1-Channel molds with different channel lengths, expressed as percentage of disk radius, using different molding configurations. Average from three filling for each disk

Pressure (kPa)	**0% (0-Channel)**	**33%**	**50%**	**67%**	**100% (unblocked)**
TK4CH	158	78.5	64.5	53.1	49.8
TN8CH	147	87.3	87.2	63.9	44.6
TN12CH	192	106	77.8	82.7	*

*Configuration does not yield meaningful pressure data.

Table 5.4 Maximum pressures (kPa) measured for 2-Channel molds with different channel lengths, expressed as percentage of disk radius, using different molding configurations. Average from three filling for each disk

Pressure (kPa)	**0% (0-Channel)**	**33%**	**50%**	**67%**	**100% (unblocked)**
TK4CH	158	66.2	56.7	40.6	26.1
TN8CH	147	73.0	63.7	42.3	26.5
TN12CH	192	92.4	48.3	44.4	*

*Configuration does not yield meaningful pressure data.

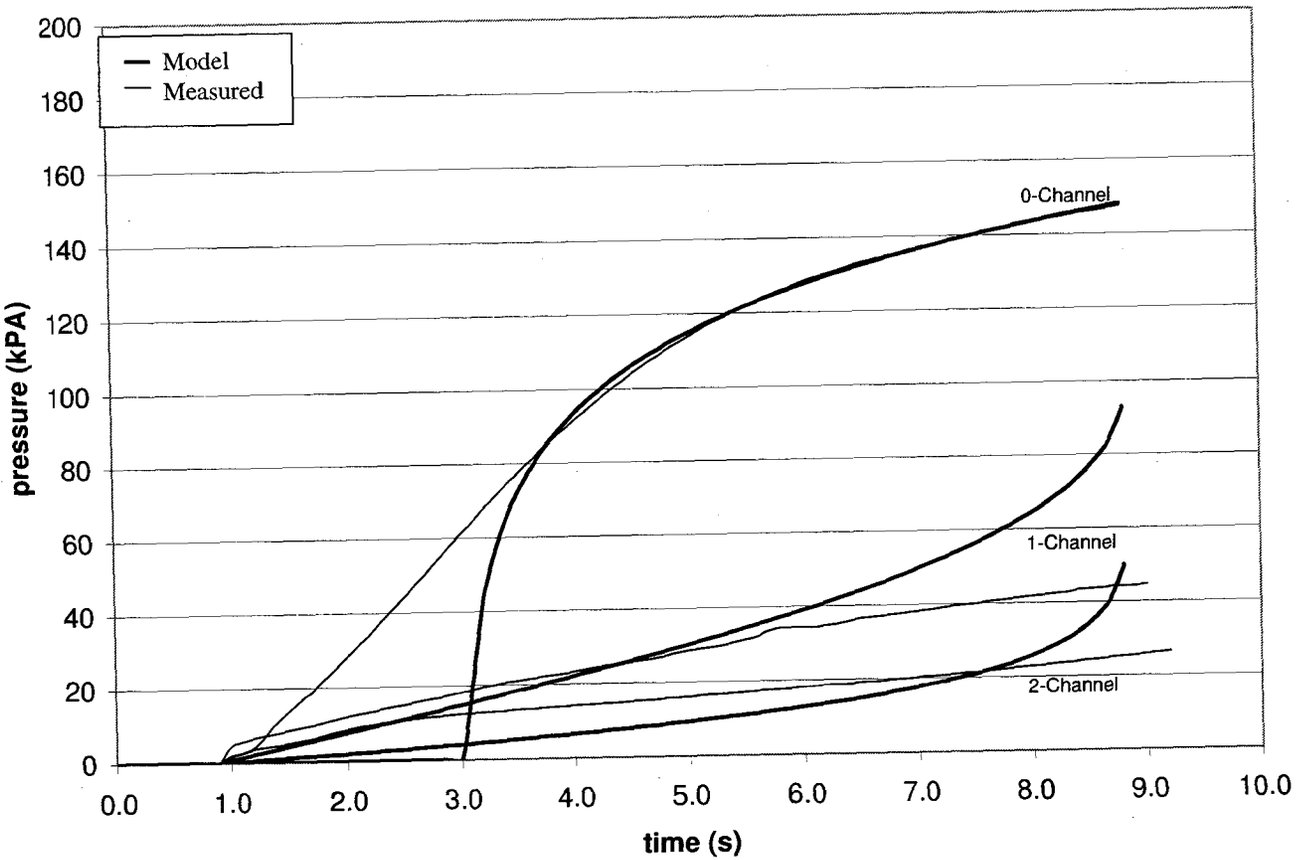

Figure 5.57 Inlet pressure measurement for 0, 1, and 2-Channel molds containing 8 layers (≅20%) of thin fiberglass preform impregnated with 138 cp corn syrup. Channel length set to disk radius. Bold curves are theoretically generated. Each experimental curve represents average of three pressure profiles

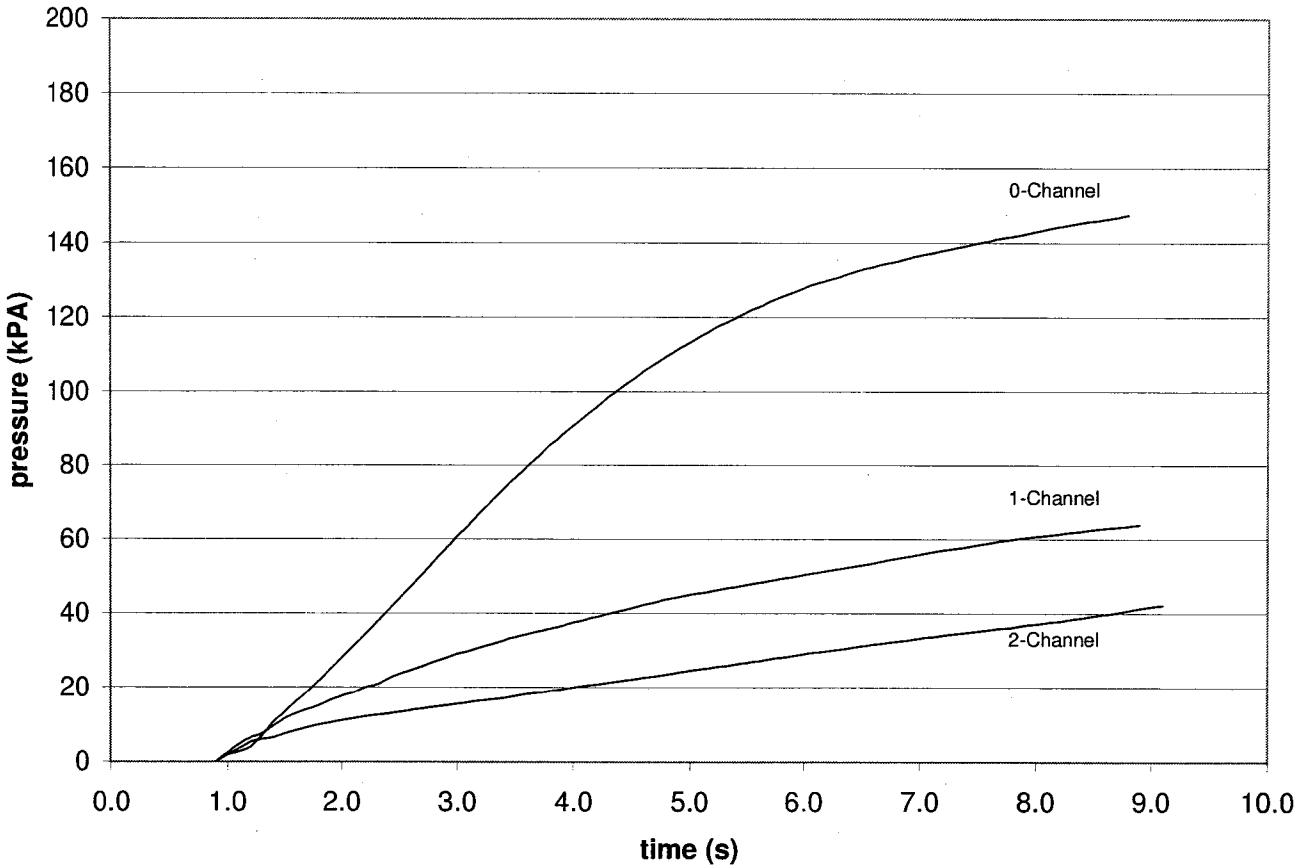

Figure 5.58 Inlet pressure measurement for 0, 1, and 2-Channel molds containing 8 layers (≅20%) of thin fiberglass preform impregnated with 138 cp corn syrup. Channel length set to 67% of disk radius. Each curve represents average of three pressure profiles

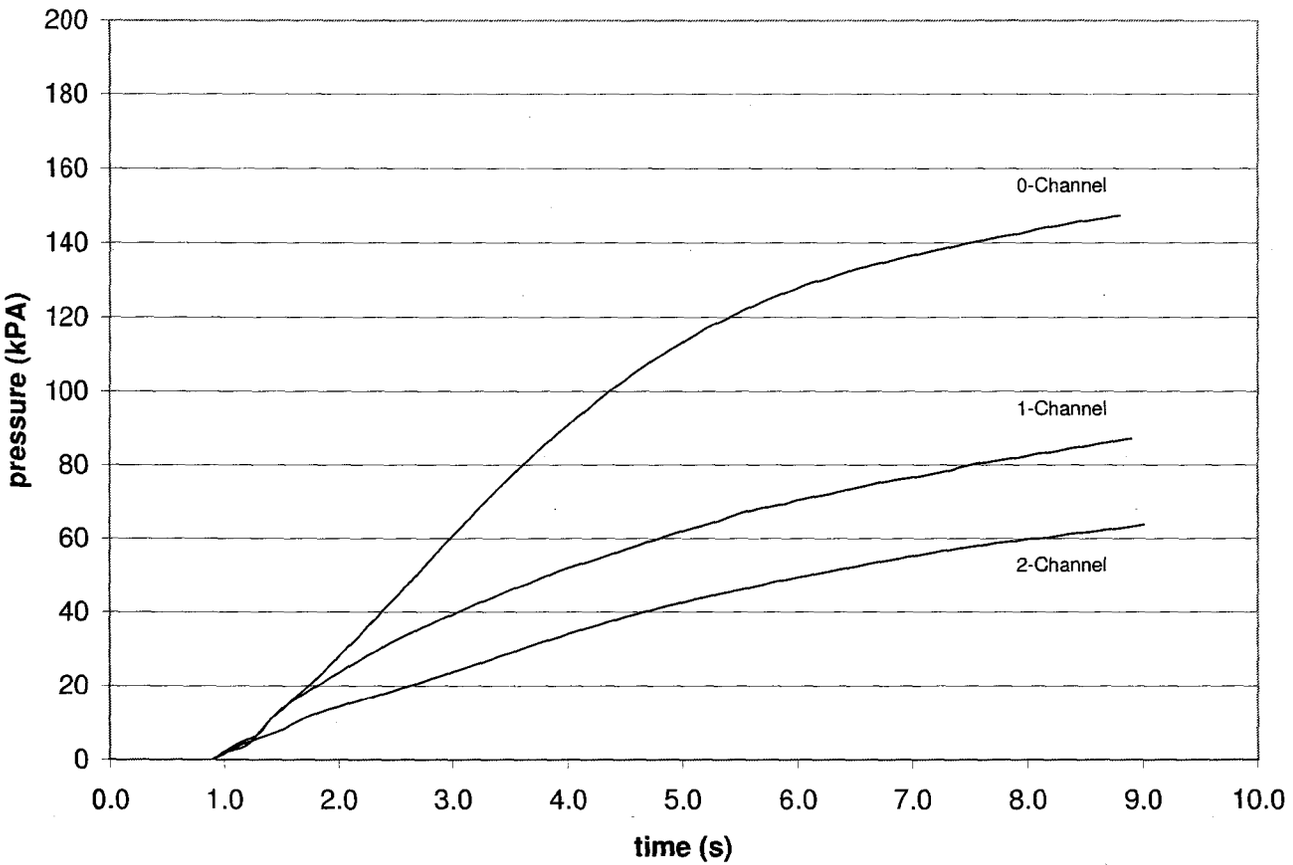

Figure 5.59 Inlet pressure measurement for 0, 1, and 2-Channel molds containing 8 layers (≅20%) of thin fiberglass preform impregnated with 138 cp corn syrup. Channel length set to 50% of disk radius. Each curve represents average of three pressure profiles

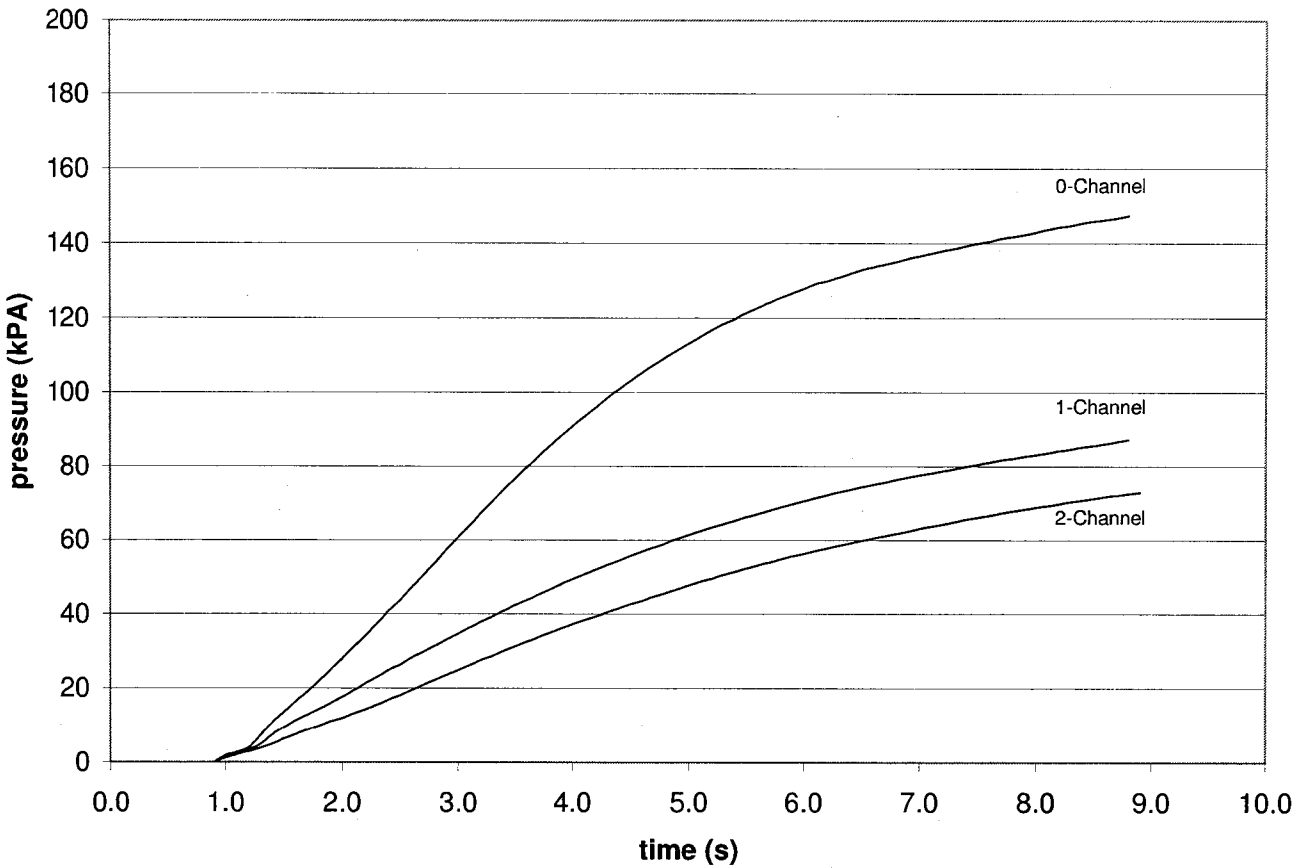

Figure 5.60 Inlet pressure measurement for 0, 1, and 2-Channel molds containing 8 layers (≅20%) of thin fiberglass preform impregnated with 138 cp corn syrup. Channel length set to 33% of disk radius. Each curve represents average of three pressure profiles

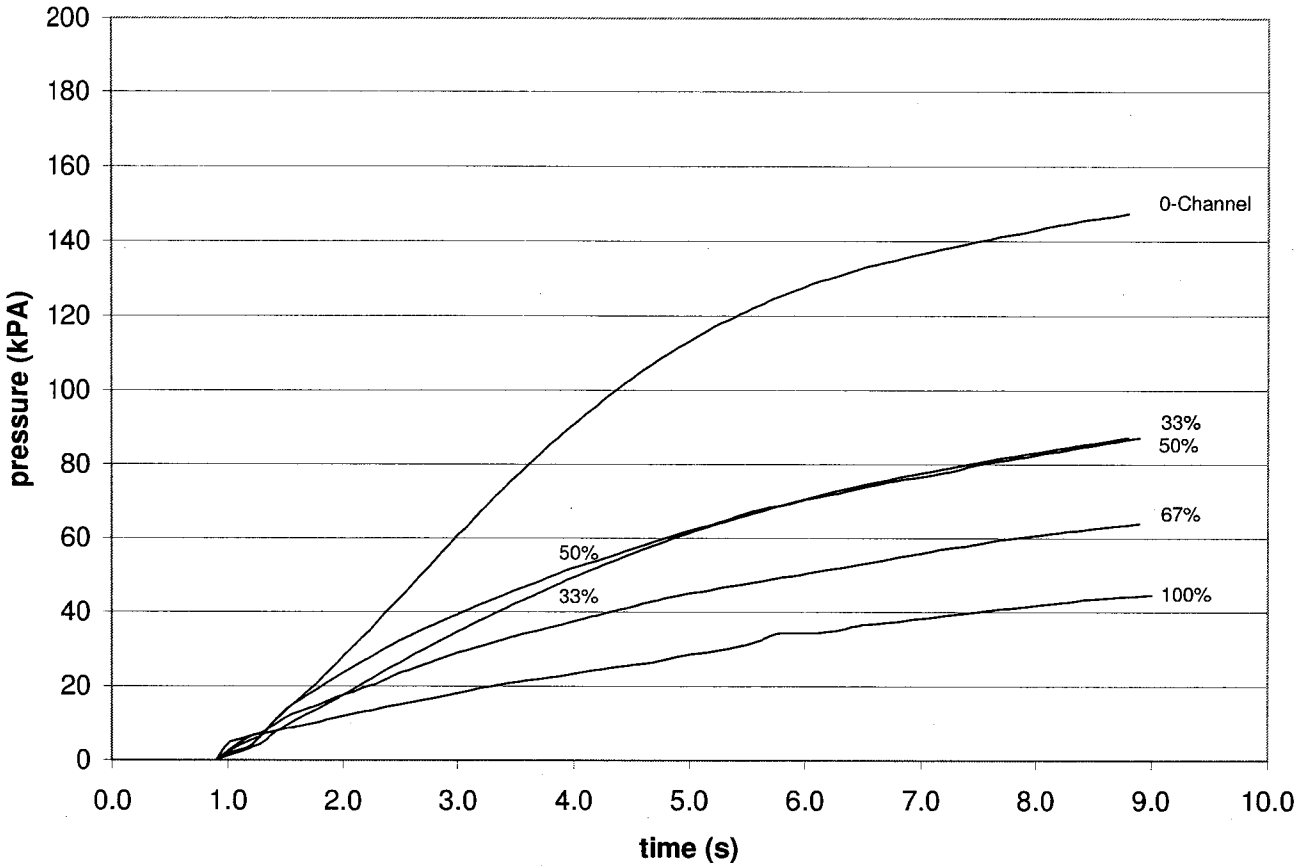

Figure 5.61 Inlet pressure measurement for 1-Channel molds containing 8 layers (≅20%) of thin fiberglass preform impregnated with 138 cp corn syrup for channel lengths blocked to 33, 50, 67, and 100% of the disk radius. Limiting case is 0% channel length, represented by 0-Channel mold. Each curve represents average of three pressure profiles

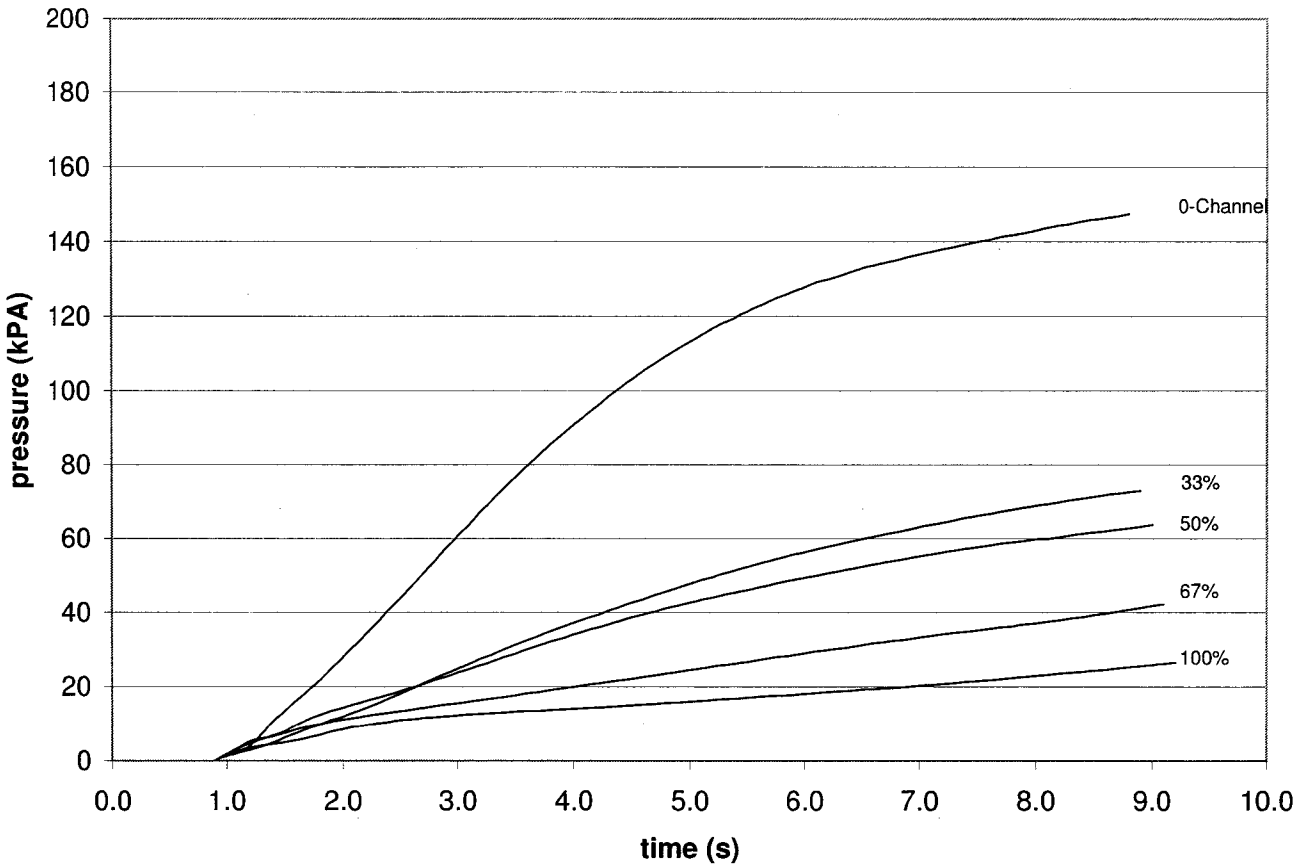

Figure 5.62 Inlet pressure measurement for 2-Channel molds containing 8 layers (≅20%) of thin fiberglass preform impregnated with 138 cp corn syrup for channel lengths blocked to 33, 50, 67, and 100% of the disk radius. Limiting case is 0% channel length, represented by 0-Channel mold. Each curve represents average of three pressure profiles

Table 5.5 Measured permeability values obtained from curve fitting inlet pressure data

Configuration	Permeability obtained from curve fit to transient inlet pressure data (10^{-10} m^2)	Reference permeabiiity from similarly volume fraction using wall mounted transducer (10^{-10} m^2)
TK4CH	12.4	5.3
TN8CH	12.7	7.8
TN12CH	10.2	2.8

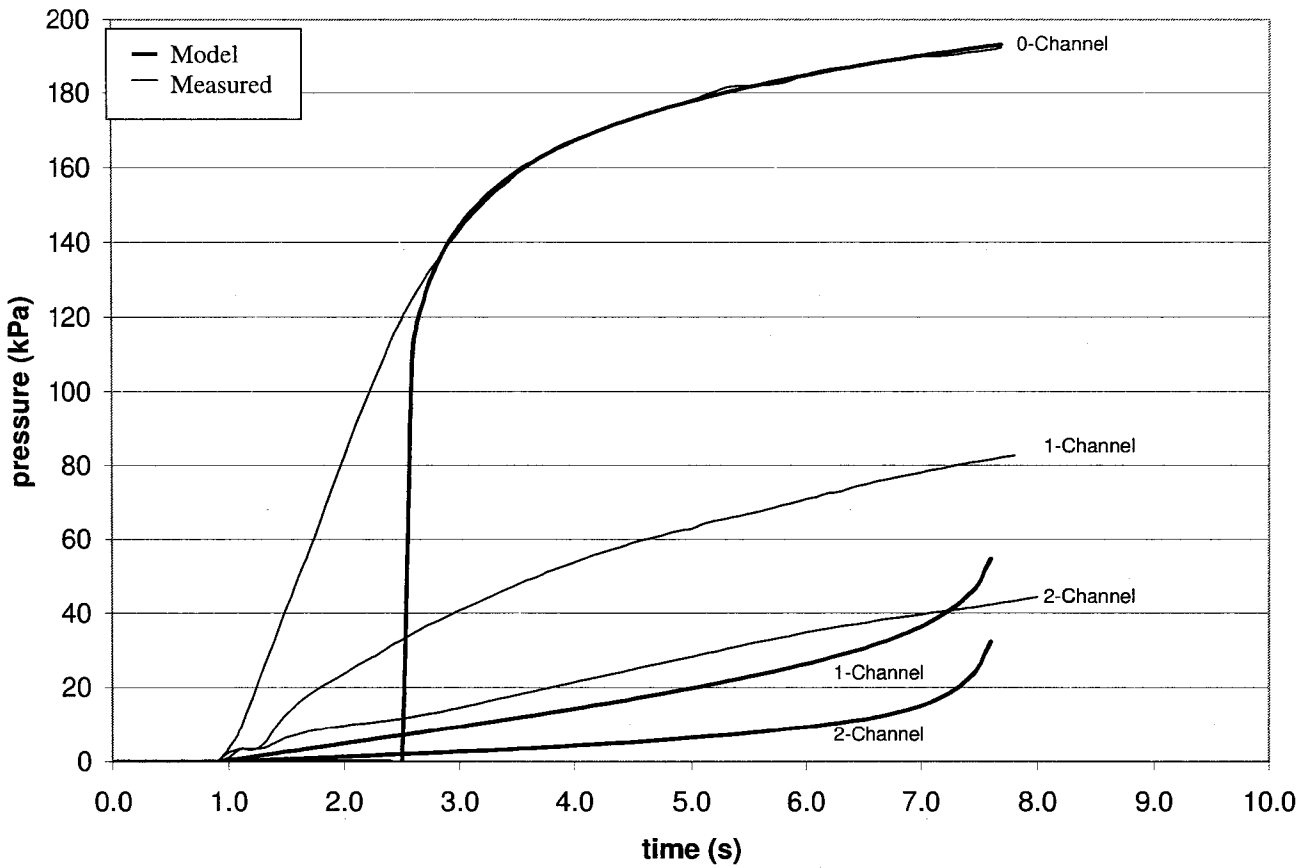

Figure 5.63 Inlet pressure measurement for 0, 1, and 2-Channel molds containing 12 layers (≅30%) of thin fiberglass preform impregnated with 63.2 cp corn syrup. Channel length set to 67% of disk radius. Bold curves are theoretically generated for 100% channel length. Each experimental curve represents average of three pressure profiles

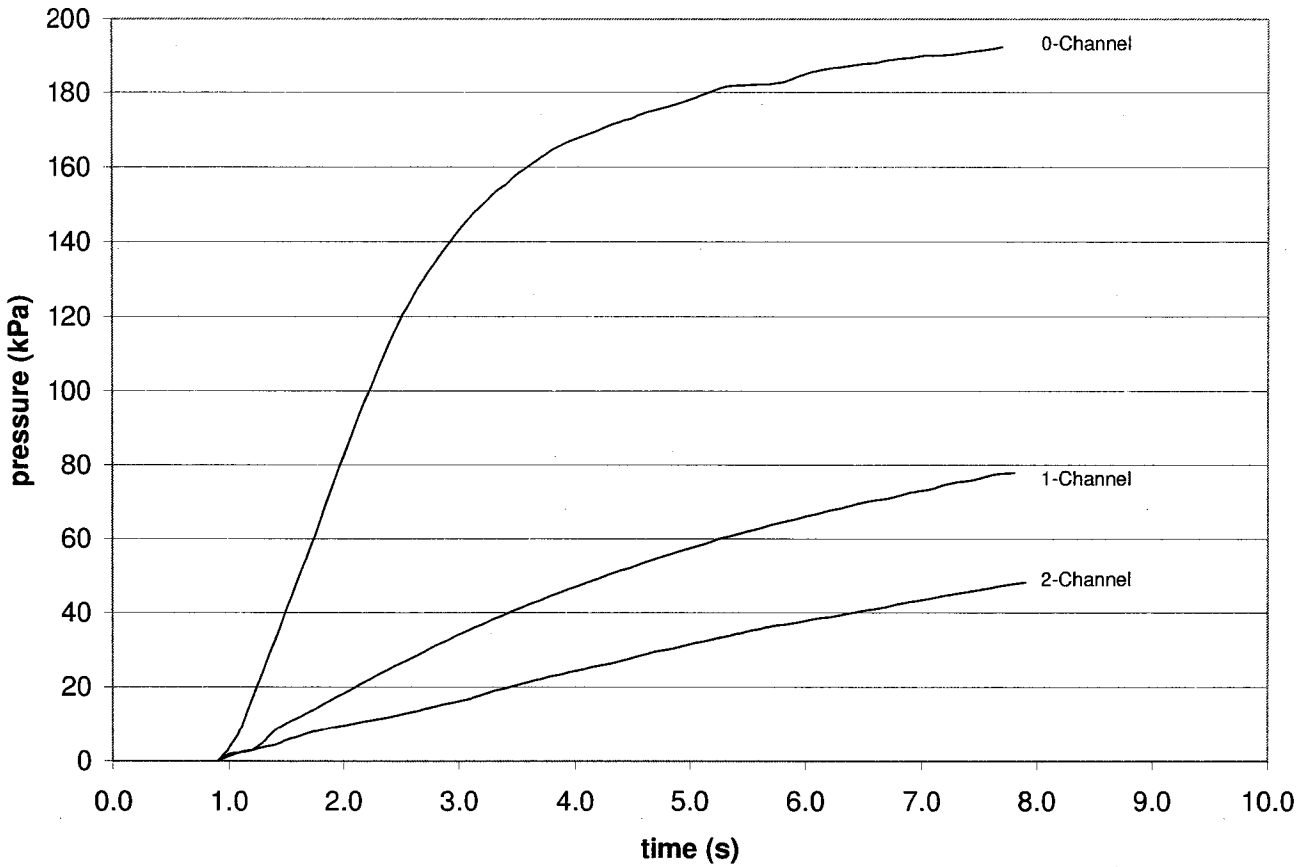

Figure 5.64 Inlet pressure measurement for 0, 1, and 2-Channel molds containing 12 layers (≅30%) of thin fiberglass preform impregnated with 63.2 cp corn syrup. Channel length set to 50% of disk radius. Each curve represents average of three pressure profiles

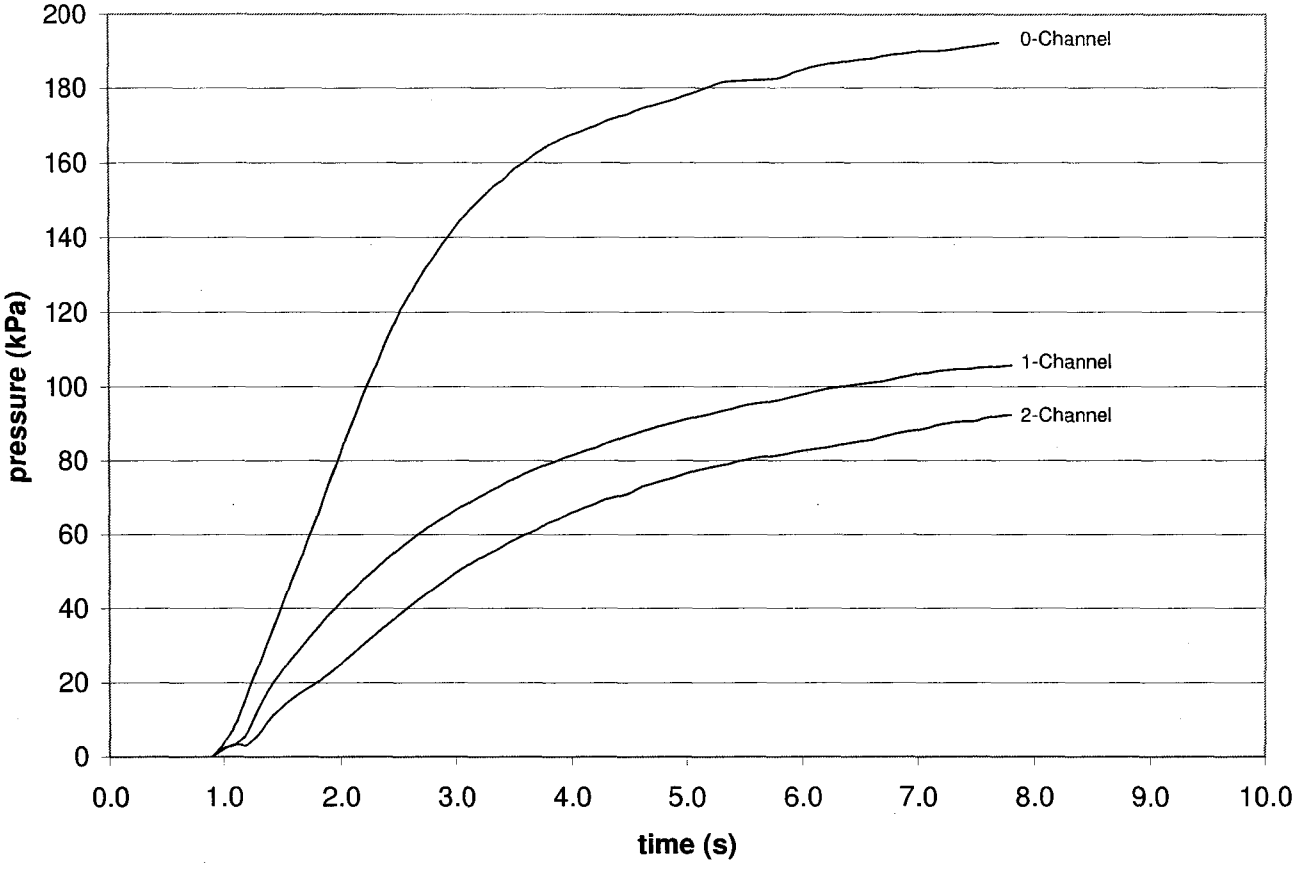

Figure 5.65 Inlet pressure measurement for 0, 1, and 2-Channel molds containing 12 layers (≅30%) of thin fiberglass preform impregnated with 63.2 cp corn syrup. Channel length set to 33% of disk radius. Each curve represents average of three pressure profiles

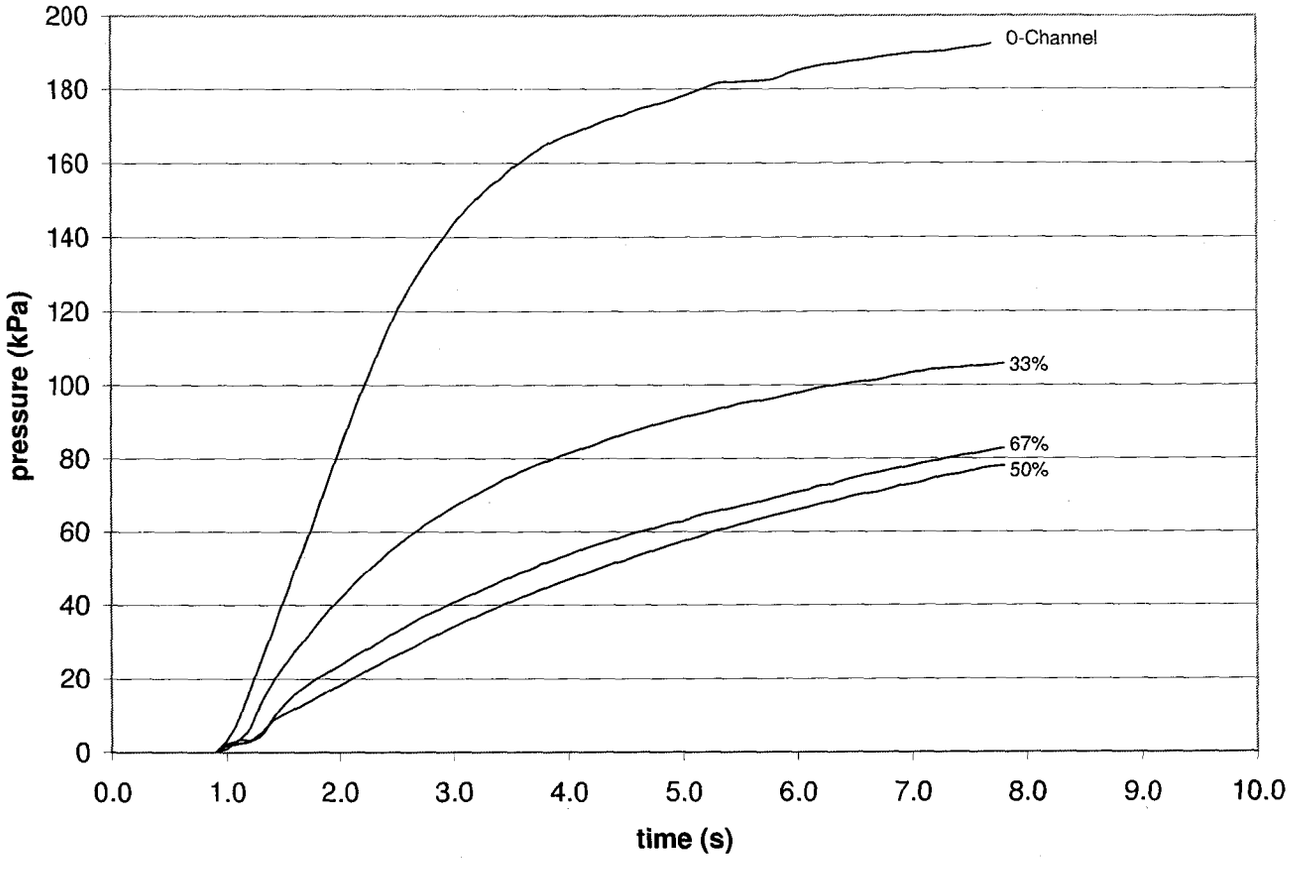

Figure 5.66 Inlet pressure measurement for 1-Channel molds containing 12 layers (≅30%) of thin fiberglass preform impregnated with 63.2 cp corn syrup for channel lengths blocked to 33, 50, and 67% of the disk radius. Limiting case is 0% channel length, represented by 0-Channel mold. Each curve represents average of three pressure profiles

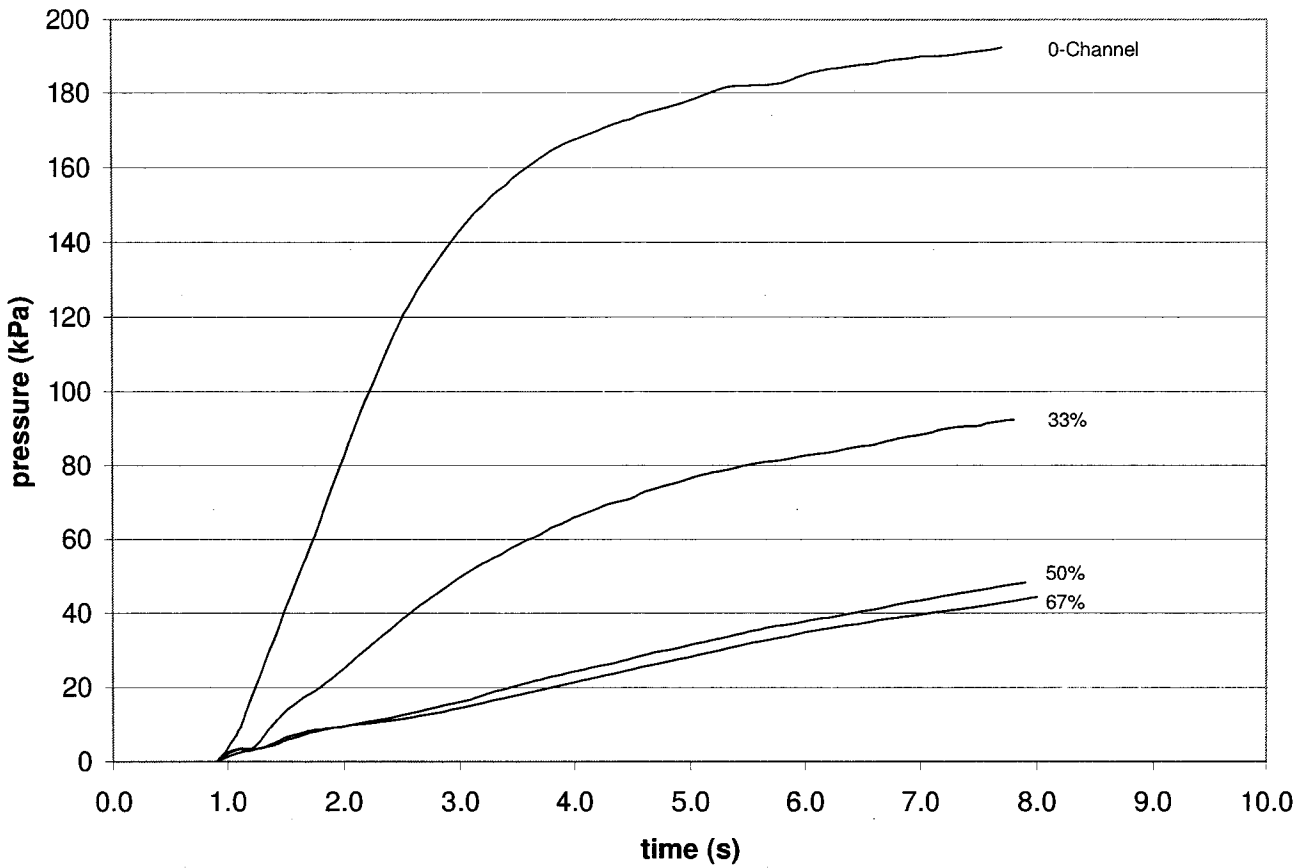

Figure 5.67 Inlet pressure measurement for 2-Channel molds containing 12 layers (≅30%) of thin fiberglass preform impregnated with 63.2 cp corn syrup for channel lengths blocked to 33, 50, and 67% of the disk radius. Limiting case is 0% channel length, represented by 0-Channel mold. Each curve represents average of three pressure profiles

6 Concluding Remarks

Effects of process parameters on resin transfer molding process are experimentally identified. Injection rate and post-fill cure pressure are varied, and resulting change in mechanical properties and observed void content recorded. Trends are observed, with increased injection rate resulting in reduced mechanical properties due to change in void shape and increase in void content. Tensile strength is found to decrease by 12% and stiffness is found to decrease by 14% over range of flow rate studied. Addition of post-fill cure pressure of 683 kPa to the process is found to reduce void content from 0.72% to 0.35%, resulting in improvements of 15% to strength and 13% to elastic modulus. Mechanical properties are correlated with void content, revealing several important trends. Properties are found to decrease with increasing void content up to 0.5%, however no degradation in properties is observed beyond 0.5% void content. Significant rate of change is observed at lowest achieved void content of 0.34%, indicating better properties are attainable. This is an important finding, as void content less than 1% is often considered "good" in literature. Total improvement in overall mechanical properties of nearly 30% is achieved by combining highest packing pressure and lowest flow rate, thus good control over these parameters is thought to have potential industrial benefit. Experimental description of effect of process parameters on molded parts is important. In industry, common practice is to vary process parameters via trial and error to find combination that yields best results. Trends observed experimentally can enhance this process with intelligent selection.

Preform used in resin transfer molding is described in the second part of the presented study. Effect of fiber volume fraction and mat thickness on mechanical properties and injection pressure of resin transfer molded disks are presented. Mechanical properties are known to increase with fiber content. Experimentally, linear increase of about 150% for ultimate tensile strength, and 100% for elastic modulus and short-beam shear strength are observed as fiber content increases from 9.8% and 33.1%. Mat thickness, or planar preform density, is observed to have insignificant effect on mechanical properties at same fiber content. Measured properties include elastic modulus, tensile strength, and short-beam shear strength. However, mat thickness is shown to have significant effect on injection pressure, resulting from up to 226% higher permeability of thin mats. The finding is significant, as ability to increase permeability without reduction in mechanical properties has several important and cost saving advantages. Higher permeabilities allow for lower molding pressure and thus less expensive molding equipment, higher injection rates at same molding pressure for greater production rate, or higher fiber content and improved properties with same molding pressure.

Preform permeability is measured using a new measurement technique. Presented method allows permeability to be measured using the transient pressure data from a single pressure transducer. Techniques currently used in the literature require use of multiple transducers or tracking of fluid front motion in addition to pressure measurement. An alternate permeability measurement technique is presented to utilize injection pressure readings. Permeability is

obtained by fitting theoretical pressure curve generated from the known injection rate to pressure measurements. Excessive inlet effects observed in the present molding setup lead to higher error in permeability measurements obtained in this manner. It is recommended that continued research be performed with an improved setup to fully demonstrate measurement technique. Injection pressure can be obtained without mounting a transducer in the mold cavity, thus method is non-intrusive and could be used to obtain preform data in industrial applications.

A new molding process is presented, in which channels are formed in mold walls and utilized in traditional RTM. Goal is to reduce molding pressure requirements in the latter process. Addition of channels is shown to considerably reduce required injection pressure, with achievements of up to 77% reduction in molding pressure. Disk-shaped parts are molded at a variety of channel configurations, varying channel length and number of channels. Parts are visually inspected for void content and defects. Ray tracing effects are identified as cause of defects for some channel configurations, as flow reaches mold edge early, however these effects are eliminated by reducing channel length and adding additional channels.

The natural next step to validate effectiveness of using channels is void content analysis and mechanical characterization of molded parts. Macrovoids resulting from the use of channels are unquestionable, however only qualitative data is available from visual comparison. Although differences in void content are obvious due to improved clarity for better parts, quantitative data is necessary to fully understand potential negative effects.

For presented results, exit gate location remained fixed, and artifacts resulting from addition of channels to the process were dealt with by changing number of channels and channel length. Many variations of this approach could yield beneficial improvements. Channel depth and width are variables that can be modified in a straightforward manner. Channels are shown to be quite effective, thus decrease in flow area may yield good pressure reduction with decreased scrap. Deeper, narrower channels could reduce effort required to remove excess material from final part. In contrast, shallow, wider channels could be used in some instances, leaving a ridge on the part that might not need to be removed at all. Tapered channel walls, or complete change in channel profile, e.g., a semicircle, could be used to allow for easier demolding and may also leave ridges that can remain permanently on the part in some cases. A T-shaped profile may result in more difficult demolding, but could combine increased flow area, with smaller contact area on the mold surface.

Numerous studies in literature address fluid front shape in RTM. Many of the presented methods could be readily applied to new molding process by assuming inlet gate shape includes channels, or by setting local permeability in area covered by channels to the much higher equivalent permeability calculated for channel flow. Numerical analysis of channel molding can more quickly cover a range of channel configurations compared with experimentally molding parts. It would also lend nicely to other optimization approaches, such as moving exit gate location to final location of flow front for any channel configuration, rather than modify the channel configuration to obtain better results.

7 References

1. Naik, R. A. Failure analysis of woven and braided fabric reinforced composites. 1995. *Journal of Composite Materials*, 29(17): 2334-2363.
2. Oksman, K. High quality flax fiber composites manufactured by the resin transfer moulding process. 2001. *Journal of Reinforced Plastics and Composites*, 20(7): 621-627.
3. Pearce, N. R. L, Summerscales, J., and Guild, F. J. Improving the resin transfer moulding process for fabric-reinforced composites by modification of the fabric architecture. 2000. *Composites Part A*, 31: 1433-1441.
4. Wang, Y. Effect of consolidation method on the mechanical properties of nonwoven fabric reinforced composites. 1999. *Applied Composite Materials*, 6: 19-34.
5. Wang, Y. and Li, J. Properties of composites reinforced with e-glass nonwoven fabric. 1995. *Journal of Advanced Materials*, 28-34.
6. Goodwin, A.A., Howe, C.A., and Paton, R.J. The role of voids in reducing the interlaminar shear strength in RTM laminates. 1997. *Proceedings of ICCM-11*. Volume IV: 11-19.
7. Lee, C.-L. and Wei K.-H. Effect of material and process variables on the performance of resin-transfer-molded epoxy fabric composites. 2000. *Journal of Applied Polymer Science*, 77: 2149-2155.
8. Patel, N., Rohatgi, V., and Lee, L. J. Influence of processing and material variables in resin-fiber interface in liquid composite molding. 1993. *Polymer Composites*, 14(2): 161-172.

9. Lee, C. -L., and Wei, K. -H. Resin transfer molding (RTM) process of high performance epoxy resin. ii: Effect of process variables on the physical, static and dynamic mechanical behavior. 2000. *Polymer Engineering and Science*, 40(4): 935-943.

10. Bickerton, S., Sozer, E. M., Graham, P. J., Advani, S.G. Fabric structure and mold curvature effects on preform permeability and mold filling in the RTM process. Part i. experiments. 2000. *Composites Part A,* 31: 423-438.

11. Bickerton, S., Sozer, E. M., Graham, P. J., Advani, S.G. Fabric structure and mold curvature effects on preform permeability and mold filling in the rtm process. Part ii. predictions and comparisons with experiments. 2000, *Composites Part A*, 31: 439-458.

12. Mogavero, J. and Advani, S. G. Experimental investigation of flow through multi-layered preforms. 1997. *Polymer Composites*, 18(5): 649-655.

13. Pearce, N. R. L, Guild, F. J. and Summerscales, J. An investigation into the effects of fabric architecture on the processing and properties of fiber reinforced composites produced by resin transfer moulding. 1998. *Composites Part A*, 29: 19-27.

14. Adams, K. L. and Rebenfeld, L. In-plane flow of fluids in fabrics: structure/flow characterization. 1987. *Textile Research Institute*, 11: 647-654.

15. Darcy, H. P. G., 1856, `Les Fontaines Publiques de la Ville de Dijon. *Dalmont*, Paris, 306.

16. Carman, P. C. Fluid flow through a granular bed. 1937. *Transcript of International Chemical Engineering*, 15: 150-166.

17. Gutowsky, T. G., Morigaki, T. and Cai, Z. The consolidation of laminate composites. 1987. *Journal of Composite Materials*, 21: 172-188.

18. Gebart, B. R. Permeability of unidirectional reinforcements for RTM. 1992. *Journal of Composite Materials*, 26(8): 1100-1133.

19. Bruschke, M. V., Advani, S. G. A finite element/control volume approach to mold filling in anisotropic porous media. 1990. *Polymer Composites*, 11(6): 398-405.

20. Ngo, N. D. and Tamma, K. K. Microscale permeability predictions of porous fibrous media. 2001. *International Journal of Heat and Mass Transfer*, 44: 3135-3145.

21. Williams, J. G., Morris, C. E. M. and Ennis, B. C. Liquid flow through aligned fiber beds. 1974. *Polymer Engineering and Science*, 14(6): 413-419.

22. Trevino, L., Rupel, K., Young, W. B., Liou, M. J. and Lee,L. J. Analysis of resin injection molding in molds with preplaced fiber mats. i: Permeability and compressibility measurements. 1991. *Polymer Composites*, 12(1): 20-29.

23. Young, W. B., Rupel, K., Lee, L. J. and Liou, M. J. Analysis of resin injection molding in molds with preplaced fiber mats. ii: Numerical simulation and experiments of mold filling. 1991. *Polymer Composites*, 12(1): 30-38.

24. Calhoun, D. R., Yalvaç, S., Wetters, D. G., and Raeck, C. A. Critical issues in model verification for the resin transfer molding process. 1996. *Polymer Composites*, 17(1): 11-22.

25. Adams, K. L., Miller, B. and Rebenfeld, L. Forced in-plane flow of an epoxy resin in fibrous network. 1986. *Polymer Engineering and Science*, 26(20): 1434-1441.

26. Adams, K. L. and Rebenfeld, L. Permeability characteristics of multilayer fiber reinforcements. Part i: Experimental observations. 1991. *Polymer Composites*, 12(3): 179-185.

27. Adams, K. L. and Rebenfeld, L Permeability characteristics of multilayer fiber reinforcements. Part ii: Theoretical model. 1991. *Polymer Composites*, 12(3): 186-190.

28. Gauvin, R., Trochu, F., Lemenn, Y. and Diallo, L. Permeability measurement and flow simulation through fiber reinforcement. 1996. *Polymer Composites*, 17(1): 34-42.

29. Sheard, J., Senft, V., Mantell, S. C. and Vogel., J. H. Determination of corner and edge permeability in resin transfer molding. 1998. *Polymer Composites*, 19(1): 96-105.

30. Ferland, P., Guittard, D. and Torchu, F. Concurrent methods for permeability measurement in resin transfer molding. 1996. *Polymer Composites*, 17(1): 149-158.

31. Dungan, F. D., Sengouz, M. T., Sastry, A. M. and Faillaci, D. A. Simulation and experiments on low pressure permeation of fabrics: Part i: 3-D

modeling of unbalenced fabric. 1999. *Journal of Reinforced Plastics and Composites*, 18(5): 472-482.

32. Thomason, J. L. The interface region in glass fibre-reinforced epoxy resin composites: 1. Sample preparation, void content and interfacial strength. 1995. *Composites*, 26: 467-475.
33. Ghiorse, S.R. Effect of void content on the mechanical properties of carbon/epoxy laminates. 1993. *SAMPE Quarterly*, 24(2): 54-59.
34. Hoppel, C., Bogetti, T., and Newill, J.F. Effects of voids on moisture diffusion in composite materials. 2000. *Proceedings of the American Society for Composites: 15th Technical Conference*: 1094-1101.
35. Varna, J., Joffe, R., Berglund, L., and Lundström, T. Effect of voids on failure mechanisms in RTM laminates. 1995. *Composites Science and Technology*, 53: 241-249.
36. Wisnom, M. R., Reynolds, T., and Gwilliam, N. Reduction in interlaminar shear strength by discrete and distributed voids. 1996. *Composites Science and Technology*, 56: 93-101.
37. Parnas, R., and Phelan, F. Effect of heterogeneous porous media on mold filling in resin transfer molding. 1991. *SAMPE Quarterly*, 22(2): 53-60.
38. Moon, K., Lee, W., and Hanh, T. Formation of Microvoids during resin-transfer molding process. 2000. *Composites Science and Technology*, 60: 2427-2434.

39. Patel, N., and Lee, L. J. Effects of fiber mat architecture on void formation and removal in liquid composite molding. 1995. *Polymer Composites*, 16(5): 386-399.

40. Stabler, W.R., Tatterson, G.B., Sadler, R.L., and El-Shiekh, A.H.M. Void minimization in the manufacture of carbon fiber composites by resin transfer molding. 1992. *SAMPE Quarterly*, 23(2): 38-42.

41. Ikegawa, N., Hamada, H., and Maekawa, Z. Effect of compression process on void behavior in structural resin transfer molding. 1996. *Polymer Engineering and Science*, 36(7): 953-962.

42. Chang, C.-Y., and Hourng, L.-W. Study on void formation in resin transfer molding. 1998. *Polymer Engineering and Science*, 38(5): 809-818.

43. Lundström, T. S., and Gebart, B. R. Influence from process parameters on void formation in resin transfer molding. 1994. *Polymer Composites*, 15(1): 25-33.

44. Lee, C.-L., and Wei, K.-H. Resin transfer molding (RTM) process of a high performance epoxy resin. ii: Effects of process variables on the physical, static and dynamic mechanical behavior. 2000. *Polymer Engineering and Science*, 40(4): 935-943.

45. Russ, J. 1986. *Practical Stereology*, New York, NY: 1st ed., Plenum Press.

46. Ghiorse, S. A comparison of void measurement methods for carbon/epoxy composites. 1991. U.S. Army Materials Technology Laboratory: Report MTL TR 91-13: 1-20.

47. Callus, P. J., Mouritz, A. P., Bannister, M. K., and Leong, K. H. Tensile properties and failure mechanisms of 3D woven GRP composites. 1999. *Composites Part A*, 30: 1277-1287.

48. De Oliveira Simões, J. A., and Marques, A. T. Determination of stiffness properties of braided composites for the design of hip prosthesis. 2001. *Composites Part A*, 32: 655-662.

49. Hillermeier, R. W., and Seferis, J. C. Interlayer toughening of resin transfer molded composites. 2001. *Composites Part A*, 32: 721-729.

50. Margueres, Ph., Meraghni, F., and Benzeggagh, M. L. Comparison of stiffness measurements and damage investigation techniques for a fatigued and post-impact fatigued GFRP composite obtained by RTM process. 2000. *Composites Part A*, 31: 151-163.

51. Mahale, A. D., Prud'Homme, R. K., and Rebenfeld, L. Quantitative measurement of voids formed during liquid impregnation of nonwoven multifilament glass networks using an optical visualization technique. 1992. *Polymer Engineering and Science,* 32(5): 319-326.

52. Patel, N., and Lee, L. J. Modeling of void formation and removal in liquid composite molding. part ii: model development and implementation. 1996. *Polymer Composites*, 17(1): 104-114.

53. Han, K., Jiang, S., Zhang, C., and Wang B. Flow modeling and simulation of SCRIMP for composites manufacturing. 2000. *Composites Part A*, 31(1): 79–86.

54. Johnson, R. J. and Pitchumani, R. Enhancement of flow in VARTM using localized induction heating. 2003. *Composites Science and Technology*, 63: 2201-2215.

55. Bre´, S. A., Bréard, J., and Bouquet G. 2002. Proc. of the 5th Intl. ESA-FORM Conf. on Material Forming, 299–302.

56. Rich R. L., Saouab, A., and Bréard, A. Coupled compression RTM and composite layup optimization. 2003. *Composites Science and Technology*, 63: 2277-2287.

57. Dhillon, I. S. Resin transfer molding of fiber reinforced composite disks. 2000. Masters thesis, University of Oklahoma, Norman, OK.

58. ASTM D3039/D3039M-95a. 1997. 15.03: 98-108.

59. ASTM D2344/D2344M-00. 2000.

60. Patel, N., Rohatgi, V., and Lee, L. J. Micro scale flow behavior and void formation mechanism during impregnation through a unidirectional stitched fiberglass mat. 1995. *Polymer Engineering and Science*, 35(10): 837-852.

61. Parnas, R. S., Flynn, K. M., and Dal-Favero, M. E. A permeability database for composites manufacturing. 1997. *Polymer Composites*, 18(5): 623-633.

62. Lai, Y-H., Khomami, B., and Kardos, J. L. Accurate permeability characterization of preforms used in polymer matrix composite fabrication processes. 1997. *Polymer Composites*, 18(3): 368-377.

63. Olivero, K. A., 2000. Gravity effects on fluid front dynamics during mold filling. Masters thesis, University of Oklahoma, Norman, OK.

64. Olivero, K. A., Barraza, H. J., O'Rear, E. A., and Altan, M. C. Effect of injection rate and post-fill cure pressure on properties of resin transfer molded disks. 2002. *Journal of Composite Materials*, 36(16): 2011-2028.

65. Han, K., Trevino, L., Lee, L. J., and Liou, M. Fiber mat deformation in liquid composite molding. i: Experimental analysis. 1993. *Polymer Composites*, 14(2): 144-150.

66. Han, K., Trevino, L., Lee, L. J., and Liou, M. Fiber mat deformation in liquid composite molding. ii: Modeling. 1993. *Polymer Composites*, 14(2): 151-160.

67. Wirth, S. and Gauvin, R. Experimental analysis of mold filling in compression resin tranfer molding. 1998. *Journal of Reinforced Plastics and Composites*, 17(16): 1414-1430.

68. Luce, T. L., Advani, S. G., Howard, J. G., and Parnas, R. S. Permeability characterization. Part 2: Flow behavior in multiple-layer preforms. 1995. *Polymer Composites*, 16(6): 446-458.

69. Kim, B. Y., Nam, G. J., and Lee, J. W. Optimization of filling processes in rtm using a genetic algorithm and experimental design method. 2002. *Polymer Composites*, 23(1): 72-86.

70. Berker, B. and Sun, J. Q. Permeability estimation in resin transfer molding. 1998. *Journal of Materials Processing & Manufacturing Science*, 6: 205-211.

71. Munson, B. R., Young, D. F., and Okiishi, T. H., 1994. *Fundamentals of Fluid Mechanics 2nd Ed.*, John Wiley & Sons, Inc.

8 Appendix A: Data Tables

Table 6.1 Tensile strength data (in kPa) for position 1 and position 2 specimens used to quantify effects of injection rate on properties for each injection rate. Packing pressure=228 kPa

0.067 cm^3/s	0.2 cm^3/s	0.6 cm^3/s	1 cm^3/s
105.8	90.0	102.5	93.2
117.3	97.5	103.1	99.0
118.3	98.1	106.0	105.6
119.8	100.3	106.4	105.9
121.3	107.7	114.7	110.5
122.0	109.4	115.3	113.7
129.8	113.4	122.5	113.8
134.8	115.5		115.9
134.9	115.5		116.8
141.7	116.7		117.0
	117.3		118.1
	117.9		124.3
	118.0		125.0
	118.4		
	122.1		
	126.7		
	126.8		
	127.3		
	131.0		
	135.5		
	144.4		

Table 6.2 Stiffness data (in kPa) for all position 1 and position 2 specimens used to quantify effects of injection rate on properties for each injection rate. Packing pressure=228 kPa

0.067 cm^3/s	0.2 cm^3/s	0.6 cm^3/s	1 cm^3/s
8233	4157	7942	7100
8724	4309	8283	7710
9344	6997	8703	7767
9501	7797	8819	8021
9651	8023	9021	8198
10040	8310	9379	8467
10063	8778	9714	8528
10269	8890		9040
10963	8973		9116
11668	8982		9311
	9167		9375
	9183		9398
	9326		10002
	9400		
	9645		
	9784		
	9994		
	10044		
	10085		
	10160		
	10523		
	11238		
	11299		

Table 6.3 Tensile strength data (in kPa) for position 1 and position 2 specimens used to quantify effects of packing pressure on properties for each packing pressure. Injection rate=0.067 cm^3/s

UTS (kPa)	0 kPa	228 kPa	455 kPa	683 kPa
Position 1	131.0	125.8	130.3	136.5
	118.0	111.3	134.5	143.9
	144.9	103.6	141.9	141.5
	124.1	147.6	132.7	134.4
	119.1	140.3	149.6	131.3
	119.8	103.4	145.0	146.6
	121.0	132.9	129.5	163.4
	138.1	128.0	127.9	143.9
		137.2		
		121.9		
Position 2	121.4	137.0	135.8	135.3
	120.0	126.8	143.3	142.3
	133.5	143.9	114.2	159.5
	121.1	146.5	136.7	154.8
	105.5	137.1	158.0	136.2
	119.8	123.9	151.7	153.5
	128.7	124.6	119.8	140.5
	136.2	93.6		136.3
		124.1		
		123.3		

Table 6.4 Stiffness data (in kPa) for position 1 and position 2 specimens used to quantify effects of packing pressure on properties for each packing pressure. Injection rate=0.067 cm^3/s

(kPa)	0 kPa	228 kPa	455 kPa	683 kPa
Position 1	10311	9794	11725	12422
	10239	11013	12128	12824
	11532	11832	12054	11426
	10605	12206	12129	11352
	10420	11499	13170	12051
	11161	9577	12023	12020
	10902	11018	10907	11501
	10828	9683	11241	12496
		10760		
		10351		
Position 2	10425	11612	11199	12014
	9868	10981	11538	11829
	11785	11389	11315	11977
	11643	11278	12533	11909
	10269	11646	12502	13489
	11198	10017	12507	13312
	10641	10425	12085	12419
	10902	9609		11278
		10907		
		10202		

Table 6.5 Void shape distribution data (in %) and total voids based on packing pressure. Injection rate=0.067 cm^3/s

	0 kPa	228 kPa	455 kPa	683 kPa
Circular (φ=12.58)	23.8	9.9	17.6	1.8
Ellipsoidal/Irregular (12.58<φ<20)	70.9	62.0	44.6	60.0
Very Irregular (φ>20)	5.3	28.2	37.8	38.2
TOTAL VOIDS	206	71	74	55

Table 6.6 Void size distribution data (in %) and total voids based on packing pressure. Injection rate=0.067 cm^3/s

SIZE (microns)	0 kPa	228 kPa	455 kPa	683 kPa
20-30	0	0.0	1.4	0.0
30-40	0	0.0	0.0	0.0
40-50	3.9	0.0	0.0	0.0
50-60	5.3	7.0	2.7	0.0
60-70	13.6	7.0	4.1	3.6
70-80	12.6	9.9	4.1	3.6
80-90	19.4	2.8	2.7	3.6
90-100	9.2	5.6	9.5	1.8
100-150	24.3	28.2	35.1	27.3
150-200	4.4	14.1	13.5	27.3
200-250	4.4	7.0	8.1	7.3
250-300	2.4	4.2	5.4	9.1
300-350	0.5	5.6	8.1	3.6
350-400	0.0	5.6	5.4	7.3
400-450	0.0	1.4	0.0	1.8
450-500	0.0	1.4	0.0	3.6
TOTAL VOIDS	206	71	74	55

Table 6.7 Tensile strength of each specimen (in kPa) used to determine effect of mat thickness and volume fraction on properties

TN4	TN8	TN12	TK2	TK4	TK6
48.8	105.0	138.8	58.9	104.8	150.4
42.9	110.0	127.7	53.0	102.5	160.3
41.0	112.2	148.7	64.5	96.6	133.2
71.9	86.2	155.3	50.2	99.0	139.7
56.2	89.1	139.4	69.8	137.4	148.9
53.4	79.4	155.3	63.5	97.9	120.8
58.2	118.4		55.4	97.2	106.4
56.0	106.4		64.7	92.5	104.9
	93.5		59.1	78.1	136.1
	93.6		68.9	96.0	130.6
	91.4		60.4	84.5	
			53.7	132.9	
			56.3		
			55.8		
			59.0		
			46.4		
			54.2		
			46.9		
			57.1		

Table 6.8 Stiffness of each specimen (in kPa) used to determine effect of mat thickness and volume fraction on properties

TN4	TN8	TN12	TK2	TK4	TK6
5329	8007	9946	6072	8189	12681
5444	8584	10025	5513	8172	11861
5746	8777	10115	5554	7494	11591
5389	7378	10561	5816	8268	11731
5033	7453	10701	6141	9120	11279
5222	7385	11246	5896	8169	10045
6004	9395	11497	4677	8006	10305
5853	9609	10863	4983	7845	8825
5802	9046	11745	5402	7741	10480
5718	7660	10813	5417	7994	9904
5278	7317	11690	5257	7600	10141
5015	7283	10971	4755	6731	
			4675	10830	
			4858	10885	
			4805	10413	
			4704		
			4662		
			5678		
			5135		
			4831		
			4849		
			4631		
			4875		